MOST (Micro-variability of Oscillations of STars) Microsatellite Structural Analysis and Design

by

Rémi Duquette

A thesis submitted in conformity with the requirements
for the degree of Masters of Applied Science
Graduate Department of Aerospace Engineering
University of Toronto, Institute for Aerospace Studies

Abstract

This work deals with the structural design and analysis of the Microvariability of Oscillations of Stars (MOST) microsat mission: Canada's first microsatellite mission and first space telescope. The preliminary study phase of the MOST mission proposes the use of the UoSAT tray stack concept as the primary bus structure. However, due to the size and requirements of the science payload (telescope enclosure), an alternative suitcase size structure (keeping the idea of a tray stack as the spinal bone of the primary structure) is conceptualised. Preliminary finite element analyses included herein highlight certain design weaknesses. Design recommendations are formulated and lead to the critical design of the MOST structure. As the design phases progress, the finite element models are refined, both at the component and at the spacecraft level. In an attempt to minimise the design cost, and following the AMSAT cost-effective philosophy, minimal mechanical testing is planned for the MOST mission. Hence, the spacecraft analysis via finite element methods is used herein to ensure structural reliability. The resulting safety margins, when the worst case load scenario is considered, adds confidence by largely surpassing the potential errors introduced by domain discretization and element formulation. The analyses confirm the MOST structure design to be adequate.

Finally, this work presents a detailed engineering analysis leading to the design of the MOST tie rods structural component. The tray stack conceptual design offers great advantages in terms of the ease of assembly. However, the sizing of tie rods for small satellites using a tray stack as a primary structure remains a challenging design problem. This work addresses the issues pertaining to tie rod design, and concludes with the appropriate tie rod design recommendations.

Acknowledgements

I would like to acknowledge those individuals who have contributed to the completion of this work. First of all, I wish to thank my co-supervisors Dr. Christopher J. Damaren and Dr. Robert E. Zee for their invaluable suggestions. The area of small satellite design is still at the infancy phase in Canada, but their sharing of many years of aerospace studies experience was truly appreciated. The USU 1999 and AMSAT 1999 conferences I attended with Dr. Robert Zee are quite memorable too. Special thanks to Dr. Peter C. Hughes who led my first steps toward defining my thesis work.

Financial assistance from the Canadian government in the form of a Natural Sciences and Engineering Research Council (NSERC) scholarship, the Canadian Space Agency NSERC supplement, as well as the University of Toronto Institute for Aerospace Studies (UTIAS) fellowship and entrance scholarship were invaluable for the completion of my dissertation.

My colleagues in the Spacecraft Dynamics and Control group have made my stay at UTIAS both enriching and entertaining. Specifically, I would like to mention the great help of Andrew Allen who edited my work and provided useful comments and suggestions that improved the scientific scope of my dissertation. James Crawford also provided some mechanical design assistance.

The staff of the Space Flight Laboratory (SFL) was also of great help. Mr. Hugh Chesser provided me with the necessary guidance along all design phases by providing judicious reviews of my finite element model results. His sharing of a professional experience in the aerospace industry is invaluable.

Special thanks to Deborah Osmond for her support and editing of the first drafts of my dissertation. Her input in terms of adding a historical perspective has had a major influence on my introduction. I would like to dedicate my first chapter to her.

Most importantly, special thanks to my mom and dad for their constant support, both financially and emotionally. It is to my family that this work is dedicated. This work would not have been the same without their words of encouragement.

Résumé

Le travail ci-inclus traite l'analyse et le design de la structure du micro-satellite MOST (*Microvariability of Oscillations of Stars*). MOST est le premier téléscope spatial Canadien et la première mission scientifique Canadienne utilisant un micro-satellite comme plateforme structurel. La phase préliminaire du design propose un design modulaire comme élément de structure primaire. Le *Surrey Space Center* et *AMSAT* ont été les premiers à utiliser ce genre de structure. Malheureusement, les dimensions et la forme du téléscope et des instruments scientifiques ont poussé les ingénieurs à modifier le design. Malgré les changements apportés, le design modulaire de la structure primaire n'a pas été modifié. Cependant, l'attachement de la structure au véhicule de lancement a due être déplacé sur le côté de la structure modulaire au lieu du dessous. Ce nouvel agancement implique des changements important au niveau de la réponse dynamique de la structure sous l'action des forces lors du lancement du satellite. Ces faiblesses sont exposées lors de l'étude préliminaire ci-incluse. Certaines modifications du design sont recommendées et appuyées sur les résultats obtenus. Le nouveau design tenant compte de l'étude préliminaire est ensuite analysé à son tour. Les résultats de l'analyse par éléments finis sont présentés afin de supporter les recommendations détailés du design final. Peu de tests expérimentaux sont prévus afin de minimiser le coût de la mission. Ainsi, les résultats des analyses par éléments finis inclus dans ce travail se veulent décisifs. Se baser seulement sur des analyses par éléments finis est généralement considéré très risqué. Cependant, les marges de sécurités découlant des analyses présentées sont largement au-dessus du seuil critique. Ce travail présente en ce sens un argument pour l'utilisation des résultats obtenus basé seulement sur l'analyse par éléments finis. L'étude de confiance prouve que les erreurs inhérentes à l'utilisation de la méthode d'analyse par éléments finis sont bien en-dessous du seuil critique.

Finalement, ce travail présente une analyse détaillée des tiges filletées servant à assembler tous les compartiments du design modulaire. Ce design présente plusieurs avantages au niveau de la facilité d'assemblage. Cependant, les tiges filletées deviennent l'une des composantes de la structure absorbant la majeure partie des forces durant le lancement du satellite. Ce travail présente donc une analyse complète visant à déterminer les dimensions, la quantité et les matériaux à utiliser pour le design des tiges filletées.

Contents

List of Notations

General Notation for All Chapters

x, y, z	Rectangular coordinates
r, θ	Polar coordinates
ξ, η	Orthogonal curvilinear coordinates
R, ψ, θ	Spherical coordinates
N	Outward normal to the surface of a body
l, m, n	Direction cosines of the outward normal
F	Force (N)
A	Cross-sectional area (m^2)
I_X, I_Y, I_Z	Moments of inertia
I_S	Specific Impulse
g	Gravitational acceleration
ρ	Density
q	Intensity of a continuously distributed load
P	Pressure
X, Y, Z	Components of a body force per unit volume
m	Mass (kg.)
M	Bending moment (N.m)
M_T	Torque (N.m)
σ	Normal (tensile) stress (Pa)
σ_{MA}	Normal maximum allowable stress (Pa)
σ_{MAX}	Normal maximum stress (Pa)
σ_{MD}	Normal maximum design stress (Pa)
σ_{MY}	Normal material yield strength (Pa)
σ_U	Normal ultimate strength (Pa)
$\sigma_X, \sigma_Y, \sigma_Z$	Normal components of stress parallel to x, y and z axes (Pa)
σ_{VM}	Von Mises stress (Pa)
τ	Shear stress (Pa)
τ_{MA}	Maximum allowable shear stress (Pa)
τ_{MS}	Material shear strength (Pa)
$\tau_{XY}, \tau_{XZ}, \tau_{YZ}$	Shear stress components in rectangular coordinates (Pa)
u, v, w	Components of displacements (m)
ε	Unit elongation

$\varepsilon_X, \varepsilon_Y, \varepsilon_Z$	Unit elongations in x, y and z directions
γ	Unit shear
E	Modulus of elasticity in tension and compression
G	Modulus of elasticity in shear or modulus of rigidity
ν	Poisson's ratio
μ_{S_Al}	Static coefficient of friction (the subscript, Al indicates on Aluminum)
μ, λ	Lamé's constants
ϕ	Stress function
U	Airy Stress Function
C	Torsional rigidity
V	Strain energy or Potential energy
SF	Safety Factor
SM	Margin of Safety
T	Temperature
t	MOST Tray wall thickness (m)

Particular Notation for Each Chapter (superseding any previous notation)

Chapter 3

U_{MAX}	Maximum Potential Energy
T_{MAX}	Maximum Kinetic Energy

Chapter 5

$_B$	Subscript denoting Bolt
$_J$	Subscript denoting Joint
A	Area (m^2)
A_B	Cross-sectional area of the body of the bolt (m^2)
A_C	Cross-sectional area of equivalent cylinder used to compute joint stiffness (m^2)
A_J	Joint cross-sectional area (m^2)
A_S	Effective tensile stress area of the threaded section of a bolt (m^2)
A_{SMAX}	Maximum bolt stress area (joint geometry limiting factor) (m^2)
A_{SMIN}	Minimum bolt stress area (m^2)
A_{SMINY}	Minimum bolt stress area for the material yielding failure mode (m^2)
A_{SMING}	Minimum bolt stress area for the tray gapping failure mode (m^2)
A_{SMINST}	Minimum bolt stress area for the bolt stripping failure mode (m^2)
A_{SMINSL}	Minimum bolt stress area for the tray slipping/bolt shearing failure mode (m^2)
A_{TS}	Cross-sectional area through which stripping shear occurs (m^2)
D	Bolt diameter (m)

E_B , E_J	Modulus of elasticity of bolt and joint material (Pa)
EQ_{P1}	Equilibrium point after pre-loading
EQ_{P2}	Equilibrium point after external load L_X is applied (from pre-loading point)
F_C	Minimum force or stress (N, Pa)
f_C	Actual design force or stress (N, Pa)
F_B , F_J	Load in bolt and joint (N)
F_{BMAX}	Maximum load in bolt (N)
F_{JMIN}	Minimum load in joint (N)
ΔF_B , ΔF_J	Change in load in bolt and joint (N)
F_P	Initial pre-load (N)
F_T	Total force computed from FBD (N)
F_X	Externally applied tension load (Fraction of force F_T calculated) (N)
F_{XCRIT}	Maximum external tension force that can be applied without gapping (N)
F_{XT}	Total external force applied in the bolt axial direction (N)
J	Total thickness of the joint (m)
ΔJ , $\Delta J'$	Compression of joint before and after application of the external load (m)
K	Nut factor (tabulated empirical values - unitless)
K_B	Stiffness of the bolt (N/m)
K_J	Stiffness of the joint (N/m)
L	Total length of the bolt (body + threads) (m)
ΔL , $\Delta L'$	Elongation of bolt before and after application of the external load (m)
L_B	Nominal length of the body (m)
L_{be}	Effective length of the body (m)
L_e	Length of thread engagement required to develop full strength (m)
L_G	Stressed length of the bolt (inner distance between nut and head) (m)
L_{se}	Effective length of the threads (m)
L_T	Thread length (m)
NT	Total number of tie rods
O_B , O_J	Origin of bolt and joint elastic curve
P	Pitch of the threads (m)
R_C	Radius of curvature of a bolt under bending load (m)
r_n	Effective radius of contact between the nut and joint surface (m)
r_t	Effective contact radius of the thread (m)
T_H	Height of head (m)
T_{in}	Torque applied to the fastener (N.m)

T_N	Height of nut (m)
T_{tor}	Maximum torque in tie rod (N.m)
β	The half-angle of the threads (30° for UN or ISO threads)
σ_B	Maximum bending stress (Pa)
σ_S	Maximum shear stress (Pa)
σ_T	Total tensile stress of each tie rods (Pa)
σ_{tor}	Maximum torsional shear stress (Pa)
μ_n	Coefficient of friction between the nut and joint at the interface
μ_t	Coefficient of friction between nut and bolt thread

List of Figures

List of Tables

List of Acronyms

AA	Aluminum Association
ACS	Attitude Control System
AIAA	American Institute of Aeronautics and Astronautics
AISC	American Institute of Steel Construction
AMSAT	The Radio Amateur Satellite Corporation
ANSI	American National Standards Institute (also referred to as ASA or USAS)
ARRL	American Radio Relay League
ASME	American Society of Mechanical Engineers
ASTM	American Society of Testing and Materials
BIPM	International Bureau of Weights and Measures
CDR	Critical Design Review
CG	Centre of Gravity
CM	Centre of Mass
CMG	Control Moment Gyro
CSA	The Canadian Space Agency
CTE	Coefficient of Thermal Expansion
ELV	Expendable Launch Vehicle
FBD	Free Body Diagram
FE	Finite Element
FEA	Finite Element Analysis
FED	Federal
FEM	Finite Element Method
FMEA	Failure Mode and Effect Analysis
HDBK	Handbook
IFI	Industrial Fasteners Institute
ISO	International Standards Organization
ITU	International Telecommunications Union
LEO	Low Earth Orbit
LHS	Left Hand Side
MIL	Military
MLI	Multilayer Insulation
MMC	Metal Matrix Composite
MOST	Microvariability of Oscillations of STars - Canada's first Space Telescope
MSC	The MacNeal-Schwendler Corporation
MSFC	Marshall Space Flight Center
NDI	Non-Destructive Inspection
PAA	Payload Adapter Assembly
PAF	Payload Attach Fitting
PDR	Preliminary Design Review
PCB	Printed Circuit Board
PRD	Program Requirements Document
RCS	Reaction Control System
RF	Radio Frequency
RHS	Right Hand Side

RMS	Root Mean Square
SAE	Society of Automotive Engineering
SFL	Space Flight Laboratory
SP	Secondary Payload
SPE	Secondary Payload Envelope
SPI	Secondary Payload Interface
SRS	Shock Response Spectrum
STD	Standard
TLV	Threshold Limit Value
TM	Telemetry
TRW	The Ramo-Wooldridge Corporation
TT&C	Telemetry, Tracking, and Command
UN	Unified Thread
UNC	Unified Coarse Thread
UNEF	Unified Extra Fine Thread
UNF	Unified Fine Thread
UNR	Unified Thread with Root Radius
USAF	United States Air Force
UTIAS	University of Toronto, Institute for Aerospace Studies

Preface

This work is about structures, and addresses analysis and design issues to ensure the structural success of the Microvariability of Oscillations of STars (MOST) micro-satellite. This section will provide a brief history of the theory of elasticity, and a survey about the emergence of small satellite missions. Wherever possible, references are provided to enable the reader to access the required background information.

Scope and Objectives

Analytical results are often regarded as *exact* results, provided that the solution to a mathematical model is numerically correct. One of the very basic principles learned during the completion of this study is that *exact* solutions of mathematical models are rarely a true representation of the physical system. Hence, questioning mathematical models, and doing research in order to find more effective and accurate solutions are both vital to the structural engineer. No engineer, nor anybody else for that matter, can predict the response of a physical problem *exactly*, because it is impractical to reproduce even in the most complex mathematical model all the chaotic material structure that exists in nature.

"Our ideas must be as broad as Nature if they are to interpret Nature." (Sir Arthur Conan Doyle. 1859–1930). *Interpretation* here is the key word. It is crucial to be careful in selecting the most appropriate mathematical model to interpret, or get accurate representation of, the physical system and to fully understand the underlying assumptions of that model. The mathematical model might inherently, on some subspace of the solution, present absurd results; the structural engineer is the one responsible to *interpret* such errors. As mentioned by Peter C. Hughes [1], there is no

such thing as an infinite number of vibration modes for a given physical system. What does it mean to have more vibration modes than the number of atoms that compose a body? Certainly, this seems absurd, but this is what the partial differential equation (PDE) based mathematical models predict. The idea of a *vibration mode* is born from the mathematical expression of a physical behaviour, and not the other way around. As also outlined by Hughes [1], it is highly unlikely that any real structure can vibrate exactly so that all its points move in unison. Obviously, the main objective is to seek mathematical or numerical results that are reasonably close to the physical system behaviours. Hence, the idea is to select vibration modes from the mathematical model that play a major role and have meaningful design implications in the analysis at hand.

The fundamental intention of any study such as this is to acquire sufficient confidence in some mathematical models over certain regimes, and to apply them to solve a set of physical problems. In this work, mathematical concepts modelling stress, vibration, and heat transfer in solid materials have been used to analyse and design the MOST small satellite structural components. The primary objective of this work, as implied in the title, is to provide the Space Flight Laboratory (SFL) with detailed structural analyses and subsequent design recommendations for the MOST microsatellite mission.

A Brief History of the Theory of Elasticity

Most of the time, the first step in research is to review the work of scholars and engineers accomplished in the field of study. Analysing stresses in structural components of a small satellite to improve the original design inherently involves having a clear understanding of the mathematical theory of elasticity. However, a pedigree of scholars has helped to develop what is now known as the *mathematical* theory of elasticity.

The history of the theory of elasticity and strength of materials has been given a thorough treatment by Isaac Todhunter, whose work was elaborated upon by Karl Pearson [2]. Unfortunately, as suggested by Clifford Truesdell [3] (1920-2000), many of the papers presented are worthless because they are too speculative to be used in any remote area of application. Moreover, research prior to 1800 is summarised in the first chapter, which lacks reference and acknowledgement of the Bernoulli family and

Leonhard Euler's major works. Another report mainly dealing with the analytical theory of vibrating bodies has been published by Heinrich Burkhardt [4] in the early 1900's. A more recent book published in 1953 by Stephen Timoshenko [5], constitutes an excellent historical survey that briefly covers Isaac Todhunter and Pearson's work, and builds up on it by covering the most influential body of work by mathematicians and engineers up to the twentieth century. Unfortunately, according to Truesdell [3], Timoshenko's work is drawn from a rather capricious selection of sources, which limit its scope. However circumscribed, Timoshenko's book has highly influenced this brief history herein. The last survey has been conducted by Clifford Truesdell [3], slightly after Timoshenko's work, between 1956-1958, and published in 1960. It is the most detailed and well-researched history of elasticity spanning the years from 1638 to 1788. Reading Truesdell's comprehensive history truly changes the way one regards the evolution of the mathematical theory of elasticity, and proves to the engineer and researcher that modern praxis is a legacy of early modern innovation. As Henry Miller (1891–1980) once suggested: "If we are always arriving and departing, it is also true that we are eternally anchored. One's destination is never a place but rather a new way of looking at things".

The brief historical survey presented herein is based on these works and on the source documents cited below. Extensive review is available in these elaborate historical surveys, and should be consulted whenever a more elaborated description is sought. Personal interest and reading "The Existential Pleasures of Engineering" by Samuel Florman [6] also became a motivating factor in the following modest and brief presentation of the roots of the strength of materials. Unveiling the major historical steps in the attempt to quantify and mathematically model the deformation of bodies will provide the reader with useful historical foundations and attempt to satisfy her/his scientific curiosity about the nature of theoretical origins and their evolution. The idea is to bring to light the primitive mathematical concepts and experiments that have led to the equations used in some modern modified forms, especially the use of finite element methods, that provides the basis for this work treating small satellite structures. The extensive use of references will allow the reader to access the sources: it is beyond the scope of this document to elaborate in sufficient detail and confer enough recognition for the work that has been done previously.

As far as can be established by modern archaeology and in print culture, Egyptians were the first to make use of empirical rules to erect pyramids and other monuments (albeit with slave labour) that can still be admired today. Following the Egyptians, the first individual to look at some primitive structural equilibrium problems was Archimedes (287-212 B.C.), who is well known for his work presenting the conditions for equilibrium of a lever. He is probably best known for discovering the law, often called "Archimedes' Principle", stating that an object immersed in fluid loses weight equal to the weight of the amount of fluid it displaces: nowadays referred to as the principle of buoyancy. After him, the main structure builders were the Greeks, the Romans, and the Persians who built structurally complex monuments. The *Pont du Gard* in France, and the many temples in Greece are impressive relics of their structural works. Most of their knowledge is believed to be based on experience, and much was lost during the Middle Ages. It is therefore a truism that crucial research, which led to the present knowledge of the strength of materials, have been derived from the period of the Renaissance in Western Europe.

The first attempt was made by Leonardo da Vinci (1452-1519) to apply what is now known as static mechanics, a principle that leads to determining the forces acting in members of a structure. Although a true masterpiece of art and engineering, da Vinci's notebooks do not present any theories per se, but constitute an amazing record of experiments based largely on his personal judgements and conclusions. These notebooks have been carefully studied and a general survey of engineering during Renaissance was published by William Parsons [7].

The first scholar to publish some original theory based on metaphysical experiments was Galileo Galilei (1564-1642), who wrote about the first theory in the field of strength of materials in the first two dialogues of his famous book "Two New Sciences". He wrote this during the last eight years of his life, while living in a villa at Arcerti in strict seclusion after being condemned by the Inquisition for supporting the Copernican theory of heliocentricity. "Two New Sciences" recapitulates all his previous works, suppositions and postulates. It was first translated into English by Henry Crew and Alfonso de Salvio [8]. Controversial issues were recently raised by Drake Stillman[9] highlighting some misleading interpretations of Galileo's true physical meaning. Translation of Italian words using English words such as *particles* that have a

modern connotation were found to be inaccurate in Crew and de Salvio's work. However presenting relatively different physical interpretations, both translations essentially expose the same newborn theory of the strength of materials. Two other books on Galileo's work are suggested: "Galileo's Life" written by Fahie [10] and the well known "The Star-Gazer" written by de Harsanyi [11]. Galileo pioneered the mathematical attempt to describing the behaviour of rods under tension, leading to the design of MOST microsatellite tie rods some 400 years later, and to determining strength in beams of similar geometry. He is also well known for developing the theory for obtaining a cantilever beam of equal strength, which can conceptually be used today for obtaining a satellite tray stack primary structure of equal strength.

The subsequent influential scholar was Robert Hooke (1635-1702), who established the linear relation between the force and the deformation of any *springy* (or in modern terms denoted as *elastic*) body, which is described today as Hooke's law. In London in 1678, he published a paper entitled "De Potentiâ Restitutiva" [12], which contains experimental results corroborating his linear relation or "Law of Nature" for elastic properties of materials. His work and life are reported by Gunther [13], Bertrand[14], and Robison [15] and should be consulted by the interested reader.

Hooke's Law has been used as the foundation upon which further development of the mechanics of elastic bodies has been made. The linear theory assumptions made for most of the structural analysis work included herein is directly derived from Hooke's work in 1678.

During the same period, Edmé Mariotte (1620-1684) established the laws of impact, demonstrating what is referred to as conservation of momentum today. In terms of his contribution to the development of the theory of elasticity, Mariotte tested tensile rods made out of wood and glass, and tested simply supported cantilever beams. From those experiments, he developed mathematical expressions to account for material elastic properties in bending of beams. In this regard, he improved the theory of bending of beams by considering simple linear elastic deformations. Mariotte also found from his tensile test experiments that the elongation was proportional to the applied forces, which is now referred to as Hooke's law. Mariotte's work has been published posthumously after 1686 which has been edited by Philippe De La Hire [16]. Hooke's famous paper[12] appeared in 1678. The succession of publications gives rise to some salient

issues, as it becomes clear that Mariotte discovered the linear relationship before Hooke did, but came up with the written evidence after Hooke. Hence, the credit solely attributed to Hooke should be revised and referred to as Hooke-Mariotte's law. However, this shall continue to be the matter of another French-English dispute. Finally, Mariotte merely introduced what is known today as fracture mechanics. He stated that a specimen under tension might fracture if a load acts for a sufficiently long time. Those preliminary experiments on fatigue and ultimate strength versus time establish Mariotte as the father of fracture mechanics.

Hooke and Mariotte had the privilege of being a part of the first group of scholars to work within the walls of the newly founded Academies of Science in Europe. Hooke was assigned to the Royal Society whose first charter was sealed in 1662 while Mariotte became amongst the first members of the French *Académie des Sciences* officially organized in 1666 by Louis XIV's minister Colbert. Similar academies were formed much later on in Russia and Germany. The St-Petersburg Academy of Sciences appeared in 1725 while the Berlin Academy of Sciences was born in 1770. Under the wing of these four Academies, the natural sciences flourished and the resulting momentum is responsible for most of the advancement that led to today's scientific knowledge.

This leads the discussion to Isaac Newton (1643-1727), who published his famous book *Philosophiae naturalis principia mathematica* [17] in 1687 in London. Although a major historical work, it did not contribute to the mathematical development of the elastic properties of bodies. However, his work suggests some philosophical hypotheses of the physical nature of elasticity based on his laws exposing the attractive properties of bodies. Hence, Newton did not advance the theory of elasticity *per se* but highlighted crucial concepts upon which other scholars further advanced the theory of elasticity.

At the same time, Gottfried Wilhelm Leibniz (1646-1716), who has been omitted in the aforementioned Timoshenko's [5] historical survey, applied calculus for the first time to find out that the bending moment is proportional to the geometrical moment of inertia of the cross-section of cantilever beams. In one of is papers, he stated that the elastic and acoustic properties of bodies are connected, which basically established him as the father of the mathematical theory of elasticity. His assertions and applied calculus results triggered great interest and drew James Bernoulli into studying elasticity. As will

be shown, Leibniz's influence on Bernouilli's work is responsible for great advancement of the mathematical theory of elasticity.

Later on, Jacopo Riccati (1676-1754), also omitted in Timoshenko's [5] historical survey, pursued a theory of elasticity based solely on the laws of mechanics, thereby rejecting the empirical Hooke's law. Basically, he wanted to show that the elastic properties of a body might be inferred from the frequency of its vibration. His mathematical result relating the material elastic modulus to be proportional to the frequency of oscillation squared is correct for the longitudinal case, but not for the transverse mode of oscillation. His work did not lead to practical results. However, the approach taken based on a dynamical theory and not a semi-metaphysical hypothesis is clearly a breakthrough in thinking.

The contest to seek a mathematical expression for the catenary was initiated in 1690 by James Bernoulli (1654-1705). He preceded Euler and hence he is truly the first mathematician to lay down the mathematical foundations of the theory of elasticity along with Leibniz and Christiaan Huygens. Actually, the Bernoulli family produced prominent mathematicians for three generations. All of them succeeded in advancing the elasticity theory at some point in their lives. John (1667-1748), participated actively to find the catenary. He also did some interesting work on the vibration of a loaded string. Nicholas I (1687-1759) did not bring anything new, although being the editor of the Opera of James; he certainly was a brilliant mathematician, too. Nicholas II (1695-1726) acted as the correspondent of Jacopo Ricatti. One of the most prolific of all the Bernoullis was undoubtedly Daniel (1700-1782). He is best known today for his book *Hydrodynamica* although his contributions to the elasticity theory are quite abundant. He worked on the frequencies and modes of vibrating bodies, but also suggested to Euler to apply his variational calculus in deriving the equations of elastic curves. Daniel's idea proposed to Euler is now known as the strain energy of a bent bar, neglecting a constant factor. Finally, John II (1710-1790), John III (1744-1807), and James II (1759-1789) also investigated, respectively, conical strings, the laws of elasticity, and the vibrations of plates.

Another great mathematician, Brook Taylor (1685-1731), published proof of the mathematical solution of most of Leibniz's and Huygens's work, especially the proof of Leibniz's solution for the catenary. John Bernoulli's own solutions have been influenced

by most of Taylor's unpublished investigations on the catenary. Nevertheless, Taylor is most well known today for his approximation, the polynomial expansion series.

As observed so far, only specific problems were solved and no true general theories were developed, except for Hooke's law. The basic principles and solutions found were mainly based on semi-metaphysical deductions. Leonhard Euler (1707-1783) introduced what shall be called the first general mathematical theory of elasticity. In 1743, Euler published his treatise on elastic curves entitled *Methodus inveniendi lineas curvas*[18]. After reading Euler's book, as mentioned above, Daniel Bernoulli suggested that he apply his variational methods to define the elastic curves. The application of Euler's isoperimetric method, known today as variational calculus methods to define the elastic curves, is a masterpiece of mathematical modelling. Indeed, the addition as an appendix to his treatise published earlier is a groundbreaking contribution to the theory of elasticity, and also to the essence of the method used in the field of mathematics. Euler's appendix has been translated in English in 1933 by W.A. Oldfather, C.A. Ellis, and D.M. Brown. Daniel Bernoulli also introduced Euler to the idea of what he called a potential force, which is equivalent to the modern expression of strain energy. Essentially, Bernoulli conveyed to Euler the physics fundamentals and ideas upon which Euler drew his mathematical researches. At the age of fifty-two, Euler published his work concerning the buckling of columns, which was printed in Berlin in 1759. Finally, Euler investigated the deflection and vibration of flexible membranes, for which he derived the partial differential equation. Truesdell's historical masterpiece [3] exposes Euler's life and work in details.

Following Euler, Thomas Young (1773-1829), who mastered over seven languages by the age of fourteen, became famous when he made his discovery of the interference of light in 1801. He was elected a member of the prestigious Royal Society a year later. His main contribution to the theory of elasticity is found in a course material book that was published in London in 1807 and entitled "A Course of Lectures on Natural Philosophy and the Mechanical Arts". He introduced the concept of the modulus of elasticity when considering tension and compression of bars. However, his definition of the modulus of elasticity differs from the modern definition of the so-called Young's modulus. His own definition was described as follows: "The modulus of elasticity of any substance is a column of the same substance, capable of producing a pressure on its base

which is to the weight causing a certain degree of compression as the length of the substance is to the diminution of its length." Nowadays, Young's modulus is defined as the constant of proportionality E linearly relating stress and strain in a material. Young highlighted the fact that permanent form deformation is incurred when the test specimen is tension-loaded over a limit that is particular to each material. Young also made some interesting statements on the fracture by dynamic loading compared with fracture by static loading. This concept is used to some extent in the equivalent static analysis of the dynamic loading of the small satellite structure. Finally, Young also presented useful and valid solutions to the problem of eccentric tension and compression of rectangular bars.

The efforts pursued after Young's discoveries, within the subject now referred to as continuum mechanics, are based on the advances in mathematics by Joseph-Louis Lagrange (1736-1813). The first publication of Lagrange's *Mécanique Analytique* appeared in 1788. A newer version of Lagrange's second edition has been edited by Bertrand and has been published in 1853. Some erroneous use of Lagrange's indeterminate multipliers by Bertrand was also corrected later on by Poisson. In addition to his introduction of new mathematical methods, Lagrange contributed to the theory of elasticity in his memoir *Sur la figure des colonnes*. His memoir treated the buckling of columns and came up with a mathematical expression highlighting the infinite number of buckling curves, which is meaningless physically, and yet provides accurate curves for the sub-space where the solution makes sense. Lagrange's main contribution to the field of structural mechanics came after his death when his method of generalized coordinates and generalized forces were applied in solving practical engineering problems.

Another major contribution during the early nineteenth century has been made by Claude-Louis-Marie-Henri Navier (1785-1836). He published in 1827 for the first time the general equations of equilibrium and motion, which must hold at every point of a body and at its surface. Those equations, in a modern modified form, referred to as Navier-Stokes equations, are being used extensively in the engineering field today. The stress concentration factor near the tie rod hole holding the tray stack of the small satellite together included later in this work is derived from an equivalent formulation of these equations in polar coordinates. Moreover, Navier's definition of the modulus of elasticity or the so-called Young's modulus was generally accepted and is still in use today. His careful assessment of the linear range over which the small deformation assumption is

valid, in addition to the seminal work of his generalised equations, establishes him as the founder of the modern theory of elasticity. His major accomplishment in the field of strength of materials appear in his book "*Résumé des Leçons données à l'école des ponts et chaussées sur l'application de la Mécanique à l'établissement des constructions et des machines*" first published in 1826. Navier revised this first edition and published a second edition in 1833. He died three years later. However, his work was revised a third time in 1863 under the supervision of Saint-Venant.

Lagrange noticed, while teaching at the *École Polytechnique* in France, the exceptional mathematical ability of one particular student from a less than privileged family: Siméon-Denis Poisson (1781-1840) graduated in 1800, two years after his entrance. He then became an instructor in mathematics and became a member of the French Academy in 1812. Poisson's main contributions are to be found in his two published memoirs [19][20] and course treatise [21]. His work is impressive from a mathematical standpoint, especially his derivation of the lateral deflection of a loaded plate with simply supported or built-in edges, and his derivation of equations for the longitudinal, torsional, and lateral vibrations of bars. The practical side of his labor accounts for today's use and application of his solutions to many problems. He is best known for the so-called Poisson's ratio used to relate strain to stress or vice-versa. The Poisson's ratio is tabulated for most isotropic and orthotropic materials used in engineering design. However, being very practical, he did not make any fundamental theoretical breakthroughs such as Navier, Cauchy, or the like.

Many French engineers like Poisson had the opportunity to be exposed to many influential mathematicians and engineers, and became prominent scholars in turn. This was the case for Augustin-Louis Cauchy (1789-1857), who had the opportunity to meet with Lagrange and read Navier's work on the deformation of elastic bodies and his derivations of the fundamental equations. Navier's work sparked interest, and Cauchy, studying hydrodynamics at the time, applied his notion of pressure on a plane. In doing so, he introduced the idea of stress within the theory of elasticity. Cauchy derived the expression of the stress components on an inclined plane of an elemental tetrahedron. One of his main proofs shows that the stress acting on any plane can be specified by six components. Along with that idea, he introduced the concept of principal stresses, which is very useful nowadays. He is also accountable for the derivation of the differential

equations of equilibrium for any rectangular parallelepiped elements. These equilibrium equations are used extensively nowadays and form the basis of many methods in finite element analysis. Moreover, he demonstrated that, within the small deformation assumption, the unit elongation in any direction and the change of the right angle between two initially perpendicular lines are expressed by six strain components. He also introduced the idea of principal strains. Finally, and certainly not the least, he derived the relationships between the six components of stress and the six components of strain for an isotropic body. His work constitutes the first complete set of equations for solving stress in isotropic bodies that is taught to engineers today. Obviously, Cauchy's work is directly embedded in the current thesis work.

Another famous graduate from the *École Polytechnique* also made breakthroughs for his brilliant engineering work concerning the theory of elasticity. Lamé (1795-1870) graduated in 1818 and was recommended to the newly formed Russian engineering school, the "Institute of Engineers of Ways of Communication" in St-Petersburg. While in Russia, Lamé invented a horizontal tensile strength testing machine. The results obtained helped in the design of iron structures in Russia. Clapeyron (1799-1864) collaborated with Lamé to publish their first important memoir *Sur l'équilibre intérieur des corps solides homogènes* [22] in 1824. This memoir shows that the equations of equilibrium using Navier's notion of the molecular forces are the same as the equations introduced by Cauchy using the concept of stresses. Moreover, it presents the so-called Lamé stress ellipsoid which can be used to measure stresses at any cross-section or at the surface of an ellipsoid. Once Lamé returned to France in 1831 because of political disruptions between France and Russia, he worked on railroad construction between Paris and St-Germain. This engineering work was abandoned quickly as he took the post of professor of physics at the *École Polytechnique* until 1844. It is only then that he started to work on his book on the theory of elasticity [23] [24] that made him famous. Lamé shows in his book published in 1852 that two elastic constants are required to determine the elastic properties of an isotropic material. He also exposes problems on vibration and presents solution for the motion of bars, membranes, and strings. Finally, he modified the relationship between stress and strain components to introduce the use of his two elastic constants. Lamé is also accountable for the introduction of the use of curvilinear coordinates and their application to mechanics. For his eminent work in Russia on the

theory of elasticity, Lamé was elected a member of the French Academy of Sciences in 1843.

As noted, the French institutions were producing talented and efficient scholars. On the other side of "*La Manche*" (the *English Channel*), the theoretical physics department at Cambridge University followed with the study and advancements made by George Gabriel Stokes (1819-1903). It is only in 1845 that Stokes published his first paper[25] on the theory of elasticity, which was presented to the Cambridge Philosophical Society the same year. Like Lamé, he established the equations of equilibrium featuring two elastic constants. In retrospect, it can be asserted that Stokes derived those equations before Lamé. Hence the so-called Lamé constants should actually be renamed when taking into consideration the work done by Stokes. This, perhaps, shall be the matter of yet another French-English dispute! Nevertheless, Stokes published his work "On the Dynamical Theory of Diffraction" in 1849. This paper introduces two theorems dictating the vibration of elastic bodies. The first of which is stated: "the part of the disturbance which is due to the initial displacements may be obtained from the part which is due to the initial velocities by differentiating with respect to time, and replacing the arbitrary functions which represent the initial velocities by those which represent the initial displacement." In short, the problem of finding the displacements is limited to that of finding the displacements due to initial velocities only. The second theorem dictates the motion of a disturbance due to a given variable force acting in a prescribed direction at a given point, the same way as within the first theorem. Stokes contributions are seen as breakthroughs in many different fields. He was elected president of the Royal Society from 1885-1890, which shows that he had an established reputation.

The last pioneer presented in this brief history of the theory of elasticity is Barré de Saint-Venant (1797-1886). Political events in Saint-Venant's early life biased the French authorities; it took long time to recognise the groundbreaking fundamental ideas brought to light by him. He contributed immensely to the theory of elasticity by introducing his semi-inverse method. Basically, he established the relationships between the strain and the displacement fields. For doing so, he introduced the well-known displacement functions u, v, and w which are arbitrary functions of the position x, y, and z. Assuming some general displacement functions, he was able to solve any stress

problem. Once some variables of the displacement and forces are assumed within the boundaries of a given problem, he argued that the remaining variables can be found easily by satisfying the equations of elasticity previously defined by Cauchy or Navier and Stokes. Saint-Venant never published a book on the subject, however, he published many papers and edited Navier's *Résumé des leçons* in 1864 and translated Clebsch's work[26] in 1883. His last work, a translation of Clebsch's book, ended up increasing threefold the volume of pages by editorial notes. This simply highlights that Saint-Venant was particularly meticulous in his work [27].

The aim of this chapter was to briefly describe how the theory of elasticity has evolved over the centuries. Since the death of Saint-Venant in 1886 to year 2000, much research and advancements have been made. The development of cars, trains, and planes, and the Industrial Revolution, to name only a few, proved the theory of elasticity useful and practical. Like many other research advancements, it also had destructive applications, especially during the two World Wars. Obviously, on the positive side, the most amazing engineering achievement has been the landing of astronaut Neil A. Armstrong onto the surface of the moon in 1969. Since then, huge strides have been made using computer technology. Engineers now use numerical techniques such as finite element modelling using computers and parallel computing facilities. Stress analysis has become increasingly easy, however, at the risk of producing nonsensical results, leading to the well-known expression "garbage in, garbage out". Hence, the understanding of fundamentals and reading of the history of the theory of elasticity has proven crucial and useful. This work has also been influenced by more contemporary scholars such as Galerkin's work on thin plates [28], Love's treatise [29], Timoshenko's theory of shell elements [30] and work on the theory of elasticity [31] [32] [33] [34], Muskhelishvili's work on elasticity [35], Novozhilov's work on nonlinear elasticity[36], Sokolnikov's work on thin shells [37], Mushtari's work on nonlinear thin shells [38], Flügge's work on shells [39] [40], Niordson's work on thin shells [41], and Bruhn's work on flight vehicle structures [42].

For brevity of this historical survey, the works of M. Mersenne (1588-1648), P. Varignon (1654-1722), A. Parent (1666-1716), P.V. Musschenbroek (1692-1761), C.A. Coulomb (1736-1806), A. Girard (1765-1836), E. Hodgkinson (1789-1861), S. Germain (1776-1831), F.J. Gerstner (1756-1832), J.M.C. Duhamel (1797-1872), G. Green (1793-

1841), J.V. Poncelet (1788-1867), B.P.E. Clapeyron (1799-1864), W. Wertheim (1815-1861), J.C. Maxwell (1831-1879), J.W.S. Rayleigh (1842-1919), A.T. Kupffer (1799-1865), and other scholars from the early twentieth century have been omitted. The above section has provided a smaller, albeit equally important, skein of the most influential scholars who have written on this subject. Subsequent to reading about the history of the development of the theory of elasticity, one would only wish that all these scholars could have lived longer in order to provide more theoretical and historical debates spanning continents and centuries. This brief historical overview may first seem incidental to the MOST project. It is, however, important to outline and recognise the lineage of the theoretical advancements from which this work is derived.

A Brief History of the Emergence of Small Satellite Missions

A brief look at the emergence of the so-called "microsatellite" missions is necessary in order to gain perspective on how this work fits in a more global picture of small satellite development work. The nickname "microsat" is used to denote satellites weighting less than 100kg. Similarly, the nickname "nanosat" was attributed to satellites weighting less than 10kg. Recently, the nickname "picosat" appeared to denote satellites weighting less than 1kg. The trend set forth by AMSAT seems to have flourished. This thesis has been mindfully guided by some AMSAT community members who have strongly influenced the conceptual ideas treated and therefore, it is important to highlight where and how the experience of these people has been gained.

At the apogee of the cold war, the former USSR launched a small transponder. The successful launch of Sputnik I occurred at 19:28:04 GMT on 4 October 1957 from Tyuratam. This marked the beginning of what has been subsequently called the Space Age [43]. Four months later, on 31 January 1958, Explorer I, the first US satellite was launched. It contained rudimental scientific instruments to measure the radiation levels in space, which was designed by physicists directed by Dr. James Van Allen, well known today for the so-called Van Allen belts.

The following major Space Age achievement has been the first manned satellite mission. Yury A. Gagarin (1934-1968), cosmonaut, born near Smolensk, Russia, became the first man to travel in space in 1961 when he rode aboard the satellite Vostok I on a single orbit of Earth. The race to the moon was sparked at that moment. In the

meantime, massive resources were put into the development of communication satellites referred to as "Comsats", most of which modified deeply the modern world as it is now: their presence on orbit brought television, global communication, and crucial scientific measurements to our world.

A large number of low-cost small satellites have been launched since then. The rate and number of new planned small satellites, or so-called microsatellites, is increasing rapidly. This trend started in the 1960's and led to the birth of the OSCAR Association organised by some radio amateurs from Sunnyvale, California, US. This community of radio amateurs made significant contributions to and have challenged traditional satellite engineering design methods and general beliefs. Many professional engineers did not believe in their chances of success. Against all odds, they launched their first transponder, OSCAR I in 1961 and OSCAR II in 1962. In January of 1969, as a result of the COMSAT Amateur Radio Club in Washington, the idea of an East Coast equivalent of Project Oscar was born. The Amateur Satellite Corporation (AMSAT) was incorporated on March 3, 1969 as a not-for-profit educational organisation. The subsequent OSCAR satellites were a modest version of the most recent AMSAT Phase 3-D satellite. However primitive these satellites were in some ways, those unsophisticated efforts truly opened the door of a new era in the aerospace field. The International Telecommunication Union (ITU) held a meeting during the 1963 Geneva Space Conference and adopted a footnote proposed by the United Kingdom, and supported by the US and Canada, authorising amateur satellite operation worldwide in the VHF (144-146 MHz) band. Much of the now established low-cost trends in developing small satellites were initiated by the early successfully flown OSCAR missions, which would not have been possible without the ITU approved amateur band. The successful achievements of AMSAT are now a part of history. The amateur handbook edited by Martin Davidoff [44] is a highly read overview of the amateur satellite history and is widely distributed today.

Following the AMSAT, as true originators of the "faster, cheaper, better" philosophy, some universities began developing small satellites for education. The well-established Surrey Space Centre at the University of Surrey is now an established leader that emerged from these early investigations. Surrey provides multiple examples of the success of small satellite missions.

Their success story began in 1981 when UoSAT 1 was launched. UoSAT 2 followed in 1984, which was their second experimental microsatellite. Since then, 12 low-cost microsatellites designed by the Surrey Space Centre together with their spin-off company Surrey Satellite Technology Limited (SSTL) have been placed in orbit piggybacking on Ariane, Tsyklon, and Zenit launchers. SSTL was formed in 1985 as a company wholly owned by the University of Surrey. Among many technological breakthroughs, SSTL introduced the modular tray stack structural design in 1990 with UoSAT 3 and 4. A similar design was proposed as a basis for MOST. Surrey's modular primary structure is qualified to carry payloads up to 35kg. In fact, most of their microsatellite total mass is under or around 70kg. Their electrical design also features commercial off the shelf (COTS) parts, which lowers the cost considerably and is most probably a vestige of AMSAT's "faster, cheaper, better" philosophy. Over the last 20 years, SSTL launched 14 small satellites, of which 11 missions are still operational and monitored from their mission operations and control centre in Guildford. Their future is also promising as 6 missions are currently preparing for launch or in progress. This is definitely the best example of the potential and innovation that is made possible through collaboration between academic research and business that can market cost-effective small satellites for rapid and affordable commercial access to space.

In the US, one of the oldest University-based aerospace programs is at Johns Hopkins University in Baltimore, Maryland. Their recent Near-Earth Asteroid Rendezvous (NEAR) mission success is anticipated to generate valuable scientific data. The properties of asteroids provide valuable clues as to the details of how planets formed both around our Sun and other stars. In addition to the manufacturing of over 55 spacecraft so far, the Applied Physics Laboratory (APL) at Johns Hopkins has also developed instrumentation for high profile missions such as Galileo, Ulysses, and Voyager.

Utah State University (USU) in Logan, Utah, is one of the oldest institutions to develop instrumentation and test facilities. Their Space Dynamics Laboratory (SDL) was formed at the height of the Cold War in the 1960's. They are established leaders in remote sensing operations. Their ground test facility features a three-axis motion table, which serves as a basis for the University of Toronto Space Flight Laboratory's motion table, currently under construction. USU hosts the largest annual international

conference on small satellites. The "Cheaper by the Dozen" slogan of their 13th conference held in August of 1999 clearly highlights the direction that is being investigated at the moment.

Weber State University's small satellite program was established in 1982, slightly after Surrey. They have designed NUSAT 1 (1986), WeberSat (1990), and JAWSAT (1996) and have been involved with the designing and manufacturing of the AMSAT Phase 3-D project space frame.

Finally, multitudes of University programs are being established and are promising for the future. The most important such programmes are those of Stanford University, Arizona State University, University of Colorado (Boulder), Penn State University, Massachusetts Institute of Technology, Boston University, University of New Hampshire, and last, but certainly not least, the Space Flight Laboratory at the University of Toronto Institute for Aerospace Studies.

The above few pages have attempted to provide a brief overview of the history of small satellites. For brevity, the history of many organisations and events have been omitted, especially information pertaining to more recent business organisations such as AeroAstro and Orbital Sciences Corporation, to name only two. However, it provides a broad historical picture necessary to understand the conceptual ideas mentored by AMSAT members for the design of MOST structural components, which are thoroughly evaluated and analysed herein.

Small Satellite Sources of Information

The most comprehensive collection of aerospace related information is found in *Jane's Space Directory* edited by Wilson [45] [46]. However, these two source documents are expensive. Cheaper sources of information are also available through other publications [47] [48] [49]. A directory by Wertz [50] is quite comprehensive. Some free sources such as the TRW Space Log [51] are also of great value. The relatively short aerospace references listed herein shall be used for further research work. Specifically, the KISS Database [52] from Germany, the AMSAT publications such as The Satellite Handbook [44], and the proceedings from the Utah State University/AIAA annual small satellite conference are invaluable sources of information. Finally,

information on launch vehicles can be found in Hujsak [53] and Isakowitz [54]. The terminology used herein was mainly based on the AIAA Guide [55].

Outline of the Thesis

This work is organised into two main parts. The first part, which includes the Preface and Chapter 1, provides a historical background, a broad discussion of previous small satellite structures, and a description of the MOST microsatellite mission objective and structural requirements. It also briefly reviews the basics upon which this work builds, in terms of spacecraft configuration, preliminary structural designs, and finite-element models. The second part, including Chapters 2 through 4, presents the preliminary and detailed design phase analyses for the MOST structure and provides design recommendations. A detailed tie rod analysis and design is covered in Chapter 4 as it is seen as one of the most critical structural components of the MOST tray stack. This second part thoroughly explains and shows why those design recommendations are proposed through analytical results, finite-element model analyses and discussions with experienced aerospace engineers.

This work is primarily in SI units, although a few examples and tie rod size results are also presented in English units. Appendix A provides the necessary conversion factors.

Chapter 1

Introduction

This chapter provides an overview of developing small satellite structures and introduces the MOST microsatellite mission. Small satellite missions, as outlined in the preface, typically run with a fraction of the traditional space programs budget. Microsat mission cost savings explain the enthusiasm shown by the aerospace industry, both in the private and public sectors. Indeed, the cost constraint for developing a small satellite is a key design factor. However, due to recent Mars exploration mission failures, one must understand the limits and design tradeoffs, and more importantly, when cost should be used as a design factor constraint and when it should not.

1.1 Introducing MOST: A Brief Summary of the Mission

The MOST mission is mainly funded by the Canadian Space Agency (CSA) through its Space Science Program. MOST is a space astronomy mission, which was proposed by Professor Jaymie Matthews, the Principal Investigator (PI). The main scientific objective of the MOST mission is to gather high-quality long-period stellar photometry data, measuring fluctuations in stellar brightness, for selected stars, from which stellar age, core composition, stability and presence of planets can be inferred. Atmospheric scintillation noise coupled with the day/night cycle of a ground based telescope set limits to astronomy observations. A terrestrial telescope cannot be used to achieve the MOST scientific goals. Hence, MOST will be Canada's first space telescope. However, to comply with CSA's budget constraints, the MOST payload was sized to fit within the envelope of a small satellite, or so-called microsat. The microsat design features a 15-cm Maksutov telescope as the primary payload. In order to meet the low

cost constraint imposed, the microsat design phase will feature few testing of the hardware. For example, the structural design will rely mainly on Finite Element Analysis (FEA). Hence, thorough analyses were performed to verify the structural design in terms of the vibration launch loads including a modal analysis and the static acceleration launch loads. The results obtained and methods used are presented in this work.

1.2 Cost Effective Approach to the Design of MOST - A Motivation for this Work

The combination of an iterative design process as outlined in Section 1.3, a small design team, a "cheaper, faster, better" philosophy, and a "simpler the better" approach will unequivocally lead to a lower cost design. However, there is often a price to be paid in terms of an increased risk of mission failure.

Many small satellites have been successfully placed in orbit as secondary payloads piggybacking on Ariane, Tsyklon, Zenit, and Delta launchers. Structural failure of a secondary payload may jeopardize its mission and, in the worst possible scenario, damage the primary payload during launch. This fact strongly motivates a thorough analysis of the MOST spacecraft structure. Moreover, a secondary motivation for the MOST spacecraft finite element analysis (FEA) included herein is drawn from the AMSAT philosophy. In an attempt to minimize the design cost, which underlies the AMSAT cost-effective philosophy, minimal mechanical testing is planned for the MOST mission.

Hence, the task of constructing reliable structural finite element models of the spacecraft and spacecraft components was an obvious research goal. Performing vibration and other mechanical analyses via finite element methods to ensure structural success is a significant challenge. Solely relying on finite element analysis results can be a risky endeavour. However, the work presented herein proves the final design to be both safe and reliable structurally within the assumptions made. The safety margins resulting from the completed analyses, when considering the worst case load scenarios, also adds confidence to the design. The challenge here is to show that the error margins obtained surpass the potential errors introduced by discretization, element formulation, and linear behavior assumptions. Those concerns will be addressed in Chapter 2 and Chapter 3 by

presenting hand calculation approximations for validation and other means of assessing the FEM results reliability. These verification procedures are quite limited for complex structural analysis, but rough-order-of-magnitude results were helpful for validating the MOST FEA.

1.3 The Process of Developing Small Satellite Structures

The scientific or commercial goals leading to the mission requirements must be well defined in order to lay out the spacecraft systems requirements, further initiate the design process, and ultimately, to clearly define the structural subsystem requirements. The mission success then largely depends on the subsequent structural design phases. Specifically, the following sections clarify the MOST structural design process undertaken in the context of a Low Earth Orbit (LEO) microsatellite mission.

Following simple design steps can curb the complexity of the design tasks. The process of outlining a general approach spanning the conceptual design up to the detailed design phase is quite straightforward and was well documented and described by Larson and Wertz[56][57], and Sarafin[58]. This is mainly due to all small satellite missions featuring more or less the same performance requirements and design constraints.

As mentioned previously, once the scientific or commercial goals are set, the mission requirements can be established. One important feature of small satellite missions, as shown in Figure 1.1, is that initial goals defining the mission requirements can be altered if cost or design issues can justify their modification. The process of developing small satellite structures can be summarised quite simply. Again, Figure 1.1 shows a generic small satellite design loop as applied to the MOST mission. The simplicity of the design hierarchy process hides some of the intricacy that one can fully discern only after going through the design loop for several iterations. Hence, the work included herein is truly a walk through that design and analysis loop, which in the end results in the MOST structure design satisfying the scientific goals and mission requirements.

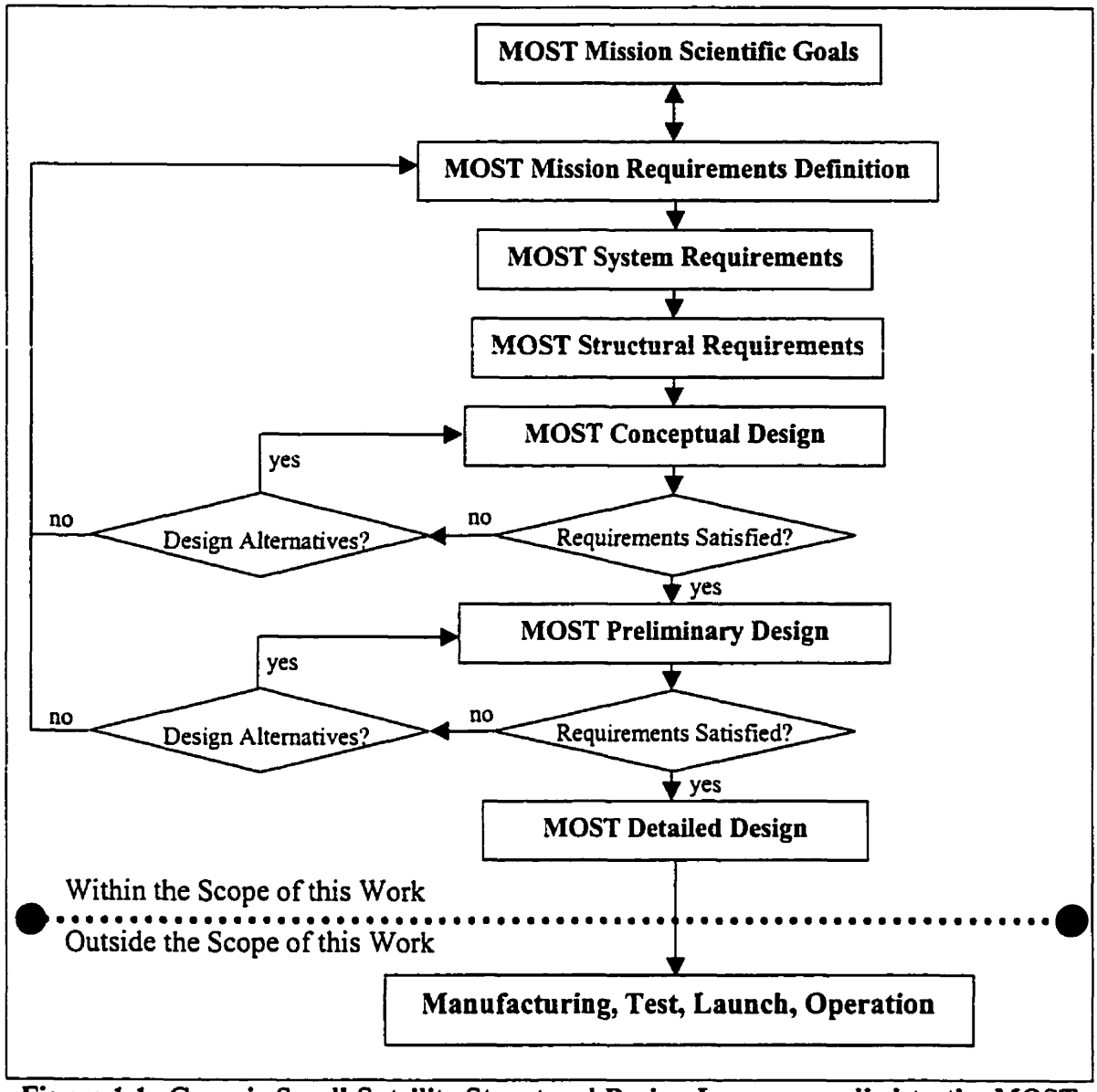

Figure 1.1: Generic Small Satellite Structural Design Loop as applied to the MOST mission

It can be observed in Figure 1.1 that the fundamental low-cost advantage of a small satellite mission may conceptually imply modifications impacting the scientific performance goals. The double-ended arrow on Figure 1.1 shows the potential interaction between scientific goals and mission requirements. For example, the scientific payload mass could be decreased in order to comply with the maximum secondary payload mass constraint (See Appendix F.4), consequently modifying the main science goals. These important modifications can be avoided, or, at the least kept to a

minimum by evaluating the conceptual design that would maximise the key performance goals.

Consequently, the primary structure conceptual and preliminary design, which can potentially instigate mission goal changes, must involve a thorough investigation of all design options. The main structural characteristics that can influence the overall design are: mass, stiffness, shape, size, volume, materials selection, thermal properties, reliability, safety, cost, manufacturing, and assembly. All these variables are dependant variables that are functions of the geometry of the structure and the materials used. Therefore, design recommendations focus on changes affecting the geometry of the structure and the materials used.

1.4 MOST Spacecraft Structural Configuration

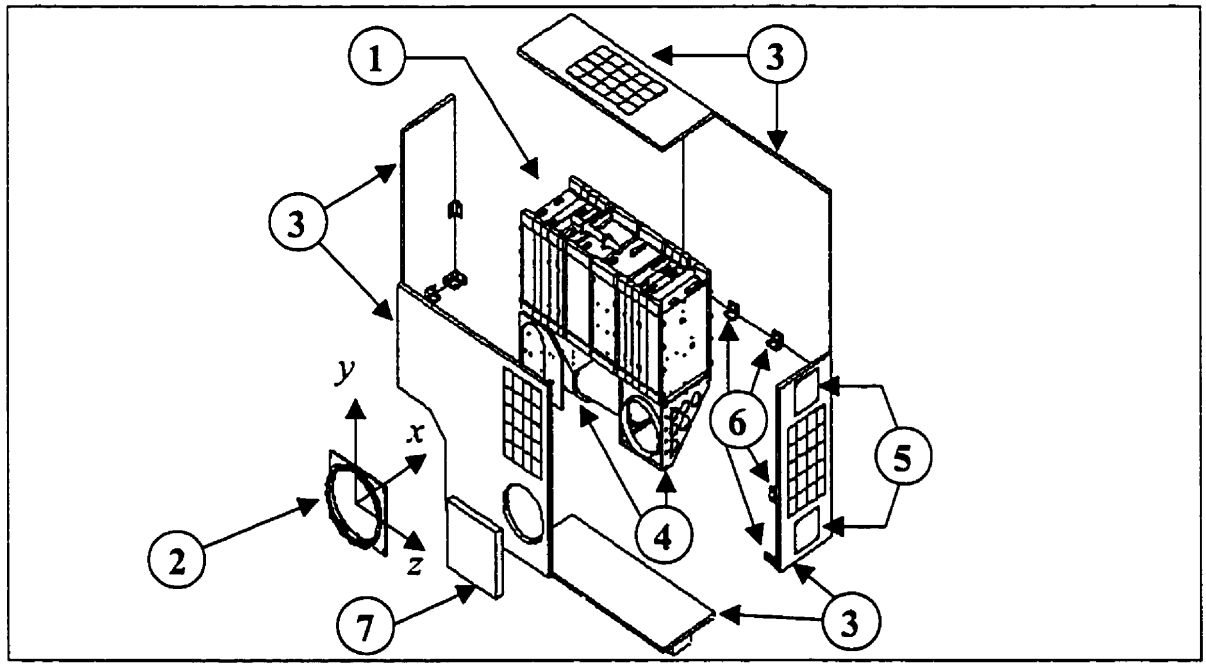

Figure 1.2: MOST Assembly Drawing (Courtesy of SFL)

The MOST rectangular coordinates system is defined in detail in Section 1.5. The MOST structure consists of seven (7) components (list numbers refer to Figure 1.2):

- The primary structure components:
  - (1) The horizontal modular assembly of fifteen trays tied up with eight tie rods
  - (2) The Payload Adapter Ring
- The secondary structure components:

(3) The six honeycomb solar panels

(4) The telescope and periscope mirror assembly

(5) The four patch antennas

- The tertiary structure components:

(6) All brackets connecting primary and secondary structural components

(7) The telescope door

Basically, the MOST microsatellite tray stack acts as the structural backbone on which all other components are attached. The fifteen (15) trays are held together by eight (8) tie rods passing through all trays and bolted at both z-side ends of the stack. The PAA ring is attached directly to the tray stack through the star-facing honeycomb panel in six locations. The PAA ring is also attached to the star-facing panel in three locations on the negative y-side. The six (6) solar panels are attached to each other via brackets on the science instrument side and mounted through thermal stand-offs directly bolted to the tray stack on the tray stack side. The telescope and periscope mirror are linked together by a non-rigid ring allowing for material thermal expansion, and are both rigidly attached separately through support brackets to the tray stack. The aperture door is to be closed during launch and is rigidly attached to the star-facing panel. The analysis assumed that the four patch antennas are rigidly attached to the two z-side panels. The solar arrays were modelled as non-structural mass smeared over the honeycomb laminate panel elements at locations shown on Figure 1.2 and Figure 1.3 since they are both glued and pinned to the honeycomb panels. The materials used and other structural details are described in Chapter 2 and Chapter 3 where appropriate. For instance, the laminate definition used for the six honeycomb panels is further defined, analysed, and validated to ensure proper modelling.

Microsatellites based on tray stack designs are mounted to the launch vehicle at one end of the stack so that the stack is along the launch vehicle thrust line. This configuration is optimal for the tray stack primary structure as all axial loads are absorbed by compression of the tray stack. Alternatively, the stiff tray stack acting as a cantilevered beam also easily absorbs lateral loads. However, the Delta II launch vehicle was selected as the baseline for MOST. Due to the space restrictions imposed by the

Delta II secondary payload envelope, MOST features a side-mounted PAA, as shown on Figure 1.4. Accordingly, the loads acting axially through the usually bottom-mounted arrangement are now transferred through the side-mounted support as severe bending and shear loads. A stiffer primary structure is therefore required for MOST. The consequences are especially important for the tie rod sizing. This issue is therefore carefully analysed and examined in Chapter 4.

1.5 MOST Dimensions and Coordinates System Definition

A rectangular coordinate system was defined as shown on Figure 1.2 and Figure 1.3 in order to present analyses results coherently throughout this work. The coordinates system is fixed with respect to the spacecraft. The positive x is meant to always point towards the sun. The positive y direction was defined to be pointing along the launch vehicle thrust line and pointing in direction away from Earth during launch. The early design phase coordinates system definition enhanced and facilitated communications between the MOST team members. The following are the general conventions that were adopted (Refer to Figure 1.2 and Figure 1.3):

- Origin of the x-y plane at centre of PAA with y-z plane located at the separation plane as described in the Delta II secondary payload document[59] [60]
- Positive x-direction Sun Facing
- Negative x-direction Star Facing
- Positive y pointed toward Tray Side
- Negative y pointed toward Telescope and Instrument Side
- Positive z pointed toward Aperture Viewing Side (Periscope Mirror Side)
- Negative z pointed toward Cryo Cooler Side

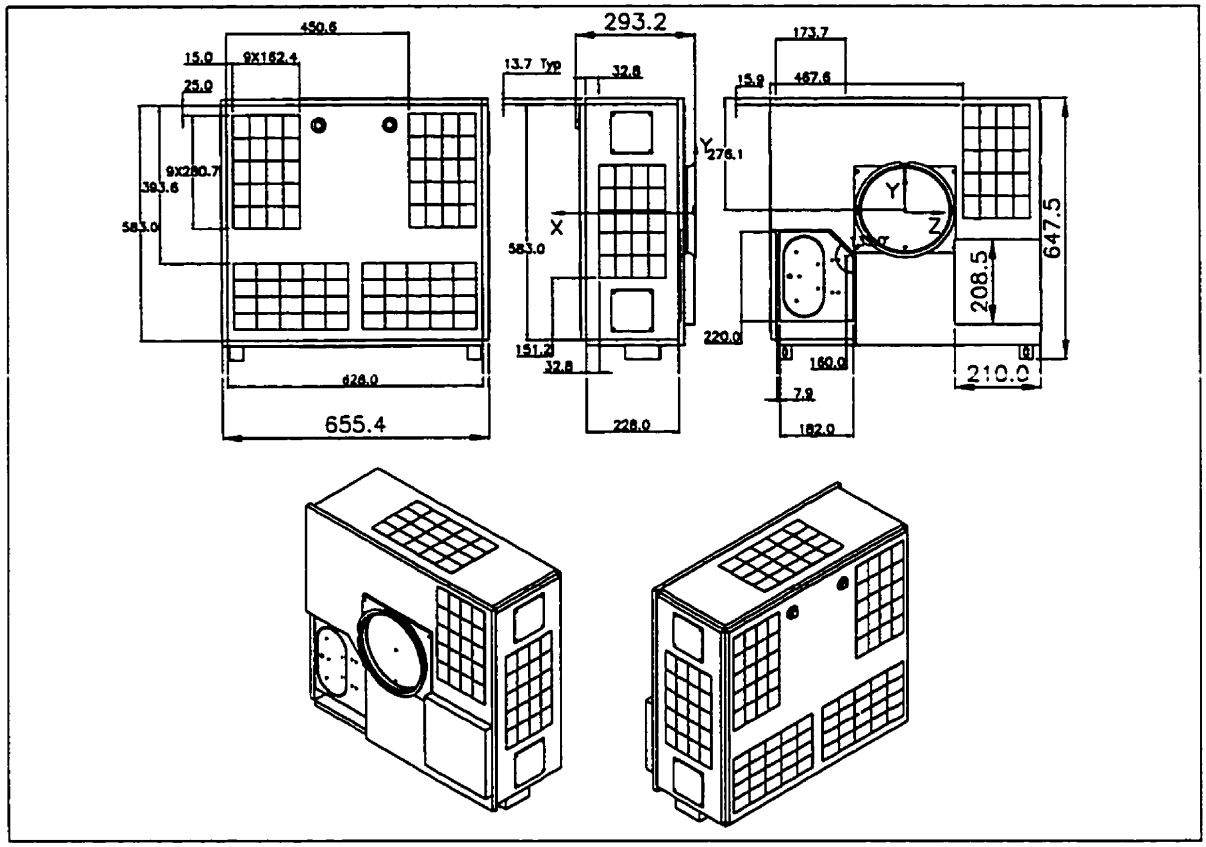

Figure 1.3: MOST Assembly and S/C Design Coordinates System Definition, Dimensions in millimetres [mm] (Courtesy of SFL)

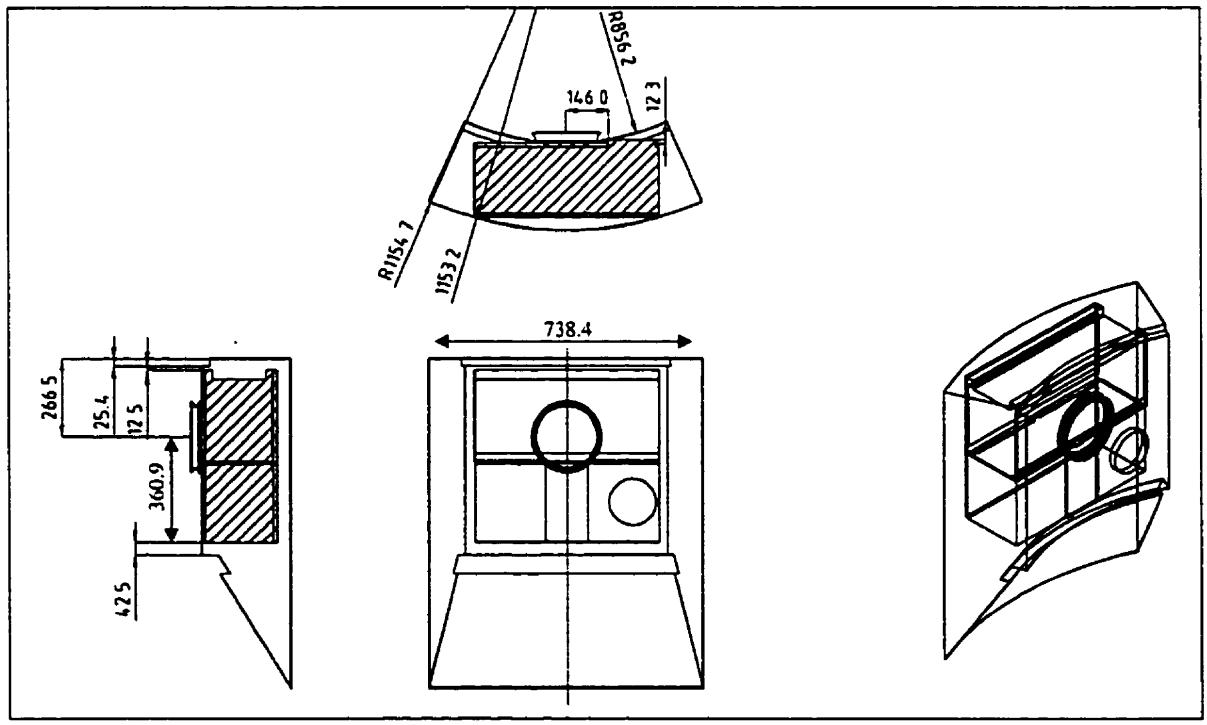

Figure 1.4: MOST within Delta II Secondary Payload Envelope, Dimensions in millimetres [mm] (Courtesy of SFL)

1.6 MOST Requirements and Constraints Definition Process

The construction of the MOST finite element (FE) models was based on all drawings provided by the SFL staff. Some assumptions made during the preliminary design analysis are outlined in Chapter 2. The detailed design configuration shown in Figure 1.2 and Figure 1.3 was used to build the final FE models.

Generally, the main design drivers constraining the material selection and conceptual geometry of a small satellite structure are the result of the requirements definition process which is outlined below within four generic steps (the values or comments in brackets {} pertain to the MOST mission):

Step 1: MOST Scientific Mission Goal

- Main Scientific Objective {Gathering high-quality long-period stellar photometry data (measuring fluctuations in stellar brightness) for selected stars, from which stellar age, core composition, stability and presence of planets can be inferred}

Step 2: MOST Mission Requirements and Parameters (Based on MOST Phase A Report[61], MOST Proposal[62], MOST scientific publications[63][64], and MOST Updated Detailed Design)

- Pointing accuracy {25 arc-sec (3σ)}
- Field-of-view {Telescope opening and cryo-cooler opening}
- Scientific Payload mass {13.7 kg. with contingency}, geometry, volume {See Appendices G and H}
- Mission life {1 year}
- Orbit altitude {785km}, Eccentricity {0}, Right Ascension of Ascending Node {6 P.M.}, and inclination {98.6 degrees (Sun-synchronous)}
- Reliability {Within low-cost AMSAT approach}

Step 3: MOST Systems Requirements

- Power requirement {Maximum power of 40W}
- Communication requirements {LEO Science Data Transfer}
- Propulsion requirements {none}
- Structure {Less than 20% of total MOST mass, Maximum mass of about 50kg.}
- Thermal {Low cost passive control whenever possible, seek ideal temperature profile for critical parts such as batteries, telescope, OBC, etc.}
- Attitude Control {Pointing Accuracy of 25 arc-sec (3σ)}

Step 4: MOST Structure Sub-System Requirements and Design Constraints

- Mass Budget Allocation {See Appendices H.1, H.2, and H.3}
- Launch vehicle {Delta II}:
  - Primary or secondary payload {Secondary payload}
  - Available volume envelope {See Figure 1.4}
  - Allowable mass vs. centre of mass {CM within 2.5mm of PAA ring centreline, See appendix F.4}
  - Constrained Vibration {1st natural frequency above 50Hz}
  - Sustain Launch Loads {$10g$ combined loads (3 axes simultaneously)}
  - Potential corrosion at the launch site {Material selection only from MIL-HDBK-5G and found in list 1 of MSFC-SPEC-522B, See Appendix E}
  - Safety {No test requirement: Safety factor of 1.65 on yield strength, and a safety factor of 2.00 on ultimate strength and other flight conditions}
- Other Design Requirements:
  - Low-cost AMSAT approach (Including use of COTS parts)
  - Transportation and manipulation between the assembly and launch sites {negligible}
  - Ease of manufacturing
  - Modular {Use of the proven spaceflight tray stack primary structure heritage from AMSAT and the Surrey Space Centre}
  - Ease of integration for assembly and disassembly for testing purposes
  - Thermal properties {Meet ideal temperature requirements for each tray}
  - Electrical conductivity {Ground for electrical components}

1.6.1 MOST Structural Requirements – A Summary

The steps described above clearly outline the structural design requirements. As observed, most of these structural requirements and constraints are a function of the launch vehicle. These requirements and constraints can be summarised as follows:

- The total mass of the structure subsystem shall not exceed 20% of the total mass of the spacecraft.
- Requirements imposed on a secondary payload onboard a Delta II launch vehicle:
  - Allowable mass vs. centre of mass {CM shall lie within 2.5mm of PAA ring centreline, See appendix F.4}
  - Constrained Vibration {1st natural frequency shall be above 50Hz}
  - Sustain Launch Loads {The structure shall be designed to sustain $10g$ combined loads (3 axes simultaneously)}
  - Safety {No test requirement: Safety factor of 1.65 on yield strength, and a safety factor of 2.00 on ultimate strength and other flight conditions}

- Other Structural Requirements:
  - The structure shall be designed to sustain all transportation loads and shall provide support points for easy manipulation of the spacecraft
- Constraints imposed on a secondary payload onboard a Delta II launch vehicle:
  - Available volume envelope {See Figure 1.4}
  - Potential corrosion at the launch site {Material selection only from MIL-HDBK-5G and found in list 1 of MSFC-SPEC-522B, See Appendix E}
  - The structure should be modular and easy to manufacture
  - The structure should facilitate integration of all parts
  - The structure should be electrically conductive

1.7 MOST Worst Case Loading Environment - Structural Analysis Requirements

The previous section leads to the layout of the structural analysis requirements, as imposed by the Delta II Secondary Payload Planner's Guide[59] [60]. The tray stack primary structure inherently satisfies some of the requirements: ease of manufacturing, ease of assembly and integration, and modularity. Good electrical conductivity mainly depends on the material, and hence, it is not the benefit of the tray stack design, as is commonly believed. The tray stack design's electrical conductivity is generally quite unpredictable. The choice of Aluminum, in the case of MOST, helps with conductivity within the tray however.

The objective of the analyses is to show that the structure is able to sustain loads expected during all mission phases with sufficient margin of safety. To be able to achieve that objective and to prove the MOST structural design reliable, the analysis requirements must be well defined.

The first key requirement that must be verified is the allowable mass as a function of the centre of mass location from the PAA ring centreline. For a 50kg spacecraft, the maximum allowable centre of mass offset in the x-direction (refer to Figure 1.2 and Figure 1.3) is 165 millimetres. This figure assumes that the centre of mass lies exactly on the PAA centreline.

Moreover, at separation from the launch vehicle, angular rates are induced as a function of the centre of mass offset from the PAA centreline in the y-z plane. The static imbalance for MOST shall be minimised to reduce tumbling at separation to a minimum. The tip-off requirement set for MOST shall be enforced by featuring a centre

of mass within 2.5 mm of the PAA centreline in the y-z plane. Typical mean tip-off rates increase by about 2°/sec per 2.5mm CM offset [59].

The analysis can be conducted only once the CM offset issues are resolved. The most severe loads are well known to occur during launch. Hence, the launch vehicle determines all the structural analysis conducted herein. The main loads sustained by the spacecraft during launch include linear acceleration loads, acoustic loads, shock, and vibrations. Some lateral acceleration loads are also transmitted during launch due to vehicle manoeuvres and wind gusts.

As outlined previously, MOST will be launched as a secondary payload on the Boeing Delta II vehicle. Appendix G presents important tables and figures taken from the Secondary Payload Planner's Guide[59].

The first analysis to be conducted is to account for the maximum acceleration of the launch vehicle. The engine thrust imparts a linear acceleration for each stage as fuel is burned. The ascending acceleration is usually at its peak at the end of the first-stage burn. The maximum acceleration load for the Delta II vehicle is around $6.3g$. However, a $10g$ load is to be used for analysis. This load features a built-in safety factor set by the Boeing Company to account for the worst possible case. The $10g$ load must also act at the centre of mass in three axes simultaneously. Additionally, a safety factor of 2.00 on the ultimate strength and 1.65 on the yield strength of all materials must be specified for structures verified by analysis only, which is the case for MOST.

The engine noise reflected off the ground also generates loads. These acoustic loads are the main source of random vibration at lift-off. The noise during the transonic flight also induces random vibrations. Appendix F.8 presents a graph of the design-level acoustic environments for different launch vehicles.

The main vibrations originate from the propulsion engine and are transmitted structurally to the spacecraft through the PAA. Aerodynamic buffeting will also induce vibrations but are often neglected in spacecraft design as their influence is negligible when compared to all other launch loads. The second analysis to be conducted is a vibration analysis for the constrained case of MOST rigidly attached to the launch vehicle through the PAA. Transmitted vibration through the payload attachment fitting (PAF)

can be sinusoidal or random. Acoustic vibrations are also transmitted to the spacecraft through air within the fairing. The constrained spacecraft must not have natural frequencies within frequency ranges specified by the launch vehicle. For spacecraft with a first natural frequency of 50Hz or greater, a coupled loads analysis is not required[59]. Secondary payloads must also avoid the 32-36Hz natural frequency range in the case of a secondary payload launch on the Delta II vehicle. Hence, the worst case first natural frequency of MOST must lie above 50Hz. That limiting case is based on the fact that no coupled loads analysis shall be necessary in order to comply with the low-cost philosophy while still getting the MOST spacecraft approved for launch by the Boeing authorities.

Obviously, the safer analysis approach used herein means that MOST's mass will not be optimum since the design is based on larger safety factors. Safety factors can only be reduced if real hardware testing is executed. This highlights the main tradeoffs between the cost of testing and minimising structural mass, and the cost savings of not testing but accepting non-optimal structural mass. The safety factors used for the analyses conducted also satisfies the NASA standard requirements[65].

Finally, shock loads will be induced in many ways during launch. These shock events include main engine ignition, staging, fairing jettison, and payload separation. The maximum flight level shock response spectrum for the Delta II vehicle is shown in Appendix F.7. Shock load analysis inherently involves a complex non-linear dynamic behaviour assessment. This is beyond the scope of this work. However, a static load equivalent to the maximum dynamic shock load expected was applied through the PAA centreline and showed large safety margins.

1.8 MOST Finite Element Design Methodology

The methodology of this work is based on an iterative design process. Figure 1.1 shows a generic small satellite iterative design loop that was applied to the MOST mission. Three levels of analyses were conducted. First, component level analyses were performed mainly to assess for the response to vibration excitation of critical parts such as printed-circuit boards (PCB). Second, analyses at the sub-assembly level were

completed to assess for the effect of connecting PCB and other lumped masses to the tray structure. Finally, the main analyses outlined in Section 1.6 were conducted at the spacecraft assembly level to assess the overall behaviours of the MOST structure. These analyses are presented in Chapter 2 and Chapter 3. In addition, Chapter 4 presents hand calculations and theoretical work that were completed to size the MOST tie rods, again by using static loads equivalent to the dynamic launch loads. Finally, the effect of temperature gradients on stresses and deflections was investigated. Design recommendations are outlined in Chapter 2, Chapter 3, and Chapter 4 where appropriate.

To begin our journey, a preliminary finite element model was constructed from the preliminary design drawings. Then, design recommendations were suggested based on the analysis results and the design was modified accordingly. This design iterative process can go on forever. However, two milestones were set to evaluate and judge if a suitable design satisfying all requirements and constraints was reached: the preliminary and critical design reviews.

The preliminary analyses, as described in detail in Chapter 3, showed satisfactory performance results. From the preliminary design, a detailed design model based on the most recent detailed design drawings was constructed and analysed again by finite element methods. Again, the same iterative process took place, producing a better structure at each step. The more detailed structural analysis results are presented in Chapter 4 and Chapter 5, and showed satisfactory structural performance too. Design recommendations are made therein to reduce the mass of the bus structure accordingly. The quality assurance and reliability issues arising from the extensive use of finite element methods were assessed and will be further described in Chapter 3 and Chapter 4.

1.9 Existing Bus Structure Concepts and Their Application to the MOST Mission

Many organisations, including AMSAT and Surrey Satellite Technology Limited (SSTL) (See Chapter 1), have successfully designed and manufactured small satellite bus structures prior to the MOST effort. The following subsections evaluate each type of satellite structural concept. This summary is intended to aid the design of future microsatellite missions after MOST.

1.9.1 Tray Design

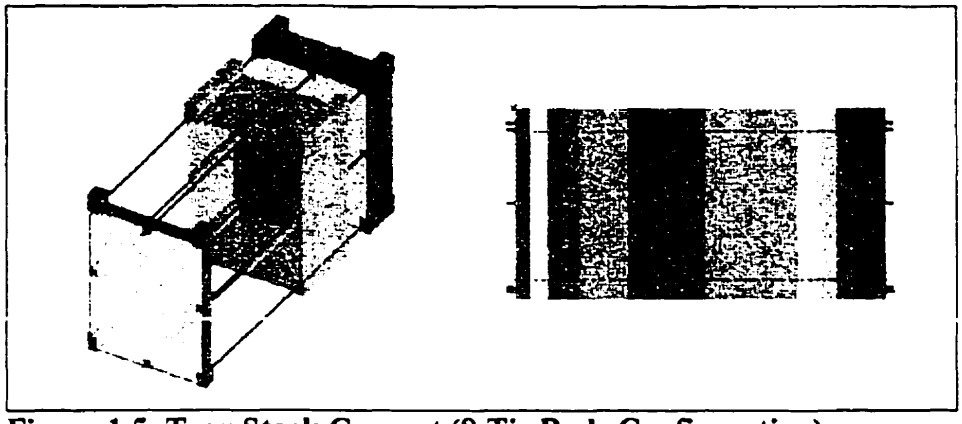

Figure 1.5: Tray Stack Concept (8-Tie Rods Configuration)

The modular tray stack concept has been used extensively in the past. It was mostly developed by the University of Surrey under the influence of AMSAT designs. This structural concept features many advantages: ease of manufacturing, modularity, and ease of integration for assembly and disassembly. The spaceflight heritage of the AMSAT and SSTL and subsequently other commercial organisations is also an important point in favour of the tray stack design. The stiffness of the tray stack is remarkably high when the Payload Adapter Assembly (PAA) is fixed at its bottom (at one end of the stack), thereby transforming the structure into a strong cantilever beam. However, there is a price to be paid in terms of mass. The minimum thickness of the tray walls is of the order of 1.5mm to avoid manufacturing problems. However, the overall benefits of such a modular primary structure in many cases supersede all other penalties for a microsat design.

1.9.2 Trusses, Skin-Frames or Chassis Design

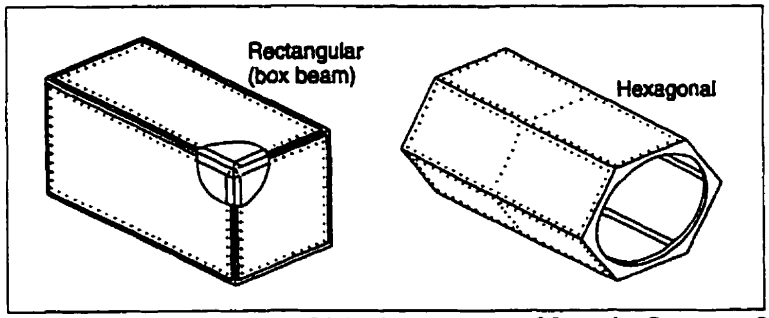

Figure 1.6: Trusses, Skin-Frames or Chassis Concept[58]

Trusses in large space structures have been used extensively in the past. Large spacecraft sustain much larger loads and the use of a tray stack would increase the mass significantly. The modularity and ease of assembly advantages of a tray stack for small spacecraft become irrelevant when the overall mass of a large spacecraft comes into play. Hence, the tradeoff between total mass, overall stiffness, modularity, and ease of assembly appears to be quite different for different spacecraft sizes. Indeed, these differences are mainly a function of the geometry (size) and materials used.

On the other hand, if the only design constraint was mass, i.e. the modularity and ease of integration did not matter; small spacecraft would definitely benefit from the trusses and skin-frames concepts. The chassis design can be made much lighter than the tray stack by simple geometrical arrangements and triangulation. However, the modularity, ease of assembly, and component number of such a structure become larger issues for small spacecraft. Furthermore, the large number of electronic and electrical connections in a small spacecraft assembly could easily lead to failures, especially since electronic component testing might require cable disconnection and reconnection or even printed-circuit board (PCB) replacement. One key factor to understand is that truss structures can be made somewhat modular in the case of large spacecraft since the larger truss and skin components can be assembled in a modular way. Similar modularity is quite difficult to attain for the case of small truss structures, as the components cannot be broken down easily. Moreover, the number of small components generated and the associated high design tolerances become main issues. These reasons coupled with cost restrictions and short design schedules usually rule out the truss concept for most small spacecraft missions.

1.9.3 Monocoque Cylinder Design

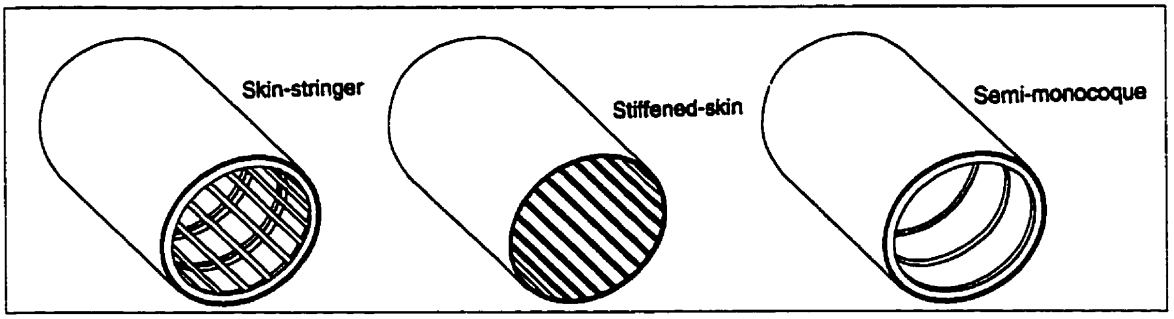

Figure 1.7: Monocoque Cylinder Concept[58]

The monocoque or semi-monocoque cylinder features extremely high stiffness to weight ratio. However, integration, assembly, and electrical conductivity become serious issues. This structure concept is therefore sometimes suitable for large spacecraft but definitely not an option for small spacecraft and microsats.

1.10 Exploring Different Geometrical Forms

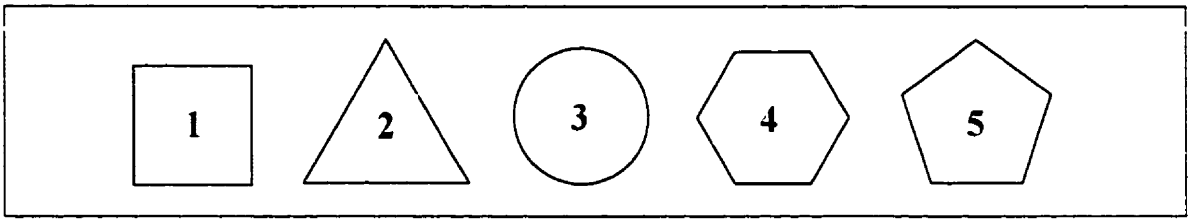

Figure 1.8: Basic Geometrical Forms

As highlighted in section 1.8, the tray stack concept is most suitable for small satellite applications. However, the basic geometry of the tray stack cross-section can be built from many different forms. Figure 1.8 presents five primary geometrical forms that can potentially be used as structural building blocks. The square, or one of its derivatives, the rectangle, was extensively used in the past because of easy PCB integration. However, easy integration of slightly smaller PCBs can be mounted in all other cross-sectional geometries presented in Figure 1.8, except for the triangular shape.

The geometry influences bending stiffness, torsional stiffness, and the first natural frequency of vibration. The effects were investigated for the case of cantilevered beams with equal masses but different cross-sectional forms, as it is an excellent and quick way of obtaining useful first approximations. The following properties were used:

- Cross-sectional area (Taken from a typical MOST tray stack): 2150 mm^2
- Wall thickness: 1.5mm
- Beam length: 600mm
- Al-6061-T6 Material Properties:

E	σ_Y	τ_U	ν	ρ
69.0 GPa	275 MPa	26.2 MPa	0.33	2715 kg/m^3

- Total mass of 5.13kg

The influence of bending stiffness can be investigated analytically. The maximum shear stress obviously occurs at the neutral axis and tends to zero at the top and

bottom along the line of symmetry of the thin-walled cross-section (for the case of a vertical load F acting along the line of symmetry, See Figure 1.9).

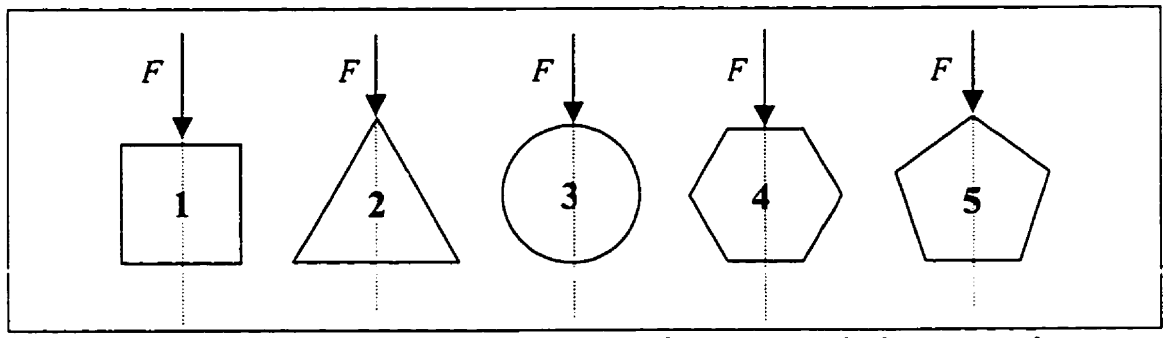

Figure 1.9: Neutral axes and line of symmetry of the geometrical cross-sections

The bending stiffness of a beam is known to be inversely proportional to the second moment of area opposing the bending moment. Equation 1.1 expresses the vertical displacement δ along the length L under the action of a bending moment M.

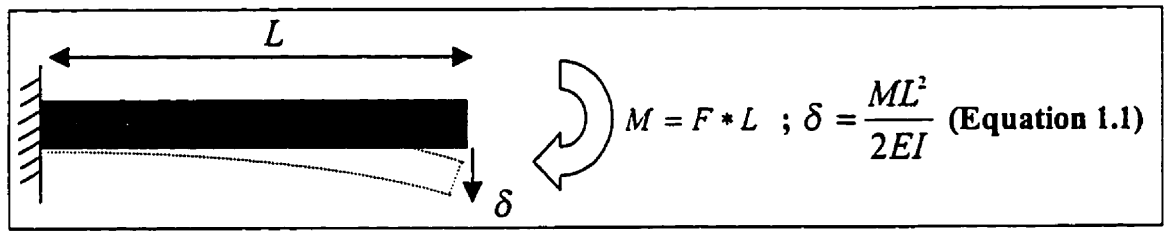

$$M = F * L \;;\; \delta = \frac{ML^2}{2EI} \quad \textbf{(Equation 1.1)}$$

Figure 1.10: Cantilevered beam analysis

Preliminary investigation using the primitive geometrical forms shown in Figure 1.9 proved the circular shape to feature the highest bending stiffness. Table 1.1 presents results comparing the bending stiffness using the strong side of a rectangular cross-section as the basis. All cantilevered beams of length L featured the same mass and same wall thickness of 1.5mm. The ratio of sides for the rectangle was of 1.5 (typical tray side ratio). The hexagonal and circular forms feature the best bending stiffness.

Form	Bending Stiffness Ratio
Rectangle (weak)	0.348
Triangle	0.599
Square	0.674
Pentagon	0.721
Hexagon	0.749
Circle	0.819
Rectangle (strong)	1.000

Table 1.1: Comparative bending stiffness for the geometrical forms investigated

A similar investigation using the same primitive geometrical forms shown in Figure 1.8 and Figure 1.9 proved the circular and hexagonal cross-sections to feature the highest torsional stiffness too. Table 1.2 presents results comparing the torsional stiffness constant computed in by the I-DEAS™, and using the circular cross-section as the basis.

Form	Torsional Stiffness Ratio
Triangle	0.366
Rectangle	0.486
Square	0.617
Pentagon	0.751
Hexagon	0.826
Circle	1.000

Table 1.2: Comparative torsional stiffness for the geometrical forms investigated

Finally, investigation using the same primitive geometrical forms shown in Figure 1.8 and Figure 1.9 proved the circular and hexagonal cross-sections to feature the highest first natural frequency of vibration. Table 1.3 presents results comparing the first natural frequency of vibration using the circular cross-section as the basis.

Form	First Natural Frequency Ratio
Rectangle (weak)	0.674
Square	0.910
Triangle	0.937
Pentagon	0.974
Hexagon	0.975
Circle	1.000

Table 1.3: Comparative 1st natural frequency for the geometrical forms investigated

These crude beam approximations of a tray stack bending stiffness, torsional stiffness, and natural frequency response serve a useful purpose. The results obtained shall guide designers at the conceptual design phase in terms of basic structural geometrical forms to be used. Although they feature the best structural properties, circular shapes are usually not suitable, especially in the case of small satellite packaging requiring integration of typical PCB square-like cross-sections. However, the hexagonal form combines both excellent packaging capability and excellent structural properties.

Hence, the hexagonal form is strongly recommended to serve as a basis for the next generation of tray stack cross-sections.

Chapter 2

MOST Preliminary Design: Structural Analysis

This chapter presents MOST's preliminary design structural analysis results and the subsequent design recommendations. The analyses performed were based on the Phase A Report [61] and were conducted from January through June 1999. The main results are based on PCB analysis, a vibration sensitivity analysis to seek optimum size of shell elements to be used in later detailed analyses, a shell thickness vibration analysis, a plate-stiffener analysis, a laminate definition reliability check, and the determination of the PAA location from a rough spacecraft level analysis.

2.1 MOST Phase A [61] Structural Design Report and Assumptions

The preliminary design structural analysis included herein is based on the MOST Phase A Report. The following information was used from the Phase A Report:

- Secondary payload on a Delta II Launch Vehicle
- 1-year science mission
- AMSAT design approach
- Stack of 10 trays
- Dimensions = 254mm x 586mm x 628mm
- No Detailed Drawings Available (At preliminary stage only)
- Mass = 48.8kg

Sub-system	Mass (kg)
Structure	13.9
Power	6.8
Telemetry & Telecommand	2.3
ACS	7.8
OBC	2.5
Thermal Control	0.6
Instrument (Total)	7.4
Distributed Mass Margin	7.5
Phase A Expected Satellite Mass	48.8

Table 2.1 Mass Allocation from the Phase A Report [61]

2.2 MOST Structural Design Objectives

The main structural requirements were presented in Chapter 1. For satellites, a well built structure usually consists of components that make up less than 20% of the total spacecraft mass. Hence the main structural design objectives can be simply stated as follows:

(1) Satisfy all structural requirements imposed by the launch vehicle and other environments taking into consideration the safety factors and margins of safety (See Section 1.6.1 for details)
(2) Ensure that the total mass of the structure sub-system components be less than 20% of the total spacecraft mass

2.3 MOST Preliminary Design Analyses

Analyses were performed to answer the following questions:

1) Is the PAA and the CG alignment within the launch vehicle allowable range?
   - Analysis: CG of preliminary 2-D Shell elements model
2) How shall PCBs be attached to tray bottoms to comply with launch vibration requirements?
   - Analysis: PCB Constrained Vibration (2-D FE Model)
   - Analysis: Tray & PCB Sub-Assembly Constrained Vibration (2-D FE Model)
3) What is the optimum tray bottom thickness?
   - Analysis: Tray Constrained Vibration (2-D FE Model)
   - Analysis: Plate Constrained Vibration (2-D FE Model & Analytical Solution)
4) How does mass distribution affect natural frequency response?
   - Analysis: Lumped mass distribution (1-D FE Model & Analytical Solution)
5) Is there a need for stiffeners on the bottom of the trays?
   - Analysis: Tray Constrained Vibration (2-D FE Model)
   - Analysis: Plate Constrained Vibration (2-D FE Model & Analytical Solution)
6) What are the recommended solar panel thickness and laminate specifications?
   - Analysis: Panel Cantilever Analysis (2-D FE Model)
   - Analysis: Panel Constrained Vibration (2-D FE Model)
   - Analysis: Panel Axial Acceleration Load (2-D FE Model)

7) Is there a need for a honeycomb panel telescope enclosure?
   - Analysis: Discussion with experienced engineers
8) Will the spacecraft satisfy all structural requirements?
   - Analysis: Spacecraft Constrained Vibration (1-D FE Model Modal Analysis)
   - Analysis: Spacecraft Constrained Vibration (2-D FE Model Modal Analysis)
   - Analysis: Spacecraft Acceleration Launch Loads (2-D FE Model)

2.4 Finite Element Model Approximation Solutions and Pitfalls

When analysing displacements and stresses of a domain in real life engineering applications, engineers are often confronted with differential or integral equations that cannot be solved in closed form using classical approaches. They are forced to use numerical methods to obtain approximate solutions. These **approximate** numerical methods always involve discretization of the system at hand into smaller elements. Hence, it is important to highlight the source of errors and pitfalls inherent to finite element modelling methods. One important fact highlighted in the introduction of this work is that these methods will only approximate solutions of partial-differential equations. The errors are therefore errors with respect to the PDE's exact solution and not errors with respect to the real problem at hand. Of course, this work assumes that the PDE solutions are fairly good approximations of the real spacecraft's behaviours. This intrinsic assumption is left for philosophical discussions that are beyond the scope of this work. However, they mark an important touchstone for the work which can and should be done in future studies. Of course, practising engineers are mostly interested in good enough answers that are conservative representations of the real phenomenon. However, one could argue that the aerospace industry would benefit immensely from research allowing safety factors to be reduced and leading to major mass savings. It is commonly acknowledged that mass is one of the primary factor used to perform a mission cost analysis.

FEM Source of Errors:

a) Discretization error: errors due to approximation of the domain.

Discretization error may be reduced by grid refinement. This can be achieved by using more elements of the same type but of smaller size or by using elements of a different type. The tradeoff here is between the number of elements, the type of elements (rectangular, triangular, etc.), and the formulation used to capture the stress gradient across each element. The structural engineers must ensure that the combination of the number, type, and formulation of element will provide accurate results.

b) Formulation error: errors due to approximation of the element behaviour.

If we model a prismatic bar under constant tensile load, the actual displacement varies linearly over the discretized domain. Hence, such elements of the discretized domain would contain no formulation error if we assumed a linear displacement formulation for those elements. However, if the same bar was cantilevered, then the actual displacements would vary quadratically and formulation error would exist for the same linear displacement formulation assumption.

c) Boundary Conditions error: errors due to modelling of boundaries.

These errors can usually be kept to a minimum by simply adding more nodes and elements at the physical boundary. The constraint equations are obviously very important and will influence the results. In that respect, the results feature high sensitivity to the applied constraints and shall therefore be given much attention.

d) Numerical error: errors due to use of finite precision arithmetic.

These errors are simply the consequence of truncation during floating-point computations and errors associated with numerical integration procedures. These are usually very small errors when compared with formulation errors in a well-designed finite element program. These numerical errors are assumed to be negligible when using MSC/NASTRAN and I-DEAS structural analysis packages. MSC/NASTRAN numerical methods have been well documented by Caffrey[66].

FEM General Steps:

All finite element methods feature the same general steps. The main differences between commercial packages such as ANSYS, I-DEAS, MSC/NASTRAN, ALGOR,

etc., are the visual interface, and the reliability and robustness of their solver. The following are the general steps taken to analyse a real system:

i) Define Geometry

ii) Define Material Properties

iii) Meshing:

- Discretization of the domain
- Element type (Formulation of the domain)

iv) Apply Boundary Conditions

- Apply Displacement Constraints
- Apply Loads (External Force, Bending Moment and Torque)
- Define time varying domain

v) Solve the discretized domain: Run program (Numerical error)

vi) Post-processing and Analysis of generated results (Requires interpretation by the structural engineer)

FEM Requirements for Accuracy: (Strongly depends on two conditions)

1- The equations of equilibrium must be satisfied throughout the model

2- Compatibility or continuity of displacements must be maintained throughout the model.

The work included herein is based on commercial package results and assumes that those two fundamental conditions are met.

FEM Requirements for Convergence:

1- The elements must be complete

The shape function must be a complete polynomial. Must not omit linear or constant terms, say in a quadratic polynomial.

2- The elements must be compatible

Continuity of displacements must be assured throughout the discretized model.

3- The elements must be capable of representing rigid-body motion and constant strain

For 2D and 3D elasticity problems, at least a complete linear polynomial must be used to describe the displacement field to insure rigid-body motion and constant strain representation. For shell elements, constant strain implies constant curvature and

constant twist. Moreover, some shell elements cannot represent rigid-body motion. One should be careful in choosing the appropriate element type.

FE Modeling Recommendations:

From the experience gained through previous structural analysis work, and from general recommendations by Bathe[67], Brenner[68], and Burnett[69], the following list of FE modelling recommendations are followed throughout this work:

1- Avoid abrupt transitions in element size and geometry

Limit the change in element stiffness (approximated by $\frac{E}{V_e}$, where V_e is the volume of the element) from one element to the next to roughly a factor of 3.

2- Avoid unnecessary element irregularity

- Keep aspect ratio less than 10:1
- Interior angles of quadrilaterals should not exceed 150° and should not be less than 30°
- Mid-side nodes on quadratic elements should be within the middle third of the edge

3- Maintain compatibility between elements

Make sure the edge of all connected elements feature same formulation so that no loss of compatibility is incurred under distortion

4- Use fine mesh only in regions of expected high stress gradient or stress concentration

5- Exploit symmetry in the geometry and loads of the physical system to build the smallest reasonable model

2.5 I-DEAS™ Finite Element Model Software Package

A complete license of the I-DEAS™ Version 6A software is used by UTIAS/SFL. Hence, the I-DEAS™ finite element solver was extensively used throughout this work for vibration and structural load analysis. Relying solely on finite element analysis is considered quite risky. However, following good finite element procedures as outlined in Section 2.4, performing FE model sensitivity analysis and convergence check, and obtaining rough hand calculation shall provide accurate results. The matrix formations and equations solver used within the I-DEAS™ software is assumed to be reliable. The MSC/NASTRAN software was also used as secondary check

as it is a time-proven software that is being used by many aerospace companies and other industries as well. Of course, running the exact same model does not guarantee that the model is a good representation of the real system's behaviours. The sensitivity analyses and convergence checks combined with some hand calculation give a better indication of the accuracy of the model.

However, for complex spacecraft structures such as MOST, or for any complex structures, it is impossible to actually come up with an alternative solution to verify the results. Any other reasonably accurate solution would lead back to the use of finite element methods. There is just no way around that problem. As a result, extensive sensitivity analyses and convergence checks are performed. The I-DEAS results presented herein have all been through these five checkpoints:

(1) Hand calculation approximation (whenever possible)

(2) Finite Element Modelling Recommendations and Procedures (see Section 2.4)

(3) Sensitivity analysis (materials properties or shell thickness varied)

(4) Convergence check (element size, type, or formulation varied)

(5) MSC/NASTRAN results comparison (whenever appropriate)

2.6 Preliminary 1-D Beam Model Analysis

The first analysis to be performed is usually a back of the envelope calculation used to get a feeling of what is expected. A 1-D beam analysis that features a continuous tray stack cross-section clamped at the PAA location and featuring the total mass of the spacecraft, with rigid links between the tray stack and the instrument's lumped masses, is expected to give a good idea of the range of the constrained frequencies of vibration of the bus structure. Obviously, this preliminary analysis cannot be used to orient the design and certainly not give accurate component level indications. However, the first natural frequency of vibration of the 1-D beam and lumped masses assembly of 343Hz obtained clearly indicates that the spacecraft bus assembly is rigid enough to avoid the principal launch load vibration regime. This quick analysis does not provide any sub-assembly or components level information where the problems are expected to occur. There is also a huge difference between a continuous beam and a tray stack held together by tie rods. This analysis does not capture any design details and therefore a 2-D shell element

analysis was conducted to obtain accurate component level, sub-assembly level, and spacecraft level results (see Section 2.7)

2.6.1 Analytical Solution of MOST Structure (1-D Bernoulli-Euler Beam Solution)

The bus structure can be roughly modelled as a cantilevered beam of half the total tray stack length. The fixed boundary condition simulates the PAA plate. Of course, this 1-D Bernoulli-Euler beam analysis is to be taken as an indication of the natural frequencies that is expected. The theoretical value of 354Hz was found as an approximate Euler beam solution using Blevins formula [70] for cantilevered beams. The moment of inertia was computed for a 300mm by 254mm thin-walled box of 1.5mm thickness. The length of the beam was taken as 314mm which is half the tray stack length. The total tray stack mass was 24.4kg, which is half the spacecraft expected mass. This gives a good indication that the bus as a whole can sustain the vibration loads. Obviously, the 2mm thick bottom of the tray plates will have excitation modes far below the 354Hz computed for the Euler beam. These component level problems need to be looked at through a more rigorous 2-D shell model analysis and verified by analytical solutions from Blevins [70].

2.6.2 1-D FE Analysis of MOST (I-DEAS^{TM} Timoshenko's Solution)

A FE model equivalent to the 1-D beam analysis was constructed in I-DEAS^{TM}. However, a slightly different result was obtained. The FE first natural frequency response for the equivalent beam was found at 343.5Hz. The difference between the analytical result presented in Section 2.6.1 and the FE result was expected since the I-DEAS^{TM} solver is based on Timoshenko's beam solution, which takes into consideration warp effects for thin-walled beam structures which, in turn, lead to a lower frequency as shown. In any case, even the more conservative Timoshenko's solution is way above the 50Hz limit set forward by the Delta II launch vehicle. Hence, the bus tray stack frame is believed to act as a rigid structure. The design problems shall be found at the sub-assembly or component levels, which requires a more accurate 2-D FEA.

2.7 Preliminary 2-D Finite Element Model Analysis

As one can expect, 1-D structural beam and lumped mass analysis is quite useful to obtain rough estimates but cannot provide enough insight for design recommendations. Hence, 2-D shell element models need to be constructed in order to obtain satisfactory results. All preliminary 2-D FE models constructed between January and June 1999 were based on the Phase A Report[61]. Many analyses were conducted and only those that are of value, in terms of guiding the final detailed design recommendations, are presented in this chapter. The updated detailed 2-D models constructed after the preliminary design review (PDR) are presented in Chapter 3.

2.7.1 Rectangular Plate: Analytical Results (Blevins [70]) vs. I-DEAS FEM Results

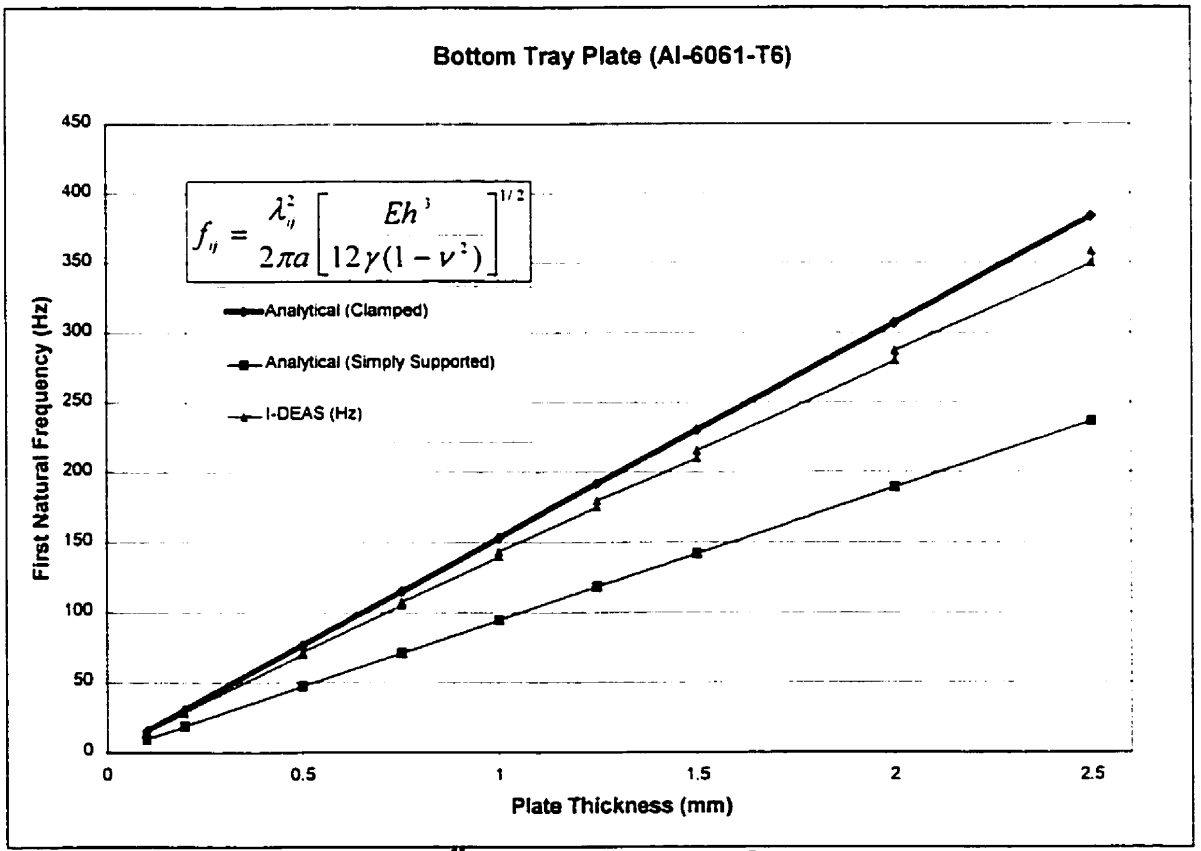

Figure 2.1 Bottom Tray Plate 1st Natural Frequency Response

The first design parameters that can be varied within the tray stack primary structure are the thicknesses of the tray walls and tray bottom. Many scholars have looked at the vibration problem of membranes and thin plates [71] [72] [73] [74]. Hence,

analytical solutions are readily available for different boundary conditions. An analytical solution was found in Blevins [70] for the case of a thin plate constrained along all 4 side edges:

$h \equiv$ Plate thickness
$a \equiv$ Plate length
$\gamma = \rho * h \equiv$ Mass per unit area
$\nu \equiv$ Poisson's ratio
$E \equiv$ Modulus of elasticity

$$f_{ij} = \frac{\lambda_{ij}^2}{2\pi a}\left[\frac{Eh^3}{12\gamma(1-\nu^2)}\right]^{1/2}$$

$\lambda_{ij} \equiv$ Dimensionless frequency parameter (a function of the edge boundary conditions)
$f_{ij} \equiv$ Frequency (Hz)

Figure 2.1 is a plot of the first natural frequency results obtained for two different boundary conditions (clamped edges with $\lambda_{11}^2 \equiv 25$ and simply supported edges with $\lambda_{11}^2 \equiv 15.42$) and for the FE bottom tray shell element results. The FE frequencies are expected to lie between the two analytical solutions as the real constraint for the bottom plate of the tray is not exactly clamped, although very close, as one side rests on the side walls of the adjacent tray. The FE results tend toward the clamped boundary analytical results, which confirms that the edges are definitely not simply supported. The results obtained from the I-DEAS tray bottom model featuring a frequency distribution between the two analytical sets of results and closer to the clamped results are therefore satisfactory. The number of elements was varied from 24 to 2400 (See I-DEAS curve in Figure 2.1). The points on the curve for the different number of elements show convergence for all plate thicknesses investigated. These analytical and FE results effectively show that we do not need stiffeners, as a 1.5mm thick plate would have a first natural frequency lying between 150Hz (edges simply supported) and 225Hz (edges clamped). This excitation frequency range is far above the 50Hz set forward by the Delta II Secondary Payload. Hence, mass can be saved by not adding stiffeners to the end of the bottom plate of the trays.

An optimisation routine would be required to find the optimum tray bottom thickness and material. Assuming that aluminum (Al-6061-T6) is the preferred material, the optimum thickness should be around 1mm. However, because the tray will be manufactured out of a single aluminum block, manufacturing vibration problems could occur. For that reason, a bottom thickness of 1.5mm is recommended. This would

ensure no vibration failure at manufacturing (during machining of the aluminum block), and obviously during launch (first natural frequency above 150 Hz).

2.7.2 2-D FE Analysis of PCB (Component Level)

The vibration analysis of the PCB was performed using I-DEAS™ software. The Lanczos method[67] was used to compute the 10 first natural frequencies of the PCB model. The purpose of the Lanczos method is to compute a relatively few number of eigenvalue and eigenvector pairs for a model defined by a large number of degrees of freedom. The Lanczos method was found to be the quickest. It is also a proven method extensively used for determining the first natural frequency for systems with a large number of degrees of freedom.

The boundary conditions were varied in order to explore different attachment alternatives or different attachment concepts. Black dots were added to show the pin locations (see Figure 2.2). Many options were considered. Attaching the PCB to the tray bottom to obtain frequencies above 50Hz was demonstrated to be possible even without using a cross stiffener at the back of the PCB. Using spacers distributed symmetrically to pin down the PCB to the bottom of the tray was found to be the lightest option while still featuring large margins of safety. The pin concept leads to an infinite number of possible strategies. Many pin arrangements and many spacer configurations were tested to obtain the highest frequency with the smallest number of spacers or pins possible. The best option is shown in Figure 2.2(C). The analysis assumes small PCB displacements because the tray stack, made out of aluminum, is expected to take most of the loads. The small deformation assumption holds provided that shell element stresses are largely below the aluminum yield point. As shown later in Chapter 3, the margins of safety obtained validate the assumption made. Within the small deformation theory, it can also be assumed that the PCB material, being an orthotropic material, will behave as a quasi-isotropic material.

PCB material quasi-isotropic properties and thickness used for analysis[76]:

E_{PCB}	ν_{PCB}	t_{PCB}	ρ_{PCB} (Including mass of typical electronic components)
13.79 GPa	0.12	0.83mm	5757.4 kg/m^3

Mass of PCB model = 0.5168 kg

Boundary conditions: The model is pinned at different locations on its contour and around the middle of the plate (See black dots on PCB's of Figure 2.2).

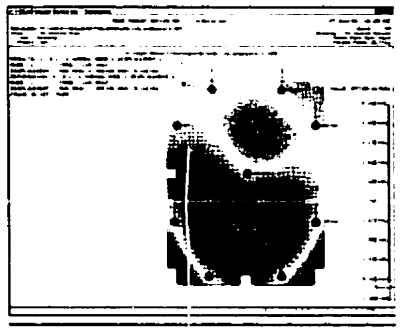

(A) 9 pins → 108.941 Hz

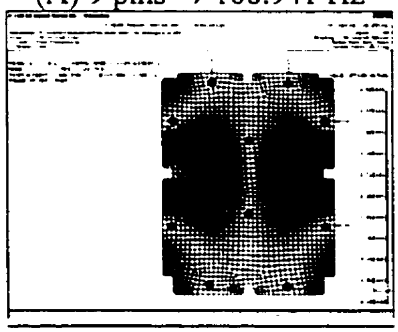

(B) 10 pins → 122.315 Hz

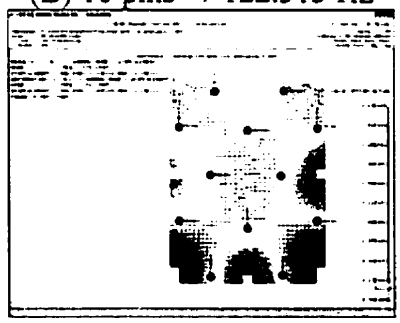

(C) 12 pins → 171.151 Hz

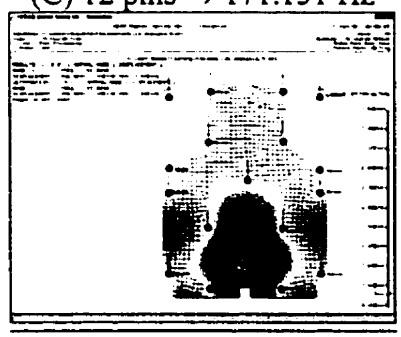

(D) 17 pins → 193.825 Hz

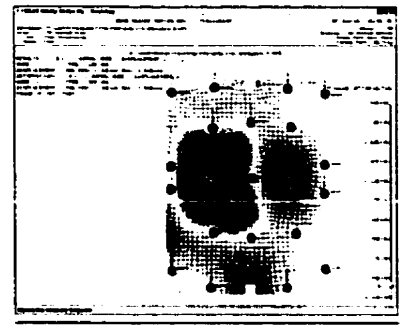

(E) 19 pins → 229.261 Hz

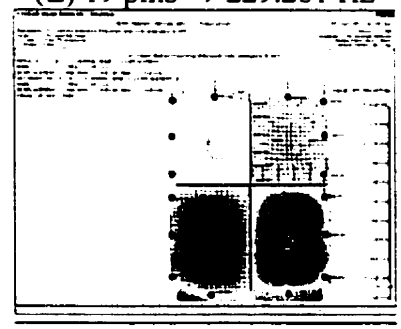

(F) 16 pins, 2 stiffeners → 245.222 Hz

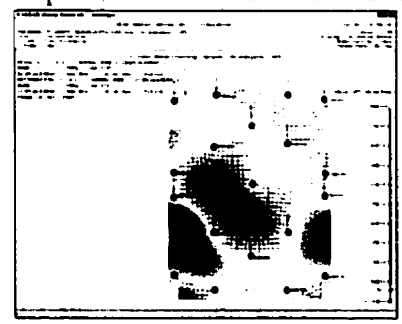

(G) 19 pins → 249.373 Hz

Figure 2.2 PCB Vibration Analysis Results

The best PCB attachment setup is the 12-pin configuration (Figure 2.2C). It features the highest ratio of frequency to number of pins, which is a good indicator of the pin arrangement dynamical effectiveness (See Table 2.2). The first natural frequency of 171.1507Hz is far above the launch critical frequency of 50Hz. Another handy feature of the diamond shape central configuration is that it leaves much space for electronic components. Hence this configuration is recommended to mount the PCB onto the tray bottom.

Figure 2.2	#Pins	Frequency (Hz)	Ratio
A	9	108.94	12.10
B	10	122.32	12.23
C	12	171.15	14.26
D	17	193.82	11.40
E	19	229.26	12.07
F	26	245.22	9.43
G	19	249.37	13.12

Table 2.2 Ratio $\frac{f(Hz)}{\#\,Pins}$ for all PCB Options Presented

2.7.3 2-D FE Analysis of PCB Mounted in a Tray (Sub-Assembly Level)

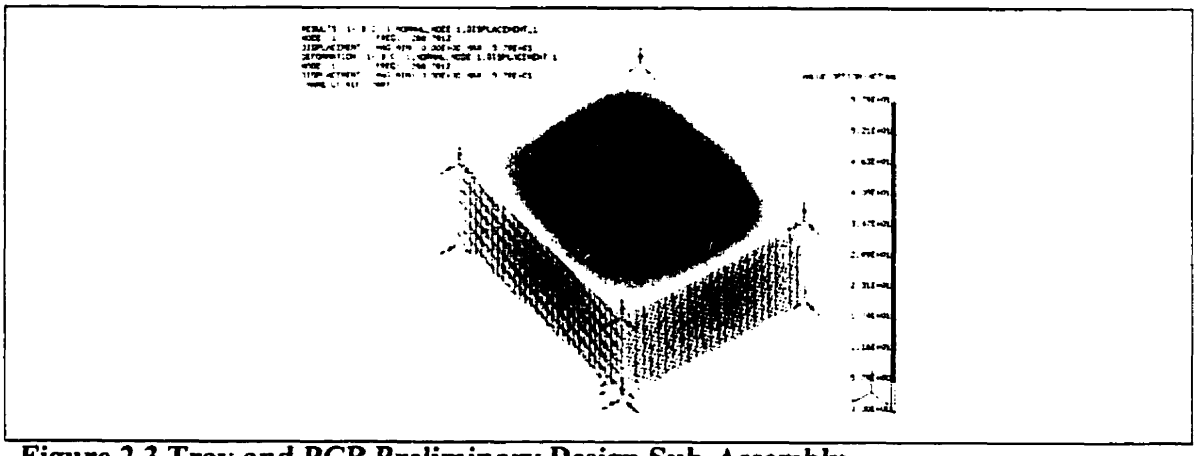

Figure 2.3 Tray and PCB Preliminary Design Sub-Assembly

Preliminary 2-D Shell Elements Tray and PCB Sub-Assembly Model Description:

- Cross-section: 251mm wide x 300mm high with a wall thickness of 1.5mm
- Material: Al-6061-T651A (material properties taken from MIL-HDBK-5[77])
- Boundary condition: Clamped edges and 8 corners to account for presence of tie rods and other trays walls
- Rigid elements used to attach the PCB to the tray bottom (See best configuration in section 2.7.2, 12-pins mounts)
- Total mass: 1.58kg

- Elements: Shell elements of 1.5mm thick (tray walls) and 2.0mm thick (tray bottom)

The tray bottom walls were set to 2.0mm thick in order to increase the safety margins. However, it is understood that the optimum design would feature 1.5mm thick tray bottoms.

A constrained vibration analysis was performed. The first natural frequency of vibration was found to be 288Hz. Again, this preliminary frequency result will only be useful for assessing convergence of the detailed design model presented in Chapter 3. However, one important conclusion can be drawn: no stiffeners were used and the high frequency result obtained indicates that there is no need to add stiffeners to the bottom of the trays.

2.7.4 2-D FE Laminate Solar Panel Analysis

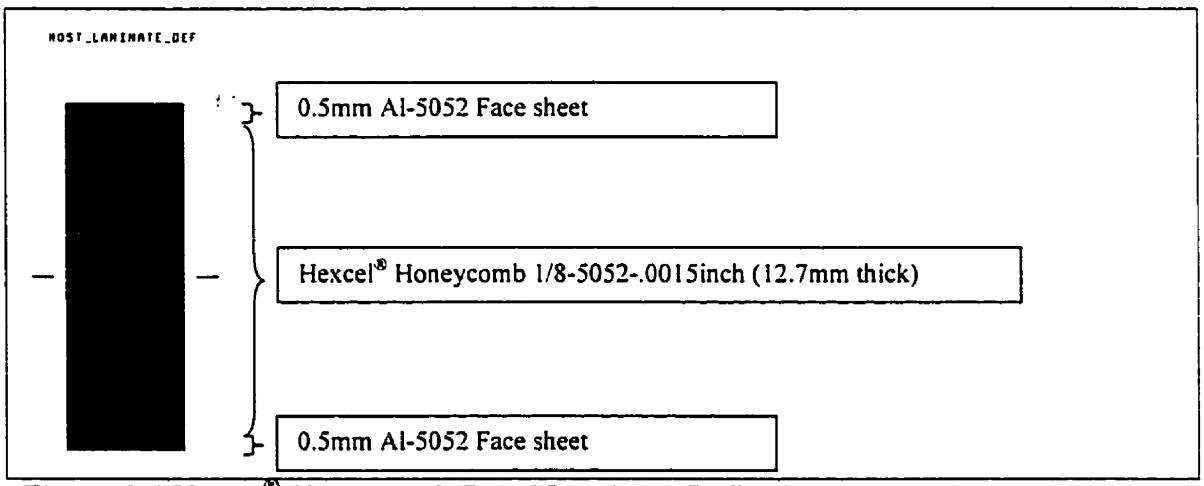

Figure 2.4 Hexcel® Honeycomb Panel Laminate Definition

The I-DEAS laminate definition task was used and tested for the case of a cantilevered plate made out of laminate shell elements. The reliability of the laminate FE shell definition was verified against examples found in the Hexcel® Honeycomb panel selection document [78] and web site[79]. The deflection results for all examples were accurate within a 1.8% maximum error, which is satisfactory for the purposes of this analysis. The modelling of the honeycomb panel was influenced by Hart-Smith's work[80].

2.7.5 Effect of Mass Distribution on the Tray Assembly First Natural Frequency

The Rayleigh method can be used to assess the effect of the mass distribution on the first natural frequency of the tray stack. All that is needed is a reasonable approximation to guide the mass distribution across the tray stack. This is assuming all trays are acting as point masses located at the middle of each tray along the z axis and fixed at the PAA location (See Figure 2.5 and Figure 2.6)

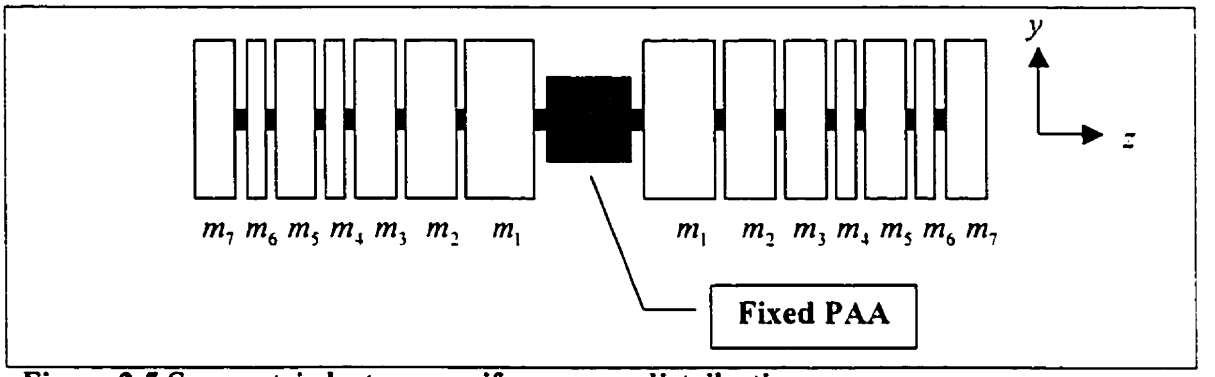

Figure 2.5 Symmetric but non-uniform mass distribution

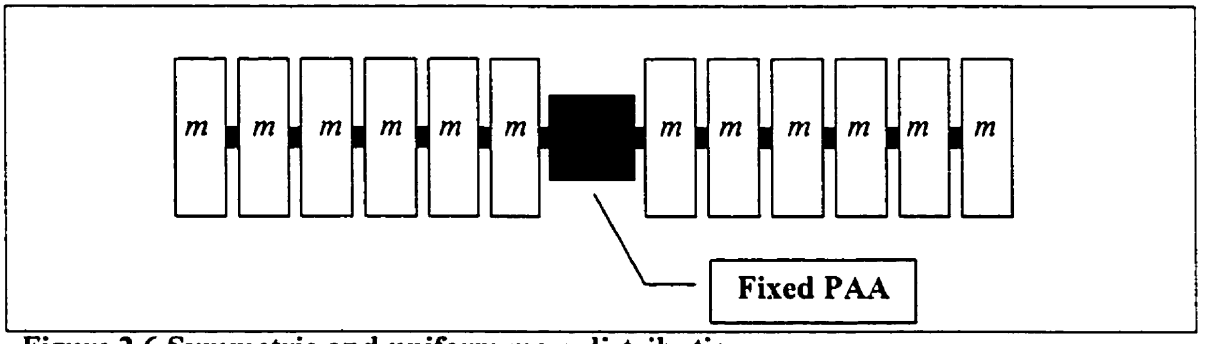

Figure 2.6 Symmetric and uniform mass distribution

A first approximation assuming the static deflection y_i due to a lumped mass m_i on a beam clamped at the PAA centreline, is accurate enough since only a comparative measure is required. The work done by these lumped masses determines the strain energy stored in the beam. The strain energy stored is assumed to be equal to the maximum kinetic energies induced by vibration. Mathematically, the first approximation of the first natural frequency of vibration can be obtained as follows:

$$U_{MAX} = T_{MAX}$$

$$\frac{1}{2} * \left[\frac{F_1^2 * z_1^3}{EI_x} + \frac{F_2^2 * z_2^3}{EI_x} + \cdots \right] = \frac{1}{2}\omega^2 \left[m_1 y_1^2 + m_2 y_2^2 + \cdots \right]$$

$$\omega_1^2 = \frac{\sum_i \frac{F_i^2 * z_i^3}{EI_x}}{\sum_i m_i y_i^2}$$

With the equation of the elastic curve for clamped beam taken as:

$$y_i = \frac{F_i}{6EI}\left[z^3 - 3Lz^2 \right]$$

We get:

$$\omega_1^2 = \frac{\sum_i \frac{F_i^2 * z_i^3}{EI_x}}{\sum_i m_i \frac{F_i^2}{36E^2 I_x^2}\left[z_i^3 - 3Lz_i^2 \right]^2} = \sum_i \frac{36 \cdot E \cdot I_x \cdot z_i^3}{m_i \cdot \left[z_i^3 - 3Lz_i^2 \right]^2}$$

Two different cases were investigated. The first one, as shown on Figure 2.5, is the actual MOST mass distribution. The first natural frequency obtained using Equation 2. was approximately 435Hz. The second case, as shown on Figure 2.6, is a uniform mass distribution. The first natural frequency was approximately 309Hz. As expected, the mass distribution does influence the first natural frequency of vibration. The closer the centre of mass is to the PAA centreline, the higher the first natural frequency will be. Hence, a general design recommendation would be to package the bus components such that the centre of mass in the z-direction shall be as close as possible to the PAA centreline.

2.7.5 2-D FE Analysis of MOST (Spacecraft Level)

Description of the Preliminary 2-D Shell Elements Spacecraft Model:

- Tray Cross-section: 251mm wide x 300mm high with a wall thickness of 1.5mm
- 10 Trays with PCBs mounted to the bottom walls with 12-pins
- Material: Al-6061-T6 (material properties taken from MIL-HDBK-5 [77])
- Boundary condition: Clamped to PAA plate (simulation of the bolt-mounted plate) with centreline at the middle of tray height (for preliminary design analysis only)
- Total mass: 48.8kg
- 5648 Elements and 5127 Nodes (about 30000 DOF)
    - Shell elements of 1.5mm thick for the tray walls and 2.0mm thick for the tray bottom + Quasi-rigid 1-D beam (no instrument model available during the preliminary design phase) + laminate plate (solar panels) + rigid elements to mount everything on the tray stack

- Hexcel® Honeycomb 1/8-5052-.0015inch (12.7mm thick), 0.5mm Al-6061-T651A Face sheets

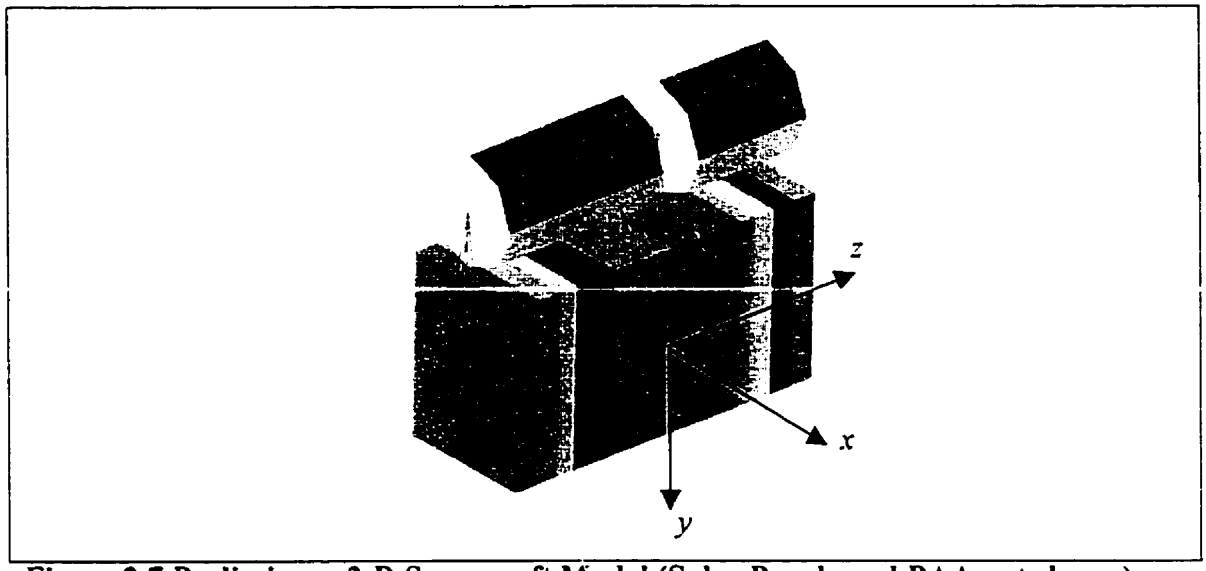

Figure 2.7 Preliminary 2-D Spacecraft Model (Solar Panels and PAA not shown)

Obviously, the results presented here for a preliminary spacecraft analysis will be subject to modification given the updated information presented in Chapter 3. However, the results obtained from this rough model provide useful information to assess the convergence of the detailed design model. For this reason, the same analyses were performed with the preliminary spacecraft model. Moreover, the CG location is found to be too far off in the negative y direction from the PAA centreline (the PAA centreline is assumed to be fixed at half the tray height for the preliminary analyses). Hence, moving the PAA plate towards the instrument enclosure in the negative y direction by 0.1219m is recommended. A more accurate position will be recommended in Chapter 3, as more details are included in the model. The preliminary CM location with respect to PAA centreline was found to be at the following point: (0.1305m,-0.1219m,-0.0012m).

Launch Vibration Load Analysis

MODE	Description	FREQUENCY	Effective Mass			% of Total Mass
		(Hz)	X	Y	Z	
1	Telescope beam rotation about x axis	114.2975	0.00001	0.00837	0.02438	3.27
2	Tray bottom	129.6964	0.00000	0.00001	0.00128	0.129

Table 2.3: Spacecraft Model – Preliminary Natural Frequency Results

Static Load Analysis

Applied Load	Element#	Description	Material	Max. Von Mises (MPa)	Allowable Stress (MPa)	MS (FS=2)
18 g in x-dir	645	Tray contour	Al-6061-T6	14.70	248.21	7.4
18 g in y-dir	103	Tray contour	Al-6061-T6	9.26	248.21	Large
18 g in z-dir	844	Tray Bottom	Al-6061-T6	30.70	248.21	3.0

Table 2.4: Spacecraft Model – Preliminary Static Load Results

Where the Margin of Safety is defined as: $MS = \frac{\sigma_{Mat}}{\sigma_{MD}} - 1$

The preliminary results obtained prove the design to be strong. Again, these results are only presented as a reference for sensitivity and convergence analysis made at the detailed design phase. These results are only rough first approximations.

2.8 MOST FE Analysis Results and Preliminary Design Recommendations

The easiest way to summarise the design recommendations made after the preliminary phase based on a coarse but reasonable FE model is to answer the questions presented in Section 2.3:

1) Is the PAA and the CG alignment within the launch vehicle allowable range?
   - Answer: No, move PAA plate in the negative y-direction by 0.1219m.
2) How must the PCBs be attached to the tray bottom to comply with launch vibration?
   - Answer: See Figure 2.2 C.
3) What is the optimum tray bottom thickness?
   - Answer: 1.5mm.
4) How does the mass distribution affect the trays natural frequency response?
   - Answer: Non-uniform mass distribution with centre of mass as close to PAA as possible will lead to higher first natural frequency (see Section 2.7.5).
5) Is there a need for stiffeners on the bottom of the trays?
   - Answer: No.
6) What are the recommended solar panel thickness and laminate specifications?
   - Answer: Hexcel® Honeycomb[78] 1/8-5052-.0015inch (12.7mm thick) with Aluminum (Al-5052) facesheets of 0.5mm thick.
7) Is there a need for a honeycomb panel telescope enclosure?
   - Answer: Yes. Moving the PAA plate means that 3 attachment points will be needed on the instrument side, which in turn forces the addition of an enclosure.
8) Will the spacecraft satisfy all structural requirements?
   - Answer: Yes, as per preliminary analysis results.

Chapter 3

MOST Detailed Design: Structural Analysis

This chapter presents the MOST detailed design structural analysis results and the subsequent design recommendations. The analyses performed were based on the Preliminary Design Updates and were conducted from July 1999 through June 2000. The main results included herein are based on tray sub-assembly and spacecraft level analyses. Many models were constructed, but only two of the detailed spacecraft design models are presented herein for brevity and for reader comprehension.

3.1 MOST Detailed Structural Design Assumptions

Some of the preliminary design recommendations presented in Chapter 2 were implemented. The preliminary design steps led to a better definition of the structural design. For example, the PAA plate was effectively moved by the amount recommended. The detailed design task required the construction of many FE models. More accurate modelling was possible as more detailed drawings became available. Each analysis influenced the design decisions. Better mass estimation was possible and a total of 57.4kg, including contingencies [81], was obtained. A detailed account of each tray mass is included in Appendices H.1 and H.3 and all spacecraft components' mass in Appendix H.2. These mass properties, along with the available detailed drawings for each tray were used to build the detailed FE models. The resulting FE models feature accurate mass distribution and accurate geometry, two of the main factors influencing dynamical and mechanical responses. Hence, all analyses presented in Chapter 3 are based on these physical properties and are therefore considered accurate representation of the real

spacecraft. The sensitivity analysis presented in Section 3.5.6 also enhances confidence in the results obtained.

3.2 MOST Critical Design Phase Analyses

The objective of the detailed analyses included herein is to prove the structure rigid enough to sustain the launch loads with a sufficient margin of safety. The main analyses to be conducted are outlined in Section 1.6.

- At the spacecraft assembly level, the following analyses were conducted to assess for the overall behaviours of the MOST structure:
    1) Centre of mass determination
    2) Rigid body modal analysis
    3) Constrained vibration analysis
    4) Axial acceleration loads (equivalent static load analysis)
- At the spacecraft sub-assembly level, the following analyses were conducted:
    1) Rigid body modal analysis and constrained vibration analysis

3.3 Detailed Design 2-D FEA of MOST (Tray Sub-Assemblies)

As the critical design progresses, more accurate models are generated to better reflect the geometrical design details and mass distribution, thereby eliminating the main source of error in finite element modelling (discretization errors). The following sections present the latest sub-assembly analysis results.

3.3.1 Models Description

The tray subassemblies were remodelled to account for design details. The trays were held together via rigid elements at the tie rod hole locations. The equipment in rigid boxes is represented by lumped masses. This assumption is based on previous component level analyses that showed rigid behaviours of these small parts. For example, the receiver and transmitter boxes can safely be assumed as acting as rigid blocks. Despite the recommendations made, stiffeners were added and modelled using beam elements of accurate cross-sectional area coupled to the bottom tray shell elements (See Section 3.3.1.1 for details on stiffener modelling). The PCBs were incorporated and pinned to the tray stack with rigid elements. The tie rod beam elements were clamped at both ends to simulate the boundary conditions as seen by the tray during launch. The resulting FE model is complex; although, only a combination of two-dimensional and

one-dimensional elements was used. Computer processing time would be quite large for a fully three-dimensional analysis. The large margins of safety obtained validate the small deformation assumption made.

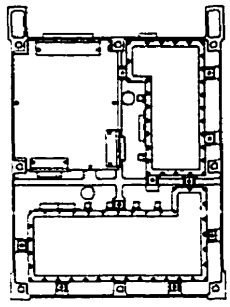

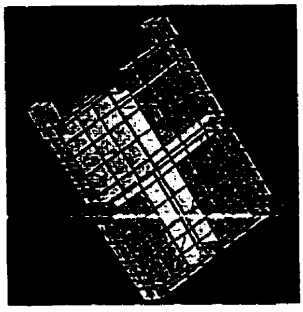

Total Mass: 2.25 kg.
Receiver Mass: 0.7 kg.
Transmitter Mass: 0.3 kg.
PCB Mass: 0.25 kg.
Tray Mass: 1.0 kg.
#Elements: 329
Side walls 1.5mm, bottom 2.0mm
#Nodes: 310
BCs: 8 Tie Rods end nodes fixed

Figure 3.1: Transceiver Tray FE Model (Masses include contingencies)

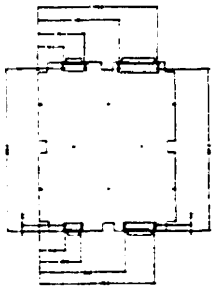

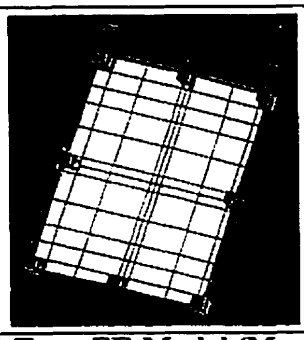

Total Mass: 1.2 kg.
PCB Mass: 0.45 kg.
Tray Mass: 0.75 kg.
#Elements: 374
Side walls 1.5mm, bottom 2.0mm
#Nodes: 375
BCs: 8 Tie Rods end nodes fixed

Figure 3.2: ACS-CCD Tray FE Model (Masses include contingencies)

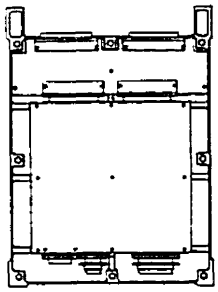

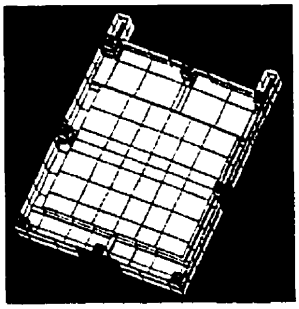

Total Mass: 2.2 kg.
Ram Disk Mass: 0.3 kg.
Stub Board Mass: 0.3 kg.
Processor Mass: 0.7 kg.
Tray Mass: 0.9 kg.
#Elements: 437
Side walls 1.5mm, bottom 2.0mm
#Nodes: 418
BCs: 8 Tie Rods end nodes fixed

Figure 3.3: OBC Tray FE Model (Masses include contingencies)

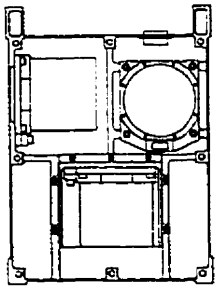

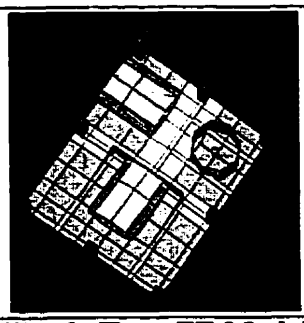

Total Mass: 4.9 kg.
Wheels Mass: 3.5 kg.
Tray Mass: 1.4 kg.
#Elements: 606
Side walls 1.5mm, bottom 2.0mm
#Nodes: 534
BCs: 8 Tie Rods end nodes fixed

Figure 3.4: Reaction Wheels Tray FE Model (Masses include contingencies)

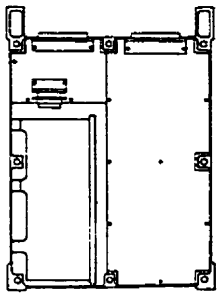

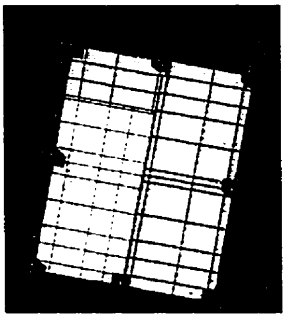

Total Mass: 4.2 kg.
Battery Box Mass: 2.7 kg.
Regulator Mass: 0.6 kg.
PCB Mass: 0.2 kg.
Tray Mass: 0.7 kg.
#Elements: 542
Side walls 1.5mm, bottom 2.0mm
#Nodes: 523
BCs: 8 Tie Rods end nodes fixed

Figure 3.5: Power Tray FE Model (Masses include contingencies)

The UTIAS/SFL team provided the detailed drawings of each tray. As previously mentioned, no stiffeners are necessary from a vibration standpoint. However, buckling is a limiting factor here. Buckling analysis was carried only by hand calculations and hence with a higher safety factor. Therefore, The tray stiffeners shall be included.

3.3.1.1 Stiffener Modelling

A combination of a 1-D beam element and the existing shell elements was used to model the tray bottom stiffeners and tie rod side stiffeners. The beam elements effectively stiffen the shell elements at the desired location. Accurate beam element cross-sections are easy to model using the beam cross-section task in I-DEAS. Figure 3.6 shows the beam and shell elements coupling combination. Many papers were found on plate stiffeners modelling in the MSC World Users' Annual Conference Proceedings(1989-93).

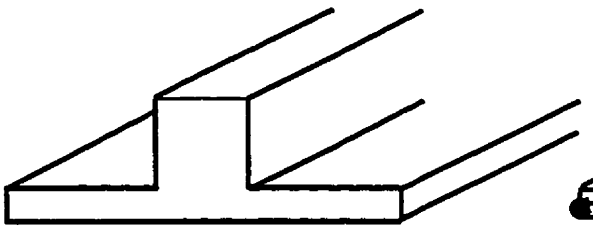

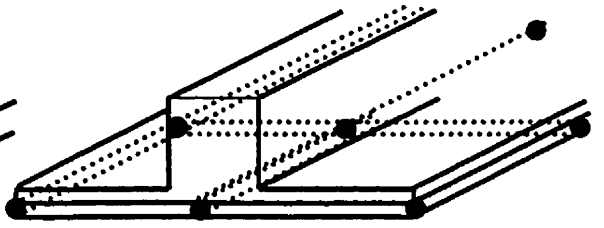

3-D Form

Beam (top) and shell (bottom) elements combination
Black dots representing the shell nodes
Gray dots representing the shared nodes

Figure 3.6: Beam and shell elements combination

3.3.2 Models Free-Body Check

All tray sub-assembly FE models described in section 3.3.1 featured 6 near zero natural frequencies.

3.3.3 Normal Modes Analysis Results

MODE	Frequency (Hz)
1	511.3836
2	511.7244
3	518.9924
4	520.5506
5	552.5204
6	736.0661
7	737.5592
8	931.3028
9	945.6621
10	1013.7976

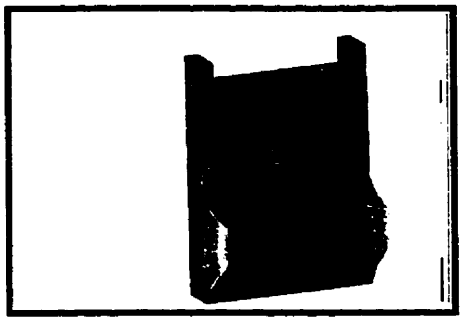

Table 3.1: Transceiver Tray Natural Frequency Results (2mm bottom thickness)

MODE	Frequency (Hz)
1	505.2486
2	505.7150
3	513.4745
4	515.2899
5	551.9481
6	734.0090
7	735.7808
8	825.8793

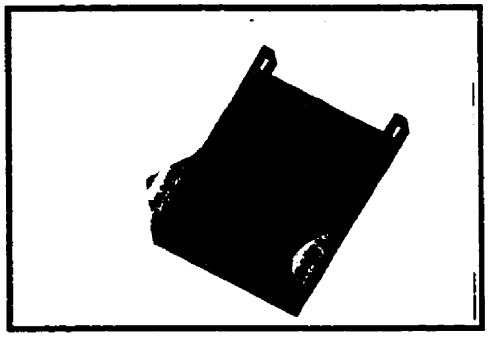

Table 3.2: Transceiver Tray Natural Frequency Results (1.5mm bottom thickness)

MODE	Frequency (Hz)
1	395.1448
2	399.9687
3	428.4827
4	448.8072
5	468.8264
6	516.6512
7	545.7824
8	552.4346
9	562.6870
10	579.1933

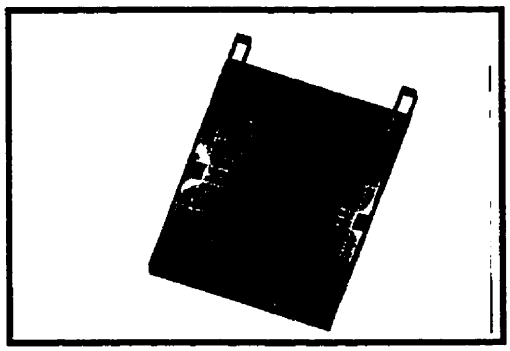

Table 3.3: ACS-CCD Tray Natural Frequency Results

MODE	Frequency (Hz)
1	251.2619
2	417.3064
3	449.5468
4	498.9978
5	515.8575
6	532.5051
7	554.7193
8	566.4124
9	603.3397
10	605.9413

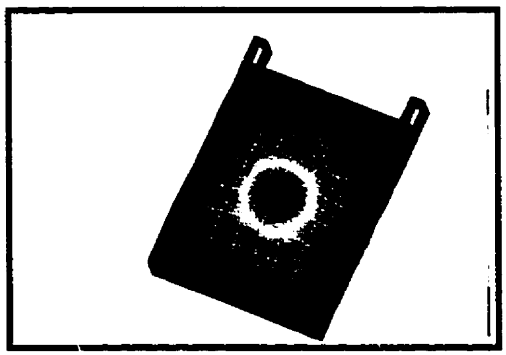

Table 3.4: OBC Tray Natural Frequency Results

MODE	Frequency (Hz)
1	173.5920
2	222.1379
3	334.6217
4	336.7406
5	344.1700
6	350.0570
7	378.7567
8	434.3723
9	528.0597
10	530.1922

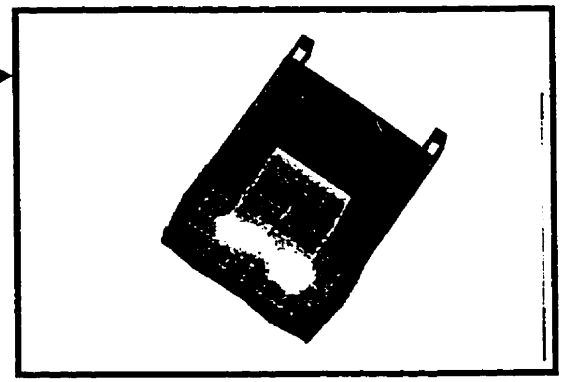

Table 3.5: Reaction Wheels Tray Natural Frequency Results

MODE	Frequency (Hz)
1	250.1386
2	336.2893
3	343.8153
4	369.8109
5	425.7237
6	435.4296
7	442.0690
8	482.6515
9	503.2261
10	524.5009

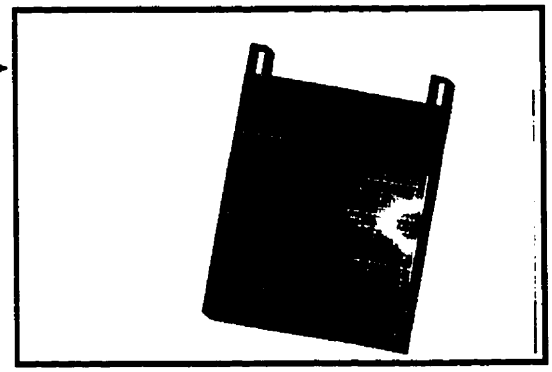

Table 3.6: Power Tray Natural Frequency Results

The above results prove the design to be very robust at the tray sub-assemblies analysis level. The first excitation frequency for all trays is largely over the critical value set forth by the Delta II launch vehicle requirements, even with a safety factor of 2.0.

3.3.4 Mass Saving Options

The results obtained in Tables 3.1 to 3.6 featured some high frequency responses. Hence, in order to save mass, the bottom plate thickness of the tray can be safely reduced to 1.5 mm. The mass saving is of the order of 125 grams per tray. Accounting for the 15 trays, this represents a mass saving of about 1.87kg. Table 3.2 presents the results obtained for the transceiver tray. As shown, reducing the bottom thickness by 0.5mm does not increase the vibration failure risk as the tray still features a high frequency response. Another option would be to remove some of the stiffeners, which was investigated in Chapter 2. Indeed, the stiffeners could be removed if buckling is ignored. However, hand calculations buckling analyses showed that stiffeners might be necessary if a safety factor of 3.0 is used. Stand off blocks could also be used to attach the PCB and

the other components to the tray bottom instead of the stiffeners. In any case, it is not recommended to both remove the stiffeners and reduce the bottom thickness of the tray, as the first natural frequency response would decrease drastically.

3.4 Detailed Design 2-D FEA of MOST (Spacecraft Level)

Two of the detailed spacecraft models constructed during the detailed design phase are presented herein. The final spacecraft model obviously provides more accurate results as the PAA plate and other components were refined. The previous version is presented as a comparative model to assess for the validity of the results obtained from the final detailed FE model and to highlight that the rigid PAA plate assumption was not a good assumption. Moreover, a previous independent model featuring less elements is shown to demonstrate convergence of the detailed model.

3.4.1 Models Description

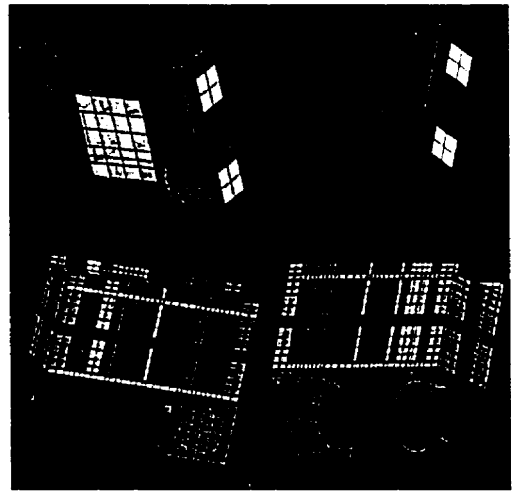

Figure 3.7: Critical Design Spacecraft FEM (Intermediate Model)

Many FE models were constructed during the various design phases. Table 3.7 presents a description of three of these models that are presented herein. The models built included modelling of the tray stack, the instruments, the solar panels, the antennas, and the PAA. All brackets were assumed to be rigid elements. The telescope and periscope mirror were mounted onto the tray stack using rigid elements with the dependant nodes only constrained in translation, releasing the rotational node dependence to allow rotational movement to account for the worst case dynamical interactions at the interface between the instruments and the tray stack. The mass properties and mass

distribution of the detailed model accounted for the detailed mass allocation provided by the SFL staff (See appendix H.3). The total mass of MOST was taken as 57.3 ±0.2kg, which include contingencies [81]. The ±200 gr. is due to the model overall inaccuracies.

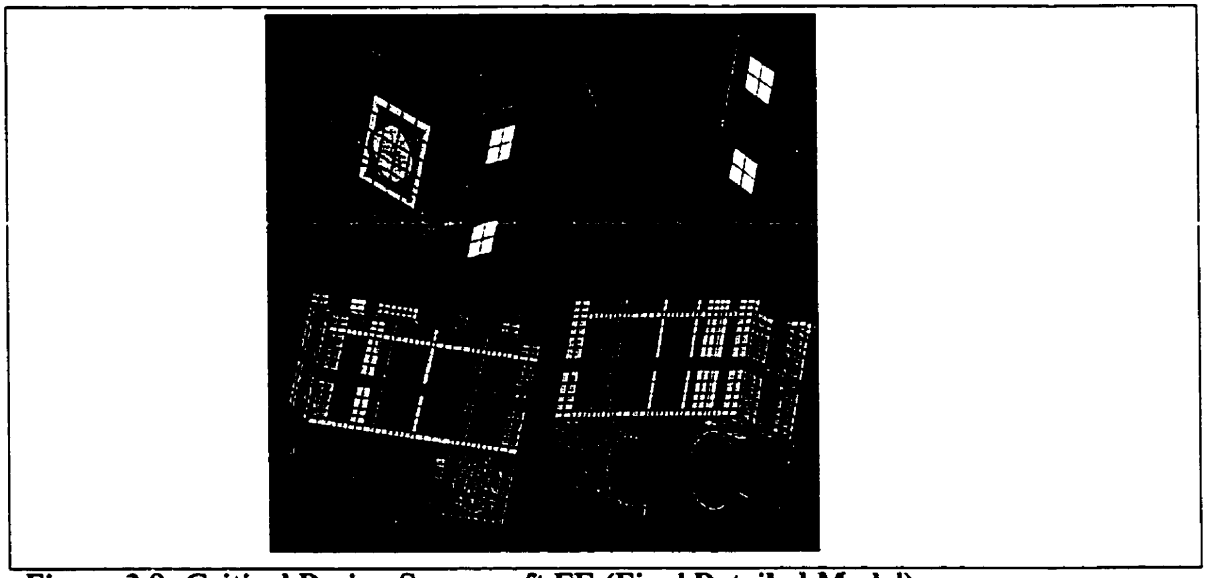

Figure 3.8: Critical Design Spacecraft FE (Final Detailed Model)

Model	Preliminary	Intermediate	Final Detailed
Picture	Figure 3.7	Figure 3.7	Figure 3.8
Total Mass	48.8 kg.	57.28 kg.	57.12 kg.
Tray Cross-section	Rectangle 251mm x 300mm	Detailed Tray Cross-section (See Figure 3.1 to 3.5)	Detailed Tray Cross-section (See Figure 3.1 to 3.5)
Tray Content	Non-structural mass evenly distributed	Lumped Masses, Detailed Tray Modeling	Lumped Masses, Detailed Tray Modeling
Number of Trays	10	15	15
Tray Material	Al-6061-T6	Al-6061-T6	Al-6061-T6
Bottom Tray Thickness	2mm	2mm	2mm
Side Tray Thickness	1.5mm	1.5mm	1.5mm
Number of Elements	5648	6118	6205
Number of Nodes	5127	5227	5303
Boundary Condition	Clamped PAA (Square) Assuming Rigid PAA Plate	9 PAA Bolts Clamped **Assuming Rigid PAA Plate**	9 PAA Bolts Clamped **PAA Plate Modelled**
PAA Location	Middle of Tray Stack Side	Bottom PAA Plate at Middle of Stack Side	Bottom PAA Plate at Middle of Stack Side
CG Location w.r.t.PAA	(0.1305m,-0.1219m,-0.0012m)	(0.1534m,0.03266m,0.0018m)	(0.1539m,0.03277m,0.0019m)
Solar Panels	Hexcel Honeycomb 1/8-5052-.0015inch (12.7mm thick), 0.5mm Al-6061-T651A Face sheets		
Telescope	Quasi-rigid 1-D beam	Detailed Model	Detailed Model
Periscope Mirror	Quasi-rigid 1-D beam	Detailed Model	Detailed Model
Patch Antennas	Not modeled	Modeled	Modeled

Table 3.7 FE Models Description

The tray order and other details on the tray assembly itself can be found in Appendix H.1.

3.4.1.1 Insertion of a Detailed 2-D Finite Element Model of the Telescope

Mayes Mullins [82] did the meshing of the telescope. His model was constructed using MSC/NASTRAN. The model was imported into I-DEAS. After adjustments of the boundary conditions that were mistranslated by I-DEAS, both models featured similar vibration frequency response for the modes of vibration looked at. The attachment points were modelled to simulate the bracket bolts as shown in Appendix G.4. The first natural frequency was found to be 124Hz when using I-DEAS and 121Hz when using MSC/NASTRAN. The 2.4% difference is satisfactory for the purposes of this analysis. Figure 3.9 shows the telescope as modelled by Mullins. It features 727 elements and 599 nodes. It weighs 9.606 kg. According to Mullins [82], the optical components were not modelled in sufficient details to examine their internal stresses or the stresses at the glass-to-metal bond. They were only modelled with sufficient details to impose their mass on the structure. Hence, the stress analysis included herein cannot conclude anything about the optical components of the telescope. The UBC/Crestech design group is responsible for the instruments and shall make sure that this critical component will sustain all launch loads described herein.

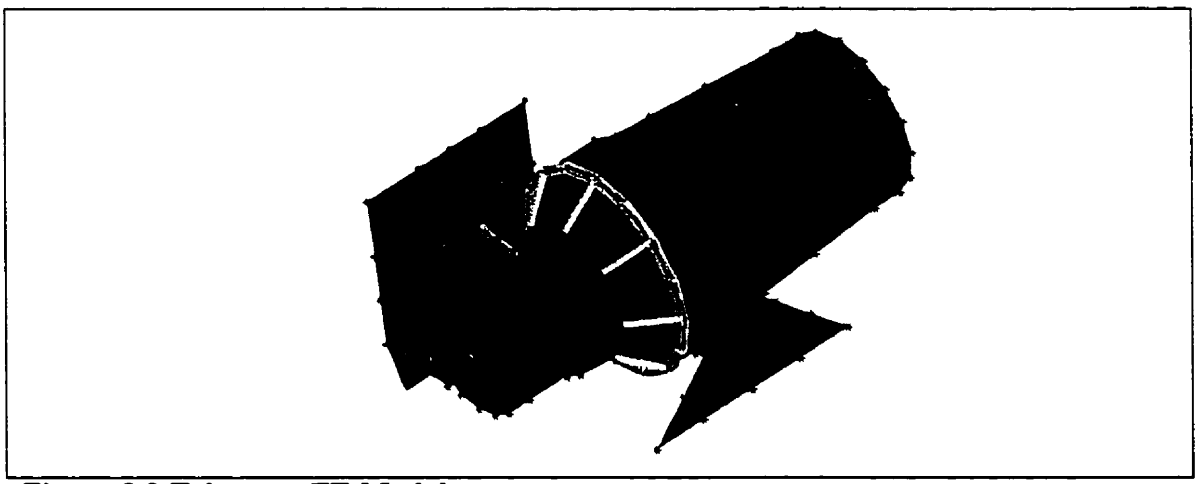

Figure 3.9 Telescope FE Model

3.4.2 Constraints and Model Free-Body Check

The 9 PAA attachment nodes were clamped for the intermediate model. However, a detailed 2-D PAA plate was modelled for the final detailed model. Also (for both models), the telescope and periscope mirror were mounted onto the tray stack using rigid elements with the dependant nodes only constrained in translation, releasing the

rotational node dependence to allow rotational movement to account for the worst case dynamical interactions at the interface between the instruments and the tray stack.

Modal analysis showed the 6 near zero frequency modes as expected, confirming that the models do not feature any extraneous constraints. The purpose of this modal analysis is solely to verify that the model is not constrained internally as it is often the case when rigid elements are used to link two parts within the overall FEM.

3.4.3 CG Assessment

The final detailed model features a CG at the following location with respect to the origin: (0.1534m, 0.03266m, 0.0018m). The 1.8mm offset in the z-direction is negligible. The 153.4mm offset in the x-direction is below the 165mm limit set forth by the Delta II launch vehicle authorities for a 57 kg payload. However, the 32.66mm offset in the y-direction could induce unwanted spin rates when the spacecraft is separated from the launch vehicle. Hence, mass should be rearranged to obtain a CG offset of the order of 2.0mm in the y-direction.

3.4.4 Normal Modes Analysis Results

The natural frequencies of vibration for the constrained spacecraft models were obtained using the Lanczos[67] method. I-DEAS featured a fully converged solution for the two models analysed. The convergence check is a built-in feature of the I-DEAS software. Tables 3.8 and 3.9 present the frequency results along with the effective mass for each excitation mode. The effective masses are computed by summing all nodal masses featuring non-zero nodal displacement. The result obtained for each direction x, y, and z is then given as a percentage of the overall mass.

Launch Vibration Load Analysis

MODE	FREQUENCY	Effective Mass			% of Total Mass	Figure#
	(Hz)	X	Y	Z		
1	124.38	0.000196	0.000161	0.007527	0.78	Table 3.10
2	152.67	0.000457	0.000000	**0.182971**	**18.33**	3.10
3	169.09	0.002984	0.001488	**0.124503**	12.91	-
4	188.26	0.032052	**0.211957**	0.004981	**24.92**	3.10
15	339.09	**0.155090**	**0.085028**	0.000981	24.12	-
18	383.41	**0.106170**	0.002723	0.009384	11.83	-

Table 3.8: Intermediate Spacecraft Model – Natural Frequency Results

MODE	FREQUENCY	Effective Mass			% of Total Mass	Figure#
	(Hz)	X	Y	Z		
1	59.7865	0.000112	**0.309346**	0.003649	31.30	Table 3.11
2	74.8578	0.000641	0.001727	**0.302056**	**30.37**	3.11
3	121.4506	0.000168	0.000316	0.001914	0.22	-
6	206.3644	**0.828015**	0.023980	0.000019	**85.19**	3.11
15	312.8301	0.024818	**0.218942**	0.015367	24.63	-
17	338.5633	0.013052	**0.084595**	**0.041242**	12.56	-

Table 3.9: Final Detailed Spacecraft Model – Natural Frequency Results

Table 3.8 presents the significant results showing the effective mass of the satellite excited at each mode. The *x* direction features the highest effective mass excited at 206Hz. However, because the frequency magnitude is largely over 50Hz, no action needs to be taken.

Tables 3.10 and 3.11 show the first ten vibration modes. As observed, the intermediate model features a first natural frequency of 124Hz, which was expected because of the telescope analysis. The intermediate model did not include modelling of the non-rigid PAA plate. The detailed model, however, accounted for the non-rigid PAA effects.

MODE	Frequency (Hz)
1	124.3854
2	152.6657
3	169.0877
4	188.2568
5	222.6753
6	246.3308
7	250.0217
8	251.8409
9	261.7961
10	264.0415

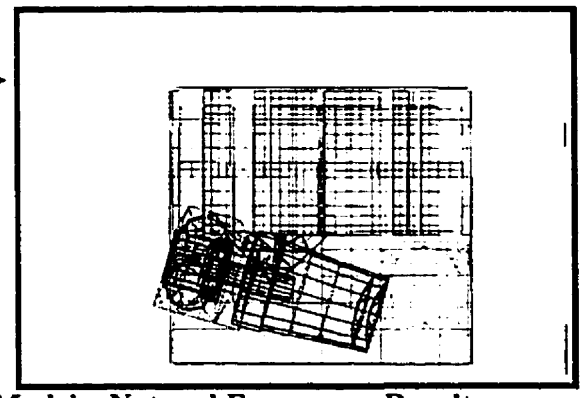

Table 3.10: Intermediate Spacecraft Model – Natural Frequency Results

MODE	Frequency (Hz)
1	59.7865
2	74.8578
3	121.4506
4	158.5967
5	181.8081
6	206.3644
7	221.2633
8	243.5012
9	249.6842
10	250.9937

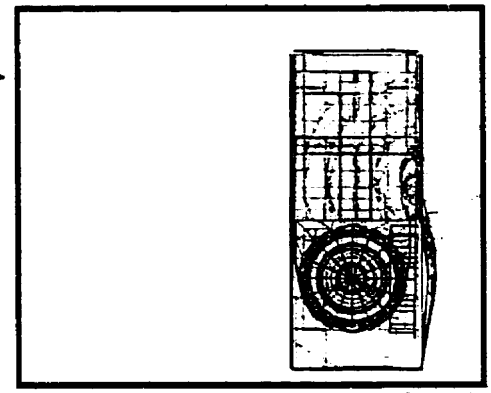

Table 3.11: Final Detailed Spacecraft Model – Natural Frequency Results

3.4.4.1 MOST 2-D FE Model Rigid PAA Plate Assumption

All the analysis prior to the final detailed model assumed a rigid PAA plate. However, the PAA plate proposed by the Delta II launch vehicle authorities is not rigid enough for MOST. The results are not shown here, but the first natural frequency response was 52Hz, which is just above the Delta II requirement.

Consequently, the SFL structural engineer designed a PAA plate that features higher strength characteristics than the Delta II baseline plate (the SFL PAA base plate features a thicker base plate). The real non-rigid effects of the PAA plate could only be fully taken into account if a 3-D model was built. However, the time and computational requirements involved in constructing a 3-D MOST spacecraft model is impractical. However, a good estimation of these effects can be obtained by modelling a 2-D PAA plate into the final detailed design model. While not as accurate, it allowed assessment of the order of magnitude of the non-rigid effects on the dynamical frequency response of the spacecraft. It is important to note that the restrictions imposed by the 2-D shell element model turn out to lead to a conservative result. The stiffening effect of having the PAA plate bolted against the honeycomb laminate panel cannot be modelled properly with shell elements. Also, a more accurate model is likely to converge to a lower frequency because the modal response results converge from above in a finite element analysis. Hence, the final detailed model is really a safe approximation of the real spacecraft dynamical behaviours.

As shown in Table 3.11, the non-rigid PAA effects induce two new excitation modes. These modes are shown in Figure 3.11 and Table 3.11. They consist of a rotation, also called a rocking mode, about the PAA plate centreline about the z and y axis respectively. The third vibration mode was found at 121Hz, which was the same telescope vibration mode as the first mode of the rigid PAA intermediate model. Then, the typical tray bottom vibration was found at 152Hz (intermediate model) and at 158Hz (detailed model), which is the AMSAT tray bottom (the only tray without any detail modelling). As no details were available yet, the AMSAT tray was left empty with a lumped mass at its CG. It is expected that the actual AMSAT tray will feature similar behaviour as the transceiver tray, which possesses a higher first natural frequency.

The modal analysis accounted for the PAA constrained boundary, without constraining the rotational degrees of freedom of the dependant nodes to account for the clamp band flexibility. The first natural frequency of the Spacecraft FEM of 59Hz is slightly above the required secondary payload requirement of 50Hz. As discussed earlier, the detailed model is a conservative model. Releasing of the rotational degrees of freedom adds to the conservative account, as the ring will be closer to being clamped than simply supported at all nodes around the circular part of the PAA plate. The first natural frequency of 59Hz is definitely a conservative number, which is higher than the Delta II no coupled load analysis requirement. Hence, no coupled load analysis is required.

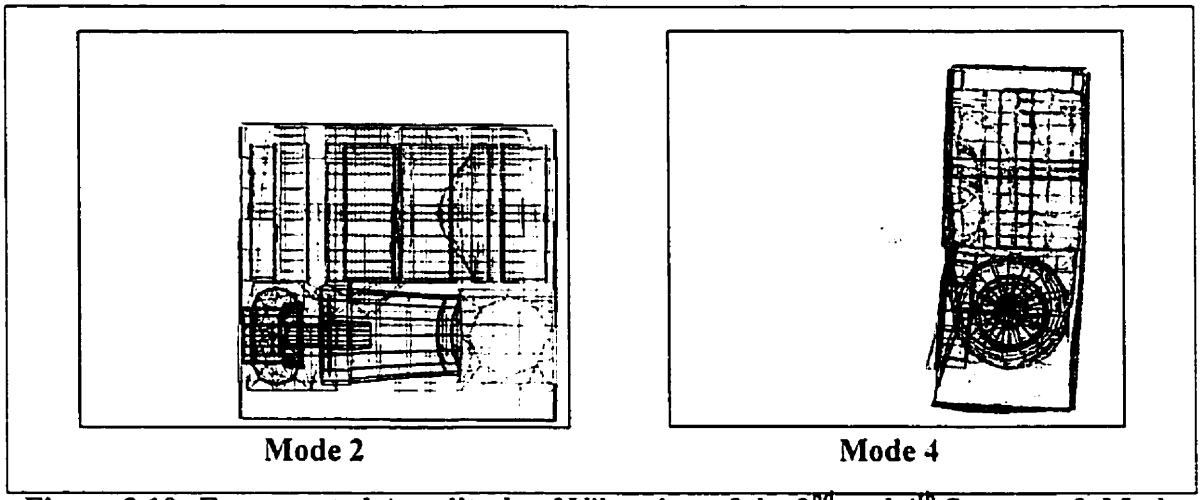

Figure 3.10: Exaggerated Amplitude of Vibration of the 2nd and 4th Spacecraft Mode (Intermediate Model)

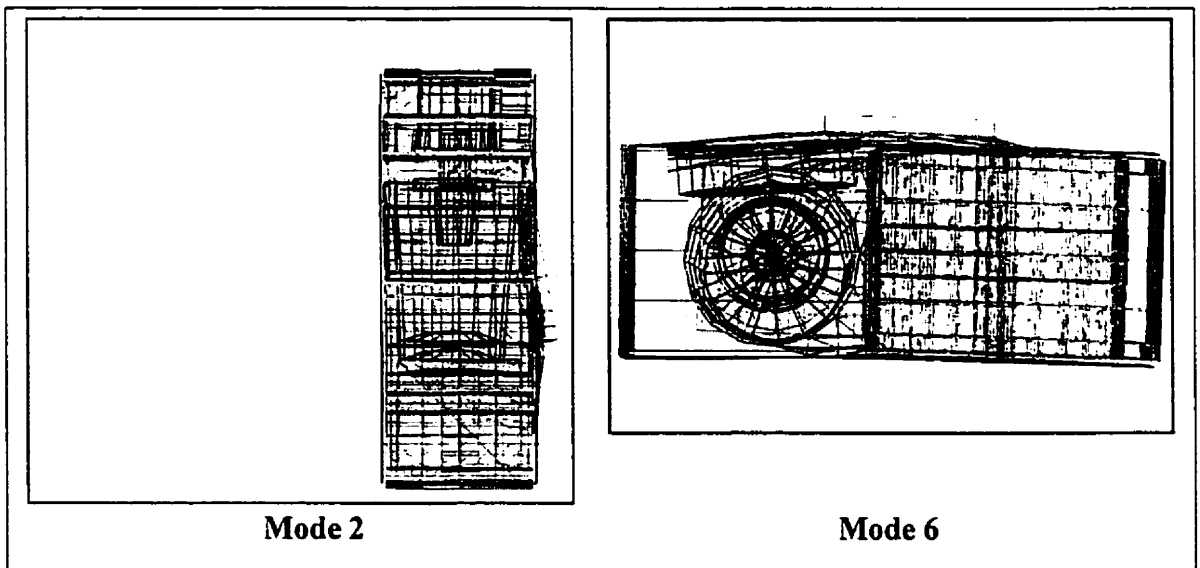

Figure 3.11: Exaggerated Amplitude of Vibration of the 2nd and 6th Spacecraft Mode (Final Detailed Model)

3.4.5 Launch Acceleration Loads

The static load analysis considered a gravity load of 20 times the gravity at sea level applied in three axes simultaneously (accounting for a safety factor of 2.0). The resulting margins of safety computed in Table 3.13 effectively establish that the small displacement and linear theory assumption is valid as the margin of safety obtained are all positive when a safety factor of 2.0 is considered.

Static Load Analysis

Applied Load	Element#	Description	Material	Von Mises (MPa)	Allowable Stress (MPa)	MS (FS=2)	Figure
20 *g* in x-dir	4170	RW Tray (side)	Al-6061-T6	43.24	248.21	4.74	-
20 *g* in y-dir	2622	ACS-CCD Tray	Al-6061-T6	35.31	248.21	6.02	3.12
20 *g* in z-dir	2622	ACS-CCD Tray	Al-6061-T6	35.47	248.21	6.00	-

Table 3.12: Intermediate Spacecraft Model – Static Load Results

Applied Load	Element#	Description	Material	Von Mises (MPa)	Allowable Stress (MPa)	MS (FS=2)	Figure
20 *g* in x-dir	8141	PAA Ring	Al-6061-T6	123.1	248.21	1.02	-
20 *g* in y-dir	8100	PAA Base Plate Contour	Al-6061-T6	242.3	248.21	0.024	3.13
20 *g* in z-dir	8142	PAA Ring	Al-6061-T6	217.1	248.21	0.14	-

Table 3.13: Final Detailed Spacecraft Model – Static Load Results

Only the ACS-CCD tray is displayed in Figure 3.13 because the Von Mises maximum stress occurs on the corner where the instrument is attached. The magnitude of the stress does not require that any actions be taken.

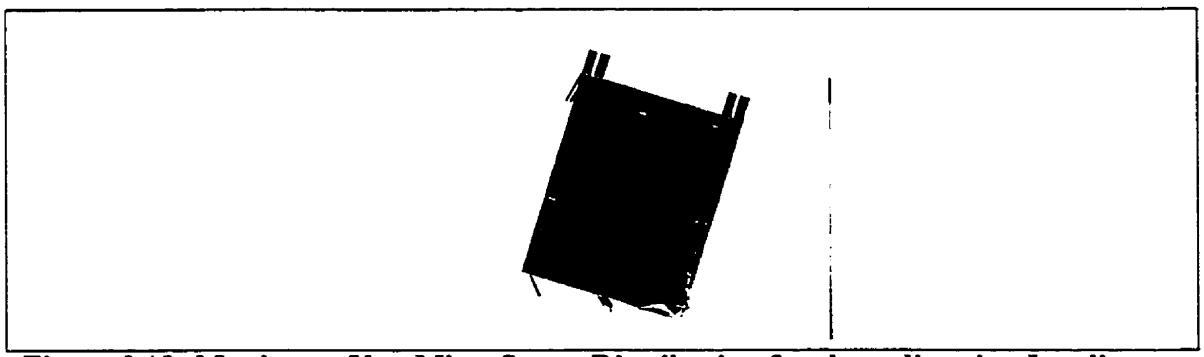

Figure 3.12: Maximum Von Mises Stress Distribution for the *x*-direction Loading (Intermediate Model)

The solar panels are not displayed in Figure 3.13 for clarity. The maximum stress occurs at the middle-top edge of the PAA base plate contour. The magnitude of the stress does not require that any actions be taken, although the margin of safety is very close to zero. It is recommended, however, that the base plate thickness be increased slightly (about 2mm) to reduce the failure risk. This would raise the margin of safety above 0.25. As observed, the non-rigid PAA ring absorbs a large share of the energy induced by launch loads. This proves again that the earlier assumption that the PAA was rigid was not a valid assumption. However, the updated results obtained from analysis only, prove the MOST structure design adequate for launch.

Figure 3.13: Maximum Von Mises Stress Distribution for the *y*-direction Loading (Final Detailed Model)

3.4.6 MOST 2-D FE Model Sensitivity Analysis

Complex geometrical structures cannot realistically be analysed via analytical tools. This is the main reason why finite element procedures were developed. However, the confidence in a FE may remain an issue. In that case, some basic sensitivity analysis (i.e. varying the number of elements, material properties, etc.) gives a fairly good indication of the model's reliability.

For MOST, the evolution of the models from the preliminary results based on analytical and finite element tools as shown in Chapter 2 to the converged model solutions shown in Chapter 3 provide some degree of confidence. Starting with a coarse model with a few number of elements, ending with the final spacecraft with a large

number of elements featuring the same order of magnitude as the earlier design models improves confidence. Seeing the results converging toward some finite value also attenuates reliability concerns. It was certainly the case for the results presented herein. Moreover, the relatively high margin of safety obtained while using a safety factor of 2.0 on all flight conditions basically leaves much room for the FEM inherent errors.

Running the same analysis on a different program does not improve confidence in the results. However, it is a nice check to make sure that the software is indeed reliable. The MOST model was therefore imported in MSC/NASTRAN and the same analyses were performed. The results obtained were almost exactly the same as expected.

To assess convergence and reliability of the final detailed model, an independent earlier model version was used. The FE model properties can be compared in Table 3.14.

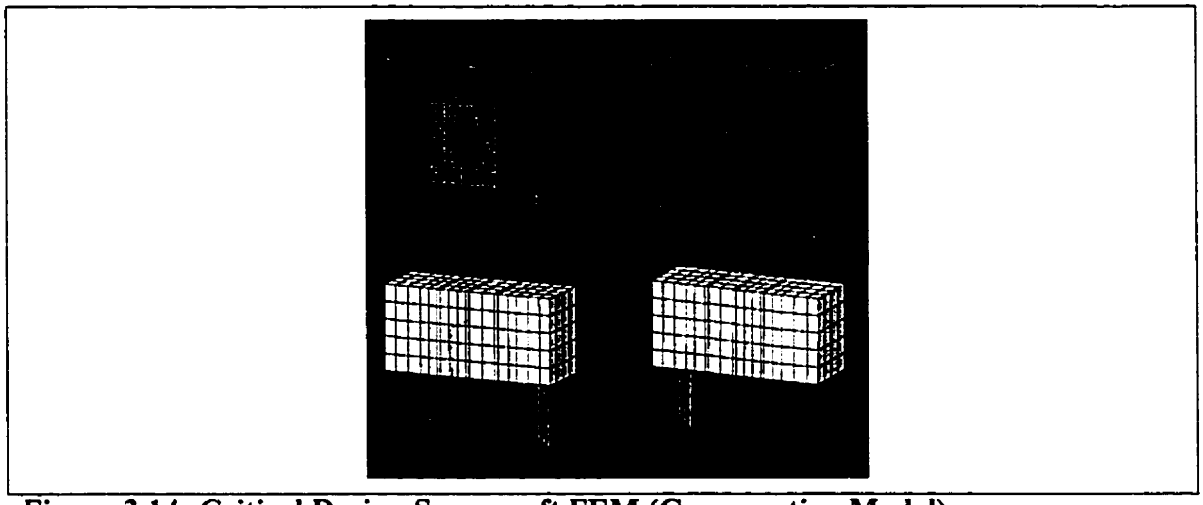

Figure 3.14: Critical Design Spacecraft FEM (Comparative Model)

All the analyses were repeated for the case of an earlier model that was constructed from the first detailed design phase iteration drawings. The telescope enclosure was clamped to the tray stack (rigid interface assumption for the telescope and periscope mounting brackets, and for the PAA plate).

As shown in Tables 3.14 through 3.16, the results for the bottom tray plate vibration modes are all around 150Hz, which turned out to be 158Hz for the case of the final detailed model. The Figure 3.15 shows the deformation of one of the major modes of vibration, with 16% effective mass involved.

The margin of safety computed for the maximum Von Mises stresses obtained in Table 3.17 are all very large because the PAA was modelled rigidly. As shown earlier,

this assumption is false. Figure 3.16 presents the location of higher stress. Again, the solar panels are not shown for clarity.

Model	Earlier Model	Final Detailed
Picture	Figure 3.14	Figure 3.8
Total Mass	57.33 kg.	57.12 kg.
Tray Cross-section	Rectangle 251mm x 300mm No stiffeners, no PCB	Detailed Tray Cross-section (See Figure 3.1 to 3.5)
Tray Content	Non-structural mass evenly distributed	Lumped Masses, Detailed Tray Modeling
Number of Trays	15	15
Tray Material	Al-6061-T6	Al-6061-T6
Bottom Tray Thickness	2mm	2mm
Side Tray Thickness	1.5mm	1.5mm
Number of Elements	**1968**	**6205**
Number of Nodes	1592	5303
Boundary Condition	9 PAA Bolts Clamped **Rigid PAA Plate**	9 PAA Bolts Clamped **Non-Rigid PAA Plate**
PAA Location	Bottom PAA at Middle of Stack Side	Bottom PAA at Middle of Stack Side
CG Location with respect to the PAA	(0.1524m,0.02844m,0.0057m)	(0.1539m,0.03277m,0.0019m)
Solar Panels	Hexcel Honeycomb 1/8-5052-.0015inch (12.7mm thick), 0.5mm Al-6061-T651A Face sheets	
Telescope	Detailed Model	Detailed Model
Periscope Mirror	2-D Shell Flat Mirror	Detailed Model
Patch Antennas	Not Modeled	Modeled

Table 3.14 FE Comparative Models Description

Launch Vibration Load Analysis

MODE	FREQUENCY	Effective Mass			% of Total Mass	Figure#
	(Hz)	X	Y	Z		
1	151.02	0.000018	0.000000	0.000679	0.07	Table 3.16
8	157.33	0.000026	0.000011	0.056658	5.67	-
19	287.49	**0.058132**	0.001276	0.000215	5.96	-
34	**429.61**	**0.095268**	**0.065394**	0.005956	**16.66**	3.15
37	456.28	0.006369	**0.096286**	**0.079747**	**18.24**	-

Table 3.15: Comparative Spacecraft Model – Natural Frequency Results

MODE	Frequency (Hz)
1	151.0205
2	152.5514
3	153.6044
4	153.8039
5	155.2878
6	155.3041
7	156.6247
8	157.3299
9	157.6070
10	157.8103

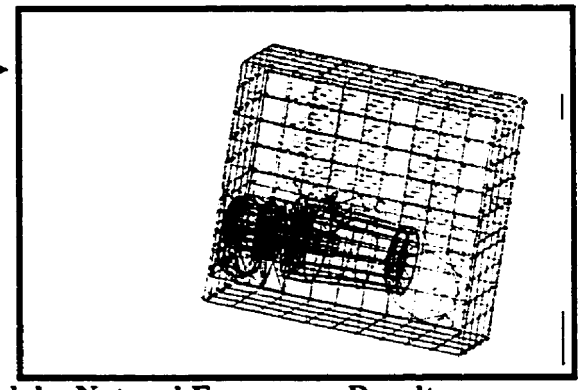

Table 3.16: Comparative Spacecraft Model – Natural Frequency Results

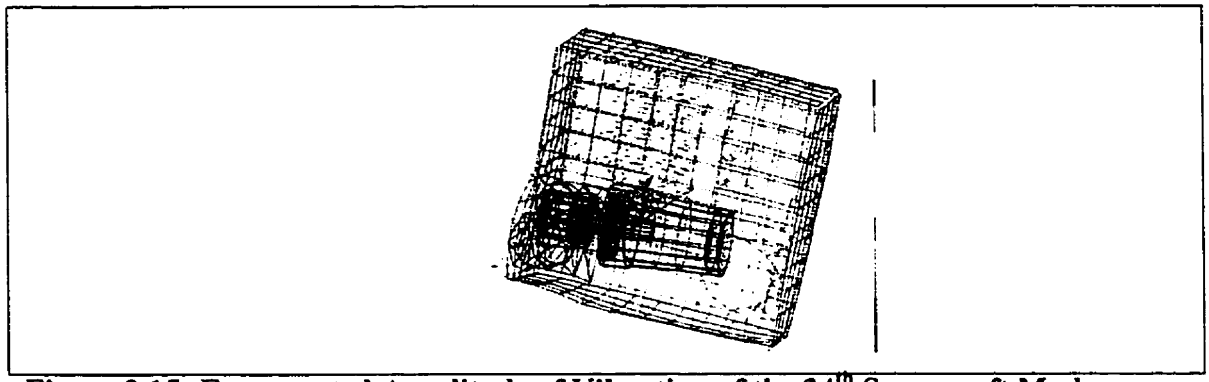

Figure 3.15: Exaggerated Amplitude of Vibration of the 34th Spacecraft Mode (Comparative Model)

Static Load Analysis

Applied Load	Element#	Description	Material	Von Mises (MPa)	Allowable Stress (MPa)	MS (FS=2)	Figure
18 g in x-dir	1275	AMSAT Tray -ve y side	Al-6061-T6	15.51	248.21	Large	3.16
18 g in y-dir	114	Telescope Mount	Ti-6Al-4V	7.04	827.37	Large	-
18 g in z-dir	744	ACS Tray Bottom	Al-6061-T6	10.74	248.21	Large	-

Table 3.17: Comparative Spacecraft Model – Static Load Results

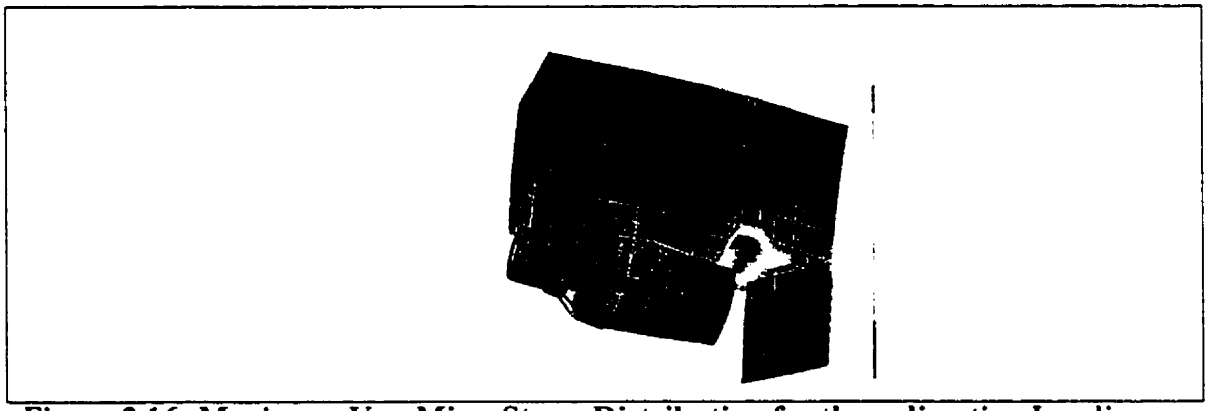

Figure 3.16: Maximum Von Mises Stress Distribution for the *x*-direction Loading (Comparative Model)

After following all good FE modelling practices highlighted in Chapter 2. verifying the convergence from one model to the next, performing basic sensitivity analysis, and correlating results to analytical results whenever possible, the MOST final detailed model results presented herein are believed to be reliable within the assumptions made. Hence, the large margin of safety obtained by finite element analysis indicates that the MOST structural design possesses adequate strength to survive the Delta II launch.

Chapter 4

MOST Tie Rod Analysis and Design

This chapter presents a detailed engineering analysis leading to the design of the MOST tie rods. The tray stack offers great advantages in terms of the ease of assembly. However, the sizing of tie rods for small satellites using a tray stack as a primary structure remains a challenging design problem. This chapter addresses the design issues, highlights the main assumptions on geometry, kinematics, material law, loading, and boundary conditions for MOST, and concludes with the appropriate design recommendations. The analysis results presented herein are intended to provide the SFL MOST engineering team with a clear understanding of tie rod design. All failure modes have been looked at extensively and the final results are presented in Table 4.3, and Appendix C.3. Although tie rod design recommendations are clearly stated in Section 4.14, all the intermediate results are presented in tables in Appendix C.3 in order to provide alternative choices for the designers of MOST.

4.1 Tie Rod Design Issues for Small Satellites and MOST

In the recent past, satellite engineers have designed tie rods in order to prevent joint failures in tray stacks assembly used as primary load carrying structures. The subject of bolted joints is far from trivial in relation to small satellite design. Excellent analytical and experimental treatments of the design and behaviour of bolted joints have been completed by Bickford[84], Eshbach[85], Fisher[86], Horsch[87], Osgood[88][89], Shigley[90], and Srinivas[91]. The reference most extensively used by engineers is Bickford[84], which covers the fundamentals of bolted joint design. The analysis presented here is motivated by the nontrivial behaviour of the bolted joint, as carefully outlined by Bickford[84].

Engineers must be careful in the selection of bolts and their applications. Microsatellite tray stack is one of the challenging applications of bolted joints. Proper tie rod design is crucial because of its impact on mission success. In fact, the design of tie rods involves a complex mechanical engineering analysis in which highly nonlinear material stress and strength considerations play a major role. The design of tie rods maintaining the microsatellite trays together is therefore far from a trivial task. The design steps required to find a viable solution are included in the following analysis. The standard military handbook of aerospace-grade materials (MIL-HDBK-5[77]) is used as a basis here for the material selection process. The utilisation of well-documented and well-known materials inherently adds safety to the design in terms of reliability of the material physical properties. Hence, the analysis restricted the material options to the extensive list given in MIL-HDBK-5[77] and in MSFC-SPEC-522[92] as fully described in Section 4.8. Cost and availability issues still remain since expensive and rare materials such as titanium or high strength steels are found in those documents. The cost and availability problems are further discussed along with other manufacturing and material treatment issues in Section 4.13.

The relative geometry of the MOST primary structure and the Payload Adapter Assembly (PAA) are certainly not optimal to resist launch loads. Hence, the structural arrangement for launch has apparent weaknesses, and leads to additional loads supported by the tie rods. The tie rods cannot realistically carry some of these loads and other structural modifications required are reported here, especially in Section 4.15. Figure 4.1 shows the optimal and intended vertical launch setup for small satellites as auxiliary payloads, and clearly exhibits the use of the tray stack assembly as a strong vertical support column. In that configuration, the primary structure basically features the same strength as a beam fixed at its base. However, aperture dimensions and other design changes forced the MOST engineers to use the weaker setup showed in Figure 1.4.

As shown in Figure 1.4, the PAA that should be fixed at the bottom of the satellite to take full advantage of the beam-like strength of a tray assembly, is fixed on the side of the tray stack instead. The analyses presented herein assume the launch setup shown in Figure 1.4. Hence, tie rod design recommendations based on the current MOST configuration are provided.

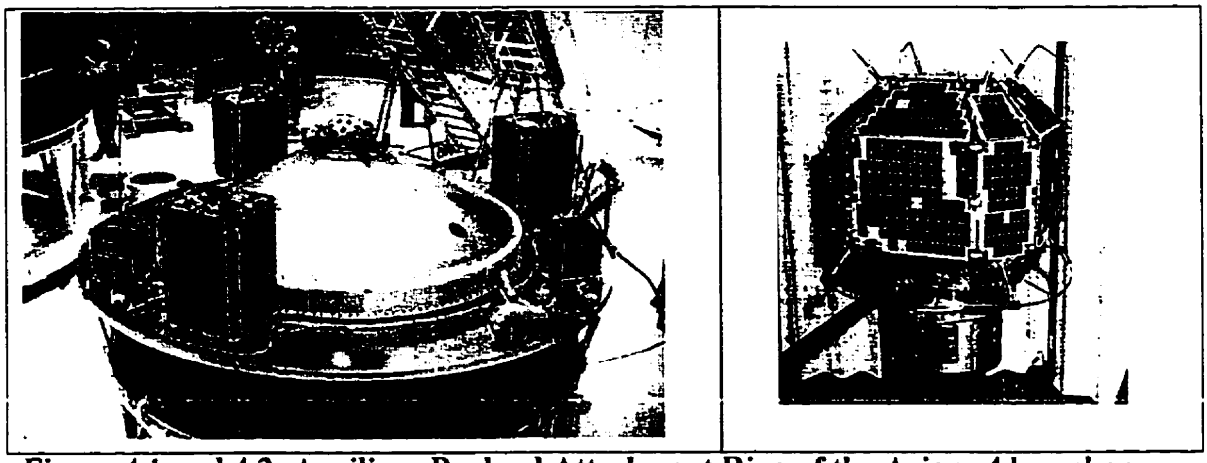

Figure 4.1 and 4.2: Auxiliary Payload Attachment Ring of the Ariane 4 launcher and example of PAA at base of JAS-2 (50kg small satellite) taken from AMSAT[44]

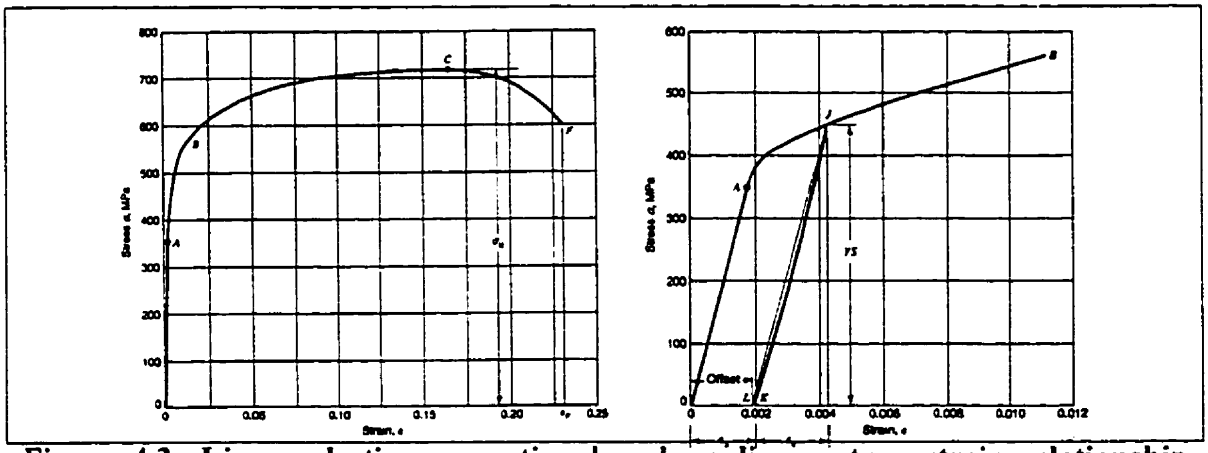

Figure 4.3: Linear elastic assumption based on linear stress-strain relationship below material yielding point A (Tension specimen of alloy steel from Boresi[93])

4.2 Tie Rod Design Theory and MOST

The basic theoretical equations for the design of bolted joints were clearly derived and explained by Bickford[84]. This thesis takes the approach that, although Bickford's work does not constitute the most rigorous mathematical treatment of the subject, his conceptualisation and applied equations can be acknowledged with accuracy within the linear material behaviour interactions between the bolt and the joint, and other fundamental assumptions of his work. Therefore, the theory on which the MOST tie rod analysis is based on has been highly influenced by the scientific papers referenced by Bickford[84]. The assumptions made herein are explained whenever appropriate.

It is well understood of course that the linear elastic material behaviour assumption is accurate as long as the material interactions take place below the yielding

point of both materials involved, which corresponds to the linear curve below Point A as shown in Figure 4.3. The main linear theory assumption is applied to obtain a bolt-joint diagram as shown in Figure 4.4. This diagram clearly reveals that the linear elastic curves for both the joint and the bolt must meet at some equilibrium point. This main assumption must be kept in mind at all times. The theoretical results are then applied to the sizing of MOST's tie rods. Relaxation effects during bolt pre-loading and other assumptions are further discussed in Section 4.11.

The elastic curves for both the joint and the bolt starting at O_B for the bolt (with initial length L) and at O_J for the joint (with initial thickness J), are easily recognised on the bolt-joint diagram in Figure 4.4. After pre-loading the bolt with force F_P and when relaxation effects are stabilised, the two curves settle at some equilibrium point EQ_{P1}. Similarly, after applying an external load F_X to the pre-loaded bolt and when relaxation effects are stabilised, the two curves settle again at some other equilibrium point EQ_{P2}. The slope of those two elastic curves represents their stiffness.

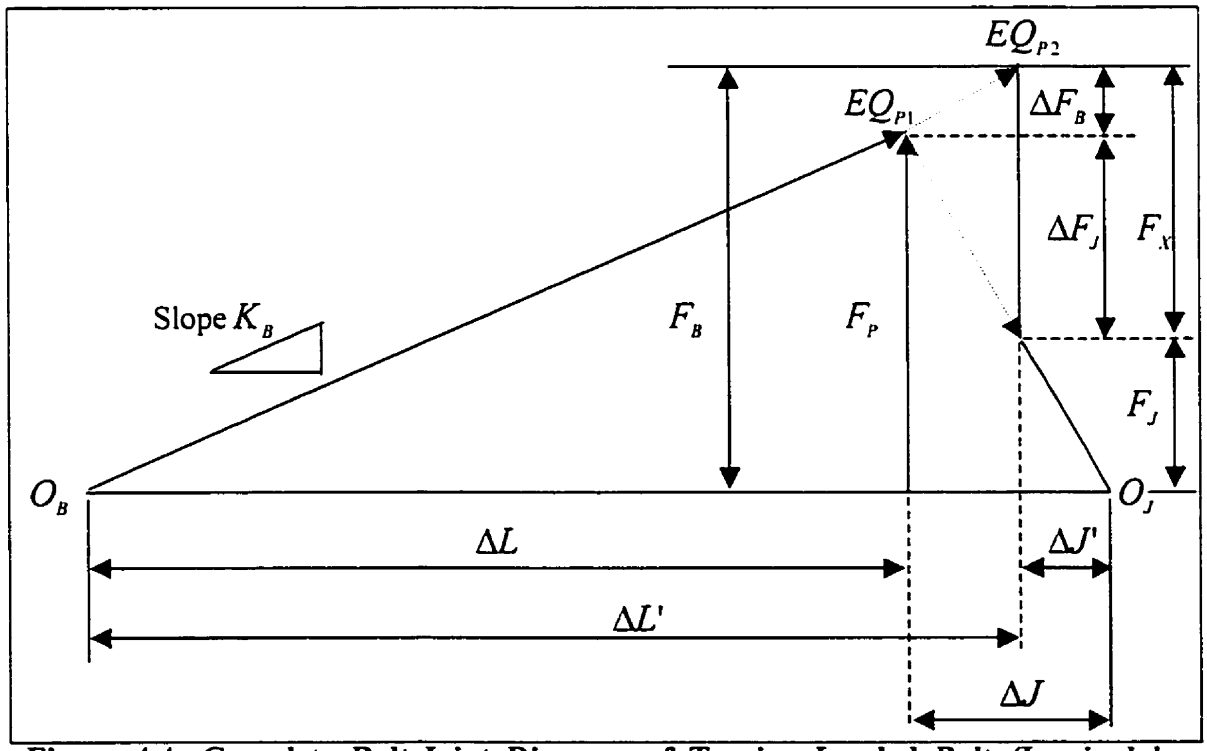

Figure 4.4: Complete Bolt-Joint Diagram of Tension Loaded Bolt (Inspired by Bickford[84])

One can appreciate that for small deformations, within the elastic range of the materials interacting, simple expressions for the bolt and joint stiffness are obtained:

$$K_B = \frac{F_P}{\Delta L} \quad \text{.....(4.1)}$$

$$K_J = \frac{F_P}{\Delta T} \quad \text{.....(4.2)}$$

This was first discovered experimentally by Hooke[12] and Mariotte and further investigated by Riccati and is qualitatively referred to as Hooke's Law. However, the pre-load tension F_P is not known, as it should be a result of the analysis. Hence, other means of computing the stiffness of the bolt K_B and the joint K_J are required.

The bolt-joint diagram (Figure 4.4) provides a useful set of relationships forming the basic system of equations required to analyse the tie rod problem at hand:

$$F_B = F_P + \Delta F_B \quad \text{.....(4.3)}$$

$$F_J = F_B - F_X \quad \text{.....(4.4)}$$

$$\Delta F_J = F_X - \Delta F_B = F_P - F_J \quad \text{.....(4.5)}$$

Similar triangle relationships applied to the bolt-joint diagram on Figure 4.4 also provide helpful equations. From those similar triangle relationships:

$$\Delta F_B = \left(\frac{K_3}{K_B + K_J} \right) * F_X \quad \text{.....(4.6)}$$

$$F_{XCRIT} = F_P * \left(1 + \frac{K_B}{K_J} \right) \quad \text{.....(4.7)}$$

It becomes obvious that values of stiffness K_B and K_J must be known in order to compute ΔF_B. In this case, F_X is known; it is defined as the external load applied. To find the limit case, F_{XCRIT} is introduced as the critical applied load that would lead to gapping of the structure (i.e.: $F_{XCRIT} = F_X$ at $F_J = 0$). Hence, if F_X is greater than F_{XCRIT}, the applied load is too large and leads to gapping failure. Finally, it appears that the initial pre-load must be calculated prior to F_{XCRIT}. The following two sections show how values for the stiffness K_B and K_J are computed for MOST.

K_B calculation:

From a general bolt stiffness definition (Bickford[84]):

$$K_B = \frac{E * A}{L} \quad \text{.....(4.8)}$$

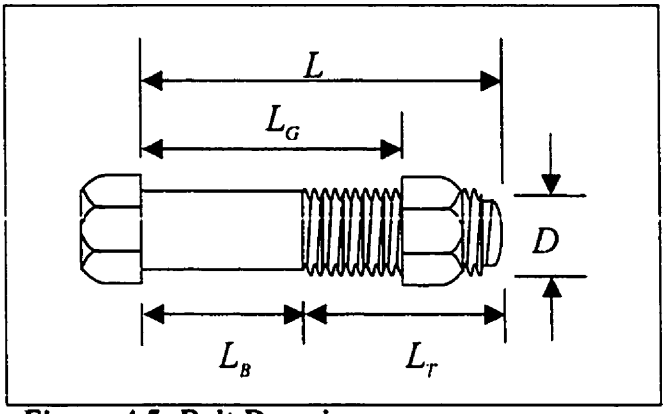

Figure 4.5: Bolt Drawing

Applying **(4.8)** to define the bolt stiffness and taking into consideration that the bolt features two distinct sections (the shank and the threads) as shown in Figure 4.5:

$$K_B = \frac{1}{\frac{L_{be}}{E_B * A_B} + \frac{L_{se}}{E_B * A_S}} \quad \text{.....(4.8a)}$$

Rearranging equation 4.8a:

$$K_B = \frac{E_B * A_B * A_S}{L_{be} * A_S + L_{se} * A_B} \quad \text{.....(4.8b)}$$

where by the definition in Figure 4.5:

$$L_{be} = L_B + \frac{T_H}{2} \quad \text{.....4.9)}$$

$$L_{se} = L_G - L_B + \frac{T_N}{2} \quad \text{.....(4.10)}$$

$$L_B = L - L_T \quad \text{.....(4.11)}$$

$$A_B = \frac{\pi * D^2}{4} \quad \text{.....(4.12)}$$

Now K_B can be calculated, as all variables on RHS of **(4.8b)** are known for any bolt diameter selected. However, this obviously leads to some iterative process as the bolt area should be a result of our analysis and not a known parameter.

K_J calculation:

The previous straightforward derivation cannot usually be applied to compute the joint stiffness as the joint features a complex cross-section. However, a hollow cylinder

of equivalent cross-section A_C can substitute the joint portion that is under compressive loading. It is easier to compute the joint stiffness of a hollow cylinder than that of the real joint and results are shown by Meyer and Strelow[94] to be equivalent or reasonably close to the actual joint stiffness. Generally, the following equation is used by Bickford[84]:

$$K_J = \frac{E_J * A_C}{J} \quad \text{.....(4.13)}$$

The total joint cross-sectional area is graphically defined in Figure 4.6 for 3 different configurations. The equivalent cylindrical cross-sectional area A_c is obtained by multiplying the simplified cross-sectional area A_J (for a single joint) highlighted in black in Figure 4.7 by the number of tie rods used. Hidden safety margin is added as the wall portion of the tray cross-section was neglected.

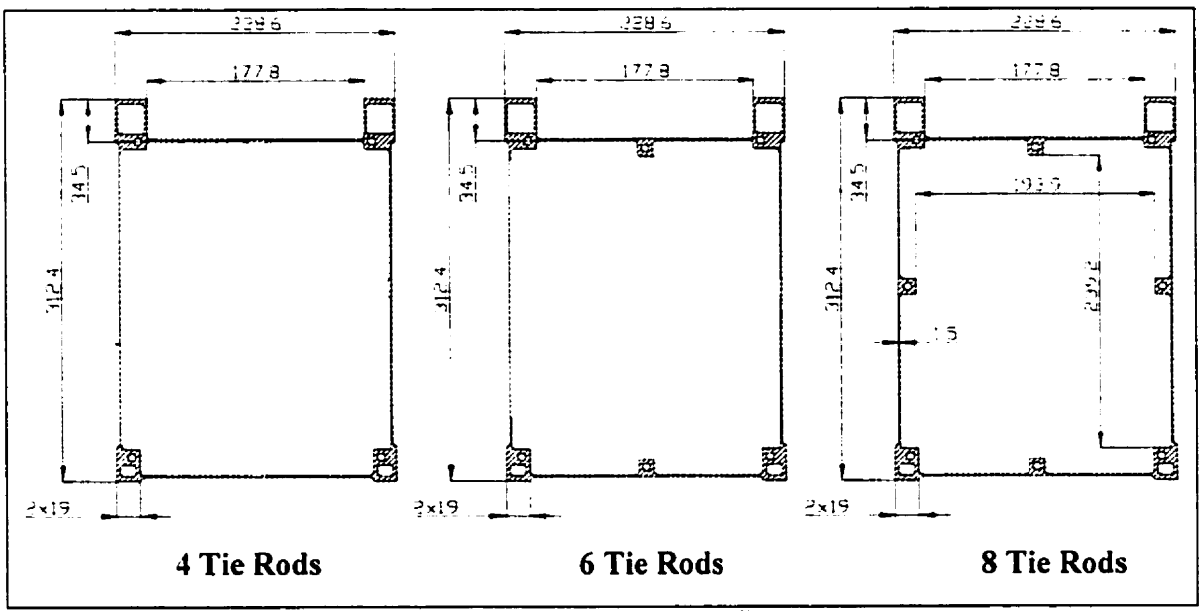

Figure 4.6 Tray cross-section (Different tie rods configurations)

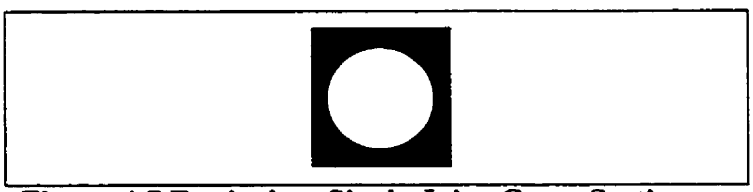

Figure 4.7 Equivalent Single Joint Cross-Section

Hence, the following relationship is obtained:

$$A_C = A_J - A_B \quad \text{.....(4.14)}$$

Linear material behaviour and progressive equilibrium or so-called quasi-static loading is assumed in the derivations. The linear material behaviour is a valid assumption for the MOST since the maximum stress actually allowed is chosen to be far below the material yielding point. Section 4.3 shows the safety factor and margin of safety used to ensure that this is actually the case.

Preloading of the tie rods can easily be made linear (quasi-static preloading assumption) by following a step-wise equilibrium path until equilibrium point EQ_{P1} is reached, and allowing enough time for relaxation effects to stabilise (See Figure 4.4).

However, dynamic loading during launch is obviously far from linear and in progressive equilibrium (quasi-static assumption), when going from EQ_{P1} to any second equilibrium point EQ_{P2} under any time varying externally applied load F_X. Hence an additional safety factor was introduced in the analysis to account for the dynamic loading effects when going from EQ_{P1} to EQ_{P2}. An equivalent static load F_X larger than the actual dynamic launch load is computed to account for dynamic loading effects. The equivalent static load determination is described in detail in Section 4.4.2. Although the dynamic stiffness response of both the joint and the bolt is expected to be highly nonlinear, the equivalent static analysis should serve as a conservative design approach to the problem at hand. EQ_{P2} will probably never be in static equilibrium, but the analysis presented assumes that the static point considered will never be exceeded under the actual dynamic launch conditions. Enormous computation and testing requirements, along with the complexity of a complete nonlinear analysis forced the less rigorous but conservative, low cost design approach taken.

The following sections describe in greater detail the design steps taken for MOST. Particularly, Section 4.4 carefully assesses the maximum loads to be supported, Section 4.5 examines each failure mode, and Section 4.6 shows derivations for each failure mode along with a sample calculation.

4.3 Safety Factors vs. Margin of Safety

Many organisations have established specifications for standards and safety: AA, ANSI, ASM, ASME, ASTM, IFI, ISO, BSI, BIPM, and SAE (See list of acronyms).

Hence, there is a need to define what is believed to characterise a safe micro-satellite structure and under what conditions and standards. The safety factors for the MOST general design analysis were set according to the Delta II Secondary Payload Planner's Guide[59] since it was chosen as the baseline launch vehicle for the MOST mission.

Obviously, the tie rods must hold the tray together, prevent gapping between trays from occurring, and sustain a clamping force avoiding natural frequency of vibration drops because of loose trays. This should be the case even when launch loads are applied to the structure considering the pre-load tension applied to the tie rods initially. The tie rods must also ensure no slipping between trays. Finally, the pre-load requirement and external loads applied must not lead to thread stripping. Hence, there is a need to define four margins of safety, each related to one of the failure modes: the first is related to the yielding of the material or so-called stress problem, the second is related to the thread stripping problem, the third is related to the gapping problem, and finally, the fourth related to the slipping problem. The tie rods must be designed to ensure safety of the structure accounting for the worst case criteria from those four potential problems or failure modes. One can readily acknowledge that the yield strength of the material selected will be a key criterion for the design problem at hand since it impacts the four failure modes. The maximum actual stress must be less than the computed maximum allowable stress, which is only dependant on the material selection and geometry. From the yield stress of the material used, the maximum allowable stress σ_{MA} is defined as:

$$\sigma_{MA} = \frac{\sigma_{MY}}{SF} \quad \text{.....(4.15)}$$

In summary, preloading of the bolts (tie rods) must be designed such that the entire structure can withstand the real launch loads, on-orbit separation loads, and transportation loads without the occurrence of bolt stripping, tray gapping, tray slipping or material yielding.

The general margin of safety for the slipping, stripping and gapping problems are defined as follows:

$$MS = \frac{f_c}{(F_c * SF)} - 1 \quad \text{.....(4.16)}$$

The general margin of safety for the stress problem:

$$MS = \frac{\sigma_{MY}}{(\sigma_{MD} * SF)} - 1 \quad \text{.....(4.17)}$$

Substituting **(4.15)** in **(4.17)**, the simplified following equation is obtained:

$$MS = \frac{\sigma_{MA}}{\sigma_{MD}} - 1 \quad \text{.....(4.18)}$$

Delta II Safety Factor Requirements [59]:

If the design is qualified by analysis only, positive margins must be shown for load safety factors of 1.65 on yield and 2.0 on ultimate strength according to the Delta II Secondary Payload Planner's Guide [59]. These figures are used throughout the analysis. After discussions with senior engineers in the aerospace field, it appears that a safety margin of 0.25 is taken as a conservative figure when a safety factor of 2.0 is considered for aerospace design excluding manned spacecraft. If a safety margin of zero is used, it means that the parts would be stressed to the maximum allowable stress limit, which can be considered as designing for maximum *constrained* or *safe* performance but not maximum reliability. Hence the trade-off value of 0.25 makes sense within the aerospace application at hand as it is very close to maximum *constrained* (safety factor of 2.0) performance without totally ignoring reliability issues of a new design.

A relatively new alternative to design based on a safety factor is to use the reliability method. It consists of a statistical measure of the probability that the mechanical part being analysed will not fail. The method of evaluating the reliability (value given from 0 to 1) is based on a normal Gaussian distribution of material properties and experimental data at hand. This method can only be used instead of the time-proven old-fashioned safety factor method when data from testing is available. In the case of the tie rod analysis, no testing is planned and hence the reliability method cannot be used. However, whenever possible, the reliability method to design should be used instead, as it constitutes a fairly accurate method to directly assess risks in design tradeoffs.

4.4 MOST Tie Rod Design Steps

To design MOST tie rods and ensure no failures, a step-by-step design procedure is adopted: identification of problem variables, problem definition including loads

determination and design goals, careful assessment of failure modes, analysis tools and equations derivation, evaluation and presentation of results. The following sections highlight these crucial design steps, and also include all required proofs, details, descriptions and justifications.

4.4.1 Identification of Tie Rod Design Parameters and Variables

The main tie rod design parameters that remain constant through a given analysis are the joint material properties and joint cross-sectional area, the applied loads, the safety factor, and the safety margin. The safety margin for each of the four failure modes examined (yielding, stripping, gapping, and slipping) is set consecutively at 0.25. The resultant safety margins for the concomitant three failure modes are computed (i.e. for yielding, the stripping, gapping, and slipping safety margins are computed). The worst case of these four analyses will govern the design of the tie rods. Following this design approach, it is possible to point out what is the limiting case only after going through each failure mode analysis. This should appear much clearer in Section 4.5 and 4.6.

The main tie rod design variables that can be varied to lead to an optimised solution are the bolt diameter and bolt material properties, the number of tie rods, the nut selection and the tie rod configuration (geometry factor). The nut selection is discussed in Section 4.5.1.2.2 where the thread-stripping problem is defined. The nut is a design variable. However, the nut selection has very little impact on the design, as a stronger nut can always be selected at little extra cost. Hence, the nut selection will not be considered a design variable throughout the analysis presented here.

4.4.2 Structural Loads Determination

Static load analysis equivalent to the actual dynamic loading problem:

- Total Mass of MOST (as of Phase A Report[61]) : 56kg
- Launch Load Expected (Acceleration): $10 * g * 2.0 * \sqrt{3} = 20\sqrt{3}\ g$ (RMS)

The factor of 2.0 was set according to the Delta II Manual for approval based on analysis only, without any real tests. The $\sqrt{3}$ factor accounts for the 3-D dynamic loading effects. This factor is quite arbitrary but makes sense after a review of the literature on stress concentration (See Peterson[95], Roark[96], and Seika[97]). Its value

is justified by stating that when a load is applied in one of the 3 axes, part of this load is "felt" by the two other axes and vice-versa, since MOST is a 3-dimensional body. Moreover, an equivalent static load is applied to the structure that is in fact loaded dynamically. Hence, there is a need to account for the fact that part of it barely moves at the constrained boundary, and that part of it sustains much worst loads, usually by a factor of 2, at the tip of the structure. On average, the structure will statically support $\sqrt{3}$ times the dynamic load when dynamic effects and 3-axis simultaneous loading are taken into account. The loading case considered here is the worst case. Assuming support at the middle of the satellite (PAA boundary condition[59]), half of the mass hangs on each side (considering DELTA II[59] maximum acceleration of $10\,g$'s RMS dynamic load), and the following force, equivalent to the real distributed tray mass loading force, acting on each side of the satellite is obtained:

$$F_T = 2.0 * \sqrt{3} * \left(\frac{56kg}{2}\right) * 10 * g = 9515.2N \quad \text{.....(4.19)}$$

Equivalent static analysis (free-body-diagram of y-z plane view):

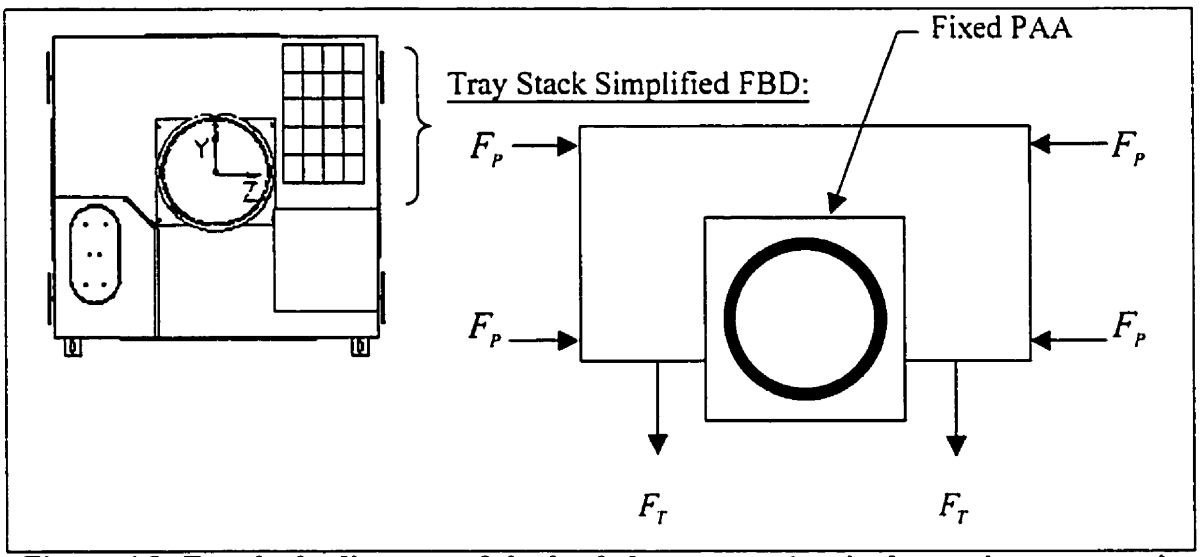

Figure 4.8: Free body diagram of the loaded structure (equivalent point mass static load)

From symmetry of the problem, top and bottom tie rods are sized equally. It is assumed that the upper tie rods take all the bending loads (restraining the entire stack from gapping). In the analysis, F_T denotes the total external force applied to the pre-tensioned upper tie rods (See y - z plane previously shown on Figure 4.8).

Launch loads are applied in three directions: x, y and z. The worst case for MOST is when the vibration launch loads are applied in the x direction, since the x-moment arm is shorter than the y-moment arm, which leads to sustain a larger force (See FBD on Figure 4.8).

For MOST (based on Detailed Design), and from FBD (Figure 4.8):

x - moment arm = 0.1252m
y - moment arm = 0.15m
z - moment arm (point mass equivalent to the distributed mass load) = 0.157m

$$F_{XT} * 0.1252\text{m} = 9515\text{ N} * 0.157\text{m} \quad \text{(4.20)}$$

Finally, from **(4.20)**, the total external applied load to the pre-tensioned tie rods is found:

$$F_{XT} = \mathbf{11932\text{ N}} \quad \text{(4.21)}$$

4.4.2.1 Bending Loads

The microsat structure should be designed not to bend much under launch loads. This is one of the reasons why the tray stack is used as a compressed joint tightened with some tie rods. In addition to the tensile stress in the tie rods due to the preload and the launch loads, the stress under tray stack bending must be added. The assumption made here is that the maximum bending stress (very small compared to all other stresses) is always present to account for the worst case scenario. However, it is understood that the real launch loads never bend the microsat structure at all times, if bending even occurs at all. Hence, the maximum bending stress is to be added to the tensile stress as a worst case scenario. From Eshbach[85], the following expression for the maximum pure bending stress was found:

$$\sigma_B = \frac{E_B * D}{2 * R_C} \quad \text{(4.22)}$$

For MOST, a maximum bending deflection of 1.5mm from the centreline of the satellite to its end, which is the limit case before shearing of trays (tray wall thickness being assumed as 1.5mm). In those limit conditions, the radius of curvature R_C can be found as:

$$R_C = \frac{\left(\frac{J}{2}\right)^2 + t^2}{2 * t} \quad \text{(4.23)}$$

with $t = 0.0015$m and $J = 0.628$m: $R_C = 38.66\text{m}$ **(4.24)**

4.4.2.2 Torsional Loads

Torsional moments are quite complex to account for when dealing with bolts. Material friction factors vary a great deal as shown in experiments. Many equations attempt to accurately measure torsional stresses induced in bolts. Motosh[98] proposed an equation from which, according to Bickford[84], the answer is in error by a negligible amount. Assuming substitution of the tie rods by an equivalent cylinder, the resulting torsional stress is found to be a function of the pre-load force F_p, and is given as:

$$T_{tor} = F_p\left[\frac{P}{2\pi} + \frac{\mu_t r_t}{\cos\beta} + \mu_n r_n\right] \quad \text{.....(4.25)}$$

Equation 4.25 shows that the input torque is resisted by three reaction torques. The first one is produced by the inclined plane action of nut threads on bolt threads. This is the effect of the bolt material stretching. The second one is created by friction between the nut and bolt threads. The last one is created by friction between the face of the nut and the joint. After giving it some thoughts, one realises that all other effects are insignificant and negligible on the torque measurement. Hence, the Motosh[98] equations should be used when comes the time to compute the torque required to assemble the trays together and achieve the desired pre-load.

And the resulting stress can be computed using equations 4.25 and 4.26 [98]:

$$\sigma_{tor} = \frac{16 * T_{tor}}{\pi * D^3} \quad \text{.....(4.26)}$$

4.5 Tie Rod Design Goal (Minimising Bolt Size)

For virtually any aerospace related design problem, the main goal is to come up with the best trade-off between maximum performance and minimum cost. This general design goal can be translated for the tie rod design problem as: designing for minimum weight and maximum stress, within safety factor and safety margin limit set previously in Section 4.3, at minimum cost. The ultimate goal in optimising our tie rod design is therefore to come up with the lightest tie rod configuration. The four main variables to achieve this goal, as outlined in Section 4.4.1, are the number of tie rods, the material used for the tie rods, the size of the tie rods, and the location of the tie rods. Assuming

there is a need to simplify the design by having a minimum of 4 tie rods, which should lead to a low-cost solution, the only remaining variables are material selection and bolt size. Ensuring satisfaction of all constraints defined by each failure mode allowing only the number of tie rods, the bolt material, and the bolt size to vary can be programmed easily. The Fortran90 program (See Appendix C.1) was then modified to accommodate more tie rods although the 4 tie rod configuration was found to be best suited for MOST.

4.5.1 Tie Rod Design Failure Modes

The main challenge when facing a design issue is to identify the primary design criteria. For the MOST tie rod design case, four major failure modes are investigated, one being related to the assembly per se or vibration issues (gapping failure), and the three other ones related to material failure issues (yielding, stripping, and slipping).

4.5.1.1 Vibration - First Natural Frequency of MOST Structure

Under the launch loads described earlier in Section 4.4.2, the primary bus structure would potentially bend as if it was a single piece (See Figure 4.9), as long as the applied load does not exceed F_{XCRIT} (See Section 4.2).

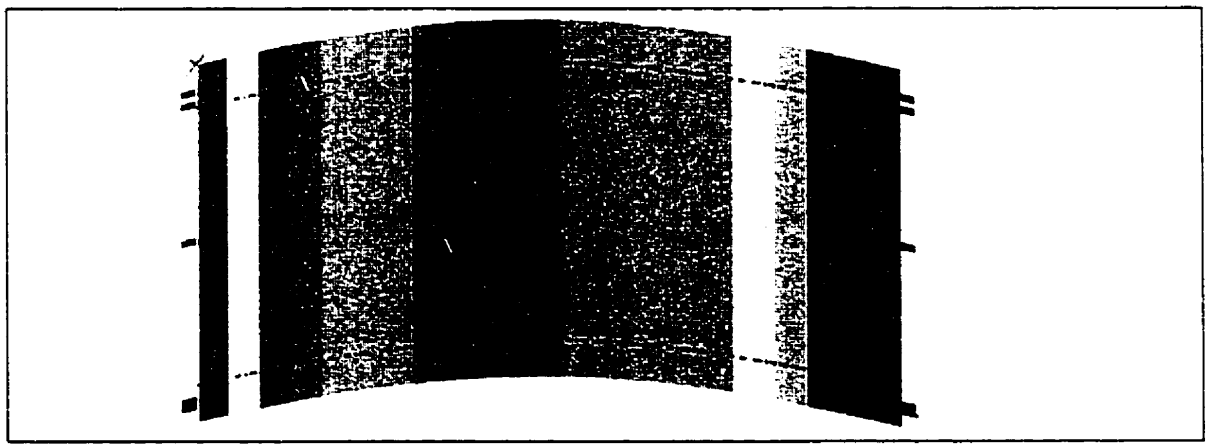

Figure 4.9: Exaggerated bending deformation of the structure (with $F_X < F_{XCRIT}$)

Unfortunately, the tray bus structure no longer acts as a one-piece structure if the external load exceeds F_{XCRIT}. It would not be possible to have a one-piece bus structure to resolve this issue, as easy integration of bus sub-systems would not be possible. This option can be discarded simply by thinking of all the electrical connections that could potentially get unplugged by assembling all sub-systems into a single shell. Hence, a

tray-like structure assembly is best suited. However, this brings up some issues in terms of the natural frequency of our entire system.

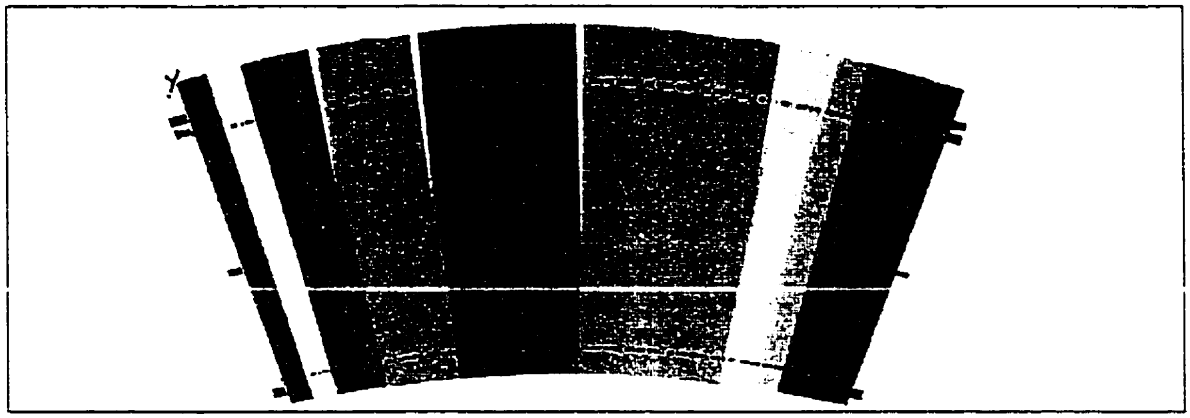

Figure 4.10: Exaggerated bending deformation of the structure (with $F_X > F_{XCRIT}$)

If not tied properly, the tray structure assembly may become loose (See top part of the bus structure in Figure 4.10) under bending induced by launch loads. As shown on Figure 4.10 the structure may become somewhat flimsy. This would lower drastically the natural frequency response of the whole satellite and potentially lead to a mission failure. Hence, there is a need to make sure that there is enough preload tension in the tie rods in order to ensure that even when the launch loads are applied, the entire structure will remain a single unit and not a weak assembly of many trays with a much lower natural frequency response.

The challenge here is to quantify this problem or potential rupture in design. When should a bunch of trays tied up together be practically considered a single strong unit, and when should it be considered as acting as if it was really composed of smaller units? To answer that question, let's say that the analysis can assume that with a safety factor of 2.0 combined with a safety margin of 25% on the critical applied load, this phenomenon cannot become an issue. The present work assumes that in all analyses, the structure is close enough to an equivalent single piece, as long as the joint part of the tied up structure is under fair compressive loading even when launch loads are applied. However, quantifying the term "fair" compressive loading still remains an issue. To be rigorous in our assertion, it is important to mention that a tray stack will never act as a single piece, since it is not. Hence, the issue is to be able to know when the assumption made leads to results that are very close to the physical behaviour of the real satellite

structure. After determining A_{SMIN} and A_{SMAX}, all the bolts considered will feature $F_J >> 0$ such that the assumption made holds true. However, it is understood that the friction forces at the interface of two separate blocks will never be as strong as the atomic cohesion forces of a continuous piece of material. However, as long as the compressive force in the joint is large ($F_J >> 0$), the assumption made is reasonable.

To achieve our design goals, it becomes first necessary to analyse and clearly describe all failure modes, which is the main focus of the following sections.

4.5.1.1.1 Tray Gapping

To prevent gapping at the top of the structure, the upper tie rods must compensate for the bending loads induced by the launch vibration loads. Only the top or bottom half of the tie rods do work or absorb energy at any maximum bending deflection, as shown in Figure 4.10. In between maximum bending and no bending, during dynamic launch loading, the top and bottom tie rods share the work done to counteract the external loads applied. Obviously, pre-tensioned tie rods when loaded in compression are not doing any useful work but are simply, in the worst case, returning to their unstressed state, which is not an issue since it is impossible to compress the joint enough for that to happen. The gapping limiting criteria on the bolt stress area are derived in Section 4.6.4.

It is of interest to note that the bending stress state changes radically within the joint from a design using a tray stack with tie rods (See Figure 4.12) to a design using a one-piece shell structure without tie rods (See Figure 4.11). The joint, the primary structure in the case of MOST, suffers much less in a tray stack design as the tie rods are carrying much of the applied external load. This obviously assumes that the tray stack is stiffer than the bolts, which is the case in MOST's tray stack assembly design.

Bolts that are subjected to external loads, at launch time for example, are tension-loaded even more on one side of the stack from bending loads. Therefore it is necessary to evaluate how the bolts and the joints are sharing this external load. This is where a complete bolt-joint diagram (Figure 4.4) can be truly appreciated for its simplicity.

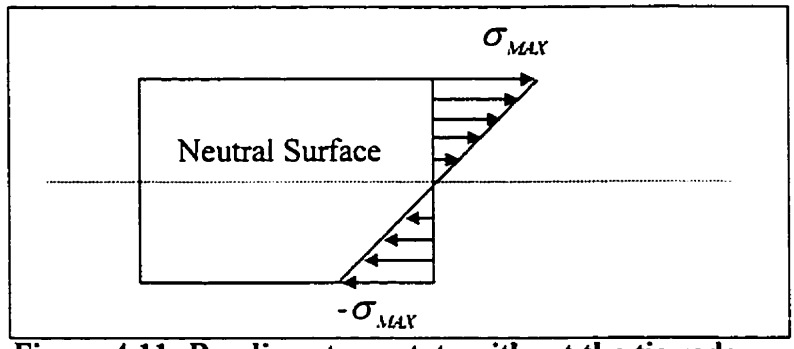

Figure 4.11: Bending stress state without the tie rods

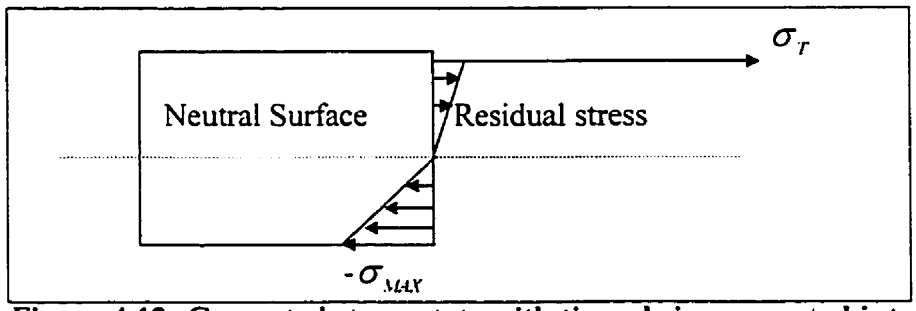

Figure 4.12: Corrected stress state with tie rods incorporated into the structure.

As mentioned earlier, the tie rods must maintain $F_J >> 0$ at any given time (to avoid vibration problems) especially when the launch loads are applied. Hence, a valid lower boundary would be to set F_J to be equal to a minimum force. This minimum compression in the joint would ensure that, indeed, the structure would act as one-piece. Here, it is observed that in the limit case ($F_J = 0$) F_X becomes equal to F_{XCRIT}. The challenge is to quantify that minimum value of F_J which will prevent the structure from becoming flimsy, i.e. to prevent the first natural frequency of the structure from stepping down drastically. One could argue that as long as F_J is greater than zero when the maximum or worst case load is applied, even slightly, the structure would almost act as a whole. However, this limit case when F_J tends to zero is very difficult to analyse. In fact, our analytical model based on the material elasticity curves does not allow drawing any conclusions or even getting meaningful results when F_J tends to zero. Indeed, the elastic resistance at the interface between two trays is missing (not a single piece), and should be compensated by the preload force of the tie rods. Hence, a constraint on F_P

has to be defined to guide the final tie rod size selection ensuring that $F_J >> 0$ at all times.

Considering the fact that in all our calculations a safety factor of 2.0 is used along with a positive margin of safety of 0.25, all bolt sizes between the limit boundaries A_{SMIN} and A_{SMAX} are considered a *failure-free* selection.

4.5.1.2 Material Issues

Although vibration and tray gapping is of great concern, a major design limiting factor is the material. The material yielding is the key design variable for tie rod sizing as presented in the sections to follow. Three major subcategories of material failure were investigated: pure tie rod material yielding under multiple loading, bolt thread stripping, and tray slipping.

4.5.1.2.1 Material Yielding

The first material failure mode investigated is, understandably, the pure material yielding under combined loading. Pre-tensioned tie rods combined with tensile launch loads and bending of the primary structure leads to a limiting case. The material yielding limit case is the minimum stress area of each tie rod. The expression for the minimum stress area is obtained in Section 4.6.2 and the basic set of equations is presented in Section 4.2.

4.5.1.2.2 Thread Stripping

The second material failure mode investigated is thread stripping. This limiting case ensures that the tie rod threads won't strip or shear under the additional applied force during launch. To achieve that task, and derive another expression for the minimum stress area required, selection of a nut and a comprehensive analysis of the thread form selection must be presented.

Nut selection

Knowing the strength of the tie rod alone is not sufficient, since it is never used alone. For a large variety of bolt sizes, a designer can find standard tables such as in

Bickford[84] (p.106-107) that indicates the best nut to use for a given application and bolt size. However, for more sophisticated or complex bolt applications, such as in the case of satellite tie rods, designers can only follow guidelines.

In general, the nut needs to support more loads than the bolt. However, it is wise to use a softer material for the nut, as it would better conform to the tie rod threads when loaded. Those two guidelines seems contradictory at first but one must understand that the strength of a part depends on dimensions and shape as well as on material properties. To increase safety or reduce strip failure, one simply needs to increase the length of thread engagement. Again, for more complex applications, Bickford[84] recommends that the nut be selected thicker and heavier than needed as it is always possible to do so. For MOST, the design will assume that the nut and bolt materials are the same and that the tie rod will fail by stripping before the nut does. Those assumptions are reasonable and simplify the issues at hand considerably.

Thread selection[99] [100] [101] [102] [103] [104] [105] [106] [107]

The threads obviously play an important role in the tie rods design. All the modern fastener thread profiles are based on an arrangement of 60° angles. In the US, there are three principal inch series thread form standards: UN, UNR and UNJ. The military standard is UNJ and they are described extensively in MIL-S-8879C. The UNJ form has generously rounded roots. The code letters M and MJ identifies the metric threads. The basic geometry of metric and inch threads is identical. Among those profiles, one can find different thread series:

1. UN, UNR or UNJ threads define the constant pitch series
2. UNC, UNCR or UNCJ threads define the coarse pitch series
3. UNF, UNFR or UNFJ threads define the fine pitch series
4. UNEF, UNEFR or UNEFJ threads define the extra fine pitch series

Metric series simply use the pitch distance between two teeth, in millimetres. It is up to the user to know if they feature extra-fine, fine or coarse pitch. For example, M6x1 would specify a thread having a nominal diameter of 6mm and a pitch distance of 1mm.

A complete description of nomenclature can be found in any good mechanical design book (Machinery's Handbook[108]) so no further comments will be made in the present document. What the designer is really looking for is a way to make sure that

threads will not fail under shear load. Many researchers have looked at this problem before. The derivation of the stripping material failure limit case is presented in Section 4.6.3 and is based primarily on readings of Alexander[109], Blake[110], Ellison[111], FED-STD-H28/2B[112], Gill[113], Sharman[114], and the Machinery's Handbook[108].

4.5.1.2.3 Tray Slipping

The last material failure mode that is considered is the slipping between two trays under launch loads. The maximum shear force can be easily determined from the previous equivalent static load analysis that accounts for the real dynamic loading. The maximum shearing force will be equal to the vertical force applied during launch time (i.e. F_S = 9515N on each side). There is a need to emphasise that this is higher than the actual maximum shear the structure will ever experience, as the satellite structure features a payload attachment assembly that is not a fixed point at the centre of the spacecraft but roughly a nine inch diameter ring, effectively reducing the amount of mass hanging on both sides of the PAA. Moreover, the tray stack features a discontinuous mass distribution, and hence a stepwise shear force distribution. However, the analysis assumed that the satellite structure is clamped at its centre as it just ensures results that are slightly safer. The derivation is done in Section 4.6.4. Slippage of more than 1.5mm is only possible if the tie rod fails in shear. Hence, the tray slipping failure mode is linked to shearing of tie rods failure mode at that point (i.e. slipping cannot be large, unless the tie rods fail in shear first). As further explained later, the tie rods cannot generate enough preload to compensate for the slipping of trays under the shear loads. Some design modifications are proposed in section 4.6.7.

4.5.1.2.4 Tie Rod Fatigue

Most bolts, which fail during normal operation, do so in fatigue. Generally, higher pre-load reduces fatigue failure risks as mentioned by Gere and Timoshenko[34]. The combined effect of higher mean stress in the bolt and lower load displacement prolongs the bolt fatigue life. That being said, the microsatellite tie rods will suffer dynamic loading only during launch time which is fairly short when compared to the

lifetime of the satellite, or even the lifetime of bolts in general. Hence, for these reasons, it can be safely assumed that no fatigue failure could possibly occur. Bolt fatigue mechanisms were investigated by Milestone[115] and Osgood[116].

4.5.1.2.5 Tie Rod Creep

The combinations of temperature, loads, and time that produces creep and possibly creep failure or creep fracture of a member depends on the material and the environment. Although very hostile, the space environment does not represent a real creep failure danger, especially since the remaining load on the tie rods when on-orbit is simply the preload. Temperature changes within the tray stack are of the order of about 60°C to 80°C in the worst cases. These variations do not occur often when considering MOST's sun-synchronous orbit. Moreover, materials such as aluminum and stainless steel can undergo much larger temperature changes before creep can be considered a possible failure. Hence, the tie rod design presented here assumes that no creep failure could possibly occur.

4.5.1.3 Pre-load and Torque Physical Limitations

Maximum preload obtained in relation to the maximum torque applied is mainly a cost concern. Hence, the analysis presented here assumes that the resulting tie rods pre-loading requirement will fall within physical limitations of maximum torque. Selection of a torque value for a given pre-load requirement and fastener material can be complex and is further discussed in Sections 4.9 and 4.11.

4.6 MOST Tie Rods Design along with a Sample Calculation

In order to demonstrate how the equations presented in Section 4.2 are applied for the design of MOST's tie rods considering all failure modes described in Section 4.5; the following sections show a sample case and numerical calculation based on well-defined typical parameters. The sample calculation shall provide the reader with a better understanding of the table of results presented in Section 4.12.

Only four failure modes are retained from all modes explained in Section 4.5: material yielding, bolt thread stripping, tray gapping, and tray slipping under launch loads. It is obvious that the maximum force F_{BMAX} acting on the bolt, when launch loads are applied, is constrained by either the material yielding or the bolt thread stripping. It is also obvious that the minimum preload force F_{PMIN} required is constrained by either the tray gapping or the tray slipping. Hence, four combinations are possible. Derivation of the minimum stress area required is derived for each combined failure problem in Section 4.6.2.

4.6.1 Sample Calculation Parameters and Variables Definition

The following subsections assign numerical values for the sample calculation considered. It provides numerical values for the bolt material, joint material, safety factor, margin of safety, applied load, number of tie rods, joint geometry, and maximum bolt stress area.

4.6.1.1 Bolt material selected for sample calculation

E_B	σ_{BMY}	τ_{BMS}	$_B$	ρ_B	μ_{BS_Al}
110.316 GPa	861.85 MPa	572.27 MPa	0.31	4428.784 kg/m^3	0.34

Table 4.1: Ti-6Al-4V-AMS-4928 Properties (ref: MIL-HDBK-5[77])

4.6.1.2 Tray material (joint material) selected for calculation

E_J	σ_{JMY}	τ_{JMS}	$_J$	ρ_J	μ_{JS_Al}
69.0 GPa	275 MPa	26.2 MPa	0.33	2715 kg/m^3	0.42

Table 4.2: Aluminum - 6061-T6, T651 Properties (ref: MIL-HDBK-5G[77] and ASTM, vol.8)

4.6.1.3 Safety factor and safety margin

The safety factor and safety margin used for all sample calculations (Delta II Manual[59]):

$$SF_{GENERAL} = 2.0,\ SF_{YIELD} = 1.65,\ SF_{ULTIMATE} = 2.0, \text{ and } MS_{GENERAL} = 0.25$$

4.6.1.4 Applied load & Number of tie rods

As computed in Section 4.4.2: $F_{XT} = \mathbf{11932\ N}$

F_X obviously decreases if there is more than one tie rod. The design must use a minimum of 4 tie rods so F_{XT} is divided by 2 ($NT = 4$: four tie rods total and two tie rods taking loads as shown in Figures 4.8 through 4.12).

$$F_X = \frac{F_{XT}}{2} \text{ for 4 tie rods total} \quad \textbf{(4.27)}$$

or

$$F_X = \frac{F_{XT}}{3} \text{ for 8 tie rods total} \quad \textbf{(4.28)}$$

The sample calculation analysis will assume the **8 tie rods** configuration case **(4.27)**:

$$F_X = \frac{F_{XT}}{3} = \mathbf{3977\ N} \quad , \quad NT = \mathbf{8}$$

4.6.1.5 Joint Geometry Information

The joint area for MOST was simplified to a square of 12.7mm by 12.7mm (Figure 4.7):

$A_J = \mathbf{0.00016129\ m^2}$

The total joint thickness is the actual width of the tray stack of the satellite:

$J = \mathbf{0.628\ m}$

The other geometrical values required are:

$T_N = \mathbf{0.004\ m}$ (approximate value, does not influence end result if neglected)

$T_H = \mathbf{0.004\ m}$ (approximate value, does not influence end result if neglected)

$L_T = J = \mathbf{0.628\ m}$ (in our case tie rods are threaded all the way)

$L_B = \mathbf{0\ m}$ (no non-threaded portion, assume off-the-shelf threaded rods)

$L_G = \mathbf{0.628\ m}$

Then, the effective length of the body L_{be} using **(4.9)** can be computed:

$L_{be} = \mathbf{0.002\ m}$

The effective length of the threads L_{se} using **(4.10)**, can also be computed:

$L_{se} = \mathbf{0.630\ m}$

4.6.1.6 Maximum Bolt area

The maximum stress area of the bolt is something that is to be determined as a geometrical limiting factor. A_{SMAX} is easy to compute, as there is a physical boundary

that cannot be exceeded, i.e. the joint size. Hence, based on the area of the joint A_J, the maximum stress area A_{SMAX} can be computed as follows:

$$A_{SMAX} = 0.625 * \frac{\left(A_J * \frac{\pi}{4}\right)}{3} \quad \text{.....(4.29)}$$

The expression in bracket, $A_J * \frac{\pi}{4}$, corresponds to the largest circle that you can draw in a square cross-section (See Figure 4.13). The factor of 3 is arbitrary and was set on the basis that the maximum stress within the joint part should not exceed half of the maximum yield strength of the joint material, which is aluminum (See Section 4.7). If this idea is expressed in terms of the percentage that the diameter takes: 57.7% of the side is taken by the hole in diameter and 21.1% is left on each side for joint thickness. The factor of 3 is shown in Figure 4.13 going from the left joint black area to the right. It basically assesses that space must be allowed between the side of the joint and the circumference of the bolt. Otherwise, there would be no joint at all. It was found that by dividing the result by 3, the joint wall thickness would be sufficient enough to ensure that stress concentration in the joint material would be under the prescribed joint maximum allowable stress. This assumption is further discussed later as stress concentration is an advanced stress subject and must be treated fully. A full derivation of the stress concentration factor of a square piece with a hole at its centre is included in Section 4.7 of the present work. The 62.5% factor accounts for the amount of material between the root and nominal diameter of the bolt that does not take much of the tension load, which is shown on the right side of Figure 4.13 as a dashed line circle. This is, of course, an additional hidden margin of safety that should ensure a conservative result.

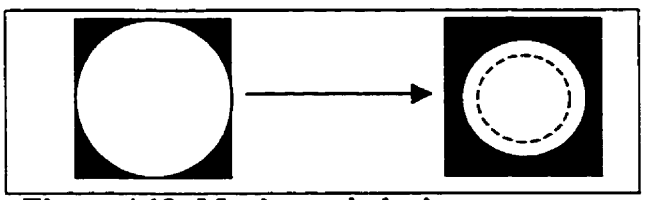

Figure 4.13: Maximum bolt size

Considering the sample case values defined previously, and using **(4.24)**, A_{SMAX} becomes:

$$A_{SMAX} = \mathbf{2.6391E\text{-}5\ m^2} \quad \text{.....(4.30)}$$

Defining the maximum bolt size A_{SMAX} is obviously of little use in determining the optimum minimum bolt size. However, it serves as a maximum boundary, which in turn constitutes a very useful basis for confining our search of the optimum design.

4.6.1.7 Sample case bolt size selection

A_S and A_B are tabulated values for any given bolt. For example, in the sample calculation, a metric bolt M6.3x1 is used where:

$$A_S = \mathbf{2.26E\text{-}5\ m^2},\ A_B = \mathbf{3.1172E\text{-}5\ m^2}, \text{ and } D = \mathbf{0.0063m} \quad \text{.....(4.31)}$$

4.6.2 MOST Tie Rods Design - Four Limiting Factors

Four failure modes were highlighted in Section 4.5. These four failure modes can be mathematically represented in terms of design constraints. The derivation of these constraint equations is presented in the following subsections.

4.6.2.1 Material yielding constraint

After determining the applied load F_X, there is a need to compute the value of F_B, which is the total force that is acting on the tie rod when the external loads are applied. This is where the design constraint is introduced. The analysis simply assumes that the bolt stress cannot exceed the material allowable stress.

$$F_{BMAX} = \frac{\sigma_{MA} * A_S}{(MS + 1)} \quad \text{.....(4.32)}$$

This stress limit ensures that the bolt will not fail because of material yielding. The stresses in the joint material are assumed to be below the joint material maximum allowable stresses under the resultant joint compression force. This assumption and a careful look at stress concentration within the joint is studied in Section 4.8.

As previously outlined in Section 4.4.2.1, the bending load assumption is taken into account by reducing the maximum allowable stress:

$$\sigma_{MA} = \sigma_{BMA} - \sigma_B \quad \text{.....(4.33)}$$

Recall that the maximum bending stress σ_B was defined in **(4.20)**:

$$\sigma_{MA} = \sigma_{BMA} - \frac{E_B * D}{2 * R_C} \quad \text{.....(4.33b)}$$

Assuming the bolt area can be $A_B = C_1 * A_S$, where C_1 is a constant of proportionality between A_B and A_S, and varies in practice from 1.6 to 1.1. As bolts get bigger, C_1 tends toward 1.1. However, to account for the worst possible scenario, the value of 1.6 is considered. The bolt diameter can be expressed as:

$$D = \sqrt{\frac{4 * C_1 * A_S}{\pi}} \quad \text{.....(4.34)}$$

Substituting D in **(4.33b)** and replacing the resulting σ_{MA} in **(4.32)**:

$$F_{BMAX} = \frac{\sigma_{BMA} * A_S - \frac{E_B * A_S}{2 * R_C} \sqrt{\frac{4 * C_1 * A_S}{\pi}}}{MS + 1} \quad \text{.....(4.32b)}$$

Where R_C was previously defined as:

$$R_C = \frac{\left(\frac{J}{2}\right)^2 + t^2}{2 * t} \quad \text{..... (From equation 4.23)}$$

4.6.2.2 Bolt thread stripping constraint:

In FED-STD-H28/2B[112], a simple way of computing the maximum force that can be applied given a bolt and a nut is presented here. This is the force required to strip the threads of a bolt or a nut:

$$F_{BMAX} = \frac{\tau_{BMA} * A_{TS}}{(MS + 1)} \quad \text{.....(4.35)}$$

Hence, the maximum force F_{BMAX} that can be applied to the bolt ensures no threads strip failure is computed. This analysis is essential in our attempt to eliminate all possible failure modes. As previously mentioned, the assumption can be made that the nut and bolt materials are the same and that the bolt will fail by stripping before the nut does. This enables easy computation of A_{TS}:

$$A_{TS} = \frac{\pi * E_S * L_e}{2} \quad \text{.....(4.36)}$$

But L_e can be defined as:

$$L_e = \frac{4 * A_S}{\pi * E_S} \quad \text{.....(4.37)}$$

Combining equations 4.36 & 4.37:

$$A_{TS} = 2 * A_S \quad \text{.....(4.38)}$$

From equation 4.35 & 4.38:

$$F_{BMAX} = \frac{\tau_{BMA} * A_{TS}}{(MS+1)} = \frac{2 * \tau_{BMA} * A_S}{(MS+1)} \quad \text{.....(4.39)}$$

4.6.2.3 Tray gapping constraint:

Tray gapping is a two-fold failure mode. First, gapping means exposure of the inside of the satellite to the outside environment and its impurities will occur. Secondly, gapping means the structure will become flimsy and the first natural frequency drastically drops (See Section 4.5.1.1.1). The design boundary relies on a design constraint that is imposed by F_{XCRIT}, since gapping is directly related to the maximum possible applied load. It is based on the fact that F_X is known. This result is then used to compute F_B and all other parameters required in the analysis. Hence, the following limit can be defined:

$$F_{XCRIT} = F_X * SF * (MS+1) \quad \text{.....(4.40)}$$

But F_{XCRIT} was defined as:

$$F_{XCRIT} = F_P * \left(1 + \frac{K_B}{K_J}\right) \quad \text{..... (From equation 4.7)}$$

Combining **(4.7)** and **(4.40)**:

$$F_{PMIN} = F_X * SF * (MS+1)\left(\frac{K_J}{K_B + K_J}\right) \quad \text{.....(4.41)}$$

4.6.2.4 Tray slipping constraint:

Analysing the interface between two trays result in what is often referred to as the so-called "no slip" condition:

$$NT * A_S * \frac{\tau_{MA}}{(MS+1)} + \mu_{S\_AI} * NT * F_N - F_S \geq 0 \quad \text{.....(4.42)}$$

Where $\mu_{S,Al}$ is the joint coefficient of friction and F_N the normal force to the surface which is equal to the total preload force F_P. F_S is the maximum external shear force that can be applied to the structure. In our case, $F_S = F_T$. It is possible to obtain a constraint on the minimum preload force that must be applied (F_{PMIN}). **(4.42)** gives:

$$F_{PMIN} = \frac{SF * F_S * (MS+1) - NT * A_S * \frac{\tau_{MA}}{(MS+1)}}{NT * \mu_{S,Al}} \quad \text{.....(4.43)}$$

Where the maximum allowable shear stress is defined as:

$$\tau_{MA} = \tau_{BMA} - \tau_{tor} \quad \text{.....(4.44)}$$

Combining **(4.25)** and **(4.26)** into **(4.44)**:

$$\tau_{MA} = \tau_{BMA} - \frac{16 * F_P}{\pi * D^3} * \left[\frac{P}{2\pi} + \frac{\mu_t r_t}{\cos\beta} + \mu_n r_n \right] \quad \text{.....(4.44b)}$$

Merging **(4.44b)** and **(4.43)**:

$$F_{PMIN} = \frac{SF * F_S * (MS+1) - NT * A_S * \frac{\left[\tau_{BMA} - \frac{16 * F_{PMIN}}{\pi * D^3} * \left[\frac{P}{2\pi} + \frac{\mu_t r_t}{\cos\beta} + \mu_n r_n \right] \right]}{(MS+1)}}{NT * \mu_{S,Al}}$$

.....**(4.45)**

Isolating F_P:

$$F_{PMIN} = \frac{SF * F_S * (MS+1)^2 - NT * A_S * \tau_{BMA}}{NT * \left\{ (MS+1) * \mu_{S,Al} - \frac{16 * A_S}{\pi * D^3} * \left[\frac{P}{2\pi} + \frac{\mu_t r_t}{\cos\beta} + \mu_n r_n \right] \right\}} \quad \text{.....(4.45b)}$$

It is observed that if the numerator is smaller than zero ($SF * F_S * (MS+1)^2 - NT * A_S * \tau_{BMA} < 0$), any pre-load force would ensure no slipping failure. However, this implies that the tie rods are loaded to the maximum allowable shear strength of the material selected. If the friction between trays under compression is to absorb the shear load instead of the tie rods, some design modifications

must be made, since the preload required would then be above its reasonable physical limit. A few alternatives that involve slight design modifications are proposed in Section 4.15, which would release the shear loads taken by the tie rods. For example, the addition of a shoulder around the tie rod as part of the tray or a shear plate between the tray stack and the science payload is proposed. Alternatives that would not modify as much the complex tray design would simply be the addition of inserts. These design alternatives are proposed on the basis that the tie rods play a major role as the main structural component that holds the whole primary structure in one piece. Failure is not an option. Hence, it would not be wise to fully load the tie rods in shear and in tension up to the maximum allowable material strength. This is definitely considered to be risky. Moreover, the shear load taken by the tie rods implies that the tray structure bends considerably, which is not a viable design considering the precision pointing requirement of the science payload. Hence, the no slip condition assuming no shear taken by the tie rods becomes:

$$\mu_{S,Al} * NT * F_N - F_S \geq 0 \quad \text{.....(4.42b)}$$

Taking F_N in **(4.42b)** to be equal to the total pre-load force F_P per tie rod gives:

$$F_{PMIN} = \frac{SF * F_S * (MS + 1)}{NT * \mu_{S,Al}} \quad \text{.....(4.43b)}$$

4.6.3 Determination of the Minimum Stress Area

The constraint equations derived (Equations 4.32b, 4.39, 4.41, and 4.43b) cannot be used alone directly to determine the minimum bolt stress area required for each material considered. The worst case combination of the above four failure constraints will be used to size MOST tie rods. The derivation of the minimum stress area based on known variables for all possible failure mode combinations is presented in the following sub-sections.

4.6.3.1 MOST Tie Rods Design Based on Material Yielding & Tray Gapping

To determine the minimum bolt stress area satisfying both **(4.32b)** and **(4.41)**, the following basic set of equations is required:

$$F_B = F_P + \Delta F_B \quad \text{..... (From equation 4.3)}$$

$$\Delta F_B = \left(\frac{K_B}{K_B + K_J} \right) * F_X \quad \text{..... (From equation 4.6)}$$

Substituting **(4.32b)** and **(4.41)** into **(4.3)**, the following result is obtained:

$$\frac{\frac{\sigma_{BMY}}{SF_Y} - \frac{E_B}{2 * R_C}\sqrt{\frac{4 * C_1 * A_S}{\pi}}}{MS_Y + 1} = \frac{F_X}{K_B + K_J} * \frac{[SF_G * (MS_G + 1) * K_J + K_B]}{A_S} \quad (4.46)$$

where:

$$K_B = \frac{E_B * A_B * A_S}{L_{be} * A_S + L_{se} * A_B} \quad \text{..... (From equation 4.8b)}$$

and

$$K_J = \frac{E_J * A_C}{J} \quad \text{..... (From equation 4.13)}$$

For brevity, the introduction of the following constant is required:

$$C = SF_G * (MS_G + 1) \quad \text{.....(4.47)}$$

Using **(4.8b)**, **(4.13)**, and **(4.47)** in **(4.46)**:

$$\frac{\frac{\sigma_{BMY}}{SF_Y} - \frac{E_B}{2 * R_C}\sqrt{\frac{4 * C_1 * A_S}{\pi}}}{MS_Y + 1} =$$

$$\frac{F_X}{A_S} * \left[\frac{C * E_J * (A_J - C_1 * A_S) * (L_{be} + L_{se} * C_1) + E_B * C_1 * A_S * J}{E_B * C_1 * A_S * J + E_J * (A_J - C_1 * A_S) * (L_{be} + L_{se} * C_1)} \right]$$

.....**(Result: Equation 4.48)**

(4.48) needs to be solved for using a Newton-Raphson or Secant root finding method. A Secant root finding method was implemented in the Fortran90 computer program (See Appendix C.1)

Sample Calculation:

From **(4.32b)**: $F_P = \mathbf{8388\ N}$

Solving **(4.48)** for A_{SMIN} :

$$A_{SMIN} = \mathbf{2.1237E\text{-}5\ m^2} \quad \text{.....(4.49)}$$

And, from **(4.30)**:

A_{SMAX} = **2.6391E-5 m^2** (this is the same for all failure modes)

These results serve as a basis for comparing the 4 different coupled failure modes and should give insight into which mode leads to the worst case scenario. It is understood that this is only a sample case for the MOST design, so no general conclusion can be drawn from the sample case numerical results.

4.6.3.2 MOST Tie Rods Design Based on Material Yielding & Tray Slipping

Similarly, to determine the minimum bolt stress area satisfying both **(4.32b)** and **(4.43b)**, the following basic set of equations is required:

$$F_B = F_P + \Delta F_B \quad \text{..... (From equation 4.3)}$$

$$\Delta F_B = \left(\frac{K_B}{K_B + K_J} \right) * F_X \quad \text{..... (From equation 4.6)}$$

Substituting **(4.32b)** and **(4.43b)** into **(4.3)**, the following result is obtained:

$$\frac{\frac{\sigma_{BMY}}{SF_Y} - \frac{E_B}{2 * R_C}\sqrt{\frac{4 * C_1 * A_S}{\pi}}}{MS_Y + 1} = \frac{SF_S * F_S * (MS_S + 1)}{A_S * NT * \mu_{S\_Al}} + \left(\frac{K_B}{K_B + K_J} \right) * \frac{F_X}{A_S} \quad \text{....(4.50)}$$

where:

$$K_B = \frac{E_B * A_B * A_S}{L_{be} * A_S + L_{se} * A_B} \quad \text{..... (From equation 4.8b)}$$

and

$$K_J = \frac{E_J * A_C}{J} \quad \text{..... (From equation 4.13)}$$

Again, for brevity, introduction of the following constant is required:

$$C = SF_S * (MS_S + 1) \quad \text{.....(4.51)}$$

Inserting **(4.8b)**, **(4.13)**, and **(4.51)** into **(4.50)**:

$$\frac{\left[\frac{\sigma_{BMY}}{SF_Y} - \frac{E_B}{2 * R_C}\sqrt{\frac{4 * C_1 * A_S}{\pi}}\right] * A_S}{MS_Y + 1} = \frac{C * F_S}{NT * \mu_{S\_Al}} + \frac{E_B * C_1 * A_S * J * F_X}{E_B * C_1 * A_S * J + E_J * (A_J - C_1 * A_S) * (L_{be} + L_{se} * C_1)} \quad \text{...(Result: Equation 4.52)}$$

(4.52) is similar to **(4.48)** and must also be solved using Newton-Raphson or Secant root finding method.

Sample Calculation:

From **(4.49)**: $F_P = \mathbf{7282\ N}$

Using **(4.52)**:

$$A_{SMIN} = \mathbf{1.9133E\text{-}5\ m^2} \quad \text{.....(4.53)}$$

And, from **(4.30)**:

$$A_{SMAX} = \mathbf{2.6391E\text{-}5\ m^2} \text{ (this is the same for all failure modes)}$$

It is observed that the minimum bolt stress area A_{SMIN} (yielding and gapping – result 4.49) is about 11% greater than the minimum bolt stress area A_{SMIN} (yielding and slipping – result 4.53). This result suggests that the gapping constraint prevail over the slipping constraint. Obviously no general conclusions can be drawn from this sample numerical calculation. However, the difference between the two numerical results for the bolt stress area is such that for MOST, it is foreseen that yielding coupled with slipping constitutes more of a concern than for yielding coupled with gapping.

4.6.3.3 MOST Tie Rods Design Based on Bolt Thread Stripping & Tray Gapping

Again, to determine the minimum bolt stress area satisfying both **(4.39)** and **(4.41)**, the following basic set of equations is required:

$$F_B = F_P + \Delta F_B \quad \text{..... (From equation 4.3)}$$

$$\Delta F_B = \left(\frac{K_B}{K_B + K_J} \right) * F_X \quad \text{..... (From equation 4.6)}$$

Substituting **(4.39)** and **(4.41)** into **(4.3)**, the following result is obtained:

$$\frac{2 * \tau_{BMY} * A_S}{SF_{ST} * (MS_{ST} + 1)} = \frac{F_X}{K_B + K_J} * \left[SF_G * (MS_G + 1) * K_J + K_B \right] \quad \text{.....(4.54)}$$

Again, for brevity, introduction of the following constant is required:

$$C = SF_G * (MS_G + 1) \quad \text{..... (From equation 4.47)}$$

Again, inserting: $$K_B = \frac{E_B * A_B * A_S}{L_{be} * A_S + L_{se} * A_B}$$ ..... **(From equation 4.8b)**

and $$K_J = \frac{E_J * A_C}{J}$$ ..... **(From equation 4.13)**

, and **(4.47)** into **(4.54)** gives:

$$\frac{2 * \tau_{BMY} * A_S}{SF_{ST} * (MS_{ST} + 1)} = F_X * \left[\frac{C * E_J * (A_J - C_1 * A_S) * (L_{be} + L_{se} * C_1) + E_B * C_1 * A_S * J}{E_B * C_1 * A_S * J + E_J * (A_J - C_1 * A_S) * (L_{be} + L_{se} * C_1)} \right]$$ .....**(4.55)**

Multiplying the LHS by the denominator of the RHS in **(4.55)**:

$$\frac{2 * \tau_{BMY} * A_S}{SF_{ST} * (MS_{ST} + 1)} * \left[E_B * C_1 * A_S * J + E_J * (A_J - C_1 * A_S) * (L_{be} + L_{se} * C_1) \right] =$$
$$F_X * \left[C * E_J * (A_J - C_1 * A_S) * (L_{be} + L_{se} * C_1) + E_B * C_1 * A_S * J \right]$$

.....**(4.56)**

(4.52c) is of the quadratic form, which can be expressed as follows:

$$a * A_{SMIN}^2 + b * A_{SMIN} + c = 0$$ .....**(4.57)**

For which the following solutions exist:

$$A_{SMIN} = \frac{-b \pm \sqrt{b^2 - 4 * a * c}}{2 * a}$$ .....**(Result: Equation 4.57)**

Where a, b and c are defined as:

$$a = \frac{2 * \tau_{BMY}}{SF_{ST} * (MS_{ST} + 1)} * \left[E_B * C_1 * J - E_J * C_1 * (L_{be} + L_{se} * C_1) \right]$$

$$b = \frac{2 * \tau_{BMY} * E_J * A_J * (L_{be} + L_{se} * C_1)}{SF_{ST} * (MS_{ST} + 1)} - F_X * \left[E_B * C_1 * J - C * E_J * C_1 * (L_{be} + L_{se} * C_1) \right]$$

$$c = -F_X * C * E_J * A_J * (L_{be} + L_{se} * C_1)$$

Sample Calculation:

From **(4.45)**: $F_P = 9118$ **N**

Using **(4.50)**:

$$A_{SMIN} = 1.9233E\text{-}5 \text{ m}^2$$ .....**(4.58)**

And, from **(4.30)**:

A_{SMAX} = **2.6391E-5 m^2** (this is the same for all failure modes)

It is observed here that the minimum bolts stress area A_{SMIN} (stripping and gapping – result 4.58), is 11% smaller than the minimum bolts stress area A_{SMIN} (yielding and gapping – result 4.49). This result provides insight that the yielding constraint, when coupled to the gapping constraint, is worst than the stripping combined with gapping for the sample numerical case. Again, no general conclusions can be drawn from this sample numerical calculation. However, the difference between the bolt stress area A_{SMIN} (stripping and gapping – result 4.58) and the bolt stress area A_{SMIN} (yielding and gapping – result 4.49) is such that it is foreseen for MOST that yielding coupled with gapping is equivalent to stripping coupled with gapping. Ultimately so far, the yielding constraint combined with the gapping constraint featured the worst (largest) minimum stress area.

4.6.3.4 MOST Tie Rods Design Based on Bolt Thread Stripping & Tray Slipping

Finally, to determine the minimum bolt stress area satisfying both **(4.39)** and **(4.43b)**, the following basic set of equations is required:

$$F_B = F_P + \Delta F_B \quad \text{..... (From equation 4.3)}$$

$$\Delta F_B = \left(\frac{K_B}{K_B + K_J}\right) * F_X \quad \text{..... (From equation 4.6)}$$

Substituting **(4.39)** and **(4.43b)** into **(4.3)**, the following result is obtained:

$$\frac{2 * \tau_{BMY} * A_S}{SF_{ST} * (MS_{ST} + 1)} = \frac{SF_S * F_S * (MS_S + 1)}{NT * \mu_{S,Al}} + \left(\frac{K_B}{K_B + K_J}\right) * F_X \quad \text{.....(4.59)}$$

With K_B, K_J, and C as previously defined, inserting **(4.8b)**, **(4.13)**, and **(4.50)** into **(4.59)** gives:

$$\frac{2 * \tau_{BMY} * A_S}{SF_{ST} * (MS_{ST} + 1)} = \frac{[E_B * C_1 * A_S * J + E_J * (A_J - C_1 * A_S) * (L_{be} + L_{se} * C_1)] * C * F_S + E_B * C_1 * A_S * J * F_X * NT * \mu_{S,Al}}{[E_B * C_1 * A_S * J + E_J * (A_J - C_1 * A_S) * (L_{be} + L_{se} * C_1)] * NT * \mu_{S,Al}} \quad \text{.....(4.60)}$$

Multiplying LHS by denominator of RHS in **(4.60)**:

$$\frac{2*\tau_{BMY}*A_S*[E_B*C_1*A_S*J+E_J*(A_J-C_1*A_S)*(L_{be}+L_{se}*C_1)]*NT*\mu_{S.Al}}{SF_{ST}*(MS_{ST}+1)} =$$
$$[E_B*C_1*A_S*J+E_J*(A_J-C_1*A_S)*(L_{be}+L_{se}*C_1)]*C*F_S+E_B*C_1*A_S*J*F_Y*NT*\mu_{S.Al}$$

.....(4.61)

(4.61) is of the quadratic form, which can be expressed as follows:

$$a*A_{SMIN}^2+b*A_{SMIN}+c=0 \quad \text{.....(4.62)}$$

For which the following solutions exist:

$$A_{SMIN}=\frac{-b\pm\sqrt{b^2-4*a*c}}{2*a} \quad \text{.....(Result: Equation 4.62)}$$

Where a, b and c are defined as:

$$a=\frac{2*\tau_{BMY}*[E_B*C_1*J-E_J*C_1*(L_{be}+L_{se}*C_1)]*NT*\mu_{S.Al}}{SF_{ST}*(MS_{ST}+1)}$$

$$b=\frac{2*\tau_{BMY}*E_J*A_J*(L_{be}+L_{se}*C_1)*NT*\mu_{S.Al}}{SF_{ST}*(MS_{ST}+1)}-$$
$$[E_B*C_1*J-E_J*C_1*(L_{be}+L_{se}*C_1)]*C*F_S-E_B*C_1*J*F_Y*NT*\mu_{S.Al}$$

$$c=-E_J*A_J*(L_{be}+L_{se}*C_1)*C*F_S$$

Sample Calculation:

From **(4.45)**: $F_P = 8428$ **N**

Using **(4.50)**:

$$A_{SMIN} = \textbf{1.6922E-5 m}^2 \quad \text{.....(4.63)}$$

And, from **(4.30)**:

$$A_{SMAX} = \textbf{2.6391E-5 m}^2 \text{ (this is the same for all failure modes)}$$

Finally, it is observed that the minimum bolt stress area A_{SMIN} (stripping and slipping – result 4.63) is 25% smaller than the minimum bolt stress area A_{SMIN} (yielding and gapping – result 4.49). This result enforces previous conclusion stating that the yielding constraint, when coupled to the gapping constraint, is the worst case scenario considering the sample numerical case. Again, no general conclusions can be drawn from this sample numerical calculation. However, the difference between the bolt stress

areas A_{SMIN} (yielding and gapping – result 4.49) and the bolt stress areas A_{SMIN} (yielding and slipping – result 4.53, stripping and gapping – result 4.58, or stripping and slipping – result 4.63) is such that for MOST, it is foreseen that yielding coupled with gapping constitutes the worst case design scenario. Again, these conclusions are only valid for the variables used in our sample calculations (see Section 4.6.1). The Fortran90 program written to size the tierods compares the four combined failure modes, and automatically provides results based on the worst case scenario, which might be different for different materials. A user's guide to the TIEROD.F90 program is provided in Section 4.16.

4.7 Joint Stress Concentration Factor Determination Using the Airy Stress Function

It is well established that non-uniformity of stress occurs because of geometric changes. This non-uniformity in stress distribution across our joint and particularly around our tie rods may result in a maximum stress that is larger than the average stress $\sigma_{AVERAGE}$.

Where $\sigma_{AVERAGE}$ can easily be computed as follows:

$$\sigma_{AVERAGE} = \frac{F_J}{A_J} \quad \text{.....(4.64)}$$

Now, let's find a theoretical value for σ_{MAX}, knowing the applied force F_J and assuming that maximum stress will occur at the edge of the joint hole.

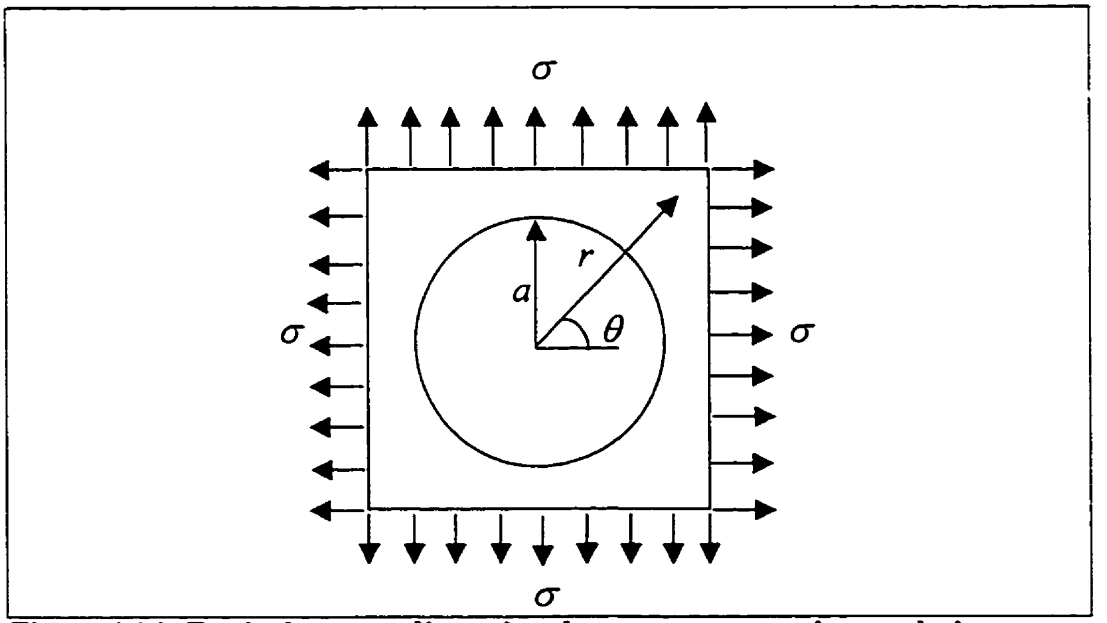

Figure 4.14: Equivalent two-dimensional stress concentration analysis

Figure 4.14 shows an approximation to the joint stress state. Obviously, the real joint is loaded in compression along the 3rd axis (out of plane of Figure 4.14) and therefore our planar tensile load distribution is really an approximation of the real 3-D effect.

First, the equilibrium equations in terms of the plane polar coordinates can be obtained where t_{rr}, $t_{\theta\theta}$, and $t_{r\theta}$ represent the polar stress components:

$$\frac{\partial t_{rr}}{\partial r}+\frac{1}{r}\frac{\partial t_{r\theta}}{\partial \theta}+\frac{1}{r}\{t_{rr}-t_{\theta\theta}\}+F_r=\rho * \ddot{u}_r \quad \text{.....(4.65)}$$

$$\frac{\partial t_{r\theta}}{\partial r}+\frac{1}{r}\frac{\partial t_{\theta\theta}}{\partial \theta}+\frac{2}{r}\{t_{r\theta}\}+F_\theta=\rho * \ddot{u}_\theta \quad \text{.....(4.66)}$$

Airy stress function method:

Let U be the Airy stress function. The stress components t_{rr}, $t_{\theta\theta}$, and $t_{r\theta}$ can be defined as follows in terms of the Airy stress function:

$$t_{rr}=\frac{1}{r}\frac{\partial U}{\partial r}+\frac{1}{r^2}\frac{\partial^2 U}{\partial \theta^2} \quad \text{.....(4.67)}$$

$$t_{\theta\theta}=\frac{\partial^2 U}{\partial r^2} \quad \text{.....(4.68)}$$

$$t_{r\theta}=\frac{1}{r^2}\frac{\partial U}{\partial \theta}-\frac{1}{r}\frac{\partial^2 U}{\partial r \partial \theta} \quad \text{.....(4.69)}$$

Solving for the maximum stress in the tie rod case is not trivial. However, the stress-state solution for an infinite plane under uni-axial tension is well known. Using this uni-axial stress state solution and applying the superposition theorem (assuming small displacement theory holds), a fairly good approximation of the stress-state in our small joint case is derived. As a result, it is possible to get an approximate stress concentration factor for the simplified MOST joint. The theoretical derivation included herein is a two-dimensional simplification of an actual three-dimensional problem. The actual joint is actually loaded by out of plane compression forces, which leads to extension (displacement) in the in-plane outward direction. Hence, the infinite plane solutions superposed provide an equivalent displacement solution of the actual three-dimensional case. Moreover, it is understood that an infinite plane solution ensures

higher stress at the radius hole location, which in turn ensures a conservative figure for the stress concentration factor.

The polar coordinate Laplacian operator is:

$$\nabla^2 = \frac{\partial^2}{\partial r^2} + \frac{1}{r}\frac{\partial}{\partial r} + \frac{1}{r^2}\frac{\partial^2}{\partial \theta^2} \quad \text{(4.70)}$$

When there are no body forces involved, we get the following compatibility equation:

$$\nabla^4 U(r,\theta) = 0 \quad \text{(4.71)}$$

Applied to the polar coordinate form Airy stress function, we get:

$$\left[\frac{\partial^2}{\partial r^2} + \frac{1}{r}\frac{\partial}{\partial r} + \frac{1}{r^2}\frac{\partial^2}{\partial \theta^2}\right]\left[\frac{\partial^2 U}{\partial r^2} + \frac{1}{r}\frac{\partial U}{\partial r} + \frac{1}{r^2}\frac{\partial^2 U}{\partial \theta^2}\right] = 0 \quad \text{(4.72)}$$

The complex part in using the Airy stress function method is to define or assume a stress function form. In the case of infinite plane uni-axial tension, a simple solution can assume the following form:

$$U(r,\theta) = F_1(r) + F_2(r)\cos(2\theta) \quad \text{(4.73)}$$

This form may seem arbitrary at first sight but it is quite general and can be used to solve most polar coordinate planar problems. The $\cos(2\theta)$ is the simplest trigonometric expression mapping the boundary conditions properly. It implies the use of an infinite Taylor expansion series, as the cosine can be expanded. The radial stress dependence and the coupled tangential-radial dependence are also expressed in **(4.73)**. Substituting **(4.73)** into **(4.72)** gives two decoupled equations:

$$\left[\frac{\partial^2}{\partial r^2} + \frac{1}{r}\frac{\partial}{\partial r}\right]\left[\frac{\partial^2 F_1}{\partial r^2} + \frac{1}{r}\frac{\partial F_1}{\partial r}\right] = 0 \quad \text{(4.74)}$$

and

$$\left[\frac{\partial^2}{\partial r^2} + \frac{1}{r}\frac{\partial}{\partial r} - \frac{4}{r^2}\right]\left[\frac{\partial^2 F_2}{\partial r^2} + \frac{1}{r}\frac{\partial F_2}{\partial r} - \frac{4}{r^2}F_2\right]\cos(2\theta) = 0 \quad \text{(4.75)}$$

A general solution for $F_1(r)$ and $F_2(r)$ that satisfies **(4.74)** and **(4.75)** would be of the following form:

$$F_1(r) = C_1 r^2 \ln(r) + C_2 r^2 + C_3 \ln(r) + C_4 \quad \text{(4.76)}$$

$$F_2(r) = C_5 r^2 + C_6 r^4 + \frac{C_7}{r^2} + C_8 \quad \text{.....(4.77)}$$

Incorporating **(4.76)** and **(4.77)** in **(4.67)**, **(4.68)**, and **(4.69)**:

$$t_{rr}(r,\theta) = C_1[1 + 2\ln(r)] + 2C_2 + \frac{C_3}{r^2} - \left[2C_5 + 6\frac{C_7}{r^4} + 4\frac{C_8}{r^2}\right]\cos(2\theta) \quad \text{.....(4.78)}$$

$$t_{\theta\theta}(r,\theta) = C_1[3 + 2\ln(r)] + 2C_2 - \frac{C_3}{r^2} + \left[2C_5 + 12C_6 r^2 + 6\frac{C_7}{r^4}\right]\cos(2\theta) \quad \text{.....(4.79)}$$

$$t_{r\theta}(r,\theta) = \left[2C_5 + 6C_6 r^2 - 6\frac{C_7}{r^4} - 2\frac{C_8}{r^2}\right]\sin(2\theta) \quad \text{.....(4.80)}$$

By inspection $C_1 = C_6 = 0$ since in the joint case, stresses are finite at $r = \infty$. To determine the remaining 5 constants, the definition of 5 boundary conditions is required:

$$t_{rr}(\infty,\theta) = \frac{1}{2}\sigma[1 + \cos(2\theta)] \quad \text{.....(4.81)}$$

$$t_{\theta\theta}(\infty,\theta) = \frac{1}{2}\sigma[1 - \cos(2\theta)] \quad \text{.....(4.82)}$$

$$t_{rr}(\infty,\theta) = -\frac{1}{2}\sigma[\sin(2\theta)] \quad \text{.....(4.83)}$$

$$t_{rr}(a,\theta) = 0 \text{ (Free surface)} \quad \text{.....(4.84)}$$

$$t_{r\theta}(a,\theta) = 0 \text{ (Free surface)} \quad \text{.....(4.85)}$$

Applying those 5 boundary conditions to **(4.78)**, **(4.79)**, and **(4.80)**:

$$C_2 = \frac{\sigma}{4} \; ; \; C_3 = -\frac{a^2\sigma}{2} \; ; \; C_5 = -\frac{\sigma}{4} \; ; \; C_7 = -\frac{a^4\sigma}{4} \text{ and } C_8 = \frac{a^2\sigma}{2} \quad \text{.....(4.86)}$$

Substituting those constants **(4.86)** into **(4.78)**, **(4.79)**, and **(4.80)**:

$$t_{rr}(r,\theta) = \frac{\sigma}{2}\left[1 - \frac{a^2}{r^2}\right] + \frac{\sigma}{2}\left[1 + 3\frac{a^4}{r^4} - 4\frac{a^2}{r^2}\right]\cos(2\theta) \quad \text{.....(4.87)}$$

$$t_{\theta\theta}(r,\theta) = \frac{\sigma}{2}\left[1 + \frac{a^2}{r^2}\right] - \frac{\sigma}{2}\left[1 + 3\frac{a^4}{r^4}\right]\cos(2\theta) \quad \text{.....(4.88)}$$

$$t_{r\theta}(r,\theta) = -\frac{\sigma}{2}\left[1 - 3\frac{a^4}{r^4} + 2\frac{a^2}{r^2}\right]\sin(2\theta) \quad \text{.....(4.89)}$$

The component-form stress-state **(4.87)** to **(4.88)** represent a solution of our infinite plane uni-axial tension problem. Now, if the same plane is kept but tension is applied on the other side of the plate, it can similarly be shown that the following equations are obtained:

$$t_{rr}(r,\theta) = \frac{\sigma}{2}\left[1-\frac{a^2}{r^2}\right] - \frac{\sigma}{2}\left[1+3\frac{a^4}{r^4}-4\frac{a^2}{r^2}\right]\cos(2\theta) \quad \textbf{(4.90)}$$

$$t_{\theta\theta}(r,\theta) = \frac{\sigma}{2}\left[1+\frac{a^2}{r^2}\right] + \frac{\sigma}{2}\left[1+3\frac{a^4}{r^4}\right]\cos(2\theta) \quad \textbf{(4.91)}$$

$$t_{r\theta}(r,\theta) = \frac{\sigma}{2}\left[1-3\frac{a^4}{r^4}+2\frac{a^2}{r^2}\right]\sin(2\theta) \quad \textbf{(4.92)}$$

Applying the superposition principle (i.e. one of the elasticity theorems: a linear combination of solutions to sub-problems is then a solution to the original problem), the final stress-state equations for our infinite plane with tension applied in both axial direction normal to the surfaces is obtained as follows:

$$t_{rr}(r,\theta) = \sigma\left[1-\frac{a^2}{r^2}\right] \quad \textbf{(4.93)}$$

$$t_{\theta\theta}(r,\theta) = \sigma\left[1+\frac{a^2}{r^2}\right] \quad \textbf{(4.94)}$$

$$t_{r\theta}(r,\theta) = 0 \quad \textbf{(4.95)}$$

Evaluating **(4.93)**, **(4.94)**, and **(4.95)** at $r = a$:

$$t_{rr}(a,\theta) = 0 \quad \textbf{(4.96)}$$

$$t_{\theta\theta}(a,\theta) = 2\sigma \quad \textbf{(4.97)}$$

$$t_{r\theta}(a,\theta) = 0 \quad \textbf{(4.98)}$$

The maximum stress at the edge of the hole resulting from that analysis is:

$$\sigma_{max} = 2 * \sigma \quad \textbf{(4.99)}$$

Hence, our stress concentration factor S_C is:

$$S_C = \frac{2*\sigma}{\sigma} = 2 \quad \textbf{(4.100)}$$

A stress concentration factor $S_C \approx 2.1$ is found using Peterson's[95] chart 5.27, which assumes an infinite cylinder with inside pressure.

The resulting joint stress concentration factor can than be used to check if the joint stress is below its maximum allowable stress.

Using the sample case numerical values:

$$\sigma_{J\max} = \frac{F_J}{A_J} * S_C = \frac{8062N}{0.00016m^2} * 2 = 0.999E8Pa \quad \text{.....(4.101)}$$

The maximum allowable stress σ_{Al} for aluminum is 1.1E8 Pa. Hence, with a stress concentration factor of 2, the maximum stress $\sigma_{J\max}$ is at 91% of the maximum allowable stress in the joint, which also includes a safety factor of 2. The computed maximum joint stress is above the real stress in the joint as outlined previously (because of assumptions made and as the tray wall cross-sectional area was not taken into account in the calculations). Hence, this represents a truly conservative analysis of the joint. It simply adds confidence in the analysis in the form of hidden safety margin. However, there is a need to verify the maximum joint stress for every tie rod selection (as this is a sample case analysis and hence cannot be generalised). These verifications shall ensure no structural failure due to the joint.

4.8 Tie Rod Material as a Design Variable (Use of MIL-HDBK-5)

The choice of material influences the size of the tie rods a great deal. Actually, the material selection is one of the two design parameters that truly impact the sizing of the tie rods. The other parameter is the number of tie rods. Many materials can be considered good options in terms of their high strength characteristics. A good point of departure in terms of material engineering is to have a look at the so-called aerospace graded materials that are listed in the MIL-HDBK-5[77] document. This extensive two-volume collection assesses aerospace graded material properties. After going through the extensive material choice listed in the MIL-HDBK-5[77] military handbook. it was decided to narrow down the material choice by using the materials that do not require MSFC approval for launch (low-cost approach). These materials are listed as alloys with

high resistance to stress corrosion cracking in table I of the MSFC-SPEC-522[92] document (See short list in Appendix E).

Titanium seems to be a material with much potential. However, the availability and cost issues in using titanium for the tie rod design might well lead designers to look at other options. The results presented in later sections and shown in Appendix C.3 include all possible options with their pros and cons along with recommendations discussed in Sections 4.14 and 4.15.

4.9 Torque Control at Assembly Time

Selecting a torque value for a given pre-load and fastener material can be complicated. Friction and material relaxation effects at assembly time can modify significantly the desired pre-load. Some tables of recommended torque values exist and are commonly used for non-critical applications. However, for the MOST micro-satellite application, accuracy is an issue. For example, even tightening speed at assembly time is critical. The use of high-speed tools to tighten the tie rods is required but many pauses should be taken to give all parts time to *relax*. This involves tightening bolts in a series of passes, rather than applying full torque required at the first pass. Hence, while torque is being applied, the nut turns, the bolt stretches, and then the desired pre-load by repeating this process is achieved. The closer control enters that chain of events, the more accuracy is obtained and the more expensive it should cost. The normal relationship between torque and pre-load is linear. The difficulty here is to define and calculate the constant of linearity. A number of equations have been derived and the one proposed here was initially defined by Motosh[198]:

$$T_{in} = F_P\left[\frac{P}{2\pi} + \frac{\mu_t r_t}{\cos\beta} + \mu_n r_n\right] \text{.... (Same as equation 4.25)}$$

Again, **(4.25)** shows that the input torque is resisted by three reaction torque. The first one is produced by the inclined plane action of nut threads on bolt threads. This is the effect of the bolt material stretching. The second one is created by friction between the nut and bolt threads. The last one is created by friction between the face of the nut and the joint. After giving it some thoughts, one realises that all other effects are insignificant and negligible on the torque measurement. Hence, the Motosh[98]

equations should be used when it is time to compute the torque required to assemble the trays together and achieve the desired pre-load.

4.10 Self-Loosening of Fasteners under Vibration

The bolt loosening mechanisms are extensively studied and investigated by Junker[117], Sakai[118], Landt[119] [120] [121], Motosh[98], Baubles et al.[122], Daadbin[123], Walker[124], and many others. It is expected that during the launch phase of the MOST mission, the bolts could self-loosen. To ensure no self-loosening, various design options are available: maintaining preload and friction (e.g. nylon inserts, disc-lock products), preventing relative slip between surfaces (e.g. addition of a shoulder, some inserts or a gasket), reducing back-off torque (e.g. using fine-pitch thread), countering back-off torque (e.g. using nylon locking collar in nut or free-spinning lock nuts or bolts), mechanically locked fasteners[125] (e.g. using lock wires and pins, welding bolt and nut, or using Huck lockbolt, truelock bolt, or Axilok nut), chemically bonded fasteners, and vibration-resistant washers.

Combining the use of a nut with a nylon locking collar, the addition of a shoulder, the use of fine-pitch thread bolt, and the use of a pin (or lock wire) would ensure no self-loosening of MOST tie rods. Those recommendations are based on simplicity and low cost. It is interesting to note that the addition of a shoulder (recommended for counteracting possible shear and slip failures – see Section 4.15) also acts to prevent self-loosening of tie rods.

Several tests can assess the residual preload in a bolt as a function of time under vibration loading. The Junker[117] test machine is probably the best and cheapest alternative to the more expensive vibration table test. However, if all recommendations are applied, no testing shall be required, as no tie rod loosening is possible considering the relatively low MOST launch vibration loads (as compared with industrial vibration loading).

4.11 Pre-load Physical Limitations and Other Assumptions

Underlying assumptions were made about pre-loading that must be well understood. For example, there exist physical limitations on the pre-load force that can

be applied. One can preload a bolt only by applying some maximum torque to it. Once pre-loaded, the relaxation effects and elastic non-linear interaction losses between the bolt and the joint come into the overall picture. The losses that will occur can be quantified. The following relationship between the average pre-load and the torque applied was taken from Bickford[84]:

$$F_{PA} = \frac{M_T}{KD} \quad \text{.....(4.102)}$$

Unfortunately, once preloaded, the bolt interacts with the joint as previously mentioned. Those material interactions effectively unload the joint. The elastic interaction losses can be quantified to find minimum and maximum effective pre-load force that remains after applying a torque M_T to the bolt. Great care has to be taken, such that the effective pre-load in the bolts remains as close as possible to the theoretical value required. Once the average pre-load (or required pre-load) has been determined by the analysis, the maximum and minimum pre-load can be computed using empirical estimates of the losses involved. From Bickford[84], in the worst case scenario:

$$\boxed{F_{PMAX} = 1.02 * F_{PA}} \text{ and } \boxed{F_{PMIN} = 0.42 * F_{PA}} \quad \text{.....(4.103)}$$

As observed, the minimum pre-load can lie quite below the expected or desired pre-load. The designers will have to bear this fact in mind when MOST is actually assembled, as less pre-load then desired might well lead to a gapping failure. As a rough figure, the torque required should be at least doubled to ensure that the minimum preload force is obtained. This rough figure shall be used only if no preload verification procedures are planned (which should be the case for MOST to keep low-cost at assembly time). Again, more elaborate and expensive equipment can be used but considering the low-cost design approach to MOST, doubling of the required torque seems a viable solution as long as it does not lead to failure of the joint or to stripping failure of the bolt. Optimum preloading was investigated by Finkelston[126].

4.12 Analysis Results for All Failure Modes and Materials Considered

As previously highlighted, the yielding and slipping failure mode is predominant. Table 4.3 presents all best bolt sizes that feature a bolt stress area A_S between boundaries A_{SMIN} and A_{SMAX} defined by the yielding and slipping failure mode. Results were

obtained from the output of the TIEROD.F90 program. As shown in Table 4.3, no choices are obtained for the 4 tie rods configuration. Also, some materials do not even appear in the case of the 8 tie rods configuration. This clearly demonstrates that a limited number of choices are viable options when slipping is considered. Additionally, more than 37 viable options are presented in Appendix C.5 for the case when the slipping failure is not considered. Hence, Section 4.15 presents design recommendations such that the slipping between trays is no longer a function of the tie rod sizing problem. The results obtained when the slipping failure is not considered also include a choice of off-the-shelf, cheap local suppliers' material choices that are not viable options otherwise. This is the main reason why some slight design changes are recommended in order to allow the use of a cheaper off-the-shelf solution.

All Viable Results Sorted by Mass (Considering Slip as a Potential Failure)							
Order	# of Rods	Bolt Material Designation	Size	Serie	Mass (kg)	Preload (N)	MS(Gapping)
1	8	Ti-13V-11Cr-3Al-SOLUTION-TREATED-AGED	M6x1	Metric	0.6841	9840	0.5265
2	8	Ti-6Al-4V-AMS-4928	M6.3x1	Metric	0.6936	8388	0.3473
3	8	Ti-6Al-4V-MIL-T-9047	M6.3x1	Metric	0.6936	8010	0.2866
4	8	Ti-6Al-4V-AMS-4928	1/4-28	UNF	0.7056	8719	0.4137
5	8	Ti-6Al-4V-MIL-T-9047	1/4-28	UNF	0.7056	8327	0.35
6	8	Ti-13V-11Cr-3Al-MIL-T-9047-ANNEALED	M6.3x1	Metric	0.7543	8093	0.2734
7	8	CUSTOM455-STAINLESS-STEEL-AMS5617-H1000	M5x0.8	Metric	0.7645	7717	0.2509
8	8	Ti-13V-11Cr-3Al-SOLUTION-TREATED-AGED	1/4-20	UNC	0.7673	10020	0.5687
9	8	Ti-13V-11Cr-3Al-MIL-T-9047-ANNEALED	1/4-28	UNF	0.7673	8412	0.3351
10	8	17-7Ph-STAINLESS-STEEL-CH900	M6x1	Metric	1.0852	8574	0.5499
11	8	PH15-7Mo-STAINLESS-STEEL-CH900	M6x1	Metric	1.0891	9582	0.732
12	8	CUSTOM450-STAINLESS-STEEL-AMS5773-H1000	M6x1	Metric	1.1009	8574	0.5499
13	8	CUSTOM450-STAINLESS-STEEL-AMS5763-H1050	M6x1	Metric	1.1009	7566	0.3677
14	8	CUSTOM450-STAINLESS-STEEL-AMS5773-H1050	M6x1	Metric	1.1009	7566	0.3677
15	8	AM-355-STAINLESS-STEEL-AMS5743-SCT1000	M6x1	Metric	1.1088	8910	0.6106
16	8	15-5Ph-STAINLESS-STEEL-AMS5659-H1025	M6x1	Metric	1.1127	8258	0.4848
17	8	17-7Ph-STAINLESS-STEEL-CH900	1/4-20	UNC	1.2171	8719	0.5992
18	8	PH15-7Mo-STAINLESS-STEEL-CH900	1/4-20	UNC	1.2215	9748	0.7879
19	8	15-5Ph-STAINLESS-STEEL-AMS5659-H1075	M6.3x1	Metric	1.2268	7787	0.4631
20	8	CUSTOM455-STAINLESS-STEEL-AMS5617-H1000	1/4-20	UNC	1.2348	11123	1.038
21	8	CUSTOM450-STAINLESS-STEEL-AMS5773-H1000	1/4-20	UNC	1.2348	8719	0.5992
22	8	CUSTOM450-STAINLESS-STEEL-AMS5763-H1050	1/4-20	UNC	1.2348	7690	0.4105
23	8	CUSTOM450-STAINLESS-STEEL-AMS5773-H1050	1/4-20	UNC	1.2348	7690	0.4105
24	8	AM-355-STAINLESS-STEEL-AMS5743-SCT1000	1/4-20	UNC	1.2436	9062	0.6621
25	8	15-5Ph-STAINLESS-STEEL-AMS5659-H1025	1/4-20	UNC	1.248	8396	0.5317
26	8	15-5Ph-STAINLESS-STEEL-AMS5659-H1075	1/4-28	UNF	1.248	8102	0.5442
27	8	15-5Ph-STAINLESS-STEEL-AMS5659-H1100	1/4-28	UNF	1.248	7317	0.3946

Table 4.3: All Viable Tie Rod Options Sorted by Mass

4.13 Material Cost and Availability Issues

The materials listed in Table 4.3 are not readily available off-the-shelf. A survey was done by Chantale Lamontagne[127], highlighting the fact that it would cost about 750$(CAN) to get 8 tie rods custom machined by local suppliers. On the other hand, off-the-shelf threaded rods are readily available. Two local distributors were contacted and the price is about 10$(CAN) per tie rod for the allowed stainless steels (See #36 and #37 in Appendix C.5). Hence, it would roughly cost 10 times more to get the tie rods custom made locally. Moreover, the lead-time would definitely be longer to obtain custom-made tie rods.

4.14 Discussion and Tie Rod Design Recommendations for MOST

As observed earlier, many material and bolt combinations can be used to achieve the no failure criteria (except for the slipping failure mode, which must be handled some other way, i.e., the addition of a shoulder, a gasket, some inserts, or an interface plate is recommended in Section 4.15). The optimum solution must consider weight, performance and cost. Appendix C.5 presents results from output of the TIEROD.F90 program for the best material and bolt combinations that would achieve the design goals. Among them, the combination of 4 tie rods (Size ¼-28) made out of AM-355 stainless steel (AMS 5743/SCT1000) is one of the lightest bolt/material solutions at around 622 grams. 8 M6.3x1 tie rods made out of Ti-6Al-4V (AMS-4928) is also one of the lightest bolt/material solutions at around 700 grams. Simplification of the design and extra weight saving are the two clear advantages of using the 4 tie rods configuration. Future MOST design shall make use of this result to reduce mass of the primary structure. As far as the current MOST design is concerned, the 8 tie rods configuration was pre-selected by engineers. In that configuration, two solutions are proposed: a custom design using titanium as mentioned earlier or some cheap off-the-shelf stainless steel tie rods. The latter has the advantage of being readily available and cheap. The obvious disadvantage is the addition of 500 grams to the primary structure. There is no performance gain other than the mass reduction in using titanium tie rods.

It is felt that cost is not a major issue when considering a stand-alone design. Hence, the titanium solution is recommended. However, if MOST was to be used within

a constellation of small satellites, or, if cost was more important than weight, the cheaper solution should be favoured. The tradeoff here is simple: 45% lighter at 10 times the cost or 45% heavier at one tenth of the cost.

Best Tie Rod Design Recommendations: ***All based on Al-6061-T6/T651 joint**

1)	**Material:**	**AM-355 stainless steel (AMS 5743/SCT1000)**
	Bolt size:	**¼-28 UNF (English)**
	Number of Tie Rods:	**4**
	Total Tie Rods Mass:	**0.6218 kg**

2)	**Material:**	**Ti-6Al-4V (AMS-4928)**	
	Bolt size:	**M6.3x1 (Metric)**	**or ¼-28 UNF (English)**
	Number of Tie Rods:	**8**	
	Total Tie Rods Mass:	**0.6936 kg**	**or 0.7056 kg**

3)	**Material:**	**316-Stainless Steel (Spaenaur)**
	Bolt size:	**¼-28 UNF (English)**
	Number of Tie Rods:	**8**
	Total Tie Rods Mass:	**1.248 kg**

4)	**Material:**	**304-Stainless Steel (Metal Supermarket)**
	Bolt size:	**¼-28 UNF (English)**
	Number of Tie Rods:	**8**
	Total Tie Rods Mass:	**1.248 kg**

4.15 MOST Tray Design Modification Recommendations

The following design recommendations or design change suggestions are based on a desire to reduce the overall weight of the primary tray stack structure. The analysis showed that the slipping constraint was the main design driver. The slipping failure mode can be solved by slightly changing the design. The addition of a shoulder at the tray interface in the vicinity of tie rod would solve the slipping problem without adding weight to the primary structure. The only disadvantage of this design change is the increased manufacturing tolerances. However, since the tray is custom made out of a single block of aluminum, it is anticipated that this change does not add unreasonable manufacturing complexity. On the positive side, it can potentially reduce the mass by a relatively large amount by allowing the 4 tie rod configuration, thereby simplifying the tray cross-section. It appears clear from the diagram on Figure 4.15 that most of the shear force, if not all, would be taken by the tray spigot or shoulder instead of the tie

rods. In the worst case where tolerances become a major problem, a shoulder can be press fitted after the tray is machined, thereby relaxing the manufacturing tolerances.

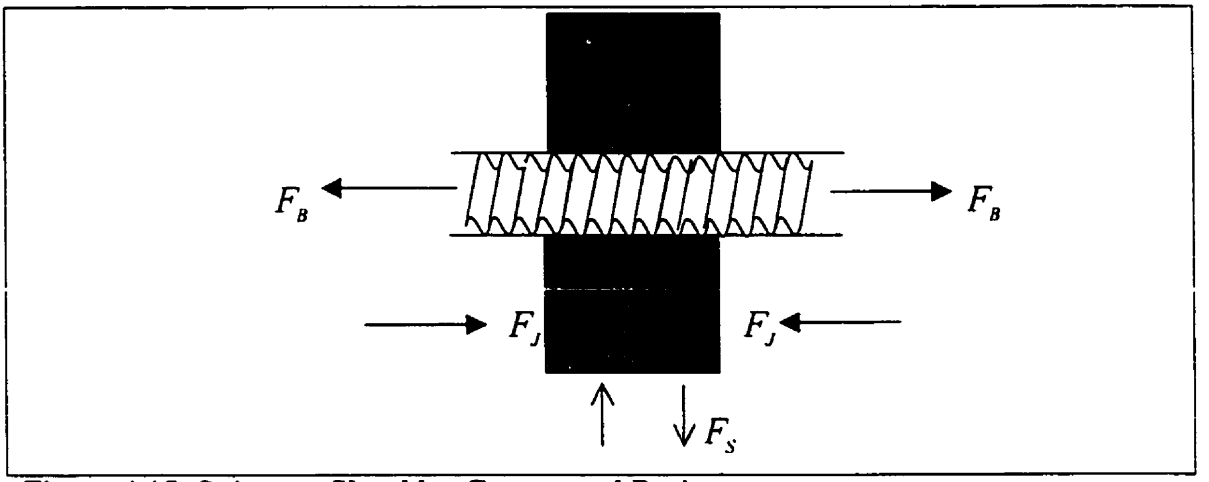

Figure 4.15: Spigot or Shoulder Conceptual Design

Another solution is the addition of a shear plate between the tray stack and the science payload. The project engineers prefer this solution, as it does not affect the manufacturing of the tray, and also provides a useful interface for ease of assembly of the science payload on top of the tray stack. The down side of this solution is that it adds weight to the structure. However, provided slight additional weight of the order of 0.5kg up to 0.75kg can be afforded, it is strongly recommended to include a shear plate for the obvious advantages mentioned previously. Alternative solutions considered are the addition of a gasket or some inserts at the interface between trays to avoid material shear or science payload misalignment, as mentioned earlier. All those additions, shear plate included, would directly solve a potential failure mode, and would reduce the sizing of tie rods to three basic problems covered previously: material yielding, bolt stripping, and tray gapping. The results presented (See Appendix C.3, C.4, and C.5) in this analysis assumed that the slipping problem was solved using one of the proposed solutions or a combination of those solutions, such that the slipping problem is out of the tie rod sizing design loop.

4.16 Fortran 90 Program – An Operator's Manual

All the results presented were generated from a custom Fortran90 program. The program was tested by comparing results of an Excel Spreadsheet and hand calculation to the output obtained from the program. All results agreed. The flexibility of custom data

management, custom output file format, and ease of input variable modifications are clear advantages of the TIEROD.F90 program developed.

The program first reads the data included in the 8 input files (See Appendix C.2 for a sample of each input files):

1) Filename: TRAY.DAT
   Description: Specification of tray information and analysis to be performed
2) Filename: SAFETY.DAT
   Description: Specification of safety factors and failure modes
3) Filename: SATGEO.DAT
   Description: Specification of satellite geometry parameters
4) Filename: TLOAD.DAT
   Description: Specification of launch loads and load factors
5) Filename: BMAT.DAT
   Description: Specification of bolt materials to be included
6) Filename: JMAT.DAT
   Description: Specification of joint materials to be included
7) Filename: EBOLT.DAT
   Description: Specification of English bolt sizes to be included
8) Filename: MBOLT.DAT
   Description: Specification of Metric bolt sizes to be included

Once the basic set of files is created, quick analysis results are obtained. Running time is of the order of less than 5 seconds. The output of the program is automatically saved in 3 output files (See Appendix C.3, C.4, and C.5):

1) Filename: TIE1.RES
   Description: All viable bolts/materials combinations for all analysis performed
2) Filename: TIE2.RES
   Description: Minimum bolt stress area for each material considered
3) Filename: TIE3.RES
   Description: Best overall results for each material considered (sorted by mass)

The Fortran90 program is run in dos mode. The 3 output files and 8 input files must be placed in the same directory as the executable file (TIEROD.EXE) for the program to run properly. To run the program, simply key-in the word TIEROD and then press the *Enter* key. The output files can then be viewed in MSWord or in any other ASCII file viewer. The tables were constructed for easy importation into MS Excel where further data treatments can be done.

Chapter 5

Conclusion

This work has presented structural analyses spanning from the preliminary design to the detailed MOST microsatellite design. The primary objective of this work was to provide the Space Flight Laboratory (SFL) with detailed structural analyses and subsequent design recommendations for the MOST microsatellite mission. In order to achieve this goal, finite element methods were extensively used. The multiple investigations presented herein mainly covered the static load stresses and normal vibration modes of the spacecraft. The main assumptions made were those inherent to the use of thin shells (assuming small deflections) to model the spacecraft: there is no deformation in the middle plane of the plate (the middle plane remains neutral during bending), the normal to the middle plane of the plate remains normal to the middle surface of the plate under bending, and the normal stresses in the direction transverse to the plate are negligible.

Under these assumptions, the preliminary results presented in Chapter 2 showed satisfactory structural behaviours. Specifically, the PCB analysis showed that four pins placed in a diamond-like shape at the middle of the PCB and eight pins on the PCB contour (See Figure 2.2 C) features a first natural frequency far above the launch vehicle requirement. Moreover, a vibration sensitivity analysis was performed for the bottom tray plate and showed optimum size of shell elements to be 1.5mm in thickness. Analysis also highlighted that no plate stiffeners are required. Subsequent analytical investigations showed that a non-uniform mass distribution with centre of mass as close to PAA as possible will lead to higher first natural frequency. The laminate definition used (Hexcel® Honeycomb[78] 1/8-5052-.0015inch, 12.7mm thick with Aluminum-5052 facesheets of 0.5mm thick) featured reliable static deformation results. Finally, it was

determined that the PAA location, from a rough spacecraft level analysis, should be modified. The PAA plate was moved in the negative y-direction by 0.1219m (towards the instrument enclosure). The PAA plate translation involved strengthening the instrument enclosure by extending the honeycomb panel surrounding the tray stack to cover the entire telescope enclosure.

The main detailed design results included herein were based on tray sub-assembly and detailed spacecraft level analyses. Many models were constructed, but only two of the detailed spacecraft design models were presented herein for brevity and for reader comprehension. Convergence and reliability of the results was demonstrated to the extent possible. The final detailed model feature all previous natural vibration modes, but two modes appeared due to the non-rigid PAA plate modelling. The frequency and stress analyses performed showed satisfactory results. After following all good FE modelling practices highlighted in Chapter 2, verifying the convergence from one model to the next, performing basic sensitivity analysis, and correlating results to analytical results whenever possible, the MOST final detailed model results presented herein are believed to be reliable within the assumptions made. Hence, the margin of safety greater than zero obtained by finite element analysis, including a safety factor of 2.0 on all launch conditions and a factor of safety of 1.65 on the materials yield strength, indicates that the MOST structural design possesses adequate strength to survive the Delta II launch.

The Delta II launch authorities expected the first natural frequency to be of the order of 50Hz. The detailed spacecraft model showed a first natural frequency of 59.8Hz. This frequency can be raised by stiffening the PAA plate and by selecting a thicker honeycomb panel. However, these modifications are felt unnecessary, as the analysis has proven to be a conservative account of the dynamical behaviours. It is important to note that the restrictions imposed by the 2-D shell element model turn out to lead to a conservative result. The stiffening effect of having the PAA plate bolted against the honeycomb laminate panel cannot be modelled properly with shell elements. The stiffness of the real spacecraft assembly will be higher then the actual finite element model, and hence the model is a weak approximation leading to safer results.

This thesis finally presents a detailed engineering analysis leading to the design of the MOST tie rods structural component. As mentioned earlier, the tray stack conceptual design offers great advantages in terms of the ease of assembly. However, the sizing of tie rods for small satellites using a tray stack as a primary structure remains a challenging design problem. The analysis results presented herein provided the SFL MOST engineering team with a clear understanding of tie rod design. All failure modes have been looked at extensively and the final results were presented in Table 4.3, and Appendix C.3. Although tie rod design recommendations were clearly stated in Section 4.14, all the intermediate results are also available in tables of Appendix C.3 in order to provide alternative choices for the designers of MOST. Four failure modes were highlighted in Section 4.5. These four failure modes were mathematically represented in terms of design constraints. The derivation of these four constraint equations were presented in this document and provided useful account of the material yielding constraint, bolt thread stripping constraint, tray gapping constraint, and tray slipping constraint. The constraint equations derived (Equations 4.32b, 4.39, 4.41, and 4.43b) cannot be used alone directly to determine the minimum bolt stress area required for each material considered. The worst case combination of the above four failure constraints were used to size MOST tierods. The derivation of the minimum stress area based on known variables for all possible failure mode combinations was presented.

As observed in Chapter 4, many material/bolt combinations can be used to achieve the no failure criteria (except for the slipping failure mode, which must be handled some other way, i.e., the addition of a shoulder, a gasket, some inserts, or an interface plate is recommended in Section 4.15). Appendix C.5 presents results from output of the TIEROD.F90 program for the best material and bolt combinations that would achieve the design goals. Among them, the combination of 4 tie rods (Size ¼-28) made out of AM-355 stainless steel (AMS 5743/SCT1000) is one of the lightest bolt/material solutions at around 622 grams. 8 M6.3x1 tie rods made out of Ti-6Al-4V (AMS-4928) is also one of the lightest bolt/material solutions at around 700 grams. Simplification of the design and extra weight saving are the two clear advantages of using the 4 tie rods configuration. Future MOST design shall make use of this result to reduce mass of the primary structure. As far as the current MOST design is concerned, the 8 tie rods configuration was pre-selected by engineers. In that configuration, two solutions are

proposed: a custom design using titanium as mentioned earlier or some cheap off-the-shelf stainless steel tie rods. The later has the advantage of being readily available and cheap. The obvious disadvantage is the addition of 500 grams to the primary structure. There is no performance gain other than the mass reduction in using titanium tie rods.

It is felt that cost is not a major issue when considering a stand-alone design. Hence, the titanium solution is recommended. However, if MOST was to be used within a constellation of small satellites, or, if cost was more important than weight, the cheaper solution should be favoured. The tradeoff here is simple: 45% lighter at 10 times the cost or 45% heavier at one tenth of the cost.

The results included in this thesis provided the SFL MOST mission design team with useful analyses indicating that, within the assumptions made, the MOST structural design possesses adequate strength to survive the Delta II launch. Modifications and other avenues were also investigated to provide the SFL design team with better alternatives supported by analytical and preliminary finite element results that should be used for future microsat missions. Hence, the primary goal of the thesis was achieved successfully and some analyses even provided results outside the scope of this document.

References

[1] Hughes, P.C., Space Structure Vibration Modes: How Many Exist? Which Ones are Important?, UTIAS Technical Note No.252, 1984

[2] Todhunter, I., Pearson, K. (ed.), A History of the Theory of Elasticity and of the Strength of Materials, Vol.I, Vol.II (Part I & II), Cambridge: At the University Press, 1886

[3] Truesdell, C., The Rational Mechanics of Flexible and Elastic Bodies (1638-1788), Leonhardi Euleri Opera Omnia, Series 2 Volume 11 part 2, Switzerland, 1960

[4] Burkhardt, H., *Entwicklungen nach oscillirenden Functionen und Integration der Differentialgleichungen der mathematischen Physik*, Parts I, II, and IV, Jahresber, 1908

[5] Timoshenko, S.P., History of Strength of Materials, Dover Publications, New York, 1983

[6] Florman, S.C., The Existential Pleasures of Engineering, 2nd Ed., St.Martins's Griffin, New York, 1994

[7] Parsons, W.B., Engineers and Engineering in the Renaissance, 1939

[8] Galileo, Two New Sciences, English translation by Henry Crew and Alfonso de Salvio, The Macmillan Company, New York, 1933

[9] Galileo, Two New Sciences, English translation by Stillman Drake, UofT Press, Toronto, 1933

[10] Fahie, J.J., Galileo, His Life and Work, New York, 1903

[11] Zsolt de Harsanyi, The Star-gazer, English translation by P. Tabor, New York, 1939

[12] Hooke, R., De Potentiâ Restitutiva, 1678

[13] Gunther, R.T., The Life and Work of Robert Hooke, Early Science in Oxford, vols. VI-VIII

[14] Bertrand, *L'Académie des Sciences et les Académiciens de 1666 a 1793*, Paris, 1869

[15] Robison, J., Elements of Mechanical Philosophy, Edinburgh, 1804

[16] de la Hire, P., The Motion of Fluids, 1686

[17] Newton, I., *Philosophiae naturalis principia mathematica*, London, 1687

[18] Euler, L., *Methodus inveniendi lineas curvas*, Berlin, 1743

[19] Poisson, S.D., *Mémoire sur l'équilibre et le mouvement des corps élastiques*, Mém. Acad., vol.8, Paris, 1829

[20] Poisson, S.D., *Mémoire sur les équation générales de l'équilibre et du mouvement des corps élastiques et des fluides*, J. école polythechnique, cahier 20, Paris, 1831

[21] Poisson, S.D., *Traité de mécanique*, 2nd ed., Paris, 1833

[22] Lamé, G., Clapeyron, B.P.E., *Sur l'équilibre intérieur des corps solides homogènes*, St-Petersburg, 1824

[23] Lamé, G., *Leçons sur la théorie mathématique de l'élasticité des corps solides*, 1e Edition, Gauthier-Villars, Paris, 1854

[24] Lamé, G., *Leçons sur la théorie mathématique de l'élasticité des corps solides*, 2e Edition, Gauthier-Villars, Paris, 1866

[25] Stokes, G. G., On the Theories of the Internal Friction of Fluids in Motion, and of the Equilibrium and Motion of Elastic Solids, presented to the Cambridge Philosophical Society, 1845

[26] Clebsch De, A., *Théorie de l'élasticité des corps solides*, Premier et Second Fascicule, Dunod, Paris, 1883

[27] Saint-Venant De, B., Pearson, K. (editor), The Elastical Researches of Barré de Saint-Venant, Cambridge: At the University Press, 1889
[28] Galerkin, B.G., Elastic Thin Plates, Moscow, 1933
[29] Love, A.E.H., A Treatise on the Mathematical Theory of Elasticity, 4th Edition, Cambridge, 1927. Russian translation Moscow-Leningrad, 1935
[30] Timoshenko, S.P., Theory of Plates and Shells, McGraw-Hill, 1940
[31] Timoshenko, S.P., Theory of Elasticity, vol.1&2, St. Petersburg, 1916
[32] Timoshenko, S.P., Gere, J.M., Theory of Elastic Stability, McGraw-Hill, 2nd Edition, 1961
[33] Timoshenko, S.P., Goodier, J.N., Theory of Elasticity, 3rd Edition, McGraw-Hill, New York, 1970
[34] Gere, J.M., Timoshenko, S.P., Mechanics of Materials, 4th Edition, PWS Publishing Company, Boston, 1997
[35] Muskhelishvili, N.I., Some Basic Problems of the Mathematical Theory of Elasticity, 3rd Edition, P. Noordhoff, 1953
[36] Novozhilov, V.V., Foundations of the Nonlinear Theory of Elasticity, Dover Publications, New York, 1953
[37] Sokolnikoff, I.S., Mathematical Theory of Elasticity, 2nd Edition, McGraw-Hill, 1956
[38] Mushtari, Kh.M., Galimov, K.Z., Nonlinear Theory of Thin Elastic Shells, S. Monson, Kazan', 1957
[39] Flügge, W., Stresses in Shells, Springer-Verlag OHG., Second printing, Berlin, 1962
[40] Flügge, W., Tensor Analysis and Continuum Mechanics, Springer-Verlag OHG., Second printing, Berlin, 1972
[41] Niordson, F.I., Theory of Thin Shells, 2nd Symposium, Copenhagen, Springer-Verlag, 1969
[42] Bruhn, E.F., Analysis and Design of Flight Vehicle Structures, S R Jacobs, 1973
[43] Curtis, A.R. (editor), Space Almanac, 2nd edition, Gulf Publishing, 1992
[44] Davidoff, M., The Satellite Experimenter's Handbook, 2nd edition, ARRL, 1990
[45] Wilson, A. (editor), Jane's Space Directory, 16th edition, Jane's Information Group, 2000
[46] Gunston, W., Jane's Aerospace Dictionary, New York, Jane's Publishing, 1988
[47] AGARD Multilingual Aeronautical Dictionary, Paris, 1980
[48] AIAA, Aerospace Design Engineers Guide, 4th edition, AIAA, Reston, 1998
[49] Dictionary of Technical Terms for Aerospace Use, NASA SP-7, 1965
[50] Wertz, J.R. (editor), 1997 Microcosm Directory of Space Technology Data Sources, Microcosm Press, Torrance, 1996
[51] Barter, N.J. (editor), TRW Space Data, 4th edition, TRW, 1992
[52] KISS Database, ZARM/University of Bremen, Germany, 1990
[53] Hujsak, Future of U.S. Rocketry, Mina-Helwig Publishers, 1994
[54] Isakowitz, S.J., International Reference to Space Launch System, 2nd edition, AIAA, 1995
[55] AIAA, Guide to Terminology for Space Launch Systems, AIAA, Washington, 1994
[56] Wertz, J.R. and Larson, W.J. (eds.), Space Mission Analysis and Design, Kluwer Academic Publishers, Norwell, MA, 1991
[57] Wertz, J.R., Larson, W.J. (editors), Reducing Space Mission Cost, Microcosm Press, Torrance, 1996
[58] Sarafin, T.P. (editor), Spacecraft Structures and Mechanisms - From Concept to Launch, Microcosm Press, Torrance, 1995
[59] McDonnell Douglas Corporation/The Boeing Company, Delta II Payload Planners Guide, MDC H3224D, April 1996
[60] NASA, Goddard Space Flight Center, Delta Launch Vehicle Secondary Payload Planner's Guide for NASA Missions, November 1993

[61] MOST Phase A Report, Internal Report, Dynacon Report 29-708/01-A, Toronto, December 1997
[62] MOST Proposal, ISTS Proposal Number ISL-063, 8 January 1997
[63] Carroll, K.A., McTavish, D.J., Matthews, J., Rucinski, S., MOST: A Space Astronomy Microsatellite Mission, paper presented at the poster session of the Eleventh Annual AIAA/UTAH State University Conference on Small Satellites, September 1997
[64] Carroll, K.A., MOST Requirements and Design Specifications, Dynacon Enterprises Limited, Version 1.3, December 12, 1997
[65] NASA, NASA-STD-5001: Structural Design and Test Factors of Safety for Spaceflight Hardware, June 21, 1996
[66] Caffrey, J.P., Lee, J.M., MSC/NASTRAN User's Guide – Linear Static analysis, MSC, Los Angeles, 1994
[67] Bathe, K.-J., Finite Element Procedures, Prentice Hall, New Jersey 07458, 1996
[68] Brenner, S.C., Scott, L.R., The Mathematical Theory of Finite Element Methods, Springer-Verlag, New York, 1994
[69] Burnett, D.S., Finite Element Analysis from Concepts to Applications, Addison-Wesley, 1987
[70] Blevins, R.D., Formulas for Natural Frequency and Mode Shape, Krieger, 1979
[71] Jones, R., An Approximate Expression for the Fundamental Frequency of Vibration of Elastic Plates, Journal of Sound and Vibration, 38 (4): 503-504, 1975
[72] Leissa, A.W., Vibration of Plates, NASA SP-160, Washington, DC, 1969
[73] Meirovitch, L., Elements of Vibration Analysis, 2nd Edition, McGraw-Hill, 1986
[74] Thomson, W.T., Theory of Vibration with Applications, 4th Edition, Prentice Hall, 1993
[75] Lanczos, C., The Variational Principles of Mechanics, 4th Edition, Dover, 1970
[76] Steinberg, D.S., Avoiding Vibration in Odd-Shaped Printed-Circuit Boards, Machine Design, May 1976
[77] Military Department-USA, MIL-HDBK-5G: Metallic Materials and Elements for Aerospace Vehicle Structures, 1990
[78] Hexcel Corporation, Technical Service Bulletin - Honeycomb, TSB124 Bonded Honeycomb Sandwich Construction,
[79] Hexcel Corporation WWW homepage, http://www.hexcel.com/
[80] Hart-Smith, L.J., Designing with Advanced Fibrous Composites, Australian bicentennial international congress in mechanical engineering, 1988
[81] ANSI/AIAA, G-020-1992, Guide for Estimating and Budgeting Weight and Power Contingencies for Spacecraft Systems, Washington, 1992
[82] Mullins, M., MOST Instrument Preliminary Structural Analysis, Issue A, Mayes Mullins Enterprises Ltd., 1999
[83] Hughes, P.C., Modal Identities for Elastic Bodies, With Application to Vehicle Dynamics and Control, Journal of Applied Mechanics, March 1980, Vol.47, pp.177-184
[84] Bickford, J.H., An Introduction to the Design and Behavior of Bolted Joints, Marcel Dekker, 3rd Edition, New York, 1995
[85] Eshbach, O.W., Handbook of Engineering Fundamentals, 2nd Edition, Wiley, New York, 1953
[86] Fisher, J.W., Struik, J.H.A., Kulak, G.L., Guide to Design Criteria for Bolted and Riveted Joints, 2nd Edition, Wiley, New York, 1987
[87] Horsch, R., Solve Complicated Force Problems with Simple Diagrams, Assembly Eng., pp.22-24, December 1972
[88] Osgood, C.C., How Elasticity Influences Bolted Joint Design - part 1, Machine Design, pp.92ff, February 24, 1972

[89] Osgood, C.C., How Elasticity Influences Bolted Joint Design - part 2, Machine Design, pp.104ff, March 9, 1972

[90] Shigley, J.E., Mechanical Engineering Design, 3rd Edition, McGraw-Hill, New York, 1977

[91] Srinivas, A.R., Determination of Torque Values for Metric Fasteners - An Approach, Space Payload Group, Space Applications Center, Indian Space Research Organization, Ahmedabad, India, Document 380 053, May 1992

[92] MSFC-SPEC-522B, Design Criteria for Controlling Stress Corrosion Cracking

[93] Boresi, A.P., Schmidt, R.J., Sidebottom, O.M., Advanced Mechanics of Materials, 5th Edition, John Wiley & Sons, 1993

[94] Meyer, G., Strelow, D., Simple Diagrams Aid in Analyzing Forces in Bolted Joints, Assembly Eng., January 1972

[95] Peterson, R.E., Stress Concentration Factors, John Wiley & Sons, New York, 1974

[96] Roark, R., Young, W.C., Formulas for Stress and Strain, 5th Edition, McGraw-Hill, New York, 1975

[97] Seika, M., Sasaki, S., Hosono, K., Measurement of Stress Concentrations in Threaded Connections, Bull. JSME, vol.17, no.111, September 1974

[98] Motosh, N., Development of Design Charts for Bolts Preloaded up to the Plastic Range, J. Eng.Ind., August 1976

[99] Metric Screw Threads - M Profile, ANSI/ASME B1.13M-1983, ASME, New York, 1983

[100] Metric Screw Threads - MJ Profile, ANSI B1.21M-1978, ASME, New York, 1991

[101] Metric Screw Threads for Commercial Mechanical Fasteners - Boundary Profile Defined, ANSI B1.18M-1982, ASME, New York, 1987

[102] Nomenclature, Definitions, and Letter Symbols for Screw Threads, ANSI/ASME B1.7M-1984, ASME, New York, 1992

[103] Screw Threads, Controlled Radius Root with Increased Minor Diameter, General Specifications for, MIL-S-8879C, U.S. Government Printing Office, Washington, DC, July 25, 1991

[104] Screw Thread Standards for Federal Services (USA), Unified Inch Screw Threads - UN and UNR Forms, FED-STD-H28/2B, 20 August 1991, Defense Industrial Supply Center, Philadelphia, PA

[105] ACME Screw Threads, ASME/ANSI B1.5-1988, ASME, New York, 1988

[106] ASME Boiler and Pressure Vessel Code, 1983 ed., ASME, New York, 1983

[107] Unified Inch Screw Threads UN and UNR Thread Forms, ASME Standard B1.1-1989, ASME, New York, 1989

[108] Machinery's Handbook, 25th Edition, The Industrial Press, New York, 1997

[109] Alexander, E.M., Design and Strength of Screw Threads, Presented at American National Metric Council Conference, Washington, DC, 1975

[110] Blake, A., What Every Engineer Should Know About Threaded Fasterners, Marcel Dekker, New York, 1986

[111] Ellison, H.W., Effects of Nut Geometry on Nut Strength, General Motors Corp., Warren, MI, 1970

[112] FED-STD-H28/2B, Screw Thread Standards for Federal Services-Section 2, Unified Inch Screw Threads - UN and UNR forms, Philadelphia, August 20, 1991

[113] Gill, P., The Static Strength of Screw Threads, G.N.K., UK.

[114] Sharman, J.M., Threaded Fastener Selection, Engineering (UK), October 1975

[115] Milestone, W.D., Fatigue Design Considerations in Bolted Joints, Presented at Using Threaded Fasteners Seminar, University of Wisconsin-Extension, Madison, WI, 1979

[116] Osgood, C.C., Fatigue Design, Wiley, New York, 1970

[117] Junker, G.H., New Criteria for Self-Loosening of Fasteners under Vibration, Reprinted

October 1973 from Trans. SAE, Vol. 78, 1969

[118] Sakai, Tomotsugu, Investigations of Bolt Loosening Mechanism, Bulletin of the JSME, Vol. 21, Paper No. 159-9, September 1978

[119] Landt, R.C., Preload Loss and Vibration Loosening, SPS Technologies, Jenkintown, PA, 1979

[120] Landt, R.C., Vibration Loosening - Causes and Cures, Presented at Using Threaded Fasteners Seminar, University of Wisconsin-Extension, Madison, WI, April 24, 1979

[121] Landt, R.C., Vibration Loosening - Causes and Cures, Presented at Using Threaded Fasteners Seminar, University of Wisconsin-Extension, Madison, WI, May, 1980

[122] Baubles, R.C., McCormick, G.J., Loosening of Fasteners by Vibration, document ER272-2177, Eng. No. 30 published by the Elastic Stop Nut Corp. of America (ESNA), Union, NJ, December 1966

[123] Daadbin, A., Chow, Y.M., A Theoretical Model to Study Thread Loosening, Department of Mechanical Engineering, University of Newcastle on Tyne, NE1 7RU, UK, 1990

[124] Walker, R.A., The Factors which Influence the Vibration Loosening of Fasteners, Presented - 1973 Design Engineering Conference, Philadelphia Civic Center, April, 1973

[125] Petras, J., Designing with Locking Fasteners, Fastener Technology International, pp.48-49, December 1993

[126] Finkelston, R.J., Preloading for Optimum Bolt Efficiency, Assembly Eng., August 1974

[127] Lamontagne, C., Microsat Design Course Final Report, Internal Document, UTIAS-SFL, Toronto, 1998

Appendix A

Conversion Factors

Input	Multiply by	Output
inch	0.0254	meter
inch	25.4	millimeter
foot	0.305	meter
yard	0.914	meter
ksi	6.89	megapascal
psi	6.89	kilopascal
pound-mass	0.454	kilogram
slug	14.6	kilogram
ton	907	kilogram
pound-foot	1.36	newton-meter
degree	0.0174	radian
foot-pound	1.35	joule
kip	4.45	kilonewton
moment of inertia lbm.ft^2	0.0421	kilogram-meter^2

Appendix B

I-DEAS Filenames and Description

I-DEAS Filename	Description	Phase
MOST_1D_BUS.mf1	Beam Elements - Bus Loads & Vibration	Preliminary
MOST_1D_SATMODEL.mf1	Beam Elements - S/C Loads & Vibration	Preliminary
MOST_2D_PCB_15.mf1	PCB Vibration Analysis (Best attachment pattern)	Preliminary
MOST_2D_TRAY.mf1	Shell Elements - Tray Loads & Vibration	Preliminary
MOST_2D_TRAY_PCB.mf1	Shell Elements - Tray and PCB Vibration	Preliminary
MOST_ENVELOPPE.mf1	Delta II Secondary Payload Enveloppe	Preliminary
LAMINATE.mf1	Laminate Definition - Test Sample	Preliminary
MOST_2D_SATMODEL_PRE.mf1	Shell Elements - S/C Loads & Vibration	Preliminary
MOST_TELESCOPE.mf1	Telescope Model (From Nastran File Provided)	Detailed
MOST_TRAY1.mf1	Detailed Transceiver1 Tray Analysis	Detailed
MOST_TRAY2.mf1	Detailed Instrument-CCD Tray Analysis	Detailed
MOST_TRAY3.mf1	Detailed ACS-CCD Tray Analysis	Detailed
MOST_TRAY4.mf1	Detailed OBC Tray Analysis	Detailed
MOST_TRAY5.mf1	Detailed Spacer1 Tray Analysis	Detailed
MOST_TRAY6.mf1	Detailed PAA1 Tray Analysis	Detailed
MOST_TRAY7.mf1	Detailed Reaction Wheels Tray Analysis	Detailed
MOST_TRAY8.mf1	Detailed PAA2 Tray Analysis	Detailed
MOST_TRAY9.mf1	Detailed Power Tray Analysis	Detailed
MOST_TRAY10.mf1	Detailed PAA3 Tray Analysis	Detailed
MOST_TRAY11.mf1	Detailed AMSAT Tray Analysis	Detailed
MOST_TRAY12.mf1	Detailed ACS1 Tray Analysis	Detailed
MOST_TRAY13.mf1	Detailed ACS2 Tray Analysis	Detailed
MOST_TRAY14.mf1	Detailed Spacer2 Tray Analysis	Detailed
MOST_TRAY15.mf1	Detailed Transceiver2 Tray Analysis	Detailed
MOST_2D_BUS.mf1	Detailed Bus Assembly Analysis	Detailed
MOST_2D_SATMODEL_DET.mf1	Detailed Spacecraft Analysis	Detailed
MOST_TIE_RODS.mf1	Tie Rod Loads Analysis	Detailed
GEOMETRICAL_FORMS.mf1	Basic Geometrical Forms Comparison	Other

Appendix C

Tie Rod Design Program

C.1 Fortran90 Source Code

```
!
!-----------------------------------------
!  TIE ROD PROGRAM FILE (REVISION 10)
!-----------------------------------------
!
PROGRAM TIEREV10
!
!-----------------------------------------
!  MAIN VARIABLES DEFINITION
!-----------------------------------------
!
!  SEE NOTATION IN CHAPTER 5
!
!-----------------------------------------
!  DECLARATION STATEMENTS
!-----------------------------------------
!
IMPLICIT NONE
!
!  REAL DOUBLE PRECISION VARIABLES
!
REAL (KIND(0D0)) :: PI,EJ(100),TYJ(100),SYJ(100),PJ(100),MRJ(100)
REAL (KIND(0D0)) :: MUJ(100),EB(100),TYB(100),SYB(100),PB(100)
REAL (KIND(0D0)) :: MRB(100),MUB(100),ASM(200),ABM(200),ASE(200)
REAL (KIND(0D0)) :: ABE(200),ASMAX,AA,BB,CC,C,ASMIN(800)
REAL (KIND(0D0)) :: SFY,SFST,SFG,SFS,MS4(100),BMAS
REAL (KIND(0D0)) :: MSY,MSST,MSG,MSS,MS1(100),MS2(100),MS3(100)
REAL (KIND(0D0)) :: SATMASS,GLL,DFACT,TSFACT,G,C1,TEMP
REAL (KIND(0D0)) :: XMOM,YMOM,ZMOM,SATW,TN,TH,LT,LB,LG,LBE,LSE,L
REAL (KIND(0D0)) :: FT,FX,AJ,THWT,FORCEDIV(100),RC,FS
REAL (KIND(0D0)) :: M0,M1,F0,F1,EE0,EE1,KB,KJ,NTIE(100)
REAL (KIND(0D0)) :: MNEW,ANSWER,MAXASMIN,MINASMIN,FB1,FB2
REAL (KIND(0D0)) :: DFB,FB,FP,FJ,DD,ASRES(100)
REAL (KIND(0D0)) :: ASMIN1(100),ASMIN2(100),ASMIN3(100),ASMIN4(100)
REAL (KIND(0D0)) :: EBOLTMA(100),EBOLTMS(100),EBOLTFP(100)
REAL (KIND(0D0)) :: MBOLTMA(100),MBOLTMS(100),MBOLTFP(100)
REAL (KIND(0D0)) :: RATIO,GRESR(100,6),JCOST(100),BCOST(100)
!
!  INTEGER VARIABLES
!
INTEGER (KIND(4)) :: I,J,II,JJ,NEBOLT,NMBOLT,CHECK,ASMAT(100)
INTEGER (KIND(4)) :: NBMAT,NJMAT,MAXASJ,MINASJ,KK
INTEGER (KIND(4)) :: NANALYSIS,LL,NTR(100),FAILIN(100),LLL
INTEGER (KIND(4)) :: III,JJJ,NRES,MNBT,ENBT,COUNT
INTEGER (KIND(4)) :: YT,STT,GT,ST
!
!  CHARACTER VARIABLES
!
CHARACTER (LEN=25) :: MBNAM(200),MBSER(200),EBOLTNA(100)
CHARACTER (LEN=25) :: EBNAM(200),EBSER(200),MBOLTNA(100)
CHARACTER (LEN=68) :: MNAJ(100),MNAB(100)
CHARACTER (LEN=25) :: EBSERIE(100),MBSERIE(100)
CHARACTER (LEN=45) :: GRESA(100,4)
!
!-----------------------------------------
!  INTERFACE FOR SUBROUTINES
!-----------------------------------------
!
INTERFACE
 SUBROUTINE SWAP(A,B)
  IMPLICIT NONE
  REAL (KIND(0D0)), INTENT(IN OUT) :: A,B
 END SUBROUTINE SWAP
 SUBROUTINE
READINPUTFILES1(NMBOLT,MBNAM,MBSER,ASM,ABM,NEBOLT,&
 &EBNAM,EBSER,ASE,ABE,NJMAT,MNAJ,EJ,TYJ,SYJ,PJ,MRJ,MUJ,JCOST)
  IMPLICIT NONE
  REAL (KIND(0D0)), INTENT(OUT) :: ASM(:),ABM(:),ASE(:),ABE(:)
  REAL (KIND(0D0)), INTENT(OUT) :: EJ(:),TYJ(:),SYJ(:),PJ(:)
  REAL (KIND(0D0)), INTENT(OUT) :: MRJ(:),MUJ(:),JCOST(:)
  INTEGER (KIND(4)), INTENT(OUT) :: NMBOLT,NEBOLT,NJMAT
  CHARACTER (LEN=25), INTENT(OUT) :: MBNAM(:),MBSER(:)
  CHARACTER (LEN=25), INTENT(OUT) :: EBNAM(:),EBSER(:)
  CHARACTER (LEN=68), INTENT(OUT) :: MNAJ(:)
 END SUBROUTINE READINPUTFILES1
 SUBROUTINE
READINPUTFILES2(NBMAT,MNAB,EB,TYB,SYB,PB,MRB,MUB,BCOST,&

&SFY,SFST,SFG,SFS,MSY,MSST,MSG,MSS,SATMASS,GLL,DFACT,TSFACT,G,
&
   &YT,STT,GT,ST)
  IMPLICIT NONE
  REAL (KIND(0D0)), INTENT(OUT) :: EB(:),TYB(:),SYB(:),PB(:),MRB(:)
  REAL (KIND(0D0)), INTENT(OUT) :: MUB(:),BCOST(:),SFY,SATMASS,GLL
  REAL (KIND(0D0)), INTENT(OUT) :: SFST,SFG,SFS,MSY,MSST,MSG,MSS
  REAL (KIND(0D0)), INTENT(OUT) :: DFACT,TSFACT,G
  INTEGER (KIND(4)), INTENT(OUT) :: NBMAT,YT,STT,GT,ST
  CHARACTER (LEN=68), INTENT(OUT) :: MNAB(:)
 END SUBROUTINE READINPUTFILES2
 SUBROUTINE
READINPUTFILES3(XMOM,YMOM,ZMOM,SATW,TN,TH,LT,LB,LG,THWT,&
   &NANALYSIS,NTR,NTIE,FORCEDIV,AJ,C1)
  IMPLICIT NONE
  REAL (KIND(0D0)), INTENT(OUT) ::
XMOM,YMOM,ZMOM,SATW,TN,TH,LT,LB
  REAL (KIND(0D0)), INTENT(OUT) :: LG,THWT,NTIE(:),FORCEDIV(:)
  REAL (KIND(0D0)), INTENT(OUT) :: AJ,C1
  INTEGER (KIND(4)), INTENT(OUT) :: NANALYSIS,NTR(:)
 END SUBROUTINE READINPUTFILES3
END INTERFACE
!
!-----------------------------------------
!  OPEN STORAGE DATA FILES
!-----------------------------------------
!
OPEN(UNIT=9,FILE='TIE1.RES',ACTION='WRITE')
OPEN(UNIT=10,FILE='TIE2.RES',ACTION='WRITE')
OPEN(UNIT=11,FILE='TIE3.RES',ACTION='WRITE')
!
!-----------------------------------------
!  INITIAL ASSIGNMENT STATEMENTS
!-----------------------------------------
!
CALL READINPUTFILES1(NMBOLT,MBNAM,MBSER,ASM,ABM,NEBOLT,&
 &EBNAM,EBSER,ASE,ABE,NJMAT,MNAJ,EJ,TYJ,SYJ,PJ,MRJ,MUJ,JCOST)
CALL
READINPUTFILES2(NBMAT,MNAB,EB,TYB,SYB,PB,MRB,MUB,BCOST,&

&SFY,SFST,SFG,SFS,MSY,MSST,MSG,MSS,SATMASS,GLL,DFACT,TSFACT,G,
&
 &YT,STT,GT,ST)
CALL
READINPUTFILES3(XMOM,YMOM,ZMOM,SATW,TN,TH,LT,LB,LG,THWT,&
 &NANALYSIS,NTR,NTIE,FORCEDIV,AJ,C1)
IF((YT==0.AND.STT==0).OR.(GT==0.AND.ST==0))THEN
PRINT *,' TOGGLE NOT SET PROPERLY IN SAFETY.DAT'
ELSE
PI=ACOS(-1.0D0)
COUNT=0
LBE=LB+(TH/2.0D0)
LSE=LG-LB+(TN/2.0D0)
L=LB+LT
```

```
AJ=AJ*AJ
ASMAX=AJ*PI/12.0D0/C1
FT=GLL*(SATMASS/2.0D0)*DFACT*TSFACT*G
FS=FT
FT=FT*ZMOM/XMOM
RC=((SATW/2.0D0)**2+THWT**2)/2.0D0/THWT
GRESR=10000.D0
!
!-----------------------------------
!  MAIN TIEROD PROGRAM
!-----------------------------------
!
DO LL=1,NANALYSIS
FX=FT.FORCEDIV(LL)
DO I=1,NJMAT
WRITE(9,*)
WRITE(9,*)
WRITE(9,*)
WRITE(9,*)
WRITE(9,*) '-------------------------------------------'
WRITE(9,*) '-------------------------------------------'
WRITE(9,*)
WRITE(9,17) MNAJ(I)
WRITE(9,*)
WRITE(9,57) NTR(LL)
WRITE(9,*) '-------------------------------------------'
WRITE(9,*) '-------------------------------------------'
WRITE(9,*)
!
17 FORMAT('JOINT MATERIAL: ',A55)
WRITE(9,*)
'-------------------------------------------------------------------
'
ASRES=100.0D5
KK=0
DO J=1,NBMAT
WRITE(9,*)
'-------------------------------------------------------------------
'
WRITE(9,*)
WRITE(9,27) MNAB(J)
WRITE(9,*)
27 FORMAT('BOLT MATERIAL: ',A55)
PRINT *,MNAB(J)
!
!-----------------------------------------------
!  FAILURE 1: COUPLING YIELDING AND GAPPING PROBLEMS
!-----------------------------------------------
!
IF(YT==1.AND.GT==1)THEN
C=(MSG+1.0D0)*SFG
M0=0.1D0*ASMAX
M1=0.9D0*ASMAX
TEMP=M0*(TYB(J)/SFY-EB(J)*SQRT(4.D0*C1*M0/PI)/2.D0/RC)/(MSY+1.0D0)
F0=FX*(C*EJ(I)*(AJ-C1*M0)*(LBE+C1*LSE)+EB(J)*C1*M0*SATW/2.D0)
F0=-F0/(EB(J)*C1*M0*SATW/2.D0+EJ(I)*(AJ-C1*M0)*(LBE+C1*LSE))
F0=F0+TEMP
EE0=F0
TEMP=M1*(TYB(J)/SFY-EB(J)*SQRT(4.D0*C1*M1/PI)/2.D0/RC)/(MSY+1.0D0)
F1=FX*(C*EJ(I)*(AJ-C1*M1)*(LBE+C1*LSE)+EB(J)*C1*M1*SATW/2.D0)
F1=-F1/(EB(J)*C1*M1*SATW/2.D0+EJ(I)*(AJ-C1*M1)*(LBE+C1*LSE))
F1=F1+TEMP
EE1=F1
IF(ABS(EE0) < ABS(EE1)) THEN
CALL SWAP(M0,M1)
CALL SWAP(EE0,EE1)
END IF
DO WHILE(ABS(EE1) > 1.0E-8)
MNEW=M1-(EE1*(M1-M0)/(EE1-EE0))
M0=M1
EE0=EE1
M1=MNEW
IF(M1<0.0D0) EXIT
TEMP=M1*(TYB(J)/SFY-EB(J)*SQRT(4.D0*C1*M1.PI)/2.D0/RC)/(MSY+1.0D0)
F1=FX*(C*EJ(I)*(AJ-C1*M1)*(LBE+C1*LSE)+EB(J)*C1*M1*SATW/2.D0)
F1=-F1/(EB(J)*C1*M1*SATW/2.D0+EJ(I)*(AJ-C1*M1)*(LBE+C1*LSE))
F1=F1+TEMP
EE1=F1
IF(ABS(EE1) < 1.0E-8) ANSWER=M1
END DO
ASMIN1(J)=ANSWER
PRINT *,' ASMIN1= ',ASMIN1(J)
ASMIN(J)=ASMIN1(J)
FAILIN(J)=1
IF(ASMIN1(J)<0.0D0)THEN
WRITE(9,*) '***** FAILURE 1: NEGATIVE MINIMUM STRESS AREA *****'
END IF
ELSE
ASMIN1(J)=-1000.D0
END IF
!
!-----------------------------------------------
!  FAILURE 2: COUPLING YIELDING AND SLIPPING PROBLEMS
!-----------------------------------------------
!
IF(YT==1.AND.ST==1)THEN
C=(MSS+1.0D0)*SFS
M0=0.5D0*ASMAX
M1=0.7D0*ASMAX
TEMP=M0*(TYB(J)/SFY-EB(J)*SQRT(4.D0*C1*M0/PI)/2.D0/RC)/(MSY+1.0D0)
F0=-FX*C1*M0*SATW/2.0D0*EB(J)
F0=F0/(EB(J)*C1*M0*SATW/2.D0+EJ(I)*(AJ-C1*M0)*(LBE+C1*LSE))
F0=F0-C*FS/NTIE(LL)/MUJ(I)+TEMP
EE0=F0
TEMP=M1*(TYB(J)/SFY-EB(J)*SQRT(4.D0*C1*M1/PI)/2.D0/RC)/(MSY+1.0D0)
F1=-FX*C1*M1*SATW/2.0D0*EB(J)
F1=F1/(EB(J)*C1*M1*SATW/2.D0+EJ(I)*(AJ-C1*M1)*(LBE+C1*LSE))
F1=F1-C*FS/NTIE(LL)/MUJ(I)+TEMP
EE1=F1
IF(ABS(EE0) < ABS(EE1)) THEN
CALL SWAP(M0,M1)
CALL SWAP(EE0,EE1)
END IF
DO WHILE(ABS(EE1) > 1.0E-8)
MNEW=M1-(EE1*(M1-M0)/(EE1-EE0))
M0=M1
EE0=EE1
M1=MNEW
IF(M1<0.0D0) EXIT
TEMP=M1*(TYB(J)/SFY-EB(J)*SQRT(4.D0*C1*M1/PI)/2.D0/RC)/(MSY+1.0D0)
F1=-FX*C1*M1*SATW/2.0D0*EB(J)
F1=F1/(EB(J)*C1*M1*SATW/2.D0+EJ(I)*(AJ-C1*M1)*(LBE+C1*LSE))
F1=F1-C*FS/NTIE(LL)/MUJ(I)+TEMP
EE1=F1
IF(ABS(EE1) < 1.0E-8) ANSWER=M1
END DO
ASMIN2(J)=ANSWER
PRINT *,' ASMIN2= ',ASMIN2(J)
IF(ASMIN2(J)>ASMIN1(J))THEN
ASMIN(J)=ASMIN2(J)
FAILIN(J)=2
END IF
IF(ASMIN2(J)<0.0D0)THEN
WRITE(9,*) '***** FAILURE 2: NEGATIVE MINIMUM STRESS AREA *****'
END IF
ELSE
ASMIN2(J)=-1000.D0
END IF
!
!-----------------------------------------------
!  FAILURE 3: COUPLING STRIPPING AND GAPPING PROBLEMS
!-----------------------------------------------
!
IF(STT==1.AND.GT==1)THEN
C=(MSG+1.D0)*SFG
AA=2.D0*SYB(J)/(SFST*(MSST+1.0D0))
AA=AA*(EB(J)*C1*SATW/2.0D0-EJ(I)*C1*(LBE+C1*LSE))
BB=2.D0*SYB(J)/(SFST*(MSST+1.0D0))*(LBE+C1*LSE)*EJ(I)*AJ
BB=BB-FX*(EB(J)*C1*SATW/2.D0-C*EJ(I)*C1*(LBE+C1*LSE))
CC=-FX*C*(LBE+C1*LSE)*EJ(I)*AJ
IF(BB**2-4.0D0*AA*CC<0.0D0)THEN
ASMIN3(J)=-100.0D0
WRITE(9,*) '***** NEGATIVE VALUE UNDER SQRT OF FAILURE 3 *****'
ELSE
ASMIN3(J)=(-BB+SQRT(BB**2-4.0D0*AA*CC))/2.0D0/AA
END IF
PRINT *,' ASMIN3= ',ASMIN3(J)
IF(ASMIN3(J)>ASMIN1(J))THEN
ASMIN(J)=ASMIN3(J)
FAILIN(J)=3
END IF
IF(ASMIN3(J)<0.0D0)THEN
WRITE(9,*) '***** FAILURE 3: NEGATIVE MINIMUM STRESS AREA *****'
END IF
ELSE
ASMIN3(J)=-1000.D0
END IF
!
!-----------------------------------------------
!  FAILURE 4: COUPLING STRIPPING AND SLIPPING PROBLEMS
!-----------------------------------------------
!
IF(STT==1.AND.ST==1)THEN
C=(MSS+1.D0)*SFS
AA=2.D0*SYB(J)*(EB(J)*C1*SATW/2.0D0-EJ(I)*C1*(LBE+C1*LSE))
AA=AA/(SFST*(MSST+1.0D0))*NTIE(LL)*MUJ(I)
BB=2.D0*SYB(J)*(LBE+C1*LSE)*EJ(I)*AJ
BB=BB*NTIE(LL)*MUJ(I)/(SFST*(MSST+1.0D0))
BB=BB-C*FS*(EB(J)*C1*SATW/2.D0-EJ(I)*C1*(LBE+C1*LSE))
BB=BB-EB(J)*C1*SATW/2.0D0*FX*NTIE(LL)*MUJ(I)
CC=-FS*C*(LBE+C1*LSE)*EJ(I)*AJ
IF(BB**2-4.0D0*AA*CC<0.0D0)THEN
ASMIN4(J)=-100.0D0
WRITE(9,*) '***** NEGATIVE VALUE UNDER SQRT OF FAILURE 4 *****'
ELSE
ASMIN4(J)=(-BB+SQRT(BB**2-4.0D0*AA*CC))/2.0D0/AA
END IF
PRINT *,' ASMIN4= ',ASMIN4(J)
IF(ASMIN4(J)>ASMIN1(J).AND.ASMIN4(J)>ASMIN2(J).AND.&
  &ASMIN4(J)>ASMIN3(J))THEN
ASMIN(J)=ASMIN4(J)
FAILIN(J)=4
```

```
END IF
IF(ASMIN4(J)<0.0D0)THEN
WRITE(9,*)'***** FAILURE 4: NEGATIVE MINIMUM STRESS AREA *****'
END IF
ELSE
ASMIN4(J)=-1000.D0
END IF
PRINT *,FAILIN(J)
!
!-----------------------------------------------
!  BOLT MATERIAL SELECTION
!-----------------------------------------------
!
IF(ASMIN(J)<0.0D0)THEN
WRITE(9,*)'***** NEGATIVE MINIMUM STRESS AREA *****'
KK=KK+1
ELSE
IF(ASMIN(J)>ASMAX)THEN
WRITE(9,*)'***** As MINIMUM IS LARGER THAN As MAXIMUM *****'
KK=KK+1
ELSE
IF(ASMIN(J)>MAXASMIN)THEN
MAXASMIN=ASMIN(J)
MAXASJ=J
END IF
IF(ASMIN(J)<MINASMIN)THEN
MINASMIN=ASMIN(J)
MINASJ=J
END IF
!
CHECK=1
DO II=1,J
IF(ASMIN(J)<ASRES(II))THEN
IF(CHECK==1)THEN
DO JJ=J,II+1,-1
ASRES(JJ)=ASRES(JJ-1)
ASMAT(JJ)=ASMAT(JJ-1)
END DO
ASRES(II)=ASMIN(J)
ASMAT(II)=J
CHECK=0
END IF
END IF
END DO
!
WRITE(9,*)'BOLT SIZE  SERIES   PRELOAD(N)  MS(Y)   MS(ST) &
     & MS(G)   MS(S)   MASS'
WRITE(9,*)'-------------------------------------------------------------'
CHECK=0
DO II=1,NMBOLT
IF(ASM(II)>ASMIN(J).AND.ASM(II)<ASMAX)THEN
KJ=EJ(I)*(AJ-ABM(II))/SATW*2.0D0
KB=EB(J)*ABM(II)*ASM(II)/(LBE*ASM(II)+LSE*ABM(II))
DFB=KB/(KB+KJ)*FX
DD=EB(J)*SQRT(4.0D0*ABM(II)/PI)/2.D0/RC
IF(FAILIN(J)==1.OR.FAILIN(J)==2)THEN
FB=(TYB(J)/SFY-DD)*ASM(II)/(MSY+1.0D0)
ELSE
FB=2.0D0*SYB(J)/SFST*ASM(II)/(MSST+1.0D0)
END IF
FP=FB-DFB
FJ=FB-FX
MS1(II)=((TYB(J)/SFY-DD)*ASM(II)/FB)-1.0D0
MS2(II)=(2.0D0*SYB(J)/SFST*ASM(II)/FB)-1.0D0
MS3(II)=(FP/FX/SFG*(KB+KJ)/KJ)-1.0D0
MS4(II)=(MUJ(I)*NTIE(LL)*FP/SFS/FS)-1.0D0
BMAS=NTIE(LL)*ABM(II)*MRB(J)*SATW
WRITE(9,77) MBNAM(II),MBSER(II),FP,MS1(II),MS2(II),MS3(II),MS4(II),BMAS
IF(CHECK==0)THEN
MBOLTMA(J)=NTIE(LL)*ABM(II)*MRB(J)*SATW
MBOLTMS(J)=MS3(II)
MNBT=MNBT+1
MBOLTNA(J)=MBNAM(II)
MBSERIE(J)=MBSER(II)
MBOLTFP(J)=FP
END IF
CHECK=1
END IF
END DO
77 FORMAT(A11,A8,1F11.0,4F8.3,1F8.4)
IF(CHECK==0) WRITE(9,*)'***** NO METRIC BOLTS FOUND WITHIN
BOUNDARIES ******'
CHECK=0
!
DO II=1,NEBOLT
IF(ASE(II)>ASMIN(J).AND.ASE(II)<ASMAX)THEN
KJ=EJ(I)*(AJ-ABE(II))/SATW*2.0D0
KB=EB(J)*ABE(II)*ASE(II)/(LBE*ASE(II)+LSE*ABE(II))
DFB=KB/(KB+KJ)*FX
DD=EB(J)*SQRT(4.0D0*ABE(II)/PI)/2.D0/RC
IF(FAILIN(J)==1.OR.FAILIN(J)==2)THEN
FB=(TYB(J)/SFY-DD)*ASE(II)/(MSY+1.0D0)
ELSE
FB=2.0D0*SYB(J)/SFST*ASE(II)/(MSST+1.0D0)
END IF
FP=FB-DFB
FJ=FB-FX
MS1(II)=((TYB(J)/SFY-DD)*ASE(II)/FB)-1.0D0
MS2(II)=(2.0D0*SYB(J)/SFST*ASE(II)/FB)-1.0D0
MS3(II)=(FP/FX/SFG*(KB+KJ)/KJ)-1.0D0
MS4(II)=(MUJ(I)*NTIE(LL)*FP/SFS/FS)-1.0D0
BMAS=NTIE(LL)*ABE(II)*MRB(J)*SATW
WRITE(9,77) EBNAM(II),EBSER(II),FP,MS1(II),MS2(II),MS3(II),MS4(II),BMAS
IF(CHECK==0)THEN
EBOLTMA(J)=NTIE(LL)*ABE(II)*MRB(J)*SATW
EBOLTMS(J)=MS3(II)
EBOLTNA(J)=EBNAM(II)
ENBT=ENBT+1
EBSERIE(J)=EBSER(II)
EBOLTFP(J)=FP
END IF
CHECK=1
END IF
END DO
IF(CHECK==0) WRITE(9,*)'***** NO ENGLISH BOLTS FOUND WITHIN
BOUNDARIES ******'
!
END IF
END IF
WRITE(9,*)
'-------------------------------------------------------------'
_'
END DO
WRITE(9,*)
'-------------------------------------------------------------'
_'
WRITE(9,*)
'-------------------------------------------------------------'
_'
!
!-----------------------------------------
!  WRITING BEST RESULTS IN FILE
!-----------------------------------------
!
WRITE(10,*)
WRITE(10,*)
WRITE(10,37) MNAJ(I)
WRITE(10,57) NTR(LL)
WRITE(10,*)
WRITE(10,*) 'BEST BOLT MATERIALS (IN ORDER OF As MINIMUM)'
WRITE(10,*)
WRITE(10,*) 'ORDER# BOLT MATERIAL NAME                    As(MIN)'
WRITE(10,*) '-------------------------------------------------'
IF(KK>=NBMAT)THEN
WRITE(10,*) '***** NO BOLTS FOUND BETWEEN BOUNDARIES *****'
ELSE
DO II=1,NBMAT-KK
JJ=ASMAT(II)
WRITE(10,47) II,MNAB(JJ),ASRES(II)
END DO
END IF
WRITE(10,*)
WRITE(10,*)
'-------------------------------------------------------------'
WRITE(10,*)
'-------------------------------------------------------------'
WRITE(10,*)
WRITE(10,*)
WRITE(10,*) 'BEST BOLT FOR ALL VIABLE MATERIALS.'
WRITE(10,*)
WRITE(10,*) 'ORDER# BOLT MATERIAL NAME                BOLT   SERIES
MASS   PRELOAD   MS(G)   '
WRITE(10,*)'-------------------------------------------------------------'
_'
NRES=0
NRES=MNBT+ENBT
IF(NRES==0)THEN
ELSE
IF(MNBT>ENBT)THEN
LLL=MNBT
ELSE
LLL=ENBT
END IF
DO II=1,LLL
IF(II<=MNBT)THEN
JJ=ASMAT(II)
RATIO=MBOLTMA(JJ)
WRITE(10,67) II,MNAB(JJ),MBOLTNA(JJ),MBSERIE(JJ),MBOLTMA(JJ),&
     &MBOLTFP(JJ),MBOLTMS(JJ)
CHECK=1
DO III=1,LL*NRES
IF(RATIO<GRESR(III,4))THEN
IF(CHECK==1)THEN
DO JJJ=LL*NRES,III+1,-1
GRESR(JJJ,1)=GRESR(JJJ-1,1)
GRESR(JJJ,2)=GRESR(JJJ-1,2)
GRESR(JJJ,3)=GRESR(JJJ-1,3)
GRESR(JJJ,4)=GRESR(JJJ-1,4)
GRESR(JJJ,5)=GRESR(JJJ-1,5)
GRESA(JJJ,1)=GRESA(JJJ-1,1)
GRESA(JJJ,2)=GRESA(JJJ-1,2)
GRESA(JJJ,3)=GRESA(JJJ-1,3)
```

```
END DO
GRESR(III,1)=MBOLTMA(JJ)
GRESR(III,2)=MBOLTFP(JJ)
GRESR(III,3)=MBOLTMS(JJ)
GRESR(III,4)=RATIO
GRESR(III,5)=NTIE(LL)
GRESA(III,1)=MNAB(JJ)
GRESA(III,2)=MBOLTNA(JJ)
GRESA(III,3)=MBSERIE(JJ)
CHECK=0
END IF
END IF
END DO
END IF
IF(II<=ENBT)THEN
JJ=ASMAT(II)
RATIO=EBOLTMA(JJ)
WRITE(10,67) II,MNAB(JJ),EBOLTNA(JJ),EBSERIE(JJ),EBOLTMA(JJ),&
      &EBOLTFP(JJ),EBOLTMS(JJ)
CHECK=1
DO III=1,LL*NRES
IF(RATIO<GRESR(III,4))THEN
IF(CHECK==1)THEN
DO JJJ=LL*NRES,III+1,-1
GRESR(JJJ,1)=GRESR(JJJ-1,1)
GRESR(JJJ,2)=GRESR(JJJ-1,2)
GRESR(JJJ,3)=GRESR(JJJ-1,3)
GRESR(JJJ,4)=GRESR(JJJ-1,4)
GRESR(JJJ,5)=GRESR(JJJ-1,5)
GRESA(JJJ,1)=GRESA(JJJ-1,1)
GRESA(JJJ,2)=GRESA(JJJ-1,2)
GRESA(JJJ,3)=GRESA(JJJ-1,3)
END DO
GRESR(III,1)=EBOLTMA(JJ)
GRESR(III,2)=EBOLTFP(JJ)
GRESR(III,3)=EBOLTMS(JJ)
GRESR(III,4)=RATIO
GRESR(III,5)=NTIE(LL)
GRESA(III,1)=MNAB(JJ)
GRESA(III,2)=EBOLTNA(JJ)
GRESA(III,3)=EBSERIE(JJ)
CHECK=0
END IF
END IF
END DO
END IF
!
END DO
END IF
WRITE(10,*)
WRITE(10,*)
'-------------------------------------------------------------------------
-------------------'
WRITE(10,*)
'-------------------------------------------------------------------------
-------------------'
WRITE(10,*)
END DO  !  END OF JOINT MATERIALS LIST
COUNT=COUNT+MNBT+ENBT
MNBT=0
ENBT=0
END DO  !  END OF ANALYSIS
37 FORMAT('BEST RESULTS FOR JOINT MADE OUT OF: ',A55)
47 FORMAT(I3,'   ',A41,1E14.5)
57 FORMAT('AND CONSIDERING THE CASE OF',I2,' TIE RODS')
67 FORMAT(I3,'   ',A41,A8,A6,1F8.4,1F8.0,1F9.4)
!
!-----------------------------------
!  PRINTING RESULTS
!-----------------------------------
!
WRITE(11,*)
WRITE(11,*)
WRITE(11,*) 'BEST OVERALL RESULTS (BASED ON MASS):'
WRITE(11,*)
WRITE(11,*) 'BEST#  #RODS - BOLT MATERIAL NAME                BOLT
SERIES   MASS   PRELOAD  MS(G)  '
WRITE(11,*)'-------------------------------------------------------------------------
-------------------'
DO I=1,COUNT
WRITE(11,97)
I,GRESR(I,5),GRESA(I,1),GRESA(I,2),GRESA(I,3),GRESR(I,1),GRESR(I,2),GRESR
(I,3)
END DO
97 FORMAT(I3,'    ',1F3.0,'   ',A41,A8,A6,1F8.4,1F8.0,1F9.4)
WRITE(11,*)''
WRITE(11,*)'-------------------------------------------------------------------------
-------------------'
WRITE(11,*)
'-------------------------------------------------------------------------
-------------------'
WRITE(11,*)''
WRITE(11,*)'-------------------------------------------------'
WRITE(11,*)'              END OF PROGRAM REACHED'
WRITE(11,*)'-------------------------------------------------'
!
!  CLOSE FILES
!
END IF
CLOSE(UNIT=9)
CLOSE(UNIT=10)
CLOSE(UNIT=11)
!
STOP
!
!-----------------------------------
!  END OF MAIN PROGRAM
!-----------------------------------
!
END PROGRAM TIEREV10
!
!-----------------------------------
!  SUBROUTINE STATEMENT DEFINITION
!-----------------------------------
!
SUBROUTINE SWAP(A,B)
IMPLICIT NONE
REAL (KIND(0D0)), INTENT(IN OUT) :: A,B
REAL (KIND(0D0)) :: C
C=A
A=B
B=C
RETURN
END SUBROUTINE SWAP
SUBROUTINE
READINPUTFILES1(NMBOLT,MBNAM,MBSER,ASM,ABM,NEBOLT,&
  &EBNAM,EBSER,ASE,ABE,NJMAT,MNAJ,EJ,TYJ,SYJ,PJ,MRJ,MUJ,JCOST)
IMPLICIT NONE
REAL (KIND(0D0)), INTENT(OUT)  :: ASM(:),ABM(:),ASE(:),ABE(:)
REAL (KIND(0D0)), INTENT(OUT)  :: EJ(:),TYJ(:),SYJ(:),PJ(:)
REAL (KIND(0D0)), INTENT(OUT)  :: MRJ(:),MUJ(:),JCOST(:)
INTEGER (KIND(4)), INTENT(OUT) :: NMBOLT,NEBOLT,NJMAT
CHARACTER (LEN=25), INTENT(OUT) :: MBNAM(:),MBSER(:)
CHARACTER (LEN=25), INTENT(OUT) :: EBNAM(:),EBSER(:)
CHARACTER (LEN=68), INTENT(OUT) :: MNAJ(:)
INTEGER (KIND(4)) :: I
CHARACTER (LEN=85) :: DUMMY
OPEN(UNIT=1,FILE='MBOLT.DAT',ACTION='READ')
OPEN(UNIT=2,FILE='EBOLT.DAT',ACTION='READ')
OPEN(UNIT=3,FILE='JMAT.DAT',ACTION='READ')
READ(1,*) DUMMY
READ(1,*) NMBOLT
DO I=1,NMBOLT
READ(1,*) MBNAM(I),MBSER(I),ASM(I),ABM(I)
END DO
READ(2,*) DUMMY
READ(2,*) NEBOLT
DO I=1,NEBOLT
READ(2,*) EBNAM(I),EBSER(I),ASE(I),ABE(I)
END DO
READ(3,*) DUMMY
READ(3,*) NJMAT
READ(3,*) DUMMY
DO I=1,NJMAT
READ(3,*) MNAJ(I),EJ(I),TYJ(I),SYJ(I),PJ(I),MRJ(I),MUJ(I),JCOST(I)
END DO
CLOSE(UNIT=1)
CLOSE(UNIT=2)
CLOSE(UNIT=3)
RETURN
END SUBROUTINE READINPUTFILES1
SUBROUTINE
READINPUTFILES2(NBMAT,MNAB,EB,TYB,SYB,PB,MRB,MUB,BCOST,&

&SFY,SFST,SFG,SFS,MSY,MSST,MSG,MSS,SATMASS,GLL,DFACT,TSFACT,G,
&
  &YT,STT,GT,ST)
 IMPLICIT NONE
 REAL (KIND(0D0)), INTENT(OUT) :: EB(:),TYB(:),SYB(:),PB(:),MRB(:)
 REAL (KIND(0D0)), INTENT(OUT) :: MUB(:),BCOST(:),SFY,SATMASS,GLL
 REAL (KIND(0D0)), INTENT(OUT) :: SFST,SFG,SFS,MSY,MSST,MSG,MSS
 REAL (KIND(0D0)), INTENT(OUT) :: DFACT,TSFACT,G
 INTEGER (KIND(4)), INTENT(OUT) :: NBMAT,YT,STT,GT,ST
 CHARACTER (LEN=68), INTENT(OUT) :: MNAB(:)
 INTEGER (KIND(4)) :: I
 CHARACTER (LEN=85) :: DUMMY
OPEN(UNIT=4,FILE='BMAT.DAT',ACTION='READ')
OPEN(UNIT=5,FILE='SAFETY.DAT',ACTION='READ')
OPEN(UNIT=6,FILE='TLOAD.DAT',ACTION='READ')
READ(4,*) DUMMY
READ(4,*) NBMAT
READ(4,*) DUMMY
DO I=1,NBMAT
READ(4,*) MNAB(I),EB(I),TYB(I),SYB(I),PB(I),MRB(I),MUB(I),BCOST(I)
END DO
READ(5,*) DUMMY
READ(5,*) DUMMY
READ(5,*) SFY,SFST,SFG,SFS
READ(5,*) MSY,MSST,MSG,MSS
READ(5,*) DUMMY
READ(5,*) DUMMY
READ(5,*) YT,STT,GT,ST
```

```
READ(6,*) DUMMY
READ(6,*) DUMMY
READ(6,*) SATMASS
READ(6,*) DUMMY
READ(6,*) GLL
READ(6,*) DUMMY
READ(6,*) DFACT
DFACT=SQRT(DFACT)
READ(6,*) DUMMY
READ(6,*) TSFACT
READ(6,*) DUMMY
READ(6,*) G
CLOSE(UNIT=4)
CLOSE(UNIT=5)
CLOSE(UNIT=6)
RETURN
END SUBROUTINE READINPUTFILES2
SUBROUTINE
READINPUTFILES3(XMOM,YMOM,ZMOM,SATW,TN,TH,LT,LB,LG,THWT,&
  &NANALYSIS,NTR,NTIE,FORCEDIV,AJ,C1)
 IMPLICIT NONE
 REAL (KIND(0D0)), INTENT(OUT) ::
XMOM,YMOM,ZMOM,SATW,TN,TH,LT,LB
 REAL (KIND(0D0)), INTENT(OUT) :: LG,THWT,NTIE(:),FORCEDIV(:)
 REAL (KIND(0D0)), INTENT(OUT) :: AJ,C1
 INTEGER (KIND(4)), INTENT(OUT) :: NANALYSIS,NTR(:)
 INTEGER (KIND(4)) :: I
 CHARACTER (LEN=85) :: DUMMY
OPEN(UNIT=7,FILE='SATGEO.DAT',ACTION='READ')
OPEN(UNIT=8,FILE='TRAY.DAT',ACTION='READ')
READ(7,*) DUMMY
READ(7,*) DUMMY
READ(7,*) XMOM
READ(7,*) DUMMY
READ(7,*) YMOM
READ(7,*) DUMMY
READ(7,*) ZMOM
READ(7,*) DUMMY
READ(7,*) SATW
READ(7,*) DUMMY
READ(7,*) TN
READ(7,*) DUMMY
READ(7,*) TH
READ(7,*) DUMMY
READ(7,*) LT
READ(7,*) DUMMY
READ(7,*) LB
READ(7,*) DUMMY
READ(7,*) LG
READ(8,*) DUMMY
READ(8,*) DUMMY
READ(8,*) THWT
READ(8,*) DUMMY
READ(8,*) NANALYSIS
READ(8,*) DUMMY
DO I=1,NANALYSIS
READ(8,*) NTR(I),NTIE(I),FORCEDIV(I)
END DO
READ(8,*) DUMMY
READ(8,*) AJ
READ(8,*) DUMMY
READ(8,*) C1
CLOSE(UNIT=7)
CLOSE(UNIT=8)
RETURN
END SUBROUTINE READINPUTFILES3
```

C.2 Input Files

FILENAME: TRAY.DAT

```
TRAY_INFORMATION
TRAY_WALL_THICKNESS
0.0015D0
NUMBER_OF_ANALYSIS_TO_BE_LOOKED_AT
2.0D0
NUMBER_OF_TIERODS(INTEGERANDREAL)_AND_FORCE_DIVIDER
4 4.0D0 2.0D0
8 8.0D0 3.0D0
JOINT_AREA_AROUND_ONE_TIE_ROD
0.0127D0
AS_TO_AB_CONVERSION
1.60D0
```

FILENAME: SAFETY.DAT

```
SAFETY_FACTORS_AND_MARGINS
YIELDING_STRIPPING_GAPPING_SLIPPING
1.65D0 2.0D0 2.0D0 2.0D0
0.25D0 0.25D0 0.25D0 0.25D0
TOGGLE_1_MEANS_CONSIDER_AS_FAILURE_MODE_0_DO_NOT
YOU_NEED_AT_LEAST_ONE_OF_THE_FIRST_AND_LAST_TWO_TO_BE_1
1 1 1 0
```

FILENAME: SATGEO.DAT

```
SATELLITE_GEOMETRY_DATA
X_MOMENT_ARM
0.1252D0
Y_MOMENT_ARM
0.15D0
Z_MOMENT_ARM
0.157D0
TOTALSATELLITE_WIDTH
0.628D0
TN
0.004D0
TH
0.004D0
LT_EFFECTIVE_LENGTH
0.314D0
LB
0.0D0
LG_EFFECTIVE_LENGTH
0.314D0
```

FILENAME: TLOAD.DAT

```
TIE_ROD_LOAD_VALUE_REQUIRED
SATELLITE_MASS(KG)
56.0D0
G_LAUNCH_LOAD
10.0D0
DYNAMIC_FACTOR_SQRT(X)
4.0D0
3_SIGMA_FACTOR
1.0D0
G_CONSTANT_ACCELERATION
9.810D0
```

FILENAME: BMAT.DAT AND JMAT.DAT

```
BOLT_MATERIALS
23
MATERIAL NAME,E,TY,SU,POISSON,DENSITY,STATIC FRICTION
Al-6061-T6-T651                                  68.258D9  248.2114D6  186.1585D6
0.33D0 2712.630D0 0.42D0 1.0D0
CARBON-STEEL-AISI-1025-AMS5046-ANNEALED         199.948D9  248.2114D6  241.3166D6
0.32D0 7861.092D0 0.35D0 2.0D0
LOW-STEEL-ALLOY-AISI-4130-4135-8630             199.948D9  517.1070D6  393.0013D6
0.32D0 7833.412D0 0.35D0 2.0D0
CUSTOM450-STAINLESS-STEEL-AMS5763-H1050         199.948D9  930.7926D6  641.2127D6
0.29D0 7750.372D0 0.35D0 10.0D0
CUSTOM450-STAINLESS-STEEL-AMS5773-H1000         199.948D9 1034.2140D6  648.1074D6
0.29D0 7750.372D0 0.35D0 10.0D0
CUSTOM450-STAINLESS-STEEL-AMS5773-H1050         199.948D9  930.7926D6  641.2127D6
0.29D0 7750.372D0 0.35D0 10.0D0
CUSTOM450-STAINLESS-STEEL-AMS5773-H1100         199.948D9  723.9498D6  572.2651D6
0.29D0 7750.372D0 0.35D0 10.0D0
CUSTOM450-STAINLESS-STEEL-AMS5773-H1150         199.948D9  517.1070D6  503.3175D6
0.29D0 7750.372D0 0.35D0 10.0D0
CUSTOM455-STAINLESS-STEEL-AMS5617-H1000         199.259D9 1275.5306D6  854.9502D6
0.29D0 7750.372D0 0.35D0 10.0D0
15-5Ph-STAINLESS-STEEL-AMS5659-H1025            196.501D9  999.7402D6  668.7917D6
0.27D0 7833.412D0 0.35D0 10.0D0
15-5Ph-STAINLESS-STEEL-AMS5659-H1075            196.501D9  861.8450D6  655.0022D6
0.27D0 7833.412D0 0.35D0 10.0D0
15-5Ph-STAINLESS-STEEL-AMS5659-H1100            196.501D9  792.8974D6  586.0546D6
0.27D0 7833.412D0 0.35D0 10.0D0
15-5Ph-STAINLESS-STEEL-AMS5659-H1150            196.501D9  723.9498D6  586.0546D6
0.27D0 7833.412D0 0.35D0 10.0D0
PH15-7Mo-STAINLESS-STEEL-CH900                  199.948D9 1137.6354D6  827.3712D6
0.28D0 7667.332D0 0.35D0 10.0D0
AM-355-STAINLESS-STEEL-AMS5743-SCT1000          199.948D9 1068.6878D6  854.9502D6
0.32D0 7805.732D0 0.35D0 8.0D0
17-7Ph-STAINLESS-STEEL-CH900                    199.948D9 1034.2140D6  772.2131D6
0.28D0 7639.652D0 0.35D0 6.0D0
Ti-5Al-2.5Sn-AMS4926_or_MIL-T-9047              106.869D9  758.4236D6  468.8437D6
0.32D0 4484.144D0 0.34D0 20.0D0
Ti-6Al-4V-MIL-T-9047                            110.316D9  827.3712D6  551.5808D6
0.31D0 4428.784D0 0.34D0 20.0D0
Ti-6Al-4V-AMS-4928                              110.316D9  861.8450D6  572.2651D6
0.31D0 4428.784D0 0.34D0 20.0D0
Ti-13V-11Cr-3Al-MIL-T-9047-ANNEALED              99.974D9  827.3712D6  634.3179D6
0.31D0 4816.303D0 0.34D0 20.0D0
Ti-13V-11Cr-3Al-SOLUTION-TREATED-AGED           106.869D9 1103.1616D6  723.9498D6
0.31D0 4816.303D0 0.34D0 20.0D0
316-STAINLESS-STEEL-SPAENAUR                    196.501D9  723.9498D6  586.0546D6
0.27D0 7833.412D0 0.35D0 9.83D0
304-STAINLESS-STEEL-METALSUPERMARKETS           196.501D9  723.9498D6  586.0546D6
0.27D0 7833.412D0 0.35D0 6.83D0
```

FILENAME: EBOLT.DAT

```
ENGLISH_BOLTS
43
0-80        UNF       1.1613D-06 1.85806D-06
1-64        UNC       1.6968D-06 2.85079D-06
1-72        UNF       1.7935D-06 2.85079D-06
2-56        UNC       2.3871D-06 3.98682D-06
2-64        UNF       2.5419D-06 3.98682D-06
3-48        UNC       3.1419D-06 5.22111D-06
3-56        UNF       3.3742D-06 5.22111D-06
4-40        UNC       3.8968D-06 6.50899D-06
4-48        UNF       4.2645D-06 6.50899D-06
5-40        UNC       5.1355D-06 8.06043D-06
5-44        UNF       5.3548D-06 8.06043D-06
6-32        UNC       5.8645D-06 9.71917D-06
6-40        UNF       6.5484D-06 9.71917D-06
8-32        UNC       9.0322D-06 1.39141D-05
8-36        UNF       9.5097D-06 1.39141D-05
10-24       UNC       1.1290D-05 1.86078D-05
10-32       UNF       1.2903D-05 1.86078D-05
"1/4-20"    UNC       2.0516D-05 3.17108D-05
"1/4-28"    UNF       2.3484D-05 3.17108D-05
"5/16-18"   UNC       3.3806D-05 4.95481D-05
"5/16-20"   UN        3.5290D-05 4.95481D-05
"5/16-24"   UNF       3.7419D-05 4.95481D-05
"5/16-28"   UN        3.9097D-05 4.95481D-05
"3/8-16"    UNC       5.0000D-05 7.13493D-05
"3/8-20"    UN        5.3935D-05 7.13493D-05
"3/8-24"    UNF       5.6645D-05 7.13493D-05
"3/8-28"    UN        5.8645D-05 7.13493D-05
"7/16-14"   UNC       6.8581D-05 9.71143D-05
"7/16-16"   UN        7.1871D-05 9.71143D-05
"7/16-20"   UNF       7.6580D-05 9.71143D-05
"7/16-32"   UN        8.3935D-05 9.71143D-05
"1/2-13"    UNC       9.1548D-05 1.26843D-04
"1/2-16"    UN        9.7419D-05 1.26843D-04
"1/2-20"    UNF       1.0316D-04 1.26843D-04
"1/2-32"    UN        1.1161D-04 1.26843D-04
"9/16-12"   UNC       1.1742D-04 1.60536D-04
"9/16-16"   UN        1.2774D-04 1.60536D-04
"9/16-18"   UNF       1.3097D-04 1.60536D-04
"9/16-20"   UN        1.3355D-04 1.60536D-04
"9/16-28"   UN        1.4129D-04 1.60536D-04
"9/16-32"   UN        1.4323D-04 1.60536D-04
"5/8-11"    UNC       1.4581D-04 1.98192D-04
"5/8-12"    UN        1.4968D-04 1.98192D-04
```

FILENAME: MBOLT.DAT

```
METRIC_BOLTS
26
M1.6x0.35       Metric    1.2700D-06  2.0106D-06
M2x0.4          Metric    2.0700D-06  3.1416D-06
M2.5x0.45       Metric    3.3900D-06  4.9087D-06
M3x0.5          Metric    5.0300D-06  7.0686D-06
M3.5x0.6        Metric    6.7800D-06  9.6211D-06
M4x0.7          Metric    8.7800D-06  1.2566D-05
M5x0.8          Metric    1.4200D-05  1.9635D-05
M6x1            Metric    2.0100D-05  2.8274D-05
M6.3x1          Metric    2.2600D-05  3.1172D-05
M8x1.25         Metric    3.6600D-05  5.0265D-05
M10x1.5         Metric    5.8000D-05  7.8540D-05
M12x1.75        Metric    8.4300D-05  1.1310D-04
M14x2           Metric    1.1500D-04  1.5394D-04
M16x2           Metric    1.5700D-04  2.0106D-04
M20x2.5         Metric    2.4500D-04  3.1416D-04
M24x3           Metric    3.5300D-04  4.5239D-04
M30x3.5         Metric    5.6100D-04  7.0686D-04
M36x4           Metric    8.1700D-04  1.0179D-03
M42x4.5         Metric    1.1200D-03  1.3854D-03
M48x5           Metric    1.4700D-03  1.8096D-03
M56x5.5         Metric    2.0300D-03  2.4630D-03
M64x6           Metric    2.6800D-03  3.2170D-03
M72x6           Metric    3.4600D-03  4.0715D-03
M80x6           Metric    4.3400D-03  5.0265D-03
M90x6           Metric    5.5900D-03  6.3617D-03
M100x6          Metric    6.9900D-03  7.8540D-03
```

C.3 Output Files

FILENAME: TIE1.RES

JOINT MATERIAL: Al-6061-T6-T651

AND CONSIDERING THE CASE OF 4 TIE RODS

BOLT MATERIAL: Al-6061-T6-T651

***** As MINIMUM IS LARGER THAN As MAXIMUM *****

BOLT MATERIAL: CARBON-STEEL-AISI-1025-AMS5046-ANNEALED

***** As MINIMUM IS LARGER THAN As MAXIMUM *****

BOLT MATERIAL: LOW-STEEL-ALLOY-AISI-4130-4135-8630

***** As MINIMUM IS LARGER THAN As MAXIMUM *****

BOLT MATERIAL: CUSTOM450-STAINLESS-STEEL-AMS5763-H1050

BOLT SIZE	SERIES	PRELOAD(N)	MS(Y)	MS(ST)	MS(G)	MS(S)	MASS
***** NO METRIC BOLTS FOUND WITHIN BOUNDARIES *****							
***** NO ENGLISH BOLTS FOUND WITHIN BOUNDARIES *****							

BOLT MATERIAL: CUSTOM450-STAINLESS-STEEL-AMS5773-H1000

BOLT SIZE	SERIES	PRELOAD(N)	MS(Y)	MS(ST)	MS(G)	MS(S)	MASS
***** NO METRIC BOLTS FOUND WITHIN BOUNDARIES *****							
***** NO ENGLISH BOLTS FOUND WITHIN BOUNDARIES *****							

BOLT MATERIAL: CUSTOM450-STAINLESS-STEEL-AMS5773-H1050

BOLT SIZE	SERIES	PRELOAD(N)	MS(Y)	MS(ST)	MS(G)	MS(S)	MASS
***** NO METRIC BOLTS FOUND WITHIN BOUNDARIES *****							
***** NO ENGLISH BOLTS FOUND WITHIN BOUNDARIES *****							

BOLT MATERIAL: CUSTOM450-STAINLESS-STEEL-AMS5773-H1100

***** As MINIMUM IS LARGER THAN As MAXIMUM *****

BOLT MATERIAL: CUSTOM450-STAINLESS-STEEL-AMS5773-H1150

***** As MINIMUM IS LARGER THAN As MAXIMUM *****

BOLT MATERIAL: CUSTOM455-STAINLESS-STEEL-AMS5617-H1000

BOLT SIZE	SERIES	PRELOAD(N)	MS(Y)	MS(ST)	MS(G)	MS(S)	MASS
M6.3x1	Metric	11639	0.250	0.417	0.465	0.027	0.6069
1/4-20	UNC	10499.	0.250	0.418	0.282	-0.073	0.6174
1/4-28	UNF	12112.	0.250	0.418	0.546	0.069	0.6174

BOLT MATERIAL: 15-5Ph-STAINLESS-STEEL-AMS5659-H1025

BOLT SIZE	SERIES	PRELOAD(N)	MS(Y)	MS(ST)	MS(G)	MS(S)	MASS
***** NO METRIC BOLTS FOUND WITHIN BOUNDARIES *****							
***** NO ENGLISH BOLTS FOUND WITHIN BOUNDARIES *****							

BOLT MATERIAL: 15-5Ph-STAINLESS-STEEL-AMS5659-H1075

***** As MINIMUM IS LARGER THAN As MAXIMUM *****

BOLT MATERIAL: 15-5Ph-STAINLESS-STEEL-AMS5659-H1100

***** As MINIMUM IS LARGER THAN As MAXIMUM *****

BOLT MATERIAL: 15-5Ph-STAINLESS-STEEL-AMS5659-H1150

***** As MINIMUM IS LARGER THAN As MAXIMUM *****

BOLT MATERIAL: PH15-7Mo-STAINLESS-STEEL-CH900

BOLT SIZE	SERIES	PRELOAD(N)	MS(Y)	MS(ST)	MS(G)	MS(S)	MASS
M6.3x1	Metric	10122.	0.250	0.543	0.275	-0.106	0.6004
1/4-28	UNF	10536.	0.250	0.543	0.347	-0.070	0.6108

BOLT MATERIAL: AM-355-STAINLESS-STEEL-AMS5743-SCT1000

BOLT SIZE	SERIES	PRELOAD(N)	MS(Y)	MS(ST)	MS(G)	MS(S)	MASS
***** NO METRIC BOLTS FOUND WITHIN BOUNDARIES *****							
1/4-28	UNF	9751.	0.250	0.701	0.246	-0.139	0.6218

BOLT MATERIAL: 17-7Ph-STAINLESS-STEEL-CH900

BOLT SIZE	SERIES	PRELOAD(N)	MS(Y)	MS(ST)	MS(G)	MS(S)	MASS
***** NO METRIC BOLTS FOUND WITHIN BOUNDARIES *****							
***** NO ENGLISH BOLTS FOUND WITHIN BOUNDARIES *****							

BOLT MATERIAL: Ti-5Al-2.5Sn-AMS4926_or_MIL-T-9047

***** As MINIMUM IS LARGER THAN As MAXIMUM *****

BOLT MATERIAL: Ti-6Al-4V-MIL-T-9047

***** As MINIMUM IS LARGER THAN As MAXIMUM *****

BOLT MATERIAL: Ti-6Al-4V-AMS-4928

***** As MINIMUM IS LARGER THAN As MAXIMUM *****

BOLT MATERIAL: Ti-13V-11Cr-3Al-MIL-T-9047-ANNEALED

***** As MINIMUM IS LARGER THAN As MAXIMUM *****

BOLT MATERIAL: Ti-13V-11Cr-3Al-SOLUTION-TREATED-AGED

BOLT SIZE	SERIES	PRELOAD(N)	MS(Y)	MS(ST)	MS(G)	MS(S)	MASS
***** NO METRIC BOLTS FOUND WITHIN BOUNDARIES *****							
***** NO ENGLISH BOLTS FOUND WITHIN BOUNDARIES *****							

BOLT MATERIAL: 316-STAINLESS-STEEL-SPAENAUR

***** As MINIMUM IS LARGER THAN As MAXIMUM *****

BOLT MATERIAL: 304-STAINLESS-STEEL-METALSUPERMARKETS

***** As MINIMUM IS LARGER THAN As MAXIMUM *****

JOINT MATERIAL: Al-6061-T6-T651

AND CONSIDERING THE CASE OF 8 TIE RODS

BOLT MATERIAL: Al-6061-T6-T651

***** As MINIMUM IS LARGER THAN As MAXIMUM *****

BOLT MATERIAL: CARBON-STEEL-AISI-1025-AMS5046-ANNEALED

***** As MINIMUM IS LARGER THAN As MAXIMUM *****

BOLT MATERIAL: LOW-STEEL-ALLOY-AISI-4130-4135-8630

***** As MINIMUM IS LARGER THAN As MAXIMUM *****

BOLT MATERIAL: CUSTOM450-STAINLESS-STEEL-AMS5763-H1050

BOLT SIZE	SERIES	PRELOAD(N)	MS(Y)	MS(ST)	MS(G)	MS(S)	MASS
M6x1	Metric	7566.	0.250	0.468	0.368	0.336	1.1009
M6.3x1	Metric	8521.	0.250	0.471	0.610	0.505	1.2138
1/4-20	UNC	7690.	0.250	0.471	0.410	0.358	1.2348
1/4-28	UNF	8866.	0.250	0.471	0.700	0.565	1.2348

BOLT MATERIAL: CUSTOM450-STAINLESS-STEEL-AMS5773-H1000

BOLT SIZE	SERIES	PRELOAD(N)	MS(Y)	MS(ST)	MS(G)	MS(S)	MASS
M6x1	Metric	8574.	0.250	0.331	0.550	0.514	1.1009
M6.3x1	Metric	9654.	0.250	0.333	0.824	0.705	1.2139
1/4-20	UNC	8719.	0.250	0.334	0.599	0.539	1.2348
1/4-28	UNF	10043.	0.250	0.334	0.925	0.773	1.2348

BOLT MATERIAL: CUSTOM450-STAINLESS-STEEL-AMS5773-H1050

BOLT SIZE	SERIES	PRELOAD(N)	MS(Y)	MS(ST)	MS(G)	MS(S)	MASS
M6x1	Metric	7566.	0.250	0.468	0.368	0.336	1.1009
M6.3x1	Metric	8521.	0.250	0.471	0.610	0.505	1.2138
1/4-20	UNC	7690.	0.250	0.471	0.410	0.358	1.2348
1/4-28	UNF	8866.	0.250	0.471	0.700	0.565	1.2348

BOLT MATERIAL: CUSTOM450-STAINLESS-STEEL-AMS5773-H1100

BOLT SIZE	SERIES	PRELOAD(N)	MS(Y)	MS(ST)	MS(G)	MS(S)	MASS
***** NO METRIC BOLTS FOUND WITHIN BOUNDARIES *****							
1/4-28	UNF	6511.	0.250	0.705	0.248	0.149	1.2348

BOLT MATERIAL: CUSTOM450-STAINLESS-STEEL-AMS5773-H1150

***** As MINIMUM IS LARGER THAN As MAXIMUM *****

BOLT MATERIAL: CUSTOM455-STAINLESS-STEEL-AMS5617-H1000

BOLT SIZE	SERIES	PRELOAD(N)	MS(Y)	MS(ST)	MS(G)	MS(S)	MASS
M5x0.8	Metric	7717.	0.250	0.410	0.251	0.362	0.7645
M6x1	Metric	10930.	0.250	0.416	0.974	0.930	1.1009
M6.3x1	Metric	12303.	0.250	0.417	1.322	1.172	1.2138
1/4-20	UNC	11123.	0.250	0.418	1.038	0.964	1.2348
1/4-28	UNF	12795.	0.250	0.418	1.450	1.259	1.2348

BOLT MATERIAL: 15-5Ph-STAINLESS-STEEL-AMS5659-H1025

BOLT SIZE	SERIES	PRELOAD(N)	MS(Y)	MS(ST)	MS(G)	MS(S)	MASS
M6x1	Metric	8258.	0.250	0.422	0.485	0.458	1.1127
M6.3x1	Metric	9298.	0.250	0.424	0.747	0.642	1.2268
1/4-20	UNC	8396.	0.250	0.424	0.532	0.482	1.2480
1/4-28	UNF	9673.	0.250	0.424	0.843	0.708	1.2480

BOLT MATERIAL: 15-5Ph-STAINLESS-STEEL-AMS5659-H1075

BOLT SIZE	SERIES	PRELOAD(N)	MS(Y)	MS(ST)	MS(G)	MS(S)	MASS
M6.3x1	Metric	7787.	0.250	0.626	0.463	0.375	1.2268
1/4-20	UNC	7025.	0.250	0.627	0.281	0.240	1.2480
1/4-28	UNF	8102.	0.250	0.627	0.544	0.431	1.2480

BOLT MATERIAL: 15-5Ph-STAINLESS-STEEL-AMS5659-H1100

BOLT SIZE	SERIES	PRELOAD(N)	MS(Y)	MS(ST)	MS(G)	MS(S)	MASS
M6.3x1	Metric	7032.	0.250	0.587	0.321	0.241	1.2268
1/4-28	UNF	7317.	0.250	0.587	0.395	0.292	1.2480

BOLT MATERIAL: 15-5Ph-STAINLESS-STEEL-AMS5659-H1150

BOLT SIZE	SERIES	PRELOAD(N)	MS(Y)	MS(ST)	MS(G)	MS(S)	MASS
***** NO METRIC BOLTS FOUND WITHIN BOUNDARIES ******							
1/4-28	UNF	6532.	0.250	0.745	0.245	0.153	1.2480

BOLT MATERIAL: PH15-7Mo-STAINLESS-STEEL-CH900

BOLT SIZE	SERIES	PRELOAD(N)	MS(Y)	MS(ST)	MS(G)	MS(S)	MASS
M6x1	Metric	9582.	0.250	0.541	0.732	0.692	1.0891
M6.3x1	Metric	10788.	0.250	0.543	1.039	0.905	1.2008
1/4-20	UNC	9748.	0.250	0.543	0.788	0.721	1.2215
1/4-28	UNF	11221.	0.250	0.543	1.151	0.981	1.2215

BOLT MATERIAL: AM-355-STAINLESS-STEEL-AMS5743-SCT1000

BOLT SIZE	SERIES	PRELOAD(N)	MS(Y)	MS(ST)	MS(G)	MS(S)	MASS
M6x1	Metric	8910.	0.250	0.698	0.611	0.573	1.1088
M6.3x1	Metric	10032.	0.250	0.700	0.896	0.771	1.2224
1/4-20	UNC	9062.	0.250	0.701	0.662	0.600	1.2436
1/4-28	UNF	10436.	0.250	0.701	1.001	0.843	1.2436

BOLT MATERIAL: 17-7Ph-STAINLESS-STEEL-CH900

BOLT SIZE	SERIES	PRELOAD(N)	MS(Y)	MS(ST)	MS(G)	MS(S)	MASS
M6x1	Metric	8574.	0.250	0.586	0.550	0.514	1.0852
M6.3x1	Metric	9654.	0.250	0.589	0.824	0.705	1.1964
1/4-20	UNC	8719.	0.250	0.589	0.599	0.539	1.2171
1/4-28	UNF	10043.	0.250	0.589	0.925	0.773	1.2171

BOLT MATERIAL: Ti-5Al-2.5Sn-AMS4926_or_MIL-T-9047

BOLT SIZE	SERIES	PRELOAD(N)	MS(Y)	MS(ST)	MS(G)	MS(S)	MASS
***** NO METRIC BOLTS FOUND WITHIN BOUNDARIES ******							
***** NO ENGLISH BOLTS FOUND WITHIN BOUNDARIES *****							

BOLT MATERIAL: Ti-6Al-4V-MIL-T-9047

BOLT SIZE	SERIES	PRELOAD(N)	MS(Y)	MS(ST)	MS(G)	MS(S)	MASS
M6.3x1	Metric	8010.	0.250	0.405	0.287	0.414	0.6936
1/4-28	UNF	9327.	0.250	0.405	0.350	0.470	0.7056

BOLT MATERIAL: Ti-6Al-4V-AMS-4928

BOLT SIZE	SERIES	PRELOAD(N)	MS(Y)	MS(ST)	MS(G)	MS(S)	MASS
M6.3x1	Metric	8388.	0.250	0.398	0.347	0.481	0.6936
1/4-28	UNF	8719.	0.250	0.398	0.414	0.539	0.7056

BOLT MATERIAL: Ti-13V-11Cr-3Al-MIL-T-9047-ANNEALED

BOLT SIZE	SERIES	PRELOAD(N)	MS(Y)	MS(ST)	MS(G)	MS(S)	MASS
M6.3x1	Metric	8093.	0.250	0.612	0.273	0.429	0.7543
1/4-28	UNF	8412.	0.250	0.612	0.335	0.485	0.7673

BOLT MATERIAL: Ti-13V-11Cr-3Al-SOLUTION-TREATED-AGED

BOLT SIZE	SERIES	PRELOAD(N)	MS(Y)	MS(ST)	MS(G)	MS(S)	MASS
M6x1	Metric	9840.	0.250	0.374	0.526	0.737	0.6841
M6.3x1	Metric	11060.	0.250	0.375	0.764	0.953	0.7543
1/4-20	UNC	10020.	0.250	0.375	0.569	0.769	0.7673
1/4-28	UNF	11495.	0.250	0.375	0.851	1.030	0.7673

BOLT MATERIAL: 316-STAINLESS-STEEL-SPAENAUR

BOLT SIZE	SERIES	PRELOAD(N)	MS(Y)	MS(ST)	MS(G)	MS(S)	MASS
***** NO METRIC BOLTS FOUND WITHIN BOUNDARIES ******							
1/4-28	UNF	6532.	0.250	0.745	0.245	0.153	1.2480

BOLT MATERIAL: 304-STAINLESS-STEEL-METALSUPERMARKETS

BOLT SIZE	SERIES	PRELOAD(N)	MS(Y)	MS(ST)	MS(G)	MS(S)	MASS
***** NO METRIC BOLTS FOUND WITHIN BOUNDARIES ******							
1/4-28	UNF	6532.	0.250	0.745	0.245	0.153	1.2480

C.4 Minimum Stress Area Results

FILENAME: TIE2.RES

Best Tierod Material (Sorted by Minimum Stress Area A_S)			
Order	Bolt Material Designation	Minimum Stress Area A_S (m^2)	
		Case of 4 Tierods	Case of 8 Tierods
1	CUSTOM455-STAINLESS-STEEL-AMS5617-H1000	2.0128E-05	1.4176E-05
2	PH15-7Mo-STAINLESS-STEEL-CH900	2.2206E-05	1.5708E-05
3	AM-355-STAINLESS-STEEL-AMS5743-SCT1000	2.3427E-05	1.6612E-05
4	Ti-13V-11Cr-3Al-SOLUTION-TREATED-AGED	2.4357E-05	1.7002E-05
5	CUSTOM450-STAINLESS-STEEL-AMS5773-H1000	2.4091E-05	1.7105E-05
6	17-7Ph-STAINLESS-STEEL-CH900	2.4091E-05	1.7105E-05
7	15-5Ph-STAINLESS-STEEL-AMS5659-H1025	2.4847E-05	1.7658E-05
8	CUSTOM450-STAINLESS-STEEL-AMS5763-H1050	2.6344E-05	1.8783E-05
9	CUSTOM450-STAINLESS-STEEL-AMS5773-H1050	2.6344E-05	1.8783E-05
10	15-5Ph-STAINLESS-STEEL-AMS5659-H1075	-	2.0140E-05
11	Ti-6Al-4V-AMS-4928	-	2.1237E-05
12	15-5Ph-STAINLESS-STEEL-AMS5659-H1100	-	2.1673E-05
13	Ti-6Al-4V-MIL-T-9047	-	2.2031E-05
14	Ti-13V-11Cr-3Al-MIL-T-9047-ANNEALED	-	2.2209E-05
15	CUSTOM450-STAINLESS-STEEL-AMS5773-H1100	-	2.3429E-05
16	15-5Ph-STAINLESS-STEEL-AMS5659-H1150	-	2.3471E-05
17	316-STAINLESS-STEEL-SPAENAUR	-	2.3471E-05
18	304-STAINLESS-STEEL-METALSUPERMARKETS	-	2.3471E-05
19	Ti-5Al-2.5Sn-AMS4926_or_MIL-T-9047	-	2.3879E-05
20	LOW-STEEL-ALLOY-AISI-4130-4135-8630	-	-
21	CUSTOM450-STAINLESS-STEEL-AMS5773-H1150	-	-

C.5 All Viable Results (sorted by mass)

FILENAME: TIE3.RES

All Viable Results Sorted by Mass (NOT Considering Slip as a Potential Failure)							
Order	# of Rods	Bolt Material Designation	Size	Serie	Mass (kg)	Preload (N)	MS(Gapping)
1	4	PH15-7Mo-STAINLESS-STEEL-CH900	M6.3x1	Metric	0.6004	10122	0.2752
2	4	CUSTOM455-STAINLESS-STEEL-AMS5617-H1000	M6.3x1	Metric	0.6069	11639	0.4646
3	4	PH15-7Mo-STAINLESS-STEEL-CH900	1/4-28	UNF	0.6108	10536	0.3467
4	4	CUSTOM455-STAINLESS-STEEL-AMS5617-H1000	1/4-20	UNC	0.6174	10499	0.2824
5	4	AM-355-STAINLESS-STEEL-AMS5743-SCT1000	1/4-28	UNF	0.6218	9751	0.2463
6	8	Ti-13V-11Cr-3Al-SOLUTION-TREATED-AGED	M6x1	Metric	0.6841	9840	0.5265
7	8	Ti-6Al-4V-AMS-4928	M6.3x1	Metric	0.6936	8388	0.3473
8	8	Ti-6Al-4V-MIL-T-9047	M6.3x1	Metric	0.6936	8010	0.2866
9	8	Ti-6Al-4V-AMS-4928	1/4-28	UNF	0.7056	8719	0.4137
10	8	Ti-6Al-4V-MIL-T-9047	1/4-28	UNF	0.7056	8327	0.35
11	8	Ti-13V-11Cr-3Al-MIL-T-9047-ANNEALED	M6.3x1	Metric	0.7543	8093	0.2734
12	8	CUSTOM455-STAINLESS-STEEL-AMS5617-H1000	M5x0.8	Metric	0.7645	7717	0.2509
13	8	Ti-13V-11Cr-3Al-SOLUTION-TREATED-AGED	1/4-20	UNC	0.7673	10020	0.5687
14	8	Ti-13V-11Cr-3Al-MIL-T-9047-ANNEALED	1/4-28	UNF	0.7673	8412	0.3351
15	8	17-7Ph-STAINLESS-STEEL-CH900	M6x1	Metric	1.0852	8574	0.5499
16	8	PH15-7Mo-STAINLESS-STEEL-CH900	M6x1	Metric	1.0891	9582	0.732
17	8	CUSTOM450-STAINLESS-STEEL-AMS5773-H1000	M6x1	Metric	1.1009	8574	0.5499
18	8	CUSTOM450-STAINLESS-STEEL-AMS5763-H1050	M6x1	Metric	1.1009	7566	0.3677
19	8	CUSTOM450-STAINLESS-STEEL-AMS5773-H1050	M6x1	Metric	1.1009	7566	0.3677
20	8	AM-355-STAINLESS-STEEL-AMS5743-SCT1000	M6x1	Metric	1.1088	8910	0.6106
21	8	15-5Ph-STAINLESS-STEEL-AMS5659-H1025	M6x1	Metric	1.1127	8258	0.4848
22	8	17-7Ph-STAINLESS-STEEL-CH900	1/4-20	UNC	1.2171	8719	0.5992
23	8	PH15-7Mo-STAINLESS-STEEL-CH900	1/4-20	UNC	1.2215	9748	0.7879
24	8	15-5Ph-STAINLESS-STEEL-AMS5659-H1075	M6.3x1	Metric	1.2268	7787	0.4631
25	8	15-5Ph-STAINLESS-STEEL-AMS5659-H1100	M6.3x1	Metric	1.2268	7032	0.3211
26	8	CUSTOM455-STAINLESS-STEEL-AMS5617-H1000	1/4-20	UNC	1.2348	11123	1.038
27	8	CUSTOM450-STAINLESS-STEEL-AMS5773-H1000	1/4-20	UNC	1.2348	8719	0.5992
28	8	CUSTOM450-STAINLESS-STEEL-AMS5763-H1050	1/4-20	UNC	1.2348	7690	0.4105
29	8	CUSTOM450-STAINLESS-STEEL-AMS5773-H1050	1/4-20	UNC	1.2348	7690	0.4105
30	8	CUSTOM450-STAINLESS-STEEL-AMS5773-H1100	1/4-28	UNF	1.2348	6511	0.2482
31	8	AM-355-STAINLESS-STEEL-AMS5743-SCT1000	1/4-20	UNC	1.2436	9062	0.6621
32	8	15-5Ph-STAINLESS-STEEL-AMS5659-H1025	1/4-20	UNC	1.248	8396	0.5317
33	8	15-5Ph-STAINLESS-STEEL-AMS5659-H1075	1/4-20	UNC	1.248	7025	0.2814
34	8	15-5Ph-STAINLESS-STEEL-AMS5659-H1100	1/4-28	UNF	1.248	7317	0.3946
35	8	15-5Ph-STAINLESS-STEEL-AMS5659-H1150	1/4-28	UNF	1.248	6532	0.2449
36	**8**	**316-STAINLESS-STEEL-SPAENAUR**	**1/4-28**	**UNF**	**1.248**	**6532**	**0.2449**
37	**8**	**304-STAINLESS-STEEL-METALSUPERMARKETS**	**1/4-28**	**UNF**	**1.248**	**6532**	**0.2449**

Appendix D

Bolt Stress Area

English Bolt Tensile Stress Areas		
Bolt Size	Series	A_S (m^2)
0-80	UNF	1.16E-06
1-64	UNC	1.70E-06
1-72	UNF	1.79E-06
2-56	UNC	2.39E-06
2-64	UNF	2.54E-06
3-48	UNC	3.14E-06
3-56	UNF	3.37E-06
4-40	UNC	3.90E-06
4-48	UNF	4.26E-06
5-40	UNC	5.14E-06
5-44	UNF	5.35E-06
6-32	UNC	5.86E-06
6-40	UNF	6.55E-06
8-32	UNC	9.03E-06
8-36	UNF	9.51E-06
10-24	UNC	1.13E-05
10-32	UNF	1.29E-05
1/4-20	UNC	2.05E-05
1/4-28	UNF	2.35E-05
5/16-18	UNC	3.38E-05
5/16-20	UN	3.53E-05
5/16-24	UNF	3.74E-05
5/16-28	UN	3.91E-05
3/8-16	UNC	5.00E-05
3/8-20	UN	5.39E-05
3/8-24	UNF	5.66E-05
3/8-28	UN	5.86E-05
7/16-14	UNC	6.86E-05
7/16-16	UN	7.19E-05
7/16-20	UNF	7.66E-05
7/16-32	UN	8.39E-05
1/2-13	UNC	9.15E-05
1/2-16	UN	9.74E-05
1/2-20	UNF	1.03E-04
1/2-32	UN	1.12E-04

Metric Bolt Tensile Stress Areas		
Bolt Size	Series	A_S (m^2)
M1.6x0.35	Metric	1.27E-06
M2x0.4	Metric	2.07E-06
M2.5x0.45	Metric	3.39E-06
M3x0.5	Metric	5.03E-06
M3.5x0.6	Metric	6.78E-06
M4x0.7	Metric	8.78E-06
M5x0.8	Metric	1.42E-05
M6x1	Metric	2.01E-05
M6.3x1	Metric	2.26E-05
M8x1.25	Metric	3.66E-05
M10x1.5	Metric	5.80E-05
M12x1.75	Metric	8.43E-05
M14x2	Metric	1.15E-04
M16x2	Metric	1.57E-04
M20x2.5	Metric	2.45E-04
M24x3	Metric	3.53E-04
M30x3.5	Metric	5.61E-04
M36x4	Metric	8.17E-04
M42x4.5	Metric	1.12E-03
M48x5	Metric	1.47E-03
M56x5.5	Metric	2.03E-03
M64x6	Metric	2.68E-03
M72x6	Metric	3.46E-03
M80x6	Metric	4.34E-03
M90x6	Metric	5.59E-03
M100x6	Metric	6.99E-03

Appendix E

Table I of MSFC-SPEC-522 [92]

Material Designation	E (Pa)	σ_y (Pa)	τ_u (Pa)	v	ρ (kg/m^3)	$\mu_{S,Al}$
Al-6061-T6/T651	6.83E+10	2.48E+08	1.86E+08	0.33	2712.63	0.42
CARBON-STEEL-AISI-1025-AMS5046-ANNEALED	2.00E+11	2.48E+08	2.41E+08	0.32	7861.09	0.35
LOW-STEEL-ALLOY-AISI-4130/4135/8630	2.00E+11	5.17E+08	3.93E+08	0.32	7833.41	0.35
CUSTOM450-STAINLESS-STEEL-AMS5763-H1050	2.00E+11	9.31E+08	6.41E+08	0.29	7750.37	0.35
CUSTOM450-STAINLESS-STEEL-AMS5773-H1000	2.00E+11	1.03E+09	6.48E+08	0.29	7750.37	0.35
CUSTOM450-STAINLESS-STEEL-AMS5773-H1050	2.00E+11	9.31E+08	6.41E+08	0.29	7750.37	0.35
CUSTOM450-STAINLESS-STEEL-AMS5773-H1100	2.00E+11	7.24E+08	5.72E+08	0.29	7750.37	0.35
CUSTOM450-STAINLESS-STEEL-AMS5773-H1150	2.00E+11	5.17E+08	5.03E+08	0.29	7750.37	0.35
CUSTOM455-STAINLESS-STEEL-AMS5617-H1000	1.99E+11	1.28E+09	8.55E+08	0.29	7750.37	0.35
15-5Ph-STAINLESS-STEEL-AMS5659-H1025	1.97E+11	1.00E+09	6.69E+08	0.27	7833.41	0.35
15-5Ph-STAINLESS-STEEL-AMS5659-H1075	1.97E+11	8.62E+08	6.55E+08	0.27	7833.41	0.35
15-5Ph-STAINLESS-STEEL-AMS5659-H1100	1.97E+11	7.93E+08	5.86E+08	0.27	7833.41	0.35
15-5Ph-STAINLESS-STEEL-AMS5659-H1150	1.97E+11	7.24E+08	5.86E+08	0.27	7833.41	0.35
PH15-7Mo-STAINLESS-STEEL-CH900	2.00E+11	1.14E+09	8.27E+08	0.28	7667.33	0.35
AM-355-STAINLESS-STEEL-AMS5743-SCT1000	2.00E+11	1.07E+09	8.55E+08	0.32	7805.73	0.35
17-7Ph-STAINLESS-STEEL-CH900	2.00E+11	1.03E+09	7.72E+08	0.28	7639.65	0.35
Ti-5Al-2.5Sn-AMS4926 or MIL-T-9047	1.07E+11	7.58E+08	4.69E+08	0.32	4484.14	0.34
Ti-6Al-4V-MIL-T-9047	1.10E+11	8.27E+08	5.52E+08	0.31	4428.78	0.34
Ti-6Al-4V-AMS-4928	1.10E+11	8.62E+08	5.72E+08	0.31	4428.78	0.34
Ti-13V-11Cr-3Al-MIL-T-9047-ANNEALED	1.00E+11	8.27E+08	6.34E+08	0.31	4816.30	0.34
Ti-13V-11Cr-3Al-SOLUTION-TREATED-AGED	1.07E+11	1.10E+09	7.24E+08	0.31	4816.30	0.34
Local Suppliers:						
316-STAINLESS-STEEL-SPAENAUR	1.97E+11	7.24E+08	5.86E+08	0.27	7833.41	0.35
304-STAINLESS-STEEL-METALSUPERMARKETS	1.97E+11	7.24E+08	5.86E+08	0.27	7833.41	0.35

Material properties from MIL-HDBK-5 []
Coefficient of static friction on Al-6061-T6 from ASM International []

Appendix F

Delta II Launch Vehicle Information [59]

F.1 Side View of the SP Envelope

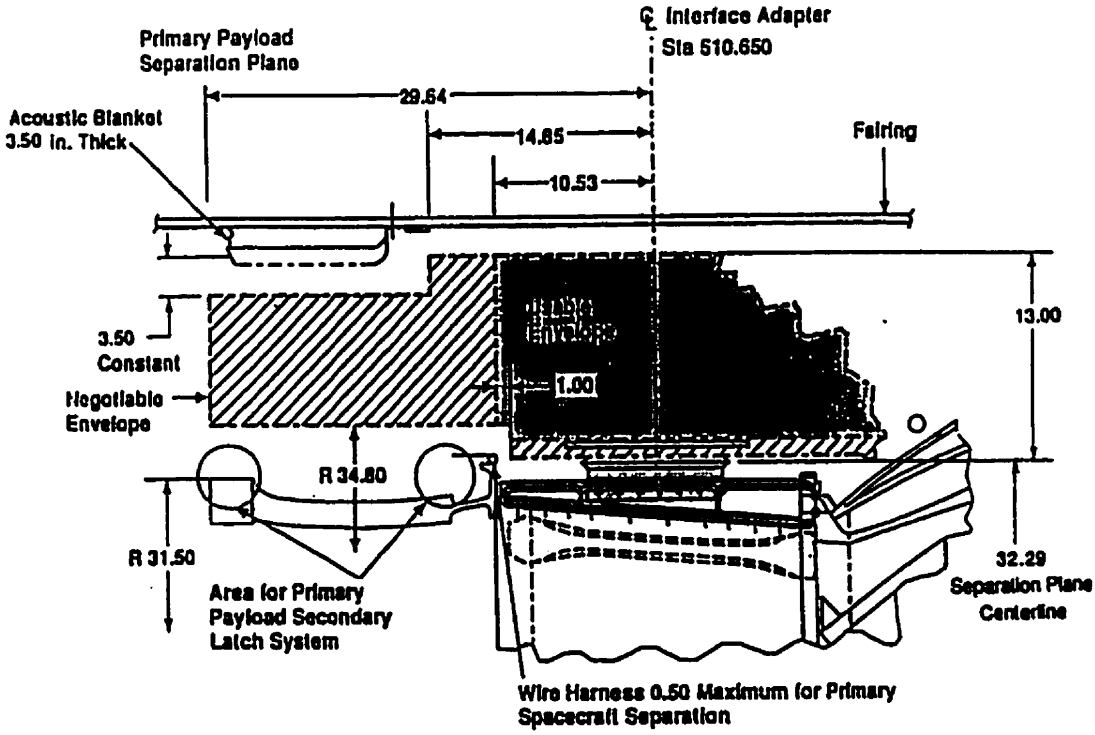

F.2 Top View of the SP Envelope

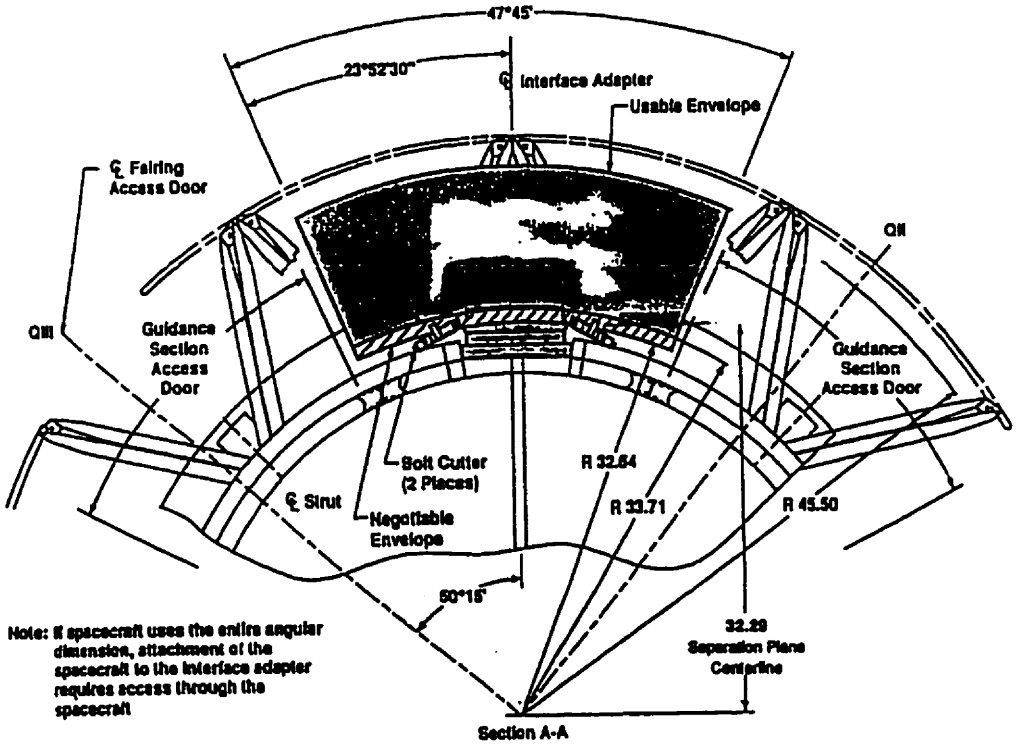

F.3 Payload Adapter Assembly (PAA)

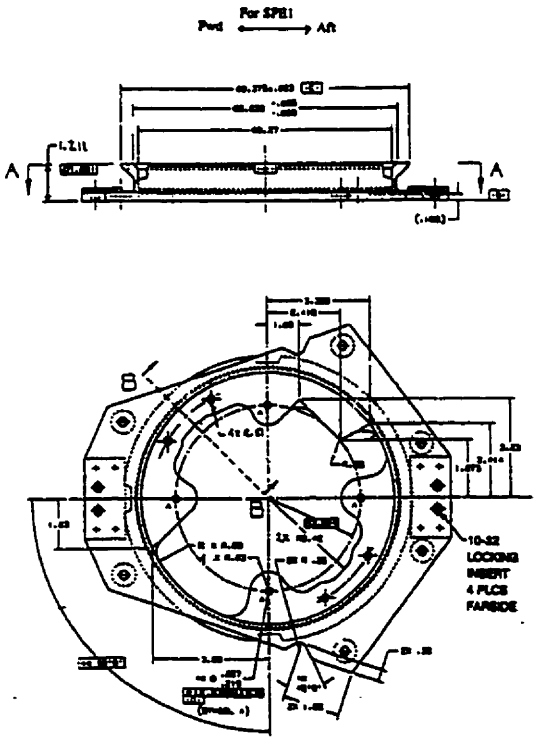

F.4 Allowable C.G. versus Payload Weight

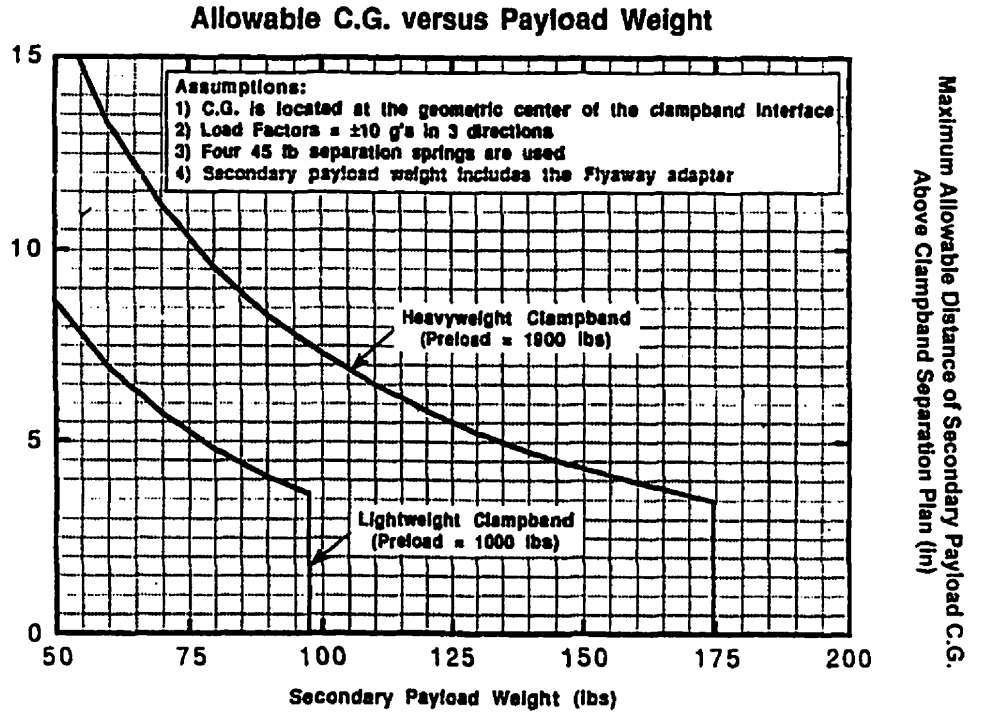

F.5 Sinusoidal Vibration Levels

MAXIMUM FLIGHT LEVEL		PROTOFLIGHT TEST LEVEL	
Frequency (Hz)	Level (Go-p)	Frequency (Hz)	Level G(o-p) (Max Flight + 3 dB)
Thrust Axis (Delta Vehicle)		Thrust Axis (Delta Vehicle)	
5 - 6.2	0.5 inch D. A.	5 - 7.4	0.5 inch D. A.
6.2 - 100	1.0	7.4 - 100	1.4
Radial and Tangential Axes (Delta Vehicle)		Radial and Tangential Axes (Delta Vehicle)	
5 - 100	0.7	5 - 6.2	0.5 inch D. A.
		6.2 - 100	1.0
Sweep Rate = 4 Octaves/Minute		Sweep Rate = 4 Octaves/Minute	

D. A. = Double Amplitude

F.6 Max Flight Level Random Vibration (Separating SP)

Frequency (Hz)	Maximum Flight Level		Protoflight Test Level (Max Flight + 3dB	
10 - 20	0.001	G^2/Hz	0.002	G^2/Hz
20 - 60	+5.7	dB/Octave	+5.7	dB/Octave
60 - 220	0.008	G^2/Hz	0.016	G^2/Hz
220 - 400	+15.7	dB/Octave	+15.7	dB/Octave
400 - 700	0.18	G^2/Hz	0.36	G^2/Hz
700 - 900	-15.4	dB/Octave	-15.4	dB/Octave
900 - 1300	0.05	G^2/Hz	0.10	G^2/Hz
1300 - 1500	+12.4	dB/Octave	+12.4	dB/Octave
1500 - 2000	0.09	G^2/Hz	0.18	G^2/Hz
Overall Grms =	12.9		18.2	
Duration =	30 Seconds/Axis 3 Axes		60 Seconds/Axis 3 Axes	

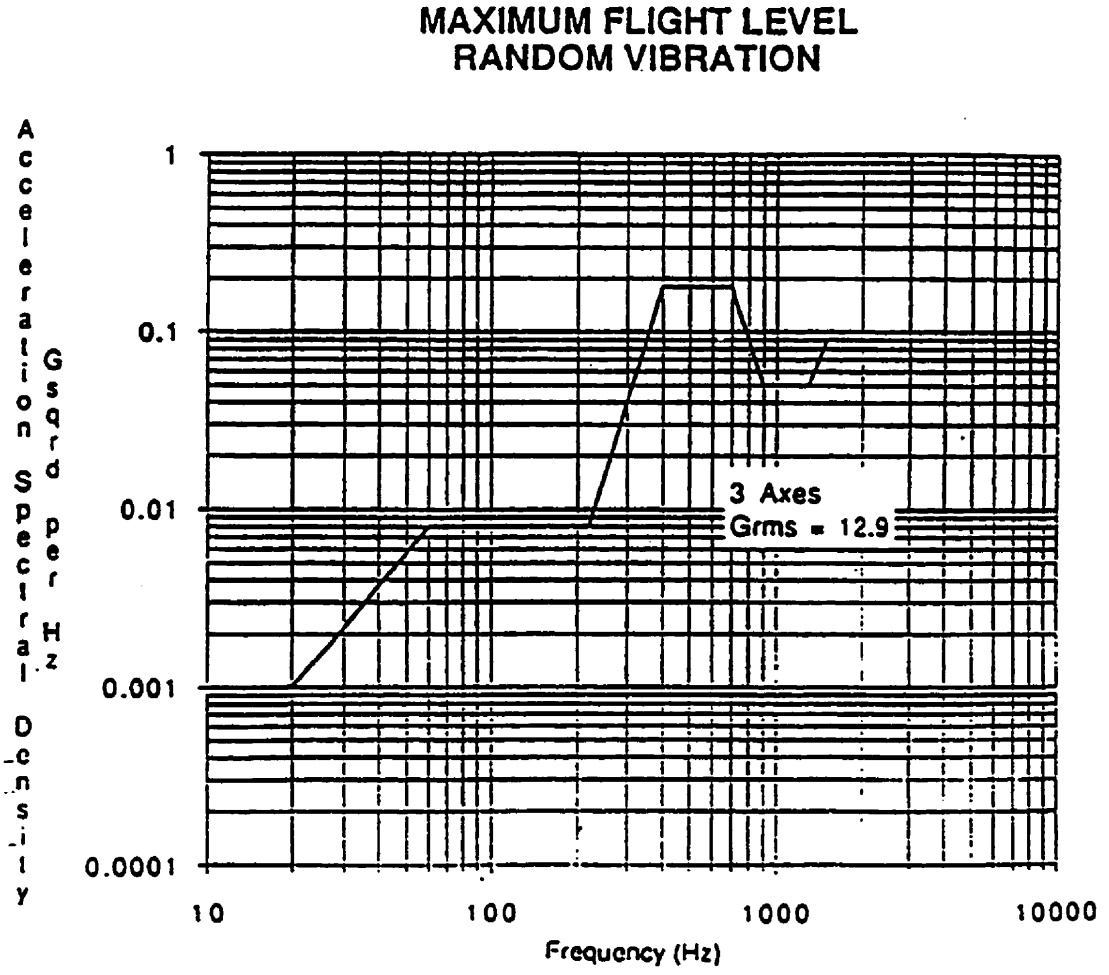

F.7 Max Flight Level Shock Spectrum (Separating SP)

Frequency (Hz)	Maximum Flight Shock Response Spectrum Level (Q=10)	
100 - 140	50	G
140 - 300	+12.7	dB/Octave
300 - 500	250	G
500 - 6000	+6.7	dB/Octave
6000 - 7000	4000	G
7000 - 10000	-1.3	dB/Octave
10000	3700	G

1 Shock/Axis
3 Mutually Perpendicular Axes

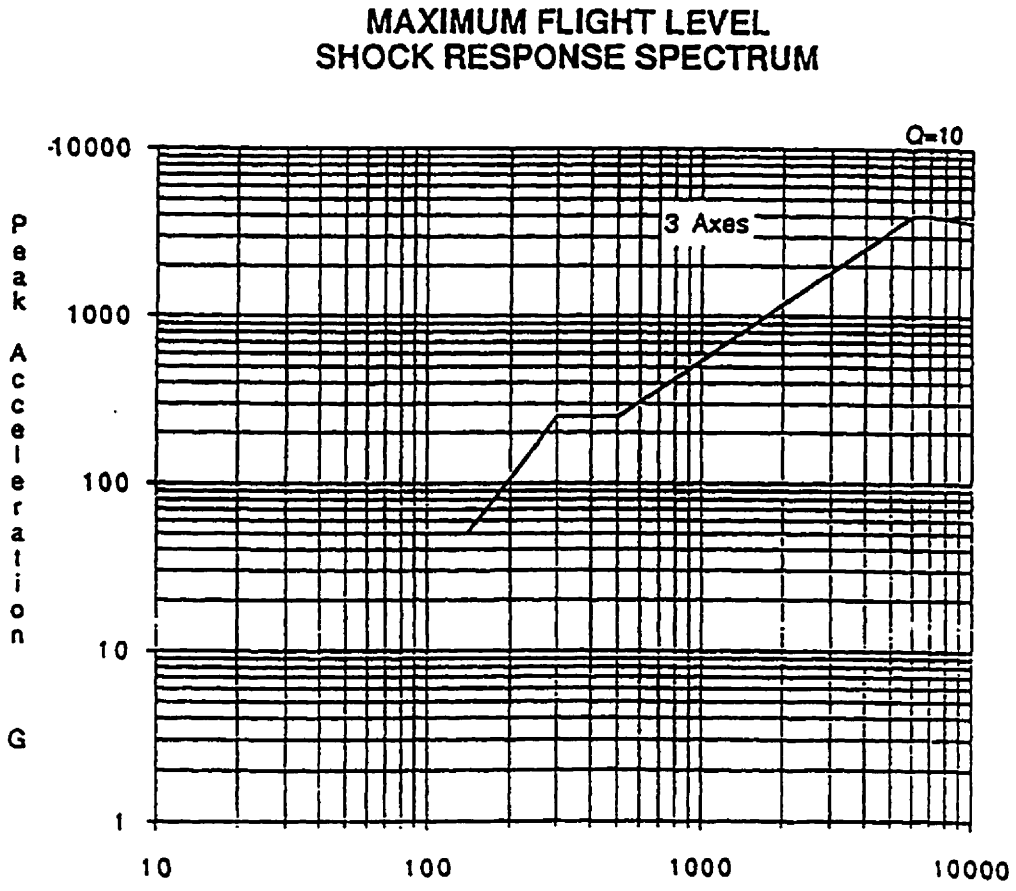

F.8 Design-Level Acoustic Environments [56] [58]

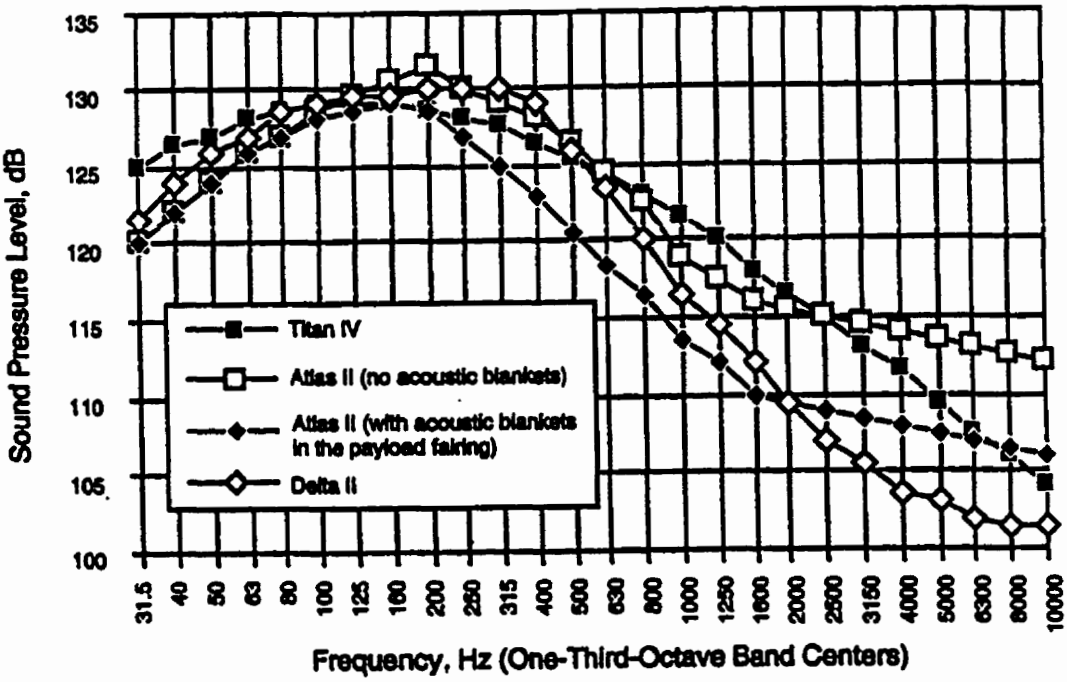

F.9 Load Factors Used in Preliminary Design [56] [58]

Launch Vehicle	Load Factors						Minimum Fundamental Frequencies (Hz)	
	Lift-off		Maximum Airloads or Other Flight Events		Stage I/II Shutdown Events			
	Axial*	Lateral	Axial	Lateral	Axial	Lateral	Axial	Lateral
Atlas-II	+0.2 -2.7	±1.0	-1.9 -2.5	±1.6	+0.5 -6.0	±2.0	15	10
Delta (max. for all series)	+0.2 -2.2	±2.0	--	--	-5.7 -6.3	--	35	15
Space Transportation System	-0.2 -3.2	±2.5	-0.2 -3.2	±2.5	-0.2 -3.2	±2.5	--	--
Titan IV	0.0 -3.0	±2.5	0.0 -3.0	±2.5	+2.0 -6.0	±1.5	--	2.5

Appendix G

Science Payload Drawings

G.1 Telescope and Periscope Assembly (Courtesy of SFL)

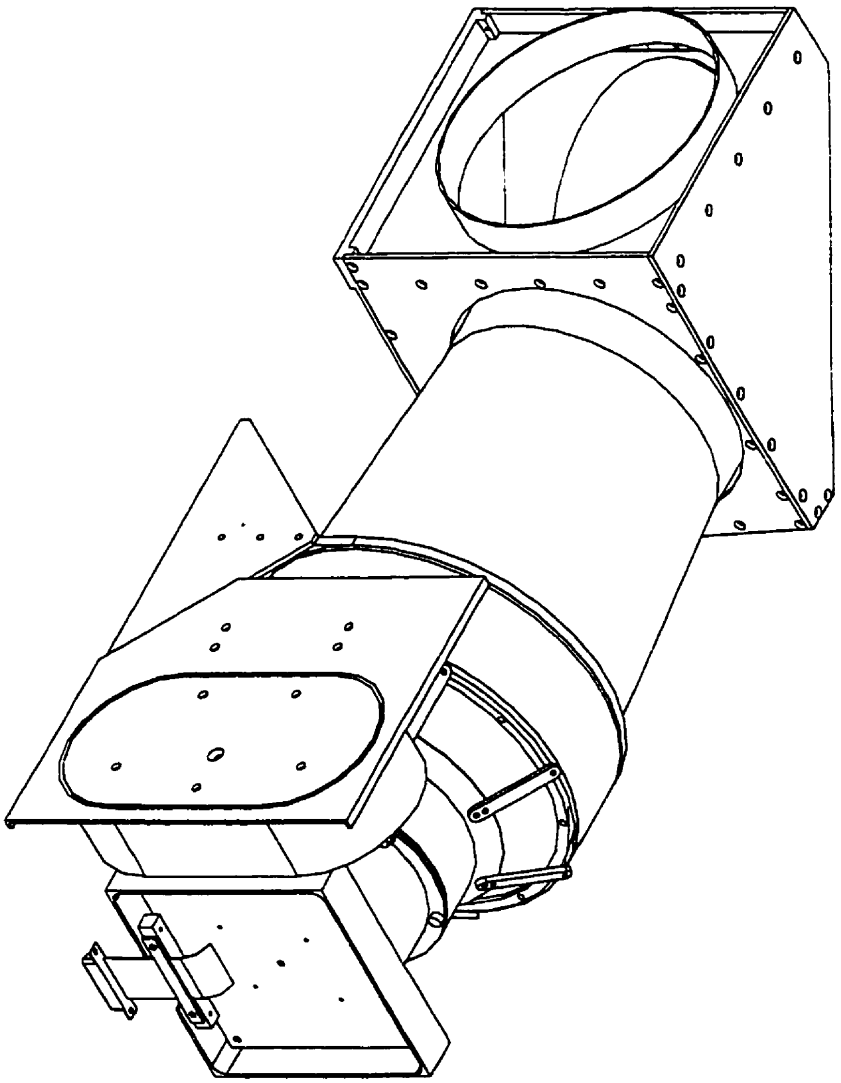

G.2 Cross-Section of the Telescope (Courtesy of SFL)

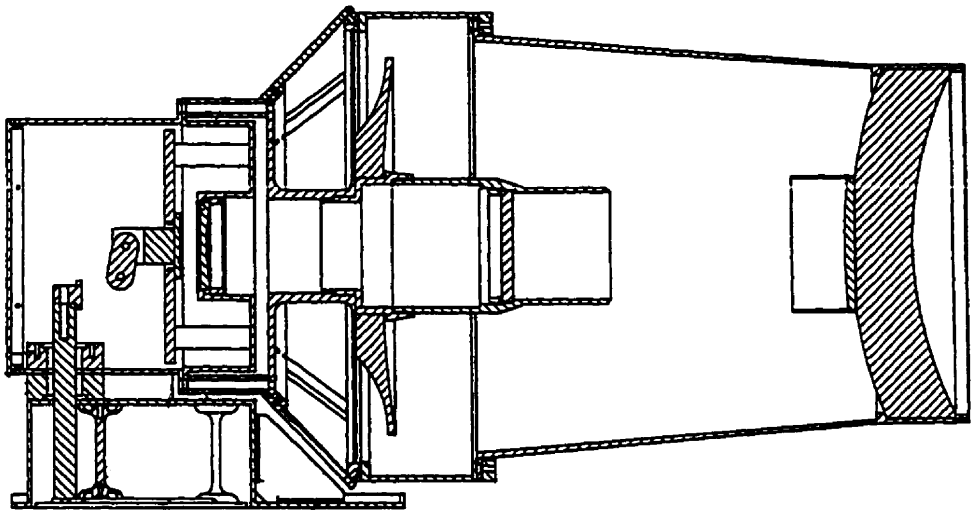

G.3 Periscope Enclosure (Courtesy of SFL)

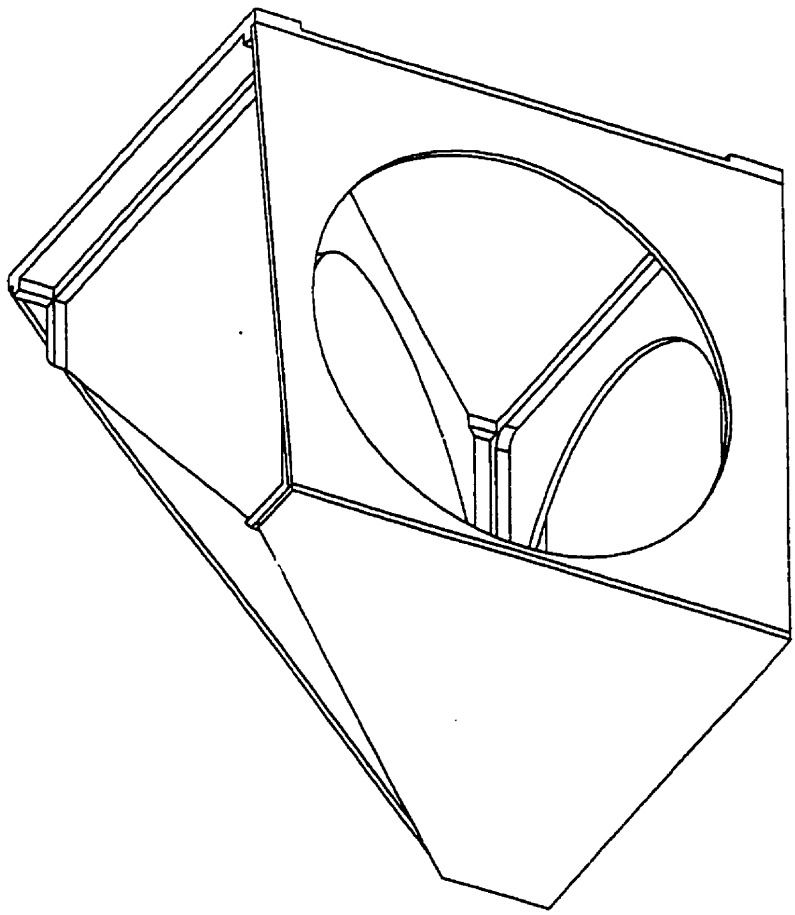

G.4 Instrument Assembly (Courtesy of SFL)

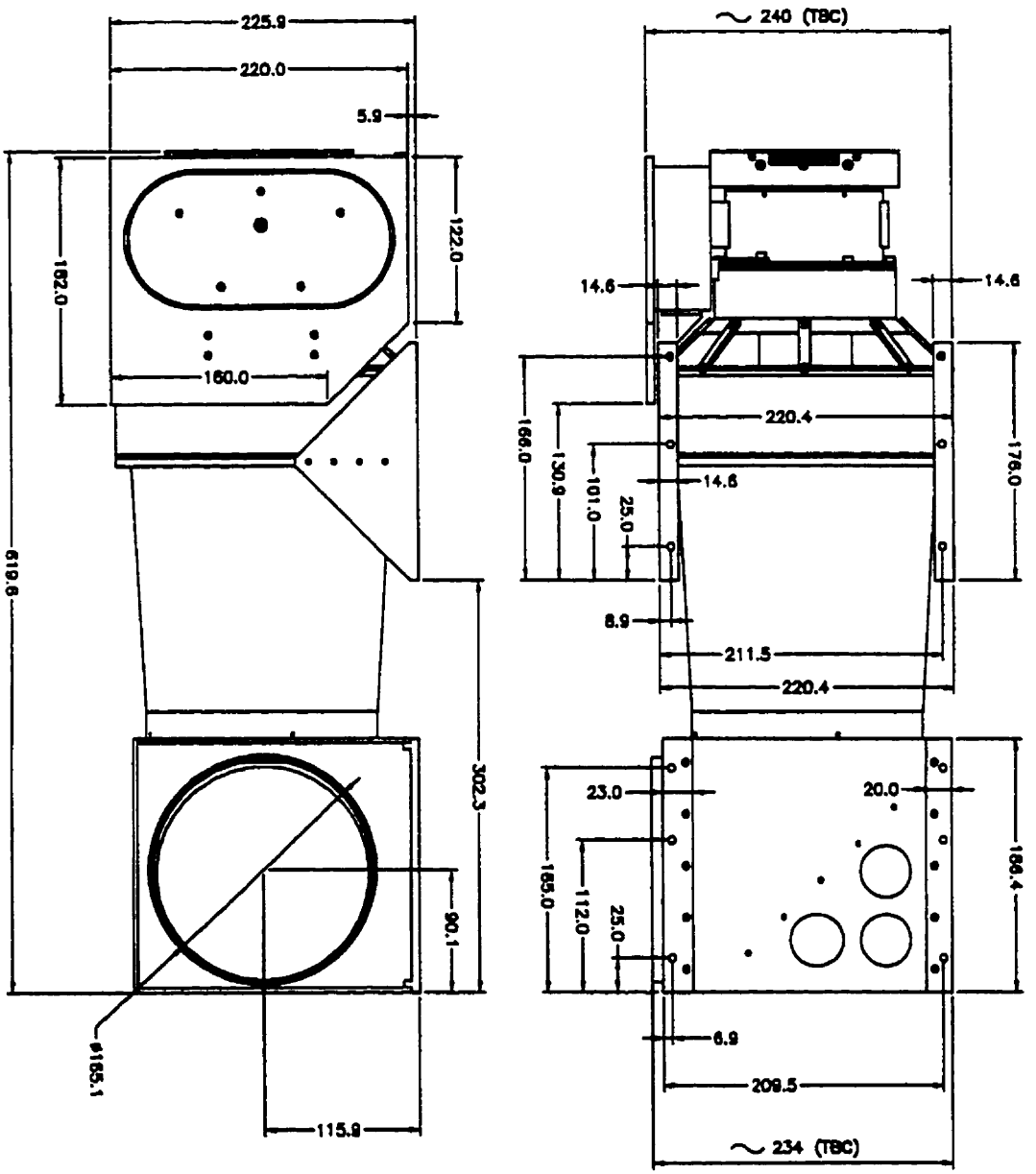

Appendix H

MOST Detailed Mass Allocation

H.1 Detailed Tray FE Model Mass Assumptions

Tray Name	#	FEM Group	-ve z start	+ve z end	Tray Bottom	PCB	Mass (kg)	Contingency (kg)	Total (kg)
Transceiver	1	trx1	-301.10	-250.10	-ve z	Yes	2.10	0.15	2.25
Instrument	2	instccd	-250.10	-218.10	-ve z	Yes	1.05	0.15	1.20
ACS-ccd	3	acsccd	-218.10	-186.10	+ve z	Yes	1.05	0.15	1.20
OBC	4	obc	-186.10	-144.10	+ve z	Yes	1.90	0.30	2.20
Spacer1	5	spacer1	-144.10	-121.10	no wall	none	0.55	0.10	0.65
PAA1	6	paa1	-121.10	-108.35	+ve z	none	0.50	0.07	0.57
Wheels	7	rw	-108.35	-6.35	+ve z	none	4.30	0.50	4.80
PAA2	8	paa2	-6.35	6.35	+ve z	none	0.50	0.07	0.57
Power	9	power	6.35	108.35	-ve z	Yes	3.90	0.50	4.40
PAA3	10	paa3	108.35	121.10	-ve z	none	0.50	0.07	0.57
AMSAT	11	amsat	121.10	153.10	+ve z	Yes	1.50	0.20	1.70
ACS1	12	acs1	153.10	183.10	+ve z	Yes	1.05	0.15	1.20
ACS2	13	acs2	183.10	213.10	+ve z	Yes	1.05	0.15	1.20
Spacer2	14	spacer2	213.10	248.10	no wall	none	0.55	0.10	0.65
Transceiver	15	trx2	248.10	301.10	+ve z	Yes	2.10	0.15	2.25

H.2 Satellite Components Mass Assumptions

Components	Quantity	Mass (kg)	Contingency (kg)	Total Mass (kg)
15 Trays	1	22.6	2.8	25.4
Torquer Coils	2	0.8	0.0	0.8
Wiring Harness	1	0.8	0.1	0.9
Power Dist. Harness	1	0.3	0.0	0.3
Solar panel harness	1	0.5	0.1	0.6
Thermal Control	1	0.6	0.1	0.7
Tie Rods	8	0.7	0.1	0.8
Brackets, misc.	1	2.0	0.3	2.3
Solar Cell Patch	9	0.7	0.1	0.8
Total Bus Mass				**32.6**
+X Sunsensor	2	0.1	0.0	**0.1**
+X Panel	1	2.0	0.3	**2.3**
-X Lens Cap	1	1.0	0.2	**1.2**
-X PAA Plate	1	1.2	0.2	**1.4**
-X Panel	1	1.4	0.2	**1.6**
+Y Panel	1	0.8	0.1	**0.9**
-Y Magnetometer	2	0.2	0.0	**0.2**
-Y Panel	1	0.8	0.1	**0.9**
-Y Least Antenna	3	0.3	0.0	**0.3**
+/- Z Antenna	4	0.4	0.0	**0.4**
+/- Z Panel	2	1.5	0.2	**1.7**
Optics	1	12.0	1.8	**13.8**
Total Satellite Mass		**50.7**	**6.7**	**57.4**

H.3 Satellite Components Mass Allocations (Courtesy of SFL)

Assembly	Item	Sum of Total Mass (kg)	Sum of Contingency (kg)	Sum of Total Estimated Mass (kg)
Transceiver	Transceiver Tray	1.7	0.3	2.0
	Receiver	1.4	0.0	1.4
	Transmitter	0.6	0.0	0.6
	T&C Smartnode	0.2	0.0	0.2
Transceiver Total (Qty 2)		**4.0**	**0.3**	**4.3**
Spacer	Spacer Tray	1.1	0.2	1.3
Spacer Total (Qty 2)		**1.1**	**0.2**	**1.3**
Instrument Drive	Telescope Electronics	0.8	0.1	0.9
	Instrument Drive Tray	1.3	0.2	1.5
Instrument Drive Total (Qty 2)		**2.1**	**0.3**	**2.4**
PAA	PAA Tray	1.5	0.2	1.7
PAA Total (Qty 3)		**1.5**	**0.2**	**1.7**
ACS	Sun Sensor	0.1	0.0	0.1
	ACS Tray	1.3	0.2	1.5
ACS Total (Qty 2)		**1.3**	**0.2**	**1.5**
OBC	OBC Tray	0.8	0.1	0.9
	Ram Disk	0.3	0.0	0.3
	Stub Board	0.3	0.0	0.3
OBC Total		**1.3**	**0.2**	**1.5**
RW	Reaction Wheel	3.1	0.4	3.5
	Reaction Wheel Tray	1.2	0.2	1.4
RW Total		**4.3**	**0.6**	**4.9**
Power	Battery Charge Regulator	0.6	0.1	0.7
	Batteries	1.7	0.2	1.9
	Power Switching Electronics	0.2	0.0	0.2
	Power Tray	0.6	0.1	0.7
Power Total		**3.1**	**0.4**	**3.5**
AMSAT	AMSAT Tray	0.7	0.1	0.8
	Least PCB	0.4	0.0	0.4
AMSAT Total		**1.1**	**0.1**	**1.2**
+X	+X Panel	2.0	0.3	2.2
	Spacecraft Processor	0.6	0.1	0.6
+X Total		**2.5**	**0.4**	**2.9**
-X	Lens Cap	1.0	0.2	1.2
	PAA Plate	1.2	0.2	1.3
	-X Panel	1.4	0.2	1.6
-X Total		**3.6**	**0.5**	**4.1**
+Y	+Y Panel	0.8	0.1	0.9
+Y Total		**0.8**	**0.1**	**0.9**
-Y	Magnetometer	0.2	0.0	0.2
	-Y Panel	0.8	0.1	0.9
	Least Antennas	0.7	0.1	0.8
-Y Total		**1.8**	**0.2**	**2.0**
+/-Z	Antenna	0.4	0.0	0.4
	+/-Z Panel	1.5	0.2	1.8
+/-Z Total (Qty 2)		**2.0**	**0.2**	**2.2**
Optics	Telescope+Periscope	12.0	1.8	13.8
Optics Total		**12.0**	**1.8**	**13.8**
Distributed Mass	Torquer Coils	0.8	0.0	0.8
	Data Wiring Harness	0.8	0.1	0.9
	Power Dist. Harness	0.3	0.0	0.3
	Solar panel wiring harness	0.5	0.1	0.6
	Thermal Control	0.6	0.1	0.7
	Tie Rods	0.7	0.1	0.8
	Brackets, Misc	2.0	0.3	2.3
	Solar Array Cell Patch	0.7	0.1	0.7
	ACS Smartnode	0.8	0.1	0.9
Distributed Mass Total		**7.0**	**0.9**	**7.9**
Grand Total		50.4	6.8	57.2